Analysis of the Role of *Bacillus oleronius* Proteins in the Induction of Rosacea and Evaluation of Novel Therapeutics for the Treatment of Dermal and Ocular Rosacea

A thesis submitted to the National University of Ireland, Maynooth for the degree of Doctor of Philosophy by

Amie Maher B. Sc.

Supervisor
Prof Kevin Kavanagh,
Medical Mycology Unit,
Dept. of Biology,
Maynooth University,
Co. Kildare

Head of Department
Prof. Paul Moynagh,
Dept. of Biology,
Maynooth University,
Co. Kildare

December 2017

Declaration

This Thesis has not been submitted in whole or in part to this or any other university for any degree, and is original work of the author except where otherwise stated.

Signed: _____

Date: _____

Acknowledgements

This PhD would not have been made possible without the support, patience, kindness and speedy reading from my supervisor, Prof Kevin Kavanagh. His encouragement and expertise throughout my PhD have never failed and I am immensely grateful to him. The early morning chats in the lab before the science day began will be remembered, as will the last days of the Mitsubishi Colt – the end of an era for us all! From trips to London and appearing on television shows and the likes with him, Kevin wealth of knowledge and experience know no end. I truly could not have wanted a better, more dedicated and committed supervisor, thank you Kevin.

My time in the Biology Department has been both a happy and homely one, all made possible by the people here at Maynooth University. From the very beginning in the Medical Mycology Unit, I was made most welcome. Thank you to Carla and Louise, two lifelong friends I have made. Both of you introduced me to lab life; from field work to running gels, to tea breaks and pub breaks! Thank you girls for the support and guidance throughout the years and for making work fun. I would like to thank Niall, my first supervisor – for answering all of those many, many questions, for being so kind and helpful and for the daily laughs in the lab. The ritual morning tea will never be forgotten with the oldies (Fred, Ahmed, Siobhán and Rónán) and the newbies (Anatte, Ger, Niall, Rosie and Ahmad). The staff in the Department have been so helpful and understanding throughout the PhD. No matter if it was borrowing items endlessly from prep lab, asking Nick or Noel to fix something or to Caroline with the mass spectrometry, your time and effort is much appreciated. I would also like to thank Michelle, Terry, Jean and Tina particularly in the last few months of my PhD.

I would like to thank Nicholas Duggan and Viadynamics Ltd, the enterprise partner involved in the PhD, who together with the Irish Research Council, have made this project possible. I owe a great deal to the NICB Centre at DCU – to Dr Finbarr O'Sullivan for taking me under his wing and Dr Joanne Keenan for introducing me to the excellent cell culture practise at the centre. I would like to especially thank Dr Clair Gallagher, whose support and encouragement throughout my time at the NICB helped me see through the good days and bad with learning the ins and outs of cell culture. From qPCR techniques to wedding dress decisions, there was never a silent moment in the culture room between us!

I would also like to give a special mention to the legend of an office buddy, Rónán (The Squire) Maguire. Between the pair of us we managed to make fun of writing-up, sometimes not knowing whether to laugh or to cry! From the ‘inspo wall’ to our daily games of Stop The Bus, Rónán kept me on my toes and lifted the spirit of the office. The morale was kept up by daily visits from Ger, especially towards the end, which will always be treasured.

Last of all, and certainly not least, I would like to thank all of my friends and family throughout my time at Maynooth University, particularly in the three years of my PhD. To the Newbridge gang for their interest and encouragement – so much so it led to a week in Greece! To the McCabe Clan, who have been in my corner all of the way spurring me on, thank you. I’d like to thank Ewan, for listening to my adrenaline fuelled rants after a day of writing. His support, love and constant confidence in me will be cherished always. To Eoin, who managed to escape the ‘boring science chats’ and grasp the highlights of my PhD. His humour and encouragement throughout my PhD has been refreshing and I am so grateful. Finally I would like to thank my parents – I would not be writing these acknowledgements without them. Their encouragement and support has been infinite. The questions, queries and quirks they have thrown my way throughout the PhD are all much appreciated, forever emphasising that there’s a solid team behind me. I would like to dedicate this thesis to them.

Publications in preparation for submission:

Maher, A., Kowalczyk, M. and Kavanagh, K. (2018). 'The role of *Demodex* mites and associated bacteria in disease in humans and animals'. Chapter in "Rola nuzenca ludzkiego (Demodex folliculorum) w schorzeniach okulistycznych i dermatologgicznych" ("*The role of Demodex folliculorum in ophthalmological and dermatological conditions*"). Collegium Stomatologicum, Poznan, Poland.

Maher, A., Staunton, K. and Kavanagh, K. (2018) Analysis of the effect of temperature on protein abundance in *Demodex*-associated *Bacillus oleronius*. *Pathogens and Disease.* 76 (4) 1-8

Publications not part of this thesis:

Browne, N., Surlis, C., **Maher, A**., Gallagher, C., Clynes, M. and Kavanagh, K. (2015). 'Duration of pre-incubation period reduces the ability of *Galleria mellonella* larvae to tolerate fungal and bacterial infection'. *Virulence* 6(5): 458-465.

Oral Presentations:

Maher, A. and Kavanagh, K. "What lies beneath: A closer look at the skin condition rosacea". February, 16th, 2016, Maynooth University. Departmental Seminar Series.

Maher, A. and Kavanagh, K. "Development of novel therapies for the treatment of erythema associated dermal rosacea". June, 13th, 2016, Maynooth University. Department Annual Research Day. (Second Prize)

Maher, A. and Kavanagh, K. "Evaluation of potential blocking agents in ocular rosacea". June, 14th, 2016, Maynooth University. Meeting with enterprise partner Viadynamics Ltd. and Dept. Commercialisation.

Maher, A. "What lies beneath: mites on your face". March, 9th, 2017, Maynooth University. 'Thesis in Three' Competition, Graduate Studies Office. (First Prize)

Maher, A. and Kavanagh, K. "Effect of temperature on protein abundance in *Bacillus oleronius*". March, 14th, 2017, Maynooth University. Departmental Seminar Series.

Maher, A. and Kavanagh, K. "Development of novel therapies for the treatment of erythema associated dermal rosacea". April, 5th, 2017, Maynooth University. Progress Meeting with enterprise partner Viadynamics Ltd.

Maher, A. and Kavanagh, K. "Development of novel therapies for the treatment of dermal and ocular rosacea". May, 10th, 2017. Viadynamics Ltd., London, UK.

Poster Presentations:

Maher, A. and Kavanagh, K. Title: Identification of immune stimulatory proteins produced by *Bacillus oleronius* that contribute to rosacea. June 12th, 2015, Maynooth University. Department Annual Research Day. (Runner-up Prize)

Maher, A. and Kavanagh, K. Title: Analysis of the effect of elevated temperature on growth and protein abundance of *Bacillus oleronius*. New Approaches and Concepts in Microbiology 27th-30th, June, 2017. EMBL Heidelberg, Germany.

Maher, A. and Kavanagh, K. Title: Development of novel therapies for the treatment of erythema associated dermal rosacea". June, 6th, 2017, Maynooth University. Department Annual Research Day.

Table of Content

Chapter 1	**Introduction**	**1**
1.1	Rosacea	2
1.2	Diagnostic features	3
1.3	Rosacea Subtypes	5
1.3.1	Subtype I: Erythematotelangiectatic Rosacea (ETR)	5
1.3.2	Subtype II: Papulopustular Rosacea (PPR)	7
1.3.3	Subtype III: Phymatous Rosacea	7
1.3.4	Ocular Rosacea	9
1.3.5	Rosacea Variants	9
1.4	Factors affecting rosacea onset	11
1.5	*Demodex* mites	12
1.5.1	Human mite ecology	14
1.5.2	*Demodex* source and transmission	18
1.5.3	Demodicosis in humans	21
1.5.4	*Demodex* density and rosacea	22
1.5.5	*Demodex*-related diseases in animals	23
1.6	Potential role of commensal skin bacteria in the pathogenesis of rosacea	26
1.6.1	*Staphylococcus epidermidis*	26
1.6.2	*Helicobacter pylori*	28
1.6.3	*Propionibacterium acnes*	28
1.6.4	*Chlamydia pneumonia*	29
1.7	*Demodex mites* and *Bacillus oleronius*	31
1.7.1	Role of *Bacillus oleronius* in rosacea	31
1.8	Innate immune response in rosacea	34
1.9	Management and Treatment	37
1.9.1	Ocular rosacea treatment	39
1.10	Aims of this study	40
Chapter 2	**Materials and Methods**	**41**
2.1	General Chemicals and Reagents	42

2.2	Sterilisation Procedures	42
2.3	Statistical Analysis	42
2.4	Culture Media	42
2.4.1	Nutrient agar	42
2.4.2	Nutirent broth	42
2.4.3	2XYT broth	43
2.5	Culture conditions	43
2.6	Phosphate buffered saline	43
2.7	*Bacillus* lysis buffer (pH 7.2)	43
2.8	Protein extraction protocol	44
2.8.1	Protein extraction from *Bacillus oleronius*	44
2.8.3	Bradford assay for protein quantification	45
2.8.4	Acetone precipitation of protein samples	45
2.9	Sodium Dodecyl Sulphate Gel Electrophoresis-Poly Acrylamide Gel Electrophoresis (SDS-PAGE)	45
2.9.1	Tris–HCl (1.5 M)	45
2.9.2	Tris-HCl (0.5 M)	46
2.9.3	10% Sodium Dodecyl Sulphate (SDS)	46
2.9.4	10% Ammonium Persulphate (APS)	46
2.9.5	10X Electrode Running Buffer	46
2.9.6	5X Solubilisation Buffer for 1D SDS-PAGE	46
2.9.7	2.9.7 Separating gel composition (12.5%)	47
2.9.8	Stacking gel composition (5%)	47
2.9.9	1D SDS-PAGE sample loading and voltages	48
2.10	2D IEF SDS-PAGE preparation and analysis	48
2.10.1	Isoelectric focussing (IEF) Buffer	48
2.10.2	Equilibration buffer (pH 6.8)	48
2.10.3	Agarose sealing solution	49
2.10.4	2-Dimensional IEF Gel Electrophoresis	49
2.11	Staining of gels and analysis of differential expression of proteins	51
2.11.1	Colloidal Coomassie staining of gels	51
2.11.2	Image J densitiometrical analysis of Western blots	51

2.11.3	Progenesis SameSpots software for analysis of 2-Dimensional IEF Gels	52
2.12	Identification of proteins from SDS-PAGE gels	52
2.12.1	Preparation for spot/band excision	52
2.12.2	Trypsin Digest of peptides from 1-Dimensional and 2-Dimensional IEF SDS-PAGE gels	52
2.12.3	Bioinformatic analysis of peptide identification results	53
2.13	Western blotting	54
2.13.1	10X Tris Buffered Saline (TBS) pH 7.6	54
2.13.2	Transfer Buffer	54
2.13.3	Blocking Buffer	54
2.13.4	Diaminobenzidine tetra-hydrochloride (DAB)	54
2.13.5	Western Blot Protocol	55
2.14	In solution digest protocol for overnight peptide digestion for label free MS/MS proteomics	57
2.14.1	Protein preparation for label free MS/MS proteomics	58
2.15	Sample clean-up prior to loading on Q-exactive MS	59
2.16	Preparation of sample prior to loading on Q-exactive MS	61
2.17	Parameters for running samples on Q-exactive MS	61
2.18	Parameters for analysing quantitative results and statistical	61
2.19	Susceptibility assay for quantifying bacterial cell growth	62
2.20	reparation of bacteria for confocal microscopy	63
2.21	Fractionation and purification of *B. oleronius* antigen with Q-Sepharose™ Performance Beads and ÄKTA-FPLC	63
2.21.1	FPLC Binding buffer (pH 4.8)	63
2.21.2	FPLC Elution buffer (pH 4.8)	63
2.21.3	Protocol for *B. oleronius* protein purification using Q-Sepharose™ charge separation	64
2.22	General HEp-2 cell culture methodology	65
2.22.1	HEp-2 cell line	65
2.22.2	Sub-culturing HEp-2 cell line	65
2.22.3	Cryopreservation of HEp-2 cell line in Liquid Nitrogen N_2	66
2.22.4	Recovery of HEp-2 cell line from Liquid N_2	66

2.23	General hTCEpi cell culture methodology	66
2.23.1	hTCEpi cell line	66
2.23.2	Sub-culturing hTCEpi cell line	67
2.23.3	Cryopreservation of HEp-2 cell line in Liquid Nitrogen N_2	67
2.23.4	Recovery of hTCEpi cell line from Liquid N_2	67
2.24	Acid phosphatase assay for determining toxicity on cell growth	68
2.25	qRT-PCR analysis of hTCEpi gene expression	68
2.25.1	RNA extraction from hTCEpi cells	68
2.25.2	cDNA synthesis	69
2.25.3	Quantitative Real-time polymerase chain reaction	69
2.26	Wound healing assay	70
2.27	ELISA protocol to detect secreted cytokine expression levels	70
2.28	Pilot study for the comparison of Oriel Sea Salt on rosacea patient skin	72
2.28.1	Parameters measured throughout patient pilot studies	72
2.28.2	Pilot Study One	73
2.28.3	Pilot Study Two	73
Chapter 3	**An Analysis of the Effect of Temperature on *Bacillus oleronius***	**74**
3.1	Introduction	75
3.2	The effect of temperature on cell growth of *B. oleronius* over 72 hours	78
3.3	The effect of temperature on the production of stimulatory 62 kDa antigen by *B. oleronius*	78
3.4	Investigating the effect of temperature on the production of *B. oleronius* antigen using confocal microscopy	82
3.5	A 2-Dimensional IEF SDS-PAGE investigation of the effect of temperature on the proteomic profile of *B. oleronius.*	86
3.6	Comparative analysis of the effect of temperature on the proteomic profile of *Bacillus oleronius* using Label free MS/MS	91

3.7	Discussion	102
Chapter 4	**An Analysis of the Effect of Oxidative Stress on *Bacillus oleronius***	**108**
4.1	Introduction	109
4.2	Investigating the effect of oxidative stress on the growth of *Bacillus oleronius*	112
4.3	Investigating the effect of aerobic and static incubation growth conditions on the production of stimulatory 62 kDa antigen by *B. oleronius*	114
4.4	A 2-Dimensional IEF SDS-PAGE investigation of the effect of oxidative stress on proteomic profile of B. oleronius	118
4.5	Comparative analysis of the effect of oxidative stress on the proteomic profile of *Bacillus oleronius* using Label Free MS/MS	124
4.6	Discussion	137
Chapter 5	**Investigation of the Potential use of Selected Blocking Agents for Preventing *B. oleronius* protein-host cell interactions**	**143**
5.1	Introduction	144
5.2	Purification of the *B. oleronius* 62 kDa antigen by ÄKTA-FPLC	147
5.2.1	SDS-PAGE and Western blot analysis of 'pure' *B. oleronius* FPLC fractions	149
5.3	Effect of purified 62 kDa *B. oleronius* antigen on human cell proliferation	152
5.3.1	The effect of *B. oleronius* antigen on hTCEpi gene expression	155
5.4	Determining the toxicity of potential blocking agents to human cells	158
5.5	The effect of potential blocking agents on human cell proliferation alone and in combination	163

5.6	The effect of B. oleronius protein on wound healing in human cells	167
5.6.1	The effect of *B. oleronius* protein on cytokine expression in response to wound healing in human cells	170
5.7	Discussion	172
Chapter 6	**Biological and Clinical Evaluation of a Novel Salt Based Formulation for the Treatment of Symptoms of Dermal Rosacea**	**179**
6.1	Introduction	180
6.2	Determining the toxicity of Oriel salt and NaCl on human cell growth	183
6.2.1	Effect of Oriel salt solution and NaCl on HEp-2 cell proliferation	186
6.3	Comparative analysis of the effect of Oriel salt on the proteomic profile of HEp-2 cells using Label free MS/MS	188
6.4	Effect of Oriel salt and NaCl on bacterial cell density	192
6.5	The effect of different Oriel formulations at inhibiting bacterial cell growth on an agar plate	196
6.6	Oriel salt as a potential treatment for symptomatic relief of ETR and PPR – Pilot Study One	198
6.7	Oriel salt as a potential treatment for symptomatic relief of ETR and PPR – Pilot Study Two	206
6.8	Discussion	214
Chapter 7	**General discussion**	**220**
Chapter 8	**Bibliography**	**229**
Chapter 9	**Appendix**	**253**

List of Figures

Chapter 1

Figure 1.1 Grading system of rosacea applied to the papulopustular subtype

Figure 1.2 Subtypes of rosacea with independently defined symptoms

Figure 1.3 Moderate grading of erythematotelangiectatic rosacea (ETR)

Figure 1.4 Phymatous rosacea featuring thickening of the skin around the nose

Figure 1.5 Ocular rosacea symptoms associated with *Demodex* mite infestation

Figure 1.6 Granulomatous rosacea

Figure 1.7 Characteristic trigger factors of rosacea may influence patient phenotype and exacerbate symptoms.

Figure 1.8 *Demodex folliculorum* mite structure and habitat

Figure 1.9 *Demodex folliculorum* mites extracted from facial region

Figure 1.10 *Demodex* mites involved in pityriasis folliculorum

Figure 1.11 Demodicosis on the skin surface of 46-year-old male patient.

Figure 1.12 Association of *Demodex* mites in bovine demodectic mange

Figure 1.13 The skin microbiome

Figure 1.14 Role of sebaceous glands in inflammatory skin conditions acne vulgaris and rosacea

Figure 1.15 Two *Bacillus oleronius* proteins that are sera reactive in rosacea patients

Figure 1.16 Proteolytic processing of cathelicidin in rosacea

Chapter 2

Figure 2.1 Isoelectric focusing Ettan IPGphor II used in 2D IEF SDS-PAGE

Figure 2.2 Western blot set-up with Mini Trans-Blot Cell by Bio-Rad

Figure 2.3 C18 spin column placed in 1.5ml micro-centrifuge tubes

Figure 2.4 ÄKTA-FPLC with attached column containing Q-Sepharose™ beads and *B. oleronius* protein sample

Figure 2.5 Example of ELISA plate with colour development following the addition of stop solution

Chapter 3

Figure 3.1 Growth of *Bacillus oleronius* in nutrient broth

Figure 3.2 Growth of *Bacillus oleronius* in 2XYT medium

Figure 3.3 Representative Western blot measuring the expression of *B. oleronius* 62 kDa protein grown from cultures under temperature stressed environments

Figure 3.4 Level of 62 kDa *B. oleronius* antigen expression under temperature stressed culture conditions.

Figure 3.5 Western blot measuring the production of stimulatory 62 kDa antigen produced at 72 hours in nutrient broth culture

Figure 3.6 Confocal images of control sample antibody specific for *B. oleronius*

Figure 3.7 Confocal images of *B. oleronius* cultured in nutrient broth at 30°C

Figure 3.8 Confocal images of *B. oleronius* cultured in nutrient broth at 37°C

Figure 3.9 Confocal images of *B. oleronius* cultured in 2XYT medium at 30°C

Figure 3.10 Confocal images of *B. oleronius* cultured in 2XYT medium at 37°C

Figure 3.11 2-Dimensional IEF SDS-PAGE gel image displaying spots identified from *Bacillus oleronius* proteome

Figure 3.12 Label free MS/MS principal component analysis and hierarchical clustering of the quantitative differences in the proteomic profile of *B. oleronius*

Figure 3.13 Volcano plot highlighting the twenty proteins most altered in abundance in *B. oleronius* when cultured at 37ºC versus 30ºC.

Figure 3.14 Biological Process Level 2 grouping of proteins found in *B. oleronius*

Figure 3.15 Molecular Function Level 2 grouping of proteins found in *B. oleronius*

Figure 3.16 Cellular Component Level 2 grouping of proteins found in *B. oleronius*

Chapter 4

Figure 4.1 Growth of *B. oleronius* in the presence of 10 mM H2O2

Figure 4.2 Representative 1-Dimensional SDS-PAGE and Western blot measuring the expression of *B. oleronius* 62 kDa protein found in secretome samples

Figure 4.3 Representative 1-Dimensional SDS-PAGE and Western blot measuring the expression of *B. oleronius* 62 kDa protein found in lysate samples

Figure 4.4 Densitometric analysis of stimulatory 62 kDa antigen expressed in aerobic or static incubation conditions

Figure 4.5 2-Dimensional IEF SDS-PAGE gel image displaying spots identified from the proteome of *Bacillus oleronius*

Figure 4.6 Label free MS/MS principal component analysis and hierarchical clustering of the quantitative differences in the proteomic profile of *B. oleronius*

Figure 4.7 Volcano plot highlighting the twenty proteins most altered in abundance in *B. oleronius* when cultured under oxidative stress

Figure 4.8 Biological Process Level 3 of proteins found in *B. oleronius*

Figure 4.9 Molecular Function Level 3 of proteins found in *B oleronius*

Figure 4.10 Cellular Components Level 3 of proteins found in *B. oleronius*

Figure 4.11 Biological Process Level 3 of altered proteins found in *B. oleronius*

Figure 4.12 Molecular Function Level 3 of altered proteins in *B. oleronius*

Figure 4.13 Cellular Component Level 3 of altered proteins in *B. oleronius*

Chapter 5

Figure 5.1 Chromatograph from ÄKTA-FPLC fractionation of *B. oleronius* protein preparation

Figure 5.2 Representative 1D SDS-PAGE of sample protein preparations collected from ÄKTA-FPLC fractions

Figure 5.3 Representative Western blot of sample protein preparations collected from ÄKTA-FPLC fractions

Figure 5.4 Representative Western Blot of *B. oleronius* 'pure' and crude protein
Figure 5.5 HEp-2 cells exposed to B. oleronius 62 kDa antigen
Figure 5.6 hTCEpi cells exposed to *B. oleronius* 62 kDa protein for 72 hours
Figure 5.7 hTCEpi cells exposed to *B. oleronius* 62 kDa protein for 144 hours
Figure 5.8 hTCEpi cells exposed to *B. oleronius* 62 kDa protein at 72 hours
Figure 5.9 Effect of pure *B. oleronius* antigen exposure on IL-1β gene expression in hTCEpi cells as measured by qRT-PCR
Figure 5.10 Effect of pure *B. oleronius* antigen exposure on IL-8 gene expression in hTCEpi cells as measured by qRT-PCR
Figure 5.11 Effect of pure *B. oleronius* antigen exposure on TNFα gene expression in hTCEpi cells as measured by qRT-PCR
Figure 5.12 Toxicity of mucin to HEp-2 cells
Figure 5.13 Toxicity of mucin to hTCEpi cells
Figure 5.14 Toxicity of BSA to HEp-2 cells
Figure 5.15 Toxicity of BSA to hTCEpi cells
Figure 5.16 Toxicity of anti-62 kDa antibody to HEp-2 cells
Figure 5.17 Toxicity of anti-62 kDa antibody to hTCEpi cells
Figure 5.18 HEp-2 cell proliferation in the presence of three potential blocking agents alone and in combination with *B. oleronius* 62 kDa antigen.
Figure 5.19 The effect of mucin as a blocking agent against *B. oleronius* 62 kDa antigen in HEp-2 cell proliferation at 72 hours.
Figure 5.20 The effect of mucin as a blocking agent against *B. oleronius* 62 kDa antigen in hTCEpi cell proliferation at 72 hours
Figure 5.21 The effect of potential blocking agent mucin and *B. oleronius* proteins on the healing of a scratch wound at 72 hours in HEp-2 cells
Figure 5.22 The effect of potential blocking agent mucin and *B. oleronius* proteins on the healing of a scratch wound at 24 hours in hTCEpi cells
Figure 5.23 The effect of *B. oleronius* protein exposure on cytokine expression during a wound healing response at 72 hours in HEp-2 cells

Figure 5.24 The effect of *B. oleronius* protein exposure on cytokine expression during a wound healing response at 72 hours in hTCEpi cells

Chapter 6

Figure 6.1 Growth of HEp-2 cells exposed to Oriel salt solution

Figure 6.2 Growth of HEp-2 cells exposed to NaCl solution

Figure 6.3 Growth of hTCEpi cells exposed to Oriel salt solution

Figure 6.4 Growth of hTCEpi cells exposed to NaCl solution

Figure 6.5 HEp-2 cells exposed to Oriel and NaCl for 72 hours

Figure 6.6 Label free MS/MS principal component analysis and hierarchical clustering of the quantitative differences in the proteomic profile of HEp-2 cells

Figure 6.7 Volcano plot highlighting the proteins altered in abundance in HEp-2 cells exposed to Oriel solution

Figure 6.8 The effect of Oriel salt solution on *B. oleronius* cell density

Figure 6.9 The effect of NaCl on *B. oleronius* cell density

Figure 6.10 The effect of Oriel salt solution on *E. coli* cell density

Figure 6.11 The effect of NaCl on *E. coli* cell density

Figure 6.12 The effect of Oriel salt solution on *S. aureus* cell density

Figure 6.13 The effect of NaCl on *S. aureus* cell density

Figure 6.14 *B. oleronius* zones of growth inhibition in response to Oriel

Figure 6.15 *B. oleronius* and *S. aureus* zones of inhibition measured in response to Oriel formulations

Figure 6.16 Erythema levels before and after one week of Oriel facial application

Figure 6.17 Melanin levels before and after one week of Oriel facial application

Figure 6.18 Sebum levels before and after one week of Oriel facial application

Figure 6.19 TEWL levels before and after one week of Oriel facial application

Figure 6.20 Moisture levels before and after one week of Oriel facial application

Figure 6.21 Effect of Oriel application on face of patient four after one week of treatment
Figure 6.22 Effect of Oriel application on face of patient fifteen after one week of treatment
Figure 6.23 Effect of Oriel application on face of patient nineteen after one week of treatment
Figure 6.24 Erythema levels before, during and after Oriel cream facial application
Figure 6.25 Average erythema levels before and after Oriel cream application
Figure 6.26 Average melanin levels before and after Oriel cream application
Figure 6.27 Average sebum levels before and after Oriel cream application
Figure 6.28 Average TEWL levels before and after Oriel cream application
Figure 6.29 Average moisture levels before and after Oriel cream application
Figure 6.30 Effect of Oriel application before and after treatment in patient E
Figure 6.31 Effect of Oriel application before and after treatment in patient G
Figure 6.32 Effect of Oriel application before and after treatment in patient H

List of Tables

Chapter 1

Table 1.1 Primary and secondary features of rosacea

Table 1.2 Differences in Demodex species which inhabit human skin

Chapter 2

Table 2.1 Constituents of 5X solubilisation buffer

Table 2.2 Constituents of separating gel for SDS-PAGE

Table 2.3 Constituents of stacking gel for SDS-PAGE

Table 2.4 Constituents of IEF buffer

Table 2.5 Constituents of Equilibration buffer

Table 2.6 Constituents of agarose sealing solution (1% w/v)

Table 2.7 Isoelectric focusing programme used for 2D IEF SDS-PAGE

Table 2.8 Colloidal Coomassie Fixing Solution

Table 2.9 Colloidal Coomassie Stain Solution

Table 2.10 Constituents of transfer buffer

Table 2.11 Constituents of DAB

Table 2.12 List of antibody dilutions

Table 2.13 Sample resuspension buffer (pH8.0)

Table 2.14 Ammonium bicarbonate (50 mM)

Table 2.15 Dithiothrietol (0.5 M)

Table 2.16 Idoacetamide (0.55 M)

Table 2.17 ProteaseMAX solution and Trypsin solution

Table 2.18 Q-exactive MS clean-up buffers

Table 2.19 ELISA buffers for detecting expression levels of cytokines

Chapter 3

Table 3.1 Protein identities of spots increased in *B. oleronius* proteomic profile at 37°C

Table 3.2 Protein identities of spots decreased in *B. oleronius* proteomic profile at 37°C

Table 3.3 Proteins identified at higher abundance in *B. oleronius* at 37ºC

Table 3.4 Proteins identified at lower abundance in B. oleronius at 37ºC

Chapter 4

Table 4.1 Identities of spots increased in abundance in *B. oleronius* proteomic profile

Table 4.2 Identities of spots decreased in abundance in *B. oleronius* proteomic profile

Table 4.3 Proteins identified at higher levels of abundance in *B. oleronius* treated with 10 mM H_2O_2 for 4 hours

Table 4.4 Proteins identified at lower levels of abundance in *B. oleronius* treated with 10 mM H_2O_2 for 4 hours

Chapter 6

Table 6.1 Proteins identified at higher and lower abundances in HEp-2 cells exposed to Oriel salt solution

Table 6.2 The mean results from pilot study one after one week of treatment with Oriel cream or gel application to the face (n=20)

Abbreviations

2XYT	2X yeast tryptone
AB	Antibody
ACN	Acetonitrile
AMP	Antimicrobial peptide
ANOVA	Analysis of variance
ATP	Adenosine triphosphate
BLAST-P	Protein-protein Basic Local Alignment Search Tool
BP	Biological process
BSA	Bovine serum albumin
°C	Degrees Celsius
CC	Cellular component
CD4+	Cluster of differentiation 4 cells
cDNA	Complementary deoxyribonucleic acid
cm	Centimetre
DAMPs	Danger associated molecular patterns
DAPI	4',6-Diamidino-2-Phenylindole, Dilactate
DMSO	Dimethyl sulfoxide
DNA	Deoxyribonucleic acid
DTT	Dithiothreitol
EDTA	Ethylene diamine tetra acetic acid
EF	Elongation factor
ELISA	Enzyme-linked immunosorbent assay
ETR	Erythematotelangiectatic rosacea
F-actin	Filamentous actin
FAD	Flavin adenine dinucleotide
FDA	Food and drug administration
FDR	False discovery rate
FPLC	Fast protein liquid chromatography

g	grams
g	g-force
G-actin	Globular-actin
GAPDH	Glyceraldehyde-3-phosphate dehydrogenase
GO	Gene ontology
h	Hour
HEp-2	Human epithelial cells
HIV	Human immunodeficiency virus
HPI	*Helicobactor pylori* infection
HSP	Heat shock protein
hTCEpi	Human telomerase-immortalized corneal epithelial cells
IAA	Iodoacetamide
IEF	Isoelectric focusing
Irr	Iron response regulator
IL	Interleukin
KAS	Beta-ketoacyl synthase
KBM	Keratinocyte basal medium
kDa	Kilodaltons
KEGG	Kyoto encyclopaedia of genes and genomics
KGDH	Ketoglutarate dehydrogenase
KLK	Kellikrein
LPS	Lipopolysaccharide
LC-MS/MS	Liquid chromatography mass spectrometry
LF-MS/MS	Label free mass spectrometry
LFQ	Label free quantification
M	Molar
mAB	Monoclonal antibody
MAM	Membrane associated mucin
MEM	Minimum Essential Medium
MF	Molecular Function

MGD	Meibomian gland dysfunction
mM	Millimolar
MMP	Matrix metalloproteases
mg	Milligram
mRNA	Messenger ribonucleic acid
MS	Mass spectrometry
µg	Microgram
µl	microliter
NADPH	Nicotinamide adenine dinucleotide phosphate
NCIMB	National Collection of Industrial Food and Marine Bacteria
NF-*k*B	Nuclear factor kappa B
NO	Nitric oxide
NRS	National rosacea society
PAMPs	Pathogen associated molecular patterns
PBS	Phosphate buffered saline
PDH	Pyruvate
PEP	Posterrior error probability
PPR	Papulopustular rosacea
PRR	Pathogen recognition receptor
p value	Probability
OD	Optical density
qRT-PCR	Quantitative real time polymerase chain reaction
ROS	Reactive oxygen species
ROSCO	ROSacea Consensus
SCTE	Stratum corneum tryptic enzyme
SDS-PAGE	Sodium dodecyl sulfate – polyacrylamide gel electrophoresis
SOD	Superoxide dismutase
SSSB	Standardised skin surface biopsy
TEMED	N,N,N',N'-Tetramethylyethlenedimine
TFA	Trifluoracetic acid

TNF	Tumour necrosis factor
TLR	Toll-like receptor
tRNA	Transfer ribonucleic acid
TRP	Transient receptor potential
TTO	Tea tree oil
UV	Ultraviolet
v/v	volume per volume
w/v	weight per volume
YEPD	Yeast extract-peptone-D-glucose

Abstract

Rosacea is a chronic inflammatory condition predominantly affecting the face on the cheeks, forehead, nose, chin and in some cases eyes. The primary diagnostic feature of rosacea is persistent erythema on the central region of the face. Distinct secondary features help to diagnose one of the four subtypes of rosacea and commonly include telangiectasia, flushing, papule and pustules, thickening of the skin and oedema. Rosacea is a debilitating condition that can impact on a patients emotional and psychological state.

The aetiology of this dermatological condition is unknown and multiple factors contribute to the onset of rosacea and exacerbate symptoms. Exogenous factors such as radiation or diet, and endogenous factors such as sebum alteration or stress, can change skin homeostasis. These factors can influence resident microbiota, which may alter skin homeostasis and induce the production of virulence factors. The increased density of *Demodex* mites in rosacea patients has been demonstrated previously. *Demodex* mites cause micro-abrasions to the skin surface and weaken the skin barrier function. *Bacillus oleronius* isolated from *Demodex* is a bacterium associated with rosacea pathogenesis and patient serum previously exposed to antigen have displayed immune reactivity.

The work in this thesis investigated the effect of different stress conditions on *B. oleronius* antigen production. The proteome of *B. oleronius* was assessed in response to temperature stress and oxidative stress to evaluate differential abundance in protein production. *B. oleronius* proteins may contribute to the over-activation of the innate immune response, leading to increased gene expression of cytokines, increased tissue damage and onset of chronic inflammation.

The treatment and management of rosacea is targeted towards symptomatic relief, predominantly with the aid of antibiotics. Some treatments demonstrate antibacterial and anti-inflammatory effects, both of which help to treat patient symptoms. Three blocking agents were evaluated in this research to determine the potential capturing of *B. oleronius* antigens. Mucin is naturally present in tear fluid and protects the epithelial barrier. This antimicrobial displayed potential as an adhesive decoy against antigen. A novel saline therapeutic was also investigated to treat rosacea patients and alleviate symptoms. The novel salt based formulation demonstrated effective anti-inflammatory properties in two pilot studies. There is no cure for rosacea, however the work presented here demonstrated potential therapeutics for rosacea patient treatment against *B. oleronius* antigens.

Chapter One

Introduction

1.1 Rosacea

Rosacea is a chronic inflammatory dermatological condition localized in the butterfly region of the face and the eyes (O'Reilly *et al*., 2012b). Rosacea currently affects 16 million Americans and up to 3% of the Irish population in an ongoing study with over 1000 individuals (Two *et al*., 2015a; McAleer & Powell, 2007). Rosacea typically affects patients between the ages of 30 and 50 years and is more prevalent in fair-skinned individuals, particularly with the Fitzpatrick skin type I-III (Jarmuda *et al*., 2012; O'Reilly *et al*., 2012c; McAleer *et al*., 2010). Men typically develop more severe symptoms of the condition, however women are three times more likely to suffer from rosacea (Gupta & Chaudhry, 2005). This common but incurable disorder is often referred to as the "curse of the Celts" and is characterised by systemic inflammation (Bevins & Liu, 2007). The pathophysiology of rosacea is an assembly of multiple factors with no defined aetiology. One such aspect is the dysregulation of the innate and adaptive immune response in rosacea patients, combined with neurovascular changes and inflammation, while the other aspect features the role of microorganisms in the skin microbiome (Weinstock & Steinhoff, 2013; Holmes, 2013).

Rosacea has been classified into four subtypes with common symptoms including erythema and telangiectasia (dermal) or keratitis and blepharitis (ocular) (McMahon *et al*., 2014; O'Reilly *et al*., 2012c). A variety of trigger factors have been associated with exacerbating symptoms, from external stimuli (e.g. UV radiation, exercise), internal stimuli (e.g. stress, genetic) and alterations in the levels of innate immunity (e.g. reactive oxygen species, inflammatory cascade) (Holmes & Steinhoff, 2017; O'Reilly *et al*., 2012a). Many treatments have proved efficient in the clearance of symptoms such as laser therapy, topical metronidazole, ivermectin and oral tetracycline (O'Reilly *et al*., 2012a, 2012c). Rosacea is a vasculature disorder consistently in a cyclic phase between relapse and remission following treatment commencement. Understanding the aetiology and pathobiology of this complex cutaneous condition has led to discoveries such as the role of associated microorganisms and immune pathways stimulated by various trigger factors. These insights into rosacea have contributed to improved management and therapies, and leave an optimistic future ahead.

1.2 Diagnostic features

The multiple triggers, undefined aetiology and clinical manifestations of rosacea lead to an array of common symptoms, each of which differ phenotypically per patient. This broad range has led to the general characterisation and classification of different rosacea subtypes and variants. This has been supported by the National Rosacea Society (NRS), an active community created to provide rosacea patients and the public with an updated forum regarding ongoing research and information about rosacea (Crawford *et al*., 2004). The NRS Expert Committee established a standard classification system to describe the primary and secondary features of rosacea, as well as the pre-rosacea phase, which is recognised when patients have rosacea but symptoms are not clinically present (Yamasaki & Gallo, 2009; Del Rosso, 2004).

A recent update in the diagnosis procedure has been formulated by the ROSacea COnsensus (ROSCO) panel which incorporates dermatologists and ophthalmologists from Europe, North and South America, Africa and Asia (Tan *et al*., 2017). ROSCO have built on the current diagnosis policy and narrowed the classification system. The primary diagnostic features of rosacea must now include persistent erythema across the central region of the face or phymatous changes only (Table 1.1). Previously, the NRS included papules, pustules and telangiectasia as primary components which have been suggested as non-diagnostic features of the cutaneous condition (Tan *et al*., 2017). The secondary features have further been divided into major and minor categories but can exist independently in some cases; flushing transient erythema, papule and pustule development, non-transient erythema, telangiectasia and ocular symptoms have been classified as major secondary features while oedema, stinging, burning and dry sensations have been classified as minor (Tan *et al*., 2017; Yamasaki & Gallo, 2009; Wilkin *et al*., 2004).

The NRS Expert Committee originally developed a grading system (Figure 1.1) to determine the severity of rosacea subtypes, including four grades ranging from absent to severe (Korting & Schöllmann, 2009; Wilkin *et al*., 2004). ROSCO have altered this system to outline a more detailed grade of severity to be based on an individual's phenotype rather than one set subtype (Tan *et al*., 2017). This grading system comprises of 5 scales; clear/none, almost clear/minimal, mild, moderate and severe.

Table 1.1 Primary and secondary features of rosacea

Primary and secondary features of rosacea outlined by the ROSCO panel. Primary features are classified into two diagnostic criteria and secondary features are categorised into major and minor, both of which are not considered diagnostic. (Tan *et al.,* 2017)

Primary Features (Diagnostic)	**Secondary Features (Non-diagnostic)**	
	Major	**Minor**
Phymatous changes	Flushing/transient erythema	Burning sensation
	Non-transient erythema	Oedema
Persistent central facial erythema	Inflammatory papules/pustules	Stinging sensation
	Telangiectasia	Dry sensation

Figure 1.1 Grading system of rosacea applied to the papulopustular subtype. Papulopustular rosacea includes persistent central facial erythema with the development of papules and/or pustules. The grading system to determine the severity of the condition includes the three latter scales which are **(A)** mild, **(B)** moderate and **(C)** severe. (Wilkin *et al.,* 2004)

1.3 Rosacea Subtypes

There are four subtypes of rosacea; erythematotelangiectatic (ETR), commonly referred to as subtype one, papulopustular (PPR), phymatous and ocular (O'Reilly *et al*., 2012a). These four subtypes (Figure 1.2) have been recognised since 2002 under the standard classification system established by the NRS Expert Committee (Yamasaki & Gallo, 2009). Each of the subtypes has recognised characteristics and is treated differently, however it is possible to suffer with two or more subtypes simultaneously (Two *et al*., 2015a; Forton *et al*., 2005). The classification and grading systems are important for the diagnosis of rosacea, along with the subtype designation as there are no serological or diagnostic assays available to confirm the skin disorder. The treatment of this relapsing condition is varied between subtypes, however the psychological impact on the patient must be considered as this cutaneous disorder can impact social and occupational states and could result in limiting patient lifestyle (Tan *et al*., 2017; Gupta & Chaudhry, 2005; Wilkin *et al*., 2004).

1.3.1 Subtype I: Erythematotelangiectatic Rosacea (ETR)

The most common form of rosacea is ETR and is recognisable by erythema and oedema of the facial region (Figure 1.3), telangiectasia and stinging of the skin (Jarmuda *et al*., 2014). Telangiectasia produces a red/purple colouring in a network of dilated capillaries while the flushed appearance throughout the face is the result of oedema and erythema (O'Reilly *et al*., 2012c). This subtype is most associated with the primary diagnostic feature of rosacea, persistent centrofacial erythema that persists periodically and intensifies, usually lasting up to 10 minutes (Tan *et al*., 2017; Barco & Alomar, 2008). ETR is commonly referred to as the" butterfly rash" as symptoms typically give a reddish/purple appearance, particularly on the malar region (Barco & Alomar, 2008; Powell, 2005).

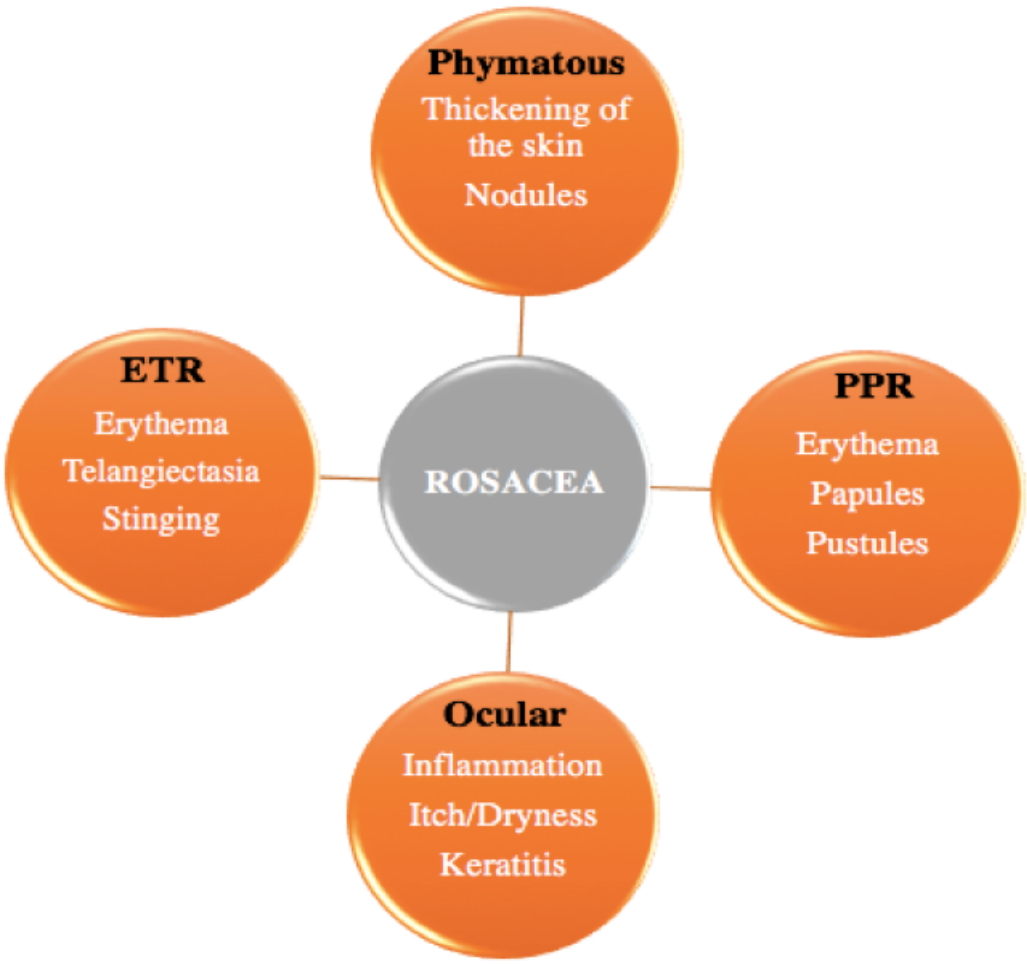

Figure 1.2 Subtypes of rosacea with independently defined symptoms.
The four subtypes of rosacea, each with the common associated characteristics. Many of the symptoms are interconnected and the rosacea condition remains central to all as it is possible to suffer with two or more subtypes simultaneously. This can contribute to the poor understanding of rosacea pathogenesis given the overlap of subtypes. (Author's image)

1.3.2 Subtype II: Papulopustular Rosacea (PPR)

Subtype two is defined by persistent papules and pustules on the skin surface, as seen previously in Figure 1.1, and is accompanied by erythema that generally presents itself symmetrically on the central region of the face (Jarmuda *et al*., 2012; Korting & Schöllmann, 2009). Episodes of flushing are less frequent in PPR in comparison to subtype one, however burning sensations and inflammatory lesions are more prominent (Barco & Alomar, 2008; Powell, 2005). PPR shares many symptoms with acne vulgaris however no link has been associated with rosacea and *Propionibacterium acnes*, the pathogen associated with acne (Jahns *et al*., 2012a). Both conditions are inflammatory skin disorders and can have papules, pustules and nodules on the skin surface (Jahns *et al*., 2012b; Zhao *et al*., 2012). PPR does not have symptoms such as comodones, microcomedomes or cysts and although similar treatments are used for rosacea and acne, the pathology, onset and management of each condition is distinct and treated separately (Zhao *et al*., 2012; Powell, 2005).

1.3.3 Subtype III: Phymatous Rosacea

The third subtype of rosacea is the disfiguring phymatous rosacea (Figure 1.4). Thickening of the nose is a predominant feature of this subtype along with nodule in irregular distribution, shape and size (Tan & Berg, 2013). Localized enlargement of the skin and nodules can result around in the nose (i.e. rhinophyma) (Korting & Schöllmann, 2009; Barco & Alomar, 2008). Phymatous rosacea is more common in men and an increased number of fibroblast cells have been associated with this type of rosacea (Two *et al*., 2015a; Steinhoff *et al*., 2013). This can result in skin fibrosis and change in sebaceous regions, most frequently observed in rhinophyma, referred to as “whiskey nose” but can also appear in areas of the ears, chin, eyelids and forehead (Powell, 2005; Crawford *et al*., 2004; Wilkin *et al*., 2004).

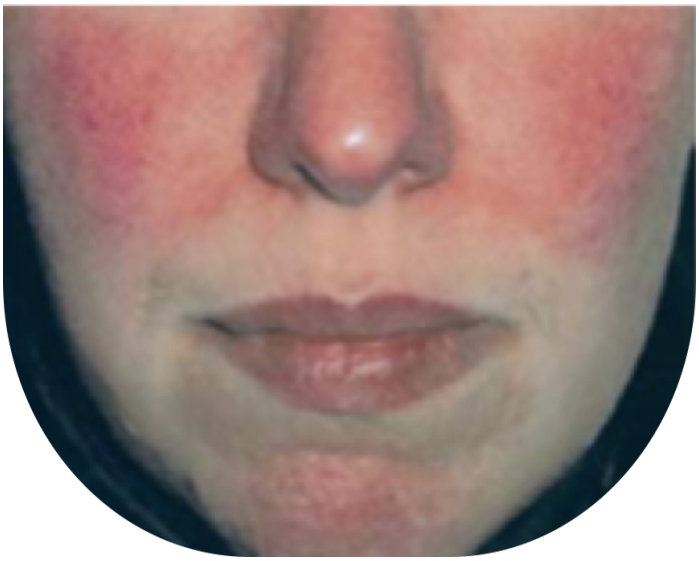

Figure 1.3 Moderate grading of erythematotelangiectatic rosacea (ETR) Subtype one of rosacea, ETR, characteristically consists transient flushing and persistent erythema across the central region of the face. Moderate grading comprises telangiectasia as a common secondary feature. (Wilkin *et al.,* 2004).

Figure 1.4 Phymatous rosacea featuring thickening of the skin around the nose. Phymatous rosacea is the third subtype and commonly features rhinophyma, thickening of the skin around the nose. Moderate scaling as seen here includes irregular facial nodules and possible marking or scarring of the skin. (Wilkin *et al.,* 2004).

1.3.4 Ocular Rosacea

Ocular rosacea is the fourth subtype and affects the eyes, eyelids and the corneal surface. It is possible to suffer from more than one subtype of rosacea at a time with almost 50% of rosacea patients manifesting ocular symptoms (O'Reilly *et al*., 2012b). This subtype typically results in marginal telangiectasia giving the eyes a bloodshot appearance. Patients manifest symptoms including itching, blurred vision, dry eyes or foreign body sensation (Tan & Berg, 2013). In severe cases of ocular rosacea corneal ulcers and keratitis may develop which can lead to blindness (McMahon *et al*., 2014). Ocular rosacea is often detected by meibomian gland dysfunction, but other signs and symptoms (Figure 1.5) include conjunctiva hyperaemia, corneal opacity, papillary hypertrophy or blepharitis (Brown *et al*., 2014; O'Reilly *et al*., 2012b). Naturally this is uncomfortable and irritating for patients. *Demodex* mites are natural inhabitants of the facial pilosebaceous unit and have been strongly associated with rosacea (Lacey *et al*., 2009). *D. folliculorum* is located in the lash follicle and *D. brevis* resides in the lash sebaceous and meibomian glands (Geerling *et al*., 2011; Gao *et al*., 2005). A correlation between *Demodex* proliferation and ocular rosacea has been well established (Li *et al*., 2010). *Demodex* mites residing in the eyelashes can induce many forms of local inflammation, thereby stimulating the immune response (Li *et al*., 2010). Cylindrical dandruff is indicative of *Demodex* presence in the ocular region and a common symptom is eyelid margin inflammation, characteristic of blepharitis (Szkaradkiewicz *et al*., 2012; Gao *et al*., 2005).

1.3.5 Rosacea Variants

Granulomatous rosacea is a recognised variant of rosacea that can be diagnosed without the presence of primary rosacea features (Wilkin *et al*., 2002, 2004). Granulomatous rosacea is more common in men and occurs across the perioral and periocular region of the face (Crawford *et al*., 2004). This variant consists of yellow/brown papules or nodules (Figure 1.6) that are uniform in size per patient and in severe cases may develop into lesions and scarring (Barco & Alomar, 2008; Wilkin *et al*., 2002). Less flushing and inflammation is observed and a reported 15% of patients develop symptoms in areas other than the face (Barco & Alomar, 2008; Crawford *et al*., 2004).

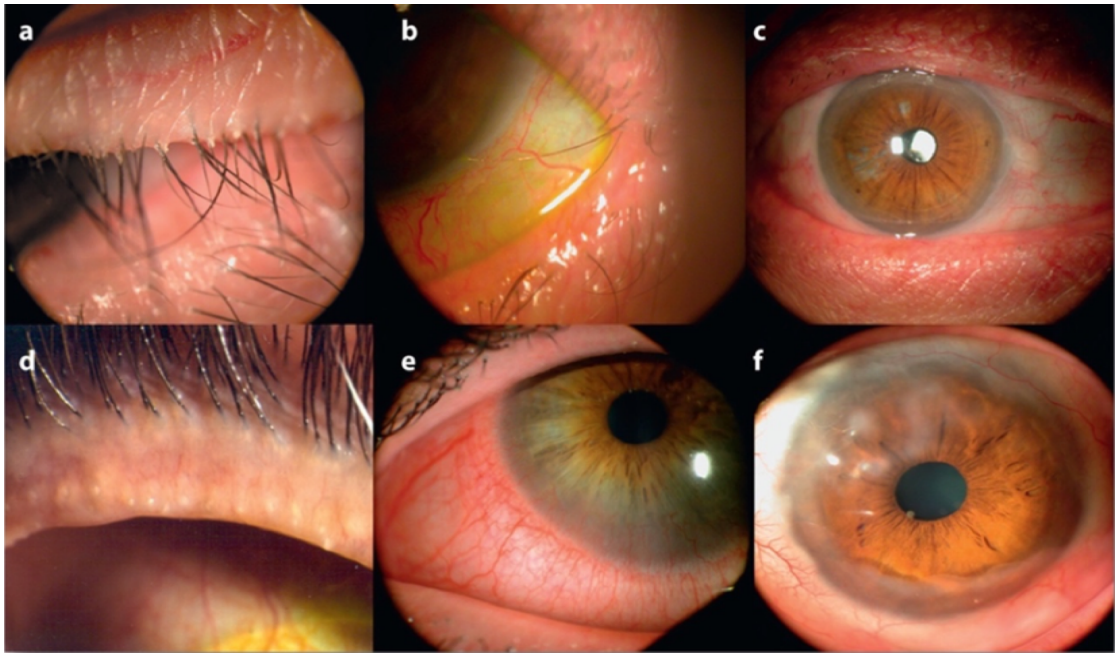

Figure 1.5 Ocular rosacea symptoms associated with *Demodex* mite infestation. Clinical features of *Demodex* infestation in the eye, all of which are symptoms of ocular rosacea. **(a)** Cylindrical dandruff; altered layout and direction of the eyelashes in toward the eye. **(b)** Trichiasis; eyelashes touch the corneal surface. **(c)** Madarosis; result of lashes falling off. **(d)** Meibomian gland dysfunction; the most common sign of ocular rosacea. **(e)** Bloodshot appearance of conjunctivitis. **(f)** Corneal lesions; result of severe ocular rosacea. (Lacey *et al.,* 2009)

Figure 1.6 Granulomatous rosacea One variant from the four classic rosacea subtypes is granulomatous rosacea. Symptoms comprise of hard erythemic papules or nodules which may develop into clusters of lesions on the face. They tend to be yellow/brown colour and are monomorphic in size to individual patients. Less inflammation is common but intensified oedema accompanies nodules. (Crawford *et al.,* 2004)

1.4 Factors affecting rosacea onset

The aetiology of this chronic dermatological disease is not clearly defined, but multiple factors may contribute to the onset, persistence and severity (Figure 1.7). Genetic factors, microbial presence on the skin, and immunological substances such as reactive oxygen species (ROS) may contribute to the appearance of symptoms (McMahon *et al*., 2014; O'Reilly *et al*., 2012a). A genetic component of rosacea has been postulated, with the identification of two single-nucleotide polymorphisms (*HLA-DRA* and *BTNL2*) (Gallo *et al*., 2017; Chang *et al*., 2015). A rosacea patient has a fourfold increased probability of a family member also developing the condition (Chang *et al*., 2015).

Many microbes live commensally on the skin and the immune system can tolerate these coexisting microbes within natural homeostasis, but as seen in many diseases, different conditions trigger the innate immune response. Normal microbiota and the microenvironment of the skin may become altered, influencing the onset and persistence of rosacea symptoms (Margalit *et al*., 2016). Environmental conditions such as diet, medication, physical exercise and exposure to varying climates can affect normal skin homeostasis (Holmes, 2013; O'Reilly *et al*., 2012a). These in turn can influence endogenous conditions including lipid composition of sebum, sweat and stress (Holmes & Steinhoff, 2017; Holmes, 2013). Papulopustular patients for example, have higher pH levels on their face than healthy individuals, as well as altered fatty acid composition with increased levels of myristic acid and linoleic acid (Ní Raghallaigh *et al*., 2012; Lacey *et al*., 2011). These multiple factors trigger dysbiosis, disrupt resident microbiota and activate immune surveillance, leading to the onset of rosacea symptoms (Tan *et al*., 2017; Margalit *et al*., 2016; Holmes, 2013).

Once the host becomes immuno-deficient, the susceptibility to certain conditions and diseases is increased. *Demodex* mites feed on human sebum and also epithelial cells (Szkaradkiewicz *et al*., 2012). This may cause skin abrasions and if the immune system is weakened by reduced cutaneous defence, this could potentially facilitate further proliferation of *Demodex* mites in the microbiota (Lacey *et al*., 2011). For example, *Demodex* mites have an exoskeleton composed of chitin, a polysaccharide that is an established trigger for the Toll-like receptor 2 (TLR2)

pathway of keratinocytes (Margalit *et al*., 2016; Steinhoff *et al*., 2013). TLR2 is a key component of the innate immune response which involves the activation and expression of pro-inflammatory cytokines (Holmes & Steinhoff, 2017).

1.5 *Demodex* mites

The *Demodex* mite was first reported by Gustav Simon, a German dermatologist examining sebaceous follicle samples from an individual with lesions (Lacey *et al*., 2011). *Demodex folliculorum* was first identified by Simon in 1842, but it was not until 1963 that *Demodex brevis* was identified as a separate species (Thoemmes *et al*., 2014). It was then that these two human mite species were classified as class Arachnida, subclass Acarin (Thoemmes *et al*., 2014; Lacey *et al*., 2011). The terms "demo" meaning lard and "dex" meaning boring worm were combined from the Greek language in 1843 by Richard Owen to create the genus "*Demodex"* (Lacey *et al*., 2011). *Demodex* mites are the most common human ectoparasite, found across a broad geographical range and on the skin of all individuals, both living and dead (Li *et al*., 2010). *Demodex* mites have been known to be associated with dermal and ocular conditions in humans and other mammals. There are over 140 species or subspecies of *Demodex* mites that have been recognized in eleven mammalian orders (Zhao *et al*., 2013). Some mammals have different *Demodex* species and more than one species can co-exist. For example, three structurally different canine species have been classified; *D. canis, D. cornei* and *D. injai* (Zhao *et al*., 2013; Thoemmes *et al*., 2014). These mites play a role in demodectic mange in dogs and the same dermatological condition can be seen in cattle caused by the two known bovine species, *D. bovis* and *D. ghanensis* (Abu Samra & Shuaib, 2014). Many others *Demodex* mites inhabit mammals including *D. caprae* in goats, *D. musculi* from mice, and different *Demodex* species in cats and white-tailed deer (Thoemmes *et al*., 2014).

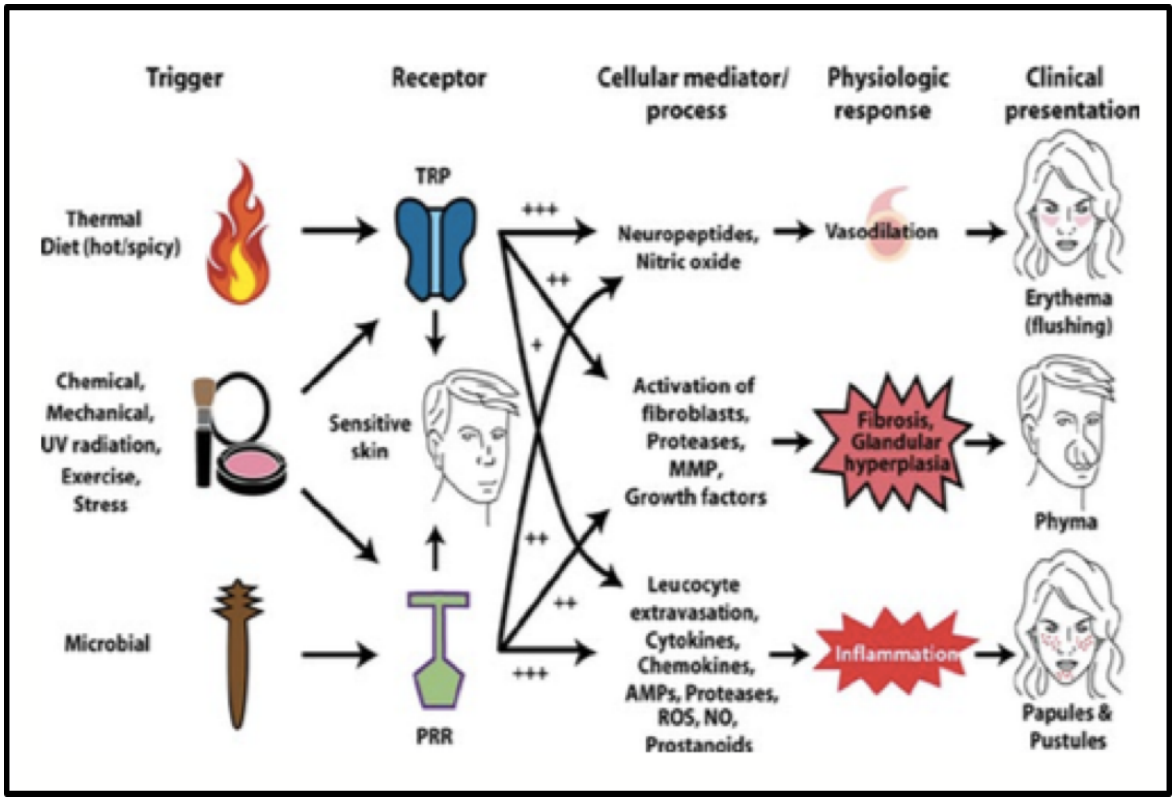

Figure 1.7 Characteristic trigger factors of rosacea may influence patient phenotype and exacerbate symptoms.

Multiple stimuli from physical, biological and endogenous factors activate different receptors in the skin innate immunity. In rosacea, this can be problematic as the skin is sensitive and individual patients are more susceptible to specific triggers. This can stimulate receptors such as TRP (transient receptor potential) or PRR (pathogen recognition receptor) and lead to cellular mediator activation including AMP's (antimicrobial peptides), ROS (reactive oxygen species), NO (nitric oxide) or MMP (matrix metalloproteases), all of which contribute towards increased inflammation and determine the onset and progression of classic rosacea symptoms. (Holmes and Steinhoff, 2016)

Demodex mites have a head and neck region called the prosoma with four pairs of articulated legs attached at one end (Lacey *et al*., 2011). The gnathosoma (Figure 1.8) contains elaborate mouth and feeding parts located at the anterior end of the mite and is more developed in *D. folliculorum* than *D. brevis* (Jing *et al*., 2005). The opisthosoma contains the gastrointestinal tract and definitive genital organs (Lacey *et al*., 2011). The typical lifespan of a *Demodex* mite is fourteen to eighteen days, from egg to larval form. The adult life stage is approximately five days for males but up to ten days for female adults to facilitate oviposition (Liu *et al*., 2010). *Demodex* mites are mobile in dark environments and more static in bright light, hence their migration from the hair follicles across the skin surface at night to locate a suitable mating partner (Lacey *et al*., 2011). This classifies them as negatively phototaxic and the mites move at a maximum speed of sixteen mm/h across the facial surface (Lacey *et al*., 2011). Copulation occurs near the surface of the pilosebaceous unit and is followed by the gravid adult female depositing the eggs back into the sebaceous gland. The eggs develop into larvae after sixty hours or so and emerge from the gland as protonymphs where they mature into the deutonymph stage of life (Jarmuda *et al*., 2012). The deutonymph is the fourth stage of the *Demodex* life cycle and is located on the cell surface but shortly enters the fifth and final adult stage upon re-entering the sebaceous canal (Lacey *et al*., 2009).

1.5.1 Human mite ecology

Humans have many different mite species such as *Sarcoptes scabiei* and the two common dust mite species *Dermatophagoides pteronyssinus* and *Dermatophagoides farina* (Chen & Plewig, 2014). However, two *Demodex* species are unique to humans and both reside simultaneously on the human body with the majority located in the malar region (Thoemmes *et al*., 2014). *D. folliculorum* is the more common mite (Figure 1.9), possibly due to it inhabiting the upper end of the hair follicle making it easier to spread by direct contact (Bikowski & Del Rosso, 2009). *D. folliculorum* resides superficially within the pilosebaceous unit and is typically found in clusters of ten to fifteen mites per follicle (Elston & Elston, 2014). This saprophytic mite colonizes the facial region commensally with *D. brevis* residing deep within the sebaceous gland of the skin and the meibomian gland of the eye (Jarmuda *et al*., 2014; Holmes, 2013). Both human *Demodex* mites coexist

commensally and share common characteristics but also have structural differences and habitual preferences (Table 1.2). *D. brevis* is the smaller of mites found in humans and is more solitarily confined deep within the glands and ducts but these are located in more widespread areas of the face such as the ear canals (Elston & Elston, 2014).

Table 1.2 Differences in *Demodex* species which inhabit human skin

Comparisons between *D. folliculorum* and *D. brevis*, the *Demodex* mites inhabiting the human skin. (Data collected from Jarmuda *et al.,* 2012)

Mite	Length	Shape	Habitat	Food source
Demodex folliculorum	0.3-0.4 mm	Elongated	Superficially on hair follicle Clusters of mites	Epidermal cells Sebum components
Demodex brevis	0.2-0.3 mm	Spindle Shorter legs	Sebaceous glands Meibomian glands	Epidermal cells Sebum components

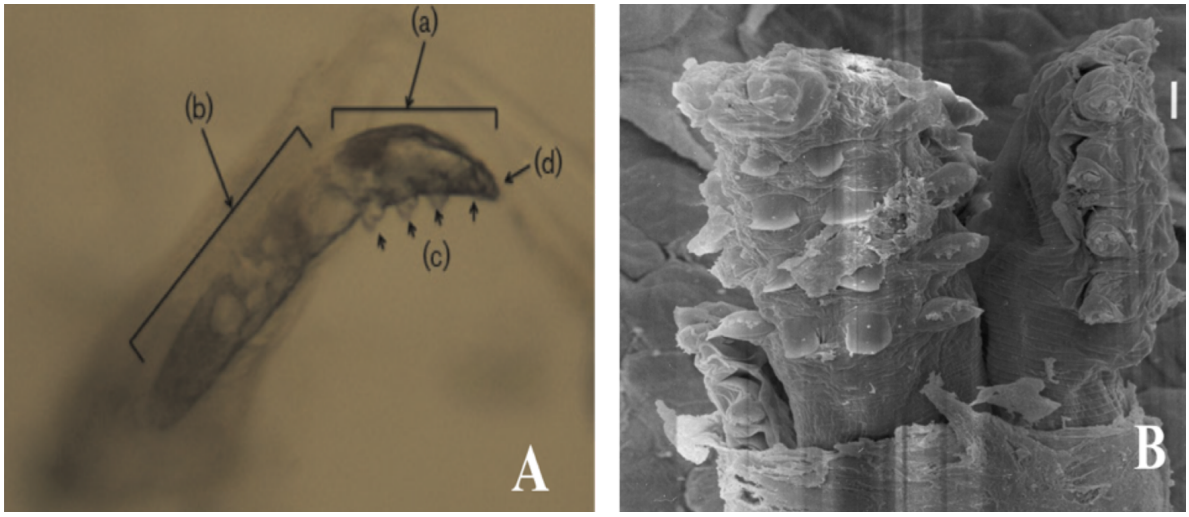

Figure 1.8 *Demodex folliculorum* mite structure and habitat.

(A) *Demodex folliculorum* mite embedded in a hair follicle with labelled body parts of the mite including (a) prosoma, (b) opisthosoma, (c) four pairs of short legs attached to the head-neck and (d) gnathosoma. Length of mite is 0.4 mm. **(B)** Detailed image of *D. folliculorum* mites side by side in the follicle under electron scanning microscopy. (Jarmuda *et al.,* 2014; Lacey *et al.,* 2009)

Figure 1.9 *Demodex folliculorum* mites extracted from facial region

Two *Demodex folliculorum* mites extracted from the malar region of a healthy individual. *D. folliculorum* resides superficially in the hair follicle and feeds on sebum and skin debris. Image taken at x100 magnification. (Image author's own)

1.5.2 *Demodex* source and transmission

Demodex mites are abundant on the skin surface across all human races and are found on the face in areas of sebum production such as the nose, chin, forehead, cheeks and also the neck and ears (Szkaradkiewicz *et al*., 2012; Bikowski & Del Rosso, 2009). *Demodex* feed on epithelial and glandular cells as well as sebum typically secreted by active pilosebaceous units (Yamashita *et al*., 2011; Bonnar *et al*., 1993). *Demodex* mites reside in the pilosebaceous units of the skin with their heads directed at the bottom of the hair follicle where the most sebum can be found (Bikowski & Del Rosso, 2009). No mites have been found on the skin of new-borns, as they do not produce sebum, hence no food source is available for the mites (Lacey *et al*., 2011). It is believed that *Demodex* mites are first transmitted during nursing, as they have been isolated from the nipple (Elston & Elston, 2014). In one particular case study, *Demodex* presence was found in nipple tissue in seventy-seven percent of mastectomy samples (Thoemmes *et al*., 2014). As children mature the sebaceous unit develops creating a suitable habitat for *Demodex* colonization, which further improves as young adults produce sebum during puberty and change its composition (Lacey *et al*., 2016). Young adults have *Demodex* mites, which most likely spread by direct contact (Lacey *et al*., 2016; Bikowski & Del Rosso, 2009). *Demodex* densities increase with age with almost ninety-five percent infestation found in individuals over the age of seventy-one (Elston & Elston, 2014).

As a result of *Demodex* feeding on sebum and epithelial cells, particularly around the nose, as it is rich in sebum, this may cause micro-abrasions to the skin surface (Figure 1.10) (Szkaradkiewicz *et al*., 2012). This can commonly lead to epithelial hyperplasia on the face or even the eyelid margin of rosacea patients and blepharitis patients (Szkaradkiewicz *et al*., 2012). It has been suggested that the composition of the sebum rather than the volume is preferred by the mite and can determine *Demodex* densities (Jarmuda *et al*., 2012; Ní Raghallaigh *et al*., 2012). Typically five mites/cm^2 is the average for a normal or healthy individual (Bikowski & Del Rosso, 2009). Demodicosis is the infestation of *Demodex* mites on the face, whereby a minimum of five mites/cm^2 exist (Figure 1.11) and induce symptoms such as redness of the skin (erythema), telangiectasia, itching, heat and scaling (Two *et al*., 2015a; Holmes, 2013). These are all relevant symptoms of rosacea subtypes as well as blepharitis and perioral dermatitis (Holmes, 2013).

In 1971, the skin surface biopsy was developed in order to detect *D. folliculorum* presence on the skin, however it was not until 1993 that the concept of assessing the *Demodex* density was first introduced (Marks & Dawber, 1971; Forton & Seys, 1993). This quickly led to the development and utilisation of the standardised skin surface biopsy (SSSB) method on the superficial part of the skin (the horny layer), immediately followed by a second deeper skin surface biopsy as outlined by Forton & De Maertelaer (2017). By combining the counts from these two consecutive samples, an improved *Demodex* density could be found, proving this method as a useful diagnostic tool. The SSSB method also has many advantages to both dermatologists and patients; it's a quick and reproducible procedure, tolerated well by patients as it's minimally invasive and is also a simple and cheap diagnostic tool. To further improve the sensitivity, which was originally only 55%, two consecutive SSSBs were introduced along with cleaning the skin and biopsy slide with ether beforehand, reaching a sensitivity of 89.3% (Forton & De Maertelaer, 2017).

Demodex mites can be obtained from the sebaceous glands of individuals by various methods such as scraping the skin gently, cellophane tape, plucking in the case of eyelashes and eyebrows and also a biopsy (Thoemmes *et al*., 2014). A standardized surface biopsy is now in place to ensure mites are obtained with a consistent and efficient method (Lacey *et al*., 2009). Thoemmes *et al.* carried out phylogenetic analysis on the 16S rRNA gene and the 18S rRNA gene to determine possible genetic diversities and the lineage history of the *Demodex* mite evolution (Thoemmes *et al*., 2014). A genetic variance between these two species has been highlighted as mites located at the eyelashes have a different CO1 mitochondrial gene to mites inhabiting the skin. The habitual preferences between *D. folliculorum* and *D. brevis* is so specific and different that it is believed the two lineages have independent evolutionary transmission to humans and it is also thought they do not share a common ancestor (Thoemmes *et al*., 2014).

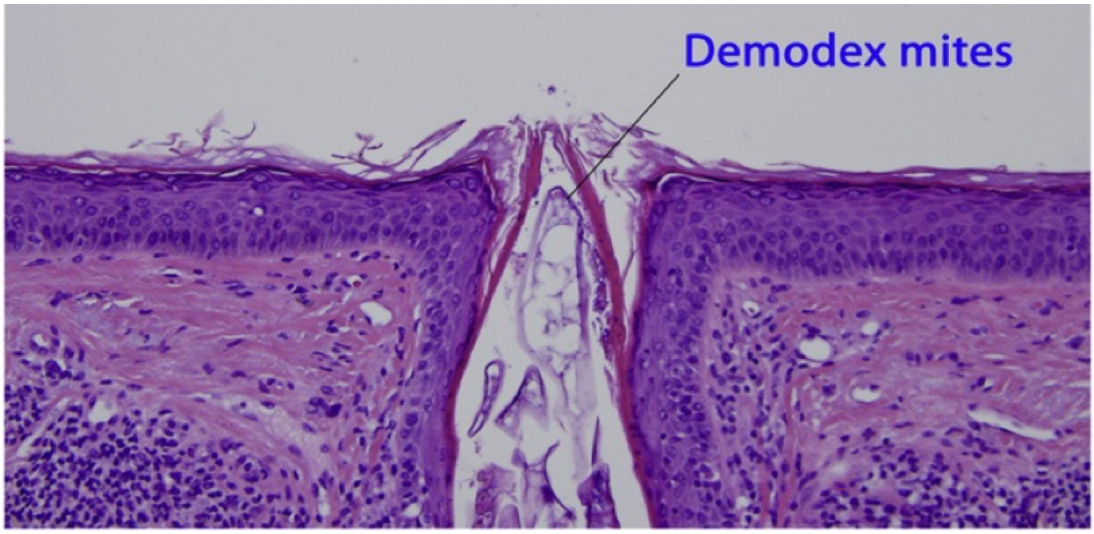

Figure 1.10 *Demodex* mites involved in pityriasis folliculorum.
Pityriasis folliculorum is the development of follicular spines/papules which is a characteristically a primary feature of subtype two rosacea, PPR. *Demodex* mites and keratin debris in the skin protrude through the follicle and give rise to such papules. (Elston and Elston, 2014)

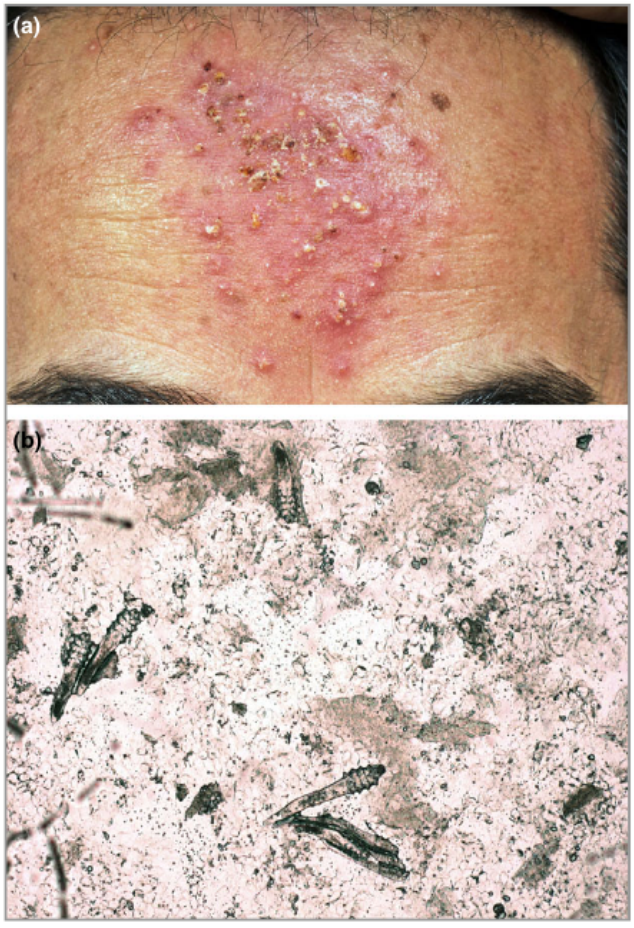

Figure 1.11 Demodicosis on the skin surface of 46-year-old male patient.
(a) Papulopustular demodicosis on patient forehead which is the infestation of *Demodex* mites leading to papule and pustule development. **(b)** Microscopic evaluation of demodicosis resulting in over 5 mites per cm^2 on a skin surface scraping. (Chen and Plewig, 2014).

1.5.3 Demodicosis in humans

Demodex mites are responsible for demodicosis in many animals and also play a role in various human diseases. A condition similar to animal mange caused by *D. folliculorum* is referred to as demodectic alopecia (Elston & Elston, 2014). The *D. folliculorum* mites typically cause symptoms such as erythema and scaling in the forehead and nose. They reside within keratin and debris in the hair follicle and as they proliferate and emerge, follicular spines develop on the skin surface. This is referred to as pityriasis folliculorum and is commonly seen in the development of papules as mites and follicular debris protrude (Elston & Elston, 2014). This leads to dry skin and pruritus, which can spread beyond the facial region to the eyelid (Jarmuda *et al*., 2012).

Demodex dermatitis, rosacea and seborrheic dermatitis are all separate dermatological conditions but have many similarities and common symptoms including erythema, facial rash, itchiness and acne-like lesions (Bikowski & Del Rosso, 2009). This facial rash typically develops around the mouth (perioral dermatitis) and can be a side effect of long-term medication such as local steroids (Fujiwara *et al*., 2010; Lacey *et al*., 2009). Demodicosis classification has yet to be defined but common diagnostic features include erythema, scaling, pruritus, skin sensitivity, perifollicular macules or papules, folliculitis, inflamed papules and atypical eczematiform eruptions (Forton & De Maertelaer, 2017).

Many dermatological conditions are the result of demodicosis, all of which can be aided by topical or oral treatments (Elston & Elston, 2014). However, immuno-suppressed individuals are more susceptible to *Demodex* proliferation and this can lead to frequent and severe conditions. For example, HIV positive patients and patients with demodicosis have a lower concentration of CD4+ cells and facial demodicosis can spread more easily (Holmes & Steinhoff, 2017; Elston & Elston, 2014). This can similarly be seen in dialysis patients, those undergoing immunosuppressive therapy or children receiving chemotherapy (Jarmuda *et al*., 2012; Lacey *et al*., 2009). An association has been established between increased densities of *Demodex* mites in diabetes patients. This can result in the vascular eye disorder diabetic retinopathy, causing intense microvascular complications and increased ocular susceptibility to infection and *Demodex* proliferation on the

eyelashes (Chang *et al*., 2015; Elston & Elston, 2014). From a study of diabetes patients, it is clear that *D. folliculorum* densities are higher in patients (27.4%) than in control patients (19%), indicative of a significant proliferation increase (Yamashita *et al*., 2011).

Demodex mites play an aetiological role in chronic blepharitis, which causes patients ocular irritation, reddening of eyelids and pruritus (severe itching) (Szkaradkiewicz *et al*., 2012). *Demodex* blepharitis has been divided into two types based on mite presence; anterior blepharitis involves *D. folliculorum* infestation in clusters at the lash root and is commonly accompanied with the clinical symptom of cylindrical dandruff (Geerling *et al*., 2011; Liu *et al*., 2010). Posterior blepharitis consists of *D. brevis* mechanically blocking the meibomian gland, giving rise to meibomian gland dysfunction (MGD) which can result in the formation of a cyst due to the gland swelling (Liu *et al*., 2010). Ocular demodicosis also features trichiasis, blepharoconjuctivitis and cylindrical dandruff (Kheirkhah *et al*., 2007). *Demodex* mites can mechanically block follicular orifices and meibomian glands and *Demodex* infestation can give rise to ocular micro-abrasions, hyperkeratinisation and follicular distension which can burden patients significantly (Jarmuda *et al*., 2012; Liu *et al*., 2010; Kheirkhah *et al*., 2007).

1.5.4 *Demodex* density and rosacea

Demodex mites have been found at a higher density on the face of patients than in unaffected (normal) individuals (McMahon *et al*., 2014; Bonnar *et al*., 1993). Normal *Demodex* densities are unusual in rosacea patients, which has been re-established by Forton with only 1.4% (3/215) of PPR patients tested had normal levels in comparison to 12.5% (6/48) (Forton *et al*., 2005). Interestingly, Forton and De Maertelaer have developed an improved consecutive standardised skin surface biopsy (SSSB) within a 1044 patient study (Forton & De Maertelaer, 2017). Approximately 254 individuals tested were PPR-suggestive, 590 had demodicosis, 180 had other facial dermatoses (such as seborrheic dermatitis and/or acne vulgaris) and finally 20 healthy control individuals. They established three different *Demodex* density cut-off values for the groups with higher *Demodex* densities (*Demodex* +) included PPR-suggestive and demodicosis while groups with lower *Demodex* densities (*Demodex* -) included other facial dermatoses and healthy controls. The

first SSSB (SSSB1) had >5 *Demodex*/cm^2 (D/cm^2), the second (SSSB2) had >10 D/cm^2 and >15 D/cm^2 for the combined (SSSB1 + SSSB2). This study found that the "*Demodex* +" group had statistically significantly higher mean *Demodex* densities than healthy controls and other facial dermatoses ($p \leq 0.001$) (Forton & De Maertelaer, 2017). *Demodex* mites are host-specific and possible opportunistic pathogens of their hosts, but the majority of the time they reside within facial sebaceous follicles and act commensally (Zhao *et al*., 2012; Lacey *et al*., 2011).

1.5.5 *Demodex*-related diseases in animals

Demodex mites have been known to be associated with dermal and ocular conditions in humans and other mammals for many years. Different *Demodex* mites are specific to host species and typically two *Demodex* species will co-exist and live commensally on the same host (Zhao *et al*., 2012). The most common example is rosacea, with *D. folliculorum* and *D. brevis* co-residing on the human hair follicles of the face or the sebaceous glands or meibomian gland of the eyelids (Tan & Berg, 2013). *Demodex* mites are most likely opportunistic pathogens of the human host, but the majority of the time they reside within the facial sebaceous follicles and act commensally (Lacey *et al*., 2011). However, *Demodex* mites can be pathogenic to animal hosts, for example, goats are affected by *D. caprae,* cats with *D. cati* and many more animal species suffer from demodectic mange (Ferrer *et al*., 2014; Lacey *et al*., 2011). This is commonly referred to as demodicosis and is defined by the presence of >5 mites/cm^2 and the proliferation of the *Demodex* mites causing penetration of the dermis (Forton *et al*., 2005). Once the host becomes immuno-compromised or the dermal immune response is altered (Margalit *et al*., 2016), the increased susceptibility to certain conditions and diseases is likely. The *Demodex* mites reside in the pilosebaceous unit, which is rich in sebum, protein and a source of epithelial cells, the food sources of the mite (Lacey *et al*., 2009; O'Reilly *et al*., 2012c). This may cause skin abrasions and if the immune system becomes weakened, this may facilitate further proliferation of *Demodex* mites in the microbiota environment, resulting in demodicosis (Lacey *et al*., 2011).

Three structurally different *Demodex* species can be found in dogs; *D. canis, D. cornei* and *D. injai* (Thoemmes *et al*., 2014). *Demodex* mites are ubiquitous in healthy dogs and reside commensally. They are opportunistic mites, whereby they colonize and spread when possible (Elston & Elston, 2014). Canine demodicosis is a prime example of how *Demodex* mites, at stages including nymph and adult, act pathogenically (Ferrer *et al*., 2014). *D. canis* has been found in cases of canine Demodicosis, which is also referred to as demodectic, follicular or red mange (Lacey *et al*., 2009). This type of canine mange is sometimes the result of a genetic defect, most commonly seen in juvenile dogs and also in purebred dogs (Ferrer *et al*., 2014; Lacey *et al*., 2009). An immune-compromised dog is more likely to develop demodectic mange caused by *D. canis*, however previously healthy dogs can develop sarcoptic mange, caused by *Sarcoptes scabei* (Elston & Elston, 2014). This form of demodectic mange causes severe itchiness as well as common symptoms including scabbing, sores and hair. This form is contagious to humans and is commonly referred to as “scabies”.

Two *Demodex* species have been isolated from orifices of the skin of cattle and are involved in bovine demodectic mange (Figure 1.12). *D. bovis* and *D. ghanensis* are opportunistic pathogens and have been isolated in lesions of demodectic mange in cattle. *D. bovis* is the predominant pathogen of mange in cattle and incurs the development of lesions on the skin, characteristically in the form of nodules, papules/pustules or cysts (Abu Samra & Shuaib, 2014). Cattle typically develop demodectic lesions around the neck, shoulders and forequarters, which can commonly spread to the eye where *D. ghanensis* is responsible for invasion of meibomian gland demodicosis (Abu Samra & Shuaib, 2014). *D. ghanensis* may induce inflammation, eyelid swelling and thickening of the eyelid which can result in the eyes physically being forced shut, thus blindness (Abu Samra & Shuaib, 2014).

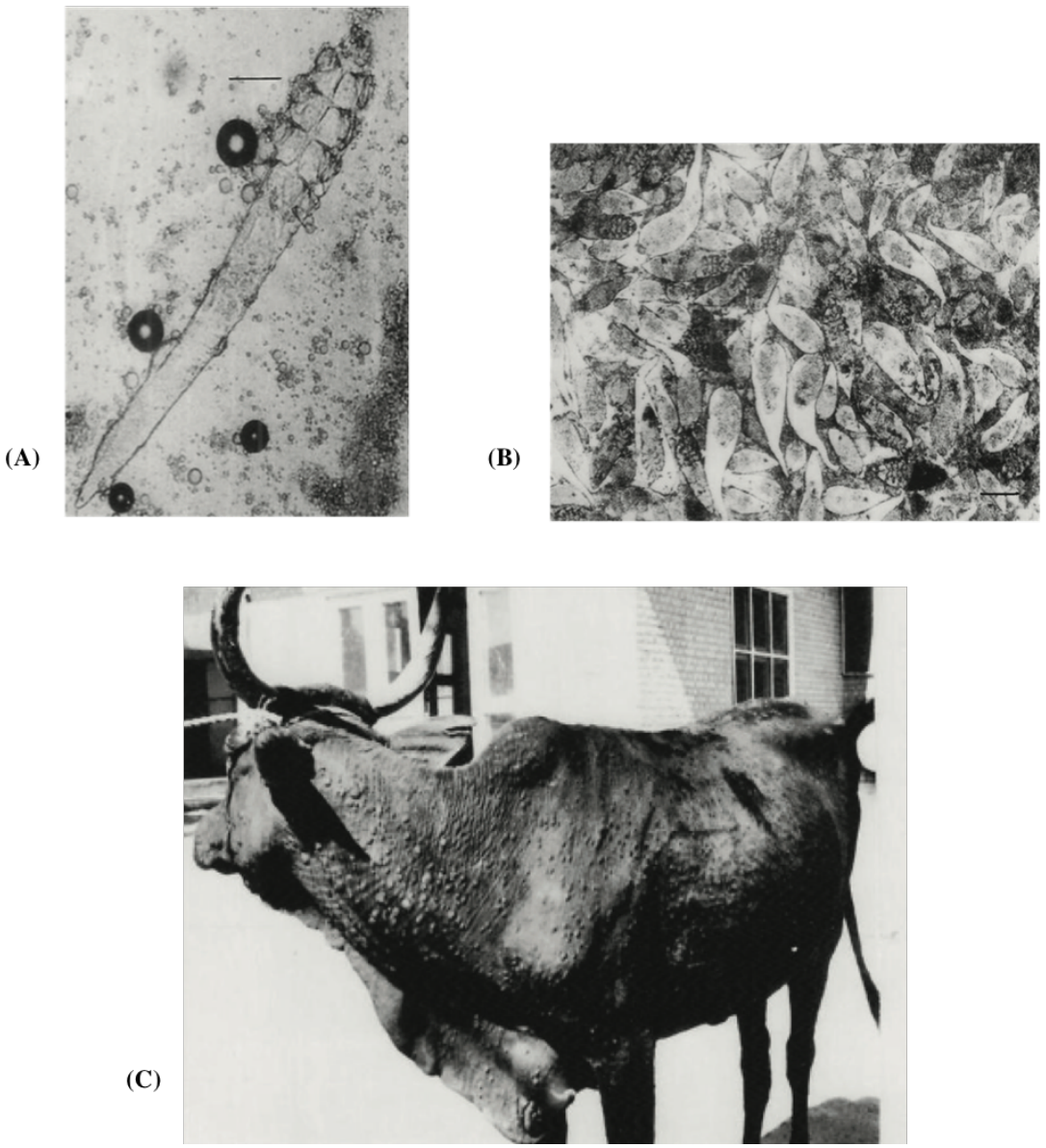

Figure 1.12 Association of *Demodex* mites in bovine demodectic mange.
(A) *Demodex ghanensis* mite extracted from infected lesion of meibomian gland in cow suffering from demodectic mange. Scale bar 50 μm. **(B)** *Demodex bovis* mites extracted from skin lesion of demodectic mange, displaying different growth stages, pus and cell debris from sample. Scale bar 70 μm. **(C)** Demodectic mange in a cow highlighting characteristic symptoms of mange including nodules and lesions. (Abu Samra and Shuaib, 2014)

1.6 Potential role of commensal skin bacteria in the pathogenesis of rosacea

The skin is colonized by a plethora of microorganisms, most of which reside commensally (Figure 1.13) (Grice & Segre, 2011). The pathology of rosacea can be explained by two possible hypotheses suggesting a role for microorganisms in rosacea; (i) microbes are responsible for this dermatological condition, or (ii) they are not responsible but accompany the condition (Holmes, 2013). The latter of the two possibilities has previously been suggested stating that some microorganisms may witness the pathogenesis of rosacea without causing it, but may act as accomplice leading to the persistence of rosacea symptoms (Chen & Plewig, 2015). Many bacterial species have been isolated from patients with all subtypes of rosacea including *Staphylococcus epidermidis, Staphylococcus albus, Chlamydophila pneumoniae*, *Helicobacter pylori* and *Bacillus oleronius* (Holmes, 2013; Lacey *et al*., 2009). One study has identified Proteobacteria and Firmicutes as the two main taxa of facial skin bacteria (Zhao *et al*., 2017). Firmicutes includes *Bacillus* and *Staphylococcus* which have both been isolated from *D. folliculorum* mites of patients with demodicosis symptoms, in comparison to no isolates being found in healthy individuals (Zhao *et al*., 2017; Tatu *et al*., 2016; Dahl *et al*., 2004). The presence of different bacteria on the skin and also within the *Demodex* mite species suggests a possible role for microorganisms in rosacea pathology.

1.6.1 *Staphylococcus epidermidis*

A common bacterial species colonizing the human skin is the Gram-positive bacterium, *Staphylococcus epidermidis* (Grice and Segre, 2011). This bacterium plays a protective role on the skin but can be an opportunistic pathogen, for example when colonizing vulnerable wounds (Holmes, 2013). *S. epidermidis* has been isolated from rosacea patient serum and some of the bacterial proteins play a virulent role in rosacea patient samples and samples from controls (Holmes, 2013; O'Reilly *et al*., 2012c). This bacterium has also been isolated from pustules of rosacea patients but was not isolated from surrounding unaffected areas of the skin (Whitfeld *et al*., 2011; Dahl *et al*., 2004). *S. epidermidis* is mesophilic with an optimum growth temperature of 37°C (O'Reilly *et al*., 2012c). This bacterium has also been isolated from the eye region of ocular rosacea patients and is consistently β-hemolytic (Dahl *et al*., 2004).

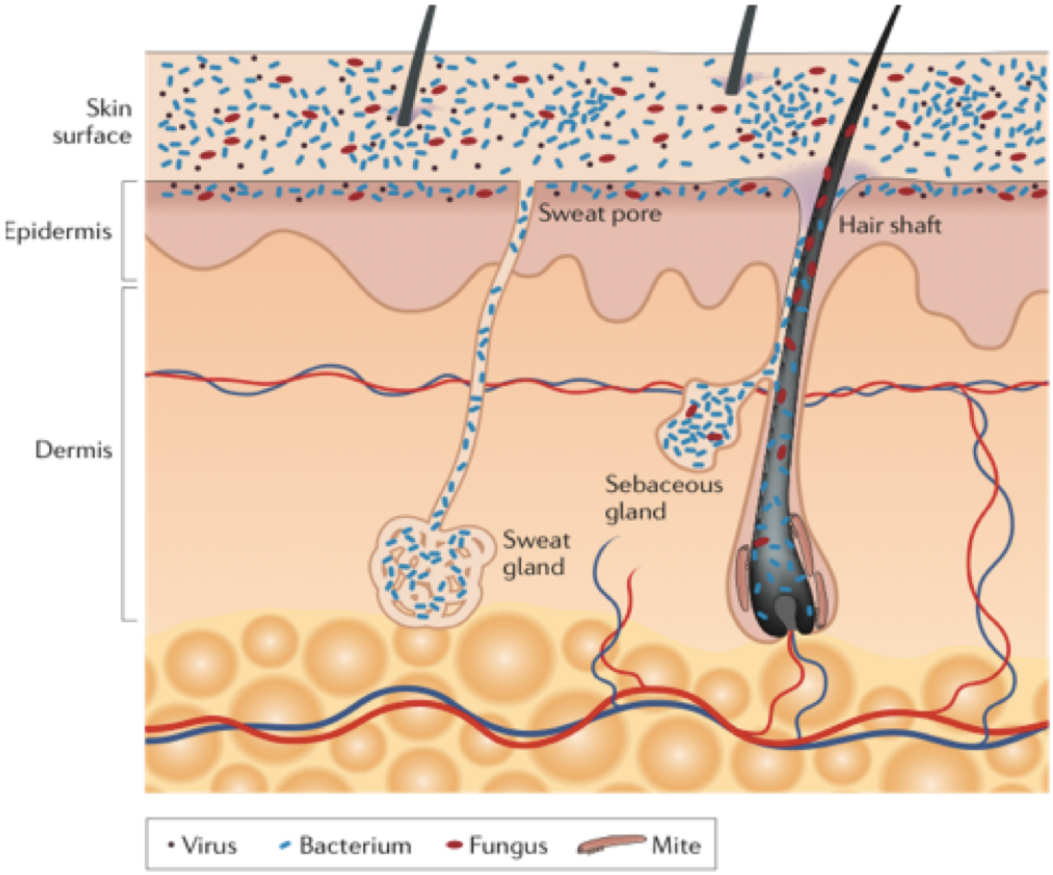

Figure 1.13 The skin microbiome.

Schematic of the skin histology in a cross-section view displaying the dermal layers, commensal microorganisms (viruses, bacteria, fungi and *Demodex* mites) and the skin components (hair follicles, sebaceous glands and sweat glands). (Grice and Segre, 2011).

Members of the phyla *Staphylococcus* have been isolated at a significantly higher prevalence from *D. folliculorum* samples from individuals with facial lesions in comparison to *D. folliculorum* controls ($p = 0.032$) and also *D. brevis* controls ($p = 0.001$) (Zhao *et al*., 2017).

1.6.2 *Helicobacter pylori*

Helicobactor pylori is a Gram-negative motile bacterium with a spiral/rod shape, located in the gastric mucosa (Del Rosso, 2004; Herr & Hee You, 2000). *H. pylori* infection (HPI) is associated with gastritis, peptic ulcer disease and hypochlorhydria symptoms (Egeberg *et al*., 2017; Utas *et al*., 1999). In some cases, an increased prevalence of HPI has been found in rosacea patients. A recent study has established that the onset of HPI is not an associated risk with rosacea patients, however the baseline for HPI prevalence is significantly increased in rosacea patients (Egeberg *et al*., 2017). Treatment for the eradication of HPI has displayed clearance or relief of rosacea symptoms in some cases, postulating an association between HPI and rosacea (Egeberg *et al*., 2017; Herr & Hee You, 2000). *H. pylori* secretes cytotoxins such as CagA and VacA which induce the release of vasoactive cytokines (Barco & Alomar, 2008; Holmes, 2013). The increased production of antibodies targeting *H. pylori* have been identified in the gastric juices and plasma of rosacea patients (Barco & Alomar, 2008; Szlachcic, 2002). The intermittence of gastrointestinal diseases and rosacea, particularly HPI and the concurrent treatment of both, has been established in many cases, thus highlighting the potential association of *H. pylori* contribution in rosacea pathophysiology.

1.6.3 *Propionibacterium acnes*

Propionibacterium acnes is a Gram positive anaerobic rod that has been associated with the inflammatory skin disorder acne vulgaris (Jahns *et al*., 2012b; Dahl *et al*., 2004). Rosacea and acne share parallels as bacteria have been associated with each condition and similar treatments improve symptoms (Crawford *et al*., 2004). However, the differentiation between the two has been separated (Figure 1.14) by the absence of comodones, truncal lesions and hormone dependency in rosacea (Holmes & Steinhoff, 2017; Two *et al*., 2015a; Tan & Berg, 2013).

P. acnes is a member of the normal skin microbiota and an opportunistic pathogen that has been found in the pilosebaceous unit and in the conjunctiva (Grice & Segre, 2011; Niazi *et al*., 2010). *P. acnes* has been found to be one of the most common *Demodex* mite microbiota from *Demodex* extracted from rosacea patient skin (Murillo *et al*., 2014). *Demodex* and *P. acnes* share the same habitat with *P. acnes* being the most abundant member of the pilosebaceous microbiota (Grice & Segre, 2011; Niazi *et al*., 2010). Recognition of *P. acnes* has been shown to induce protective human defensin-2 by sebocytes in the pilosebaceous unit (Zouboulis *et al*., 2016). There is no direct association between *P. acnes* and rosacea, however the abundance of *P. acnes* as pilosebaceous microbiota and presence within *Demodex* mites, may act as a contributing microorganism in the pathogenesis of rosacea (Murillo *et al*., 2014; Jahns *et al*., 2012a; Grice & Segre, 2011).

1.6.4 *Chlamydophila pneumonia*

Chlamydophila pneumoniae is a Gram negative intracellular pathogen and is a known causative agent of the respiratory condition pneumonia (Holmes, 2013). The role of commensal microorganisms in the pathogenesis of rosacea includes *C. pneumonia* but no definitive link has been associated with the condition (Lazaridou *et al*., 2011). The effect of inflammation on the skin microbiome of rosacea patients may enhance proliferation of bacteria such as *C. pneumonia*. For example, serum antibodies against *C. pneumonia* and antigens of the pathogen were detected in rosacea patients (Lazaridou *et al*., 2011). Altered homeostasis in the skin microenvironment of rosacea patients may result in such detections however further controlled studies with this association are required. *C. pneumonia* has been shown to activate macrophages via the secretion of purified heat shock protein (HSP) 60 during infection, which can stimulate of TLR2 and TLR4 pathways and result in the production of pro-inflammatory cytokines such as tumour necrosis factor alpha and interleukin 6 (Prazeres *et al*., 2002). Similar pathways are associated with rosacea pathogenesis. As microbes live commensally on the skin and other organs, a broad variety of factors may influence natural homeostasis and the microbiome, which can lead to many of the microorganisms adapting and inducing an immune response. Some of these adaptions may be observed in the development of different rosacea subtypes but may accompany the condition rather than induce it (Holmes, 2013).

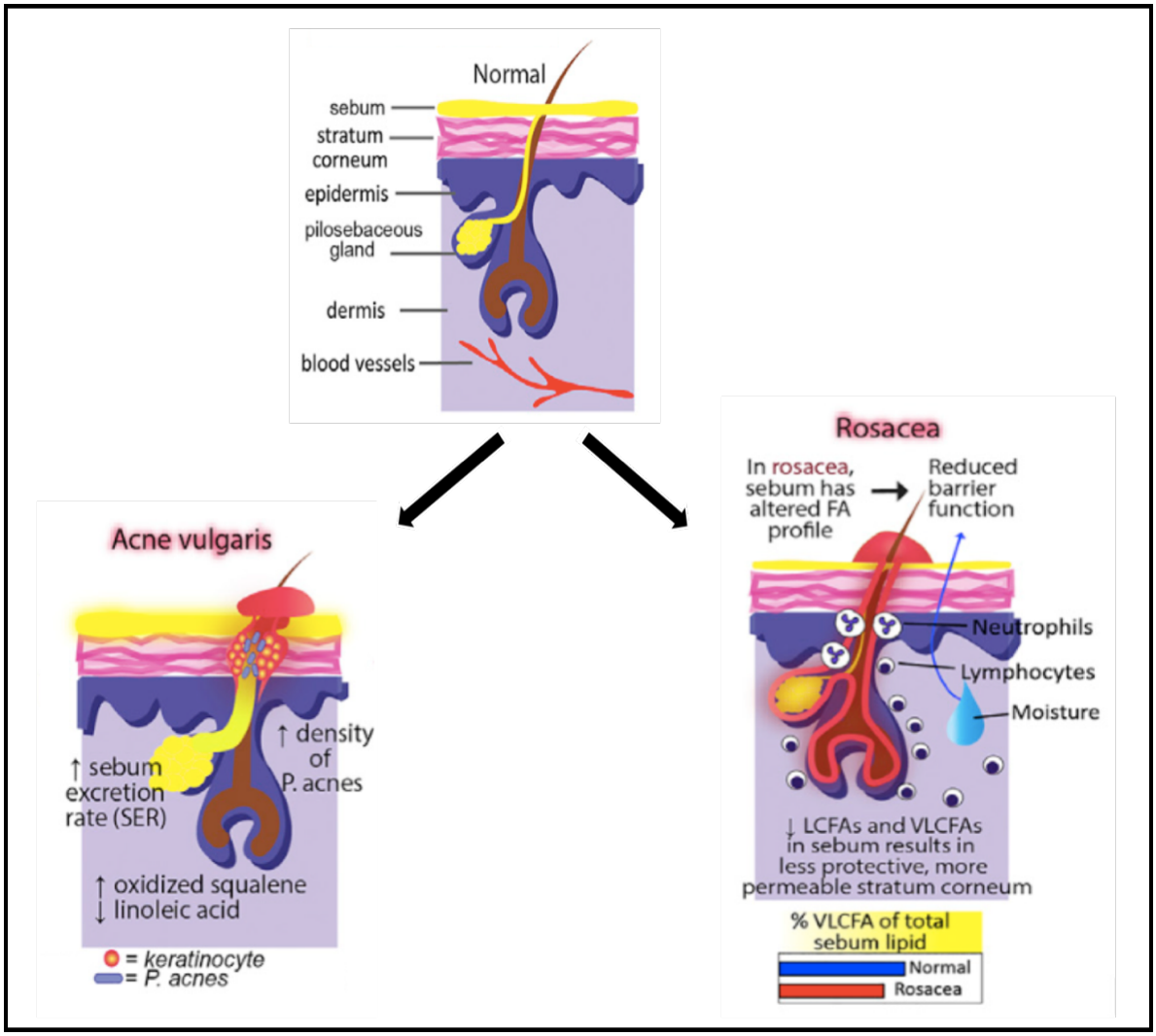

Figure 1.14 Role of sebaceous glands in inflammatory skin conditions acne vulgaris and rosacea.

Normal skin layer with pilosebaceous gland located in the hair follicle. Acne differentiation present with increased sebum excretion and presence of the pathogenic bacterium *P. acnes* associated with the condition. Increased inflammation and innate immune cells are characteristic of rosacea. The abundance of sebum secretion in the pilosebaceous unit remain consistent with altered fatty acid profile. (Shi *et al*., 2015)

1.7 *Demodex* mites and *Bacillus oleronius*

Bacillus oleronius is an aerobic, non-motile, rod-shaped bacterium and was first isolated from the termite *Reticulitermes santonesis* in 1995 (Kuhnigk *et al*., 1995). The termite hindgut has been described as the world's smallest bioreactor (Brune, 1998). The *Demodex* mite may represent a parallel example to the termite, as both termite and mite digestive systems provide an appropriate habitat for microbial communities. This suggests a possible symbiotic relationship between the mite and microbiota in its digestive system. Delaney first isolated *B. oleronius* in the digestive tract of *Demodex* mites from a PPR patient (Delaney, 2004). It is now believed that *B. oleronius* and other closely related *Bacillus* species are endosymbionts of *D. folliculorum* and *D. brevis*. *Demodex* mites flourish on the skin and eyelashes as they feed on sebum and epithelial cells, which is broken down in their digestive tract by microbial endosymbionts (Szkaradkiewicz *et al*., 2012; Li *et al*., 2010). Lacey *et al.* confirmed *B. oleronius* is Gram-negative, but like other *Bacillus* species, it shares cell wall components of Gram-positive bacteria (Lacey *et al*., 2007). *B. oleronius* has two forms of growth, the first is endosporic allowing the bacterium to encounter potential hosts such as the *Demodex* mite. Once inside the digestive tract the *Bacillus* enter their vegetative stage of life where the endosymbiosis begins with the host (Jarmuda *et al*., 2014; Szkaradkiewicz *et al*., 2012). These two cellular morphologies have been shown clearly by culturing the *B. oleronius* in nutrient broth media to demonstrate the rapid germination of the bacterium into its vegetative state (Szkaradkiewicz *et al*., 2012).

1.7.1 Role of *Bacillus oleronius* in rosacea

The consequence of higher *Demodex* densities in rosacea skin compared with normal skin and its role in the aetiology of the disorder is controversial. *Demodex* mites are a mobile reservoir of microorganisms that reside deep within the pilosebaceous unit. This can prove problematic as once the mites do not get rid of waste during life so once they die they release the internal microbes, including *B. oleronius,* and toxins within the sebaceous gland of the face or from the eyelash (Jarmuda *et al*., 2014; Szkaradkiewicz *et al*., 2012). This may result in a localised innate immune response with inflammation acting as the first line of defence on the skin, represented by erythema on the central region of the face. When bacterial cells

and antigens are released within the sebaceous glands, inflammation is centred on this structure (Jarmuda *et al*., 2014). The two antigenic proteins from *B. oleronius* that are sera reactive in rosacea patients are 62kDa and 83kDa in size. The 62kDa protein shares homology with the mammalian heat shock protein (HSP) groEL chaperonin while the 83kDa protein is homologous to aconitate hydratase, a bacterial protein that is induced during oxidative stress (O'Reilly *et al*., 2012c). It has been shown that rosacea patients are immune-reactive to the *B. oleronius* antigens. For example, ETR patient serum and control serum were extracted and used to probe reactivity on membranes containing the 62kDa and 83kDa *B. oleronius* antigens. This study highlighted the signifcant difference in immune reactivity, with 82.6% of ETR patients showing reactivity to one or both antigens in comparison to 26.9% of controls showing reactivity (Jarmuda *et al*., 2014). This immuno-reactivity to *B.* oleronius antigens has further been shown in PPR and ocular rosacea (Lacey *et al*., 2007; O'Reilly *et al*., 2012b).

The correlation between *Demodex* density and *B. oleronius* antigen response has been established with patient sebum having a higher concentration of mites than control sebum, thus more antigenic proteins are 'leaked' from the hair follicle into surrounding tissue, resulting in localized inflammation (Jarmuda *et al*., 2012; Szkaradkiewicz *et al*., 2012; Li *et al*., 2010). However not all rosacea patients are reactive to the two *B. oleronius* antigens. Some patients are serum positive to both the 62kDa and 83kDa antigens (Figure 1.15), while others are reactive to only one (Jarmuda *et al*., 2014). The strongest immune response and most severe rosacea symptoms have been the result of reactivity to *Bacillus* 62kDa protein alone, 83kDa protein alone and the simultaneous presence of both proteins, respectively (O'Reilly *et al*., 2012c).

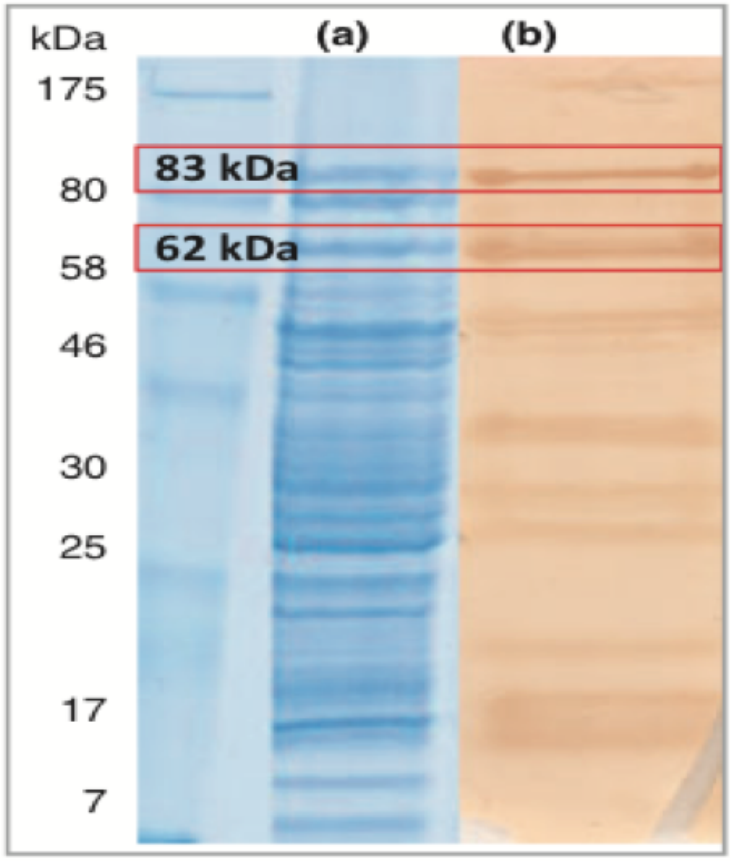

Figure 1.15 Two *Bacillus oleronius* proteins that are sera reactive in rosacea patients.

(a) *B. oleronius* proteins separated by 1D SDS-PAGE with 62 kDa and 83 kDa proteins identified. **(b)** Western blot analysis of patient sera to immune-reactive protein bands, displaying intense staining of the 62 kDa and 83 kDa proteins. (O'Reilly *et al.,* 2012c)

1.8 Innate immune response in rosacea

Rosacea patients display an altered immune response in the skin which may be due to increased *Demodex* densities, exposure to microorganisms harboured by the *Demodex* or residing in the pilosebaceous unit, differences in sebum composition and excessive inflammation (Margalit *et al*., 2016; Weinstock & Steinhoff, 2013). *Demodex* mites inhabiting eyelashes can induce eyelid margin inflammation and possibly lead to corneal scarring and neo-vascularization (Li *et al*., 2010). The development of pathologies similar to corneal ulcers has been shown in a corneal epithelial cell line (hTCEpi) following exposure to *B. oleronius* sera reactive proteins (O'Reilly *et al*., 2012b). Cells exposed to the *Bacillus* proteins show increased migration and elevated matrix metalloprotease (MMP) 9 activity. Treated cells also displayed an uncoordinated wound healing response which could be indicative of the early stages of scarring on the corneal surface *in vivo* (O'Reilly *et al*., 2012b).

The two antigens secreted by *B. oleronius* are highly immunogenic to rosacea patients and may be responsible for the induction and persistence of this chronic inflammatory condition. Once the 62kDa and 83kDa serum reactive antigens escape from the pilosebaceous unit, the innate immune system may be activated due to the presence of pathogenic foreign material. If the antigenic load reaches a critical level, this induces an inflammatory cascade resulting in the visible erythema symptoms of rosacea (Szkaradkiewicz *et al*., 2012; Li *et al*., 2010; Lacey *et al*., 2009). Increased antigenic load recruits neutrophils to the site, one of the characteristic innate immune cells (O'Reilly *et al*., 2012a). In healthy individuals, neutrophils induce an inflammatory cascade to target pathogens. Immune-compromised individuals, have an abnormal innate immune response whereby neutrophils can be over-activated. This can have a damaging effect on the skin as excessive tissue degradation may occur resulting in excessive inflammation and onset of rosacea symptoms (Margalit *et al*., 2016).

In order for neutrophils to become activated, they must convert from G- to F-actin in the cytoskeleton; a functional requirement following pathogen detection in the innate immune response (McMahon *et al*., 2016). The heightened immune response of rosacea patients highlights the abnormal activation of neutrophils which

subsequently may contribute to erythema and inflammation (McMahon *et al*., 2016). Neutrophils exposed to *B. oleronius* antigens show chemotaxis significantly increased (3.9 fold increase) indicating migration towards the pathogenic target (McMahon *et al*., 2016). Neutrophil activation leads to the secretion of pro-inflammatory cytokines *in vivo* such as tumour necrosis factor (TNF-α) and IL-8, inducing further neutrophil migration (Jarmuda *et al*., 2014; Holmes, 2013). The downstream effects of the innate immune defence induce inflammation and tissue degradation at the sebaceous unit site which is commonly seen in rosacea, particularly in PPR where inflammation is localized in the form of papules and pustules (Jarmuda *et al*., 2012; O'Reilly *et al*., 2012a).

The aetiology of rosacea is influenced by many factors and symptoms can be exacerbated by the various trigger factors, commensals of the skin microbiome and the dysregulation of the innate immune response, all of which can lead to chronic inflammation. Toll-like receptors (TLRs) are a pattern recognition receptor (PRR) and is commonly associated with the inflammatory role of rosacea (Holmes & Steinhoff, 2017). Pathogen-associated molecular patterns (PAMPs) and danger-associated molecular patterns (DAMPs) can stimulate PRRs located on the membranes of innate cells such as keratinocytes and mast cells (Holmes & Steinhoff, 2017; Tan *et al*., 2017). TLR-2 activation leads to the production of many pro-inflammatory cytokines, chemokines and the innate peptide cathelicidin, a key contributor to inflammation in rosacea (Holmes & Steinhoff, 2017; Margalit *et al*., 2016). Cathelicidins play a major role in the innate immune response acting as internal antibiotics, initiating wound healing responses, coordinating cell migration, signalling and vascular functions (Two *et al*., 2015a; Bevins & Liu, 2007). TLR pathways activate cathelicidin which in turn upregulates MMP and kallikrein 5 (KLK5) expression in keratinocytes (Holmes & Steinhoff, 2017). In rosacea, stratum corneum tryptic enzyme (SCTE, also known as KLK5) and cathelicidin peptides are elevated (Figure 1.16), resulting in the increased cleavage of cathelicidin (pro-peptide) by SCTE into the active version LL-37 (Holmes & Steinhoff, 2017; Two *et al*., 2015a; Bevins & Liu, 2007). LL-37 cleavage promotes inflammation and angiogenesis which are characteristic to rosacea and may impact patient phenotypes (Tan *et al*., 2017; Holmes & Steinhoff, 2017; Bevins & Liu, 2007).

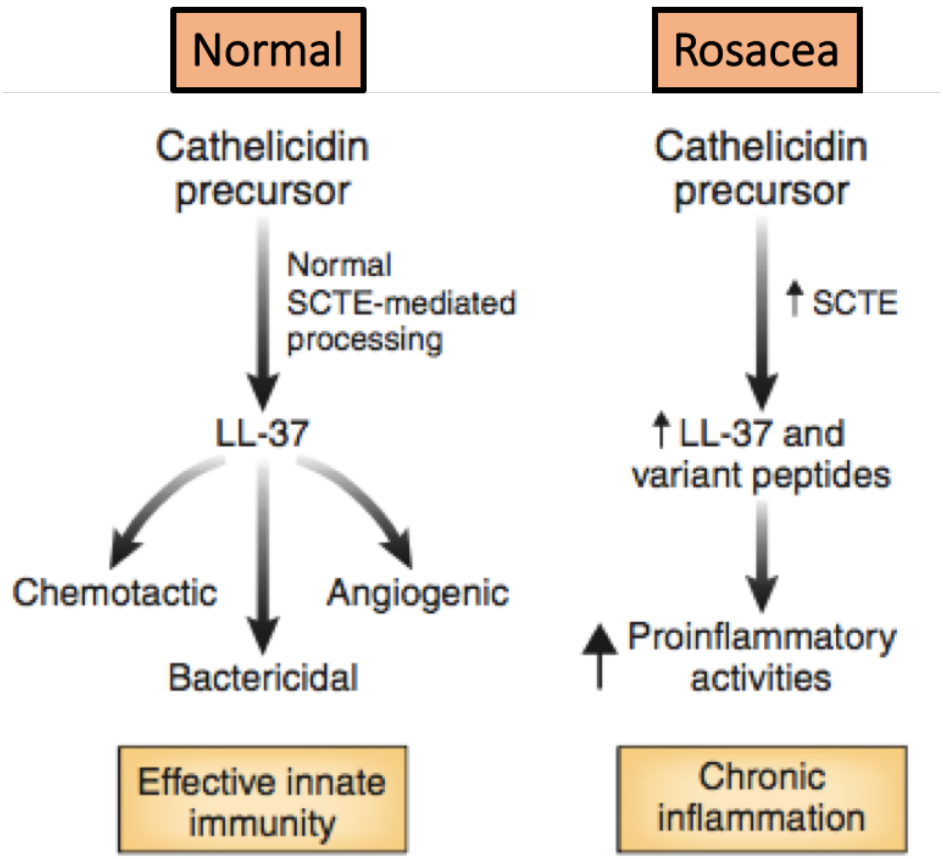

Figure 1.16 Proteolytic processing of cathelicidin in rosacea.
In normal individuals, the pro-peptide cathelicidin is cleaved by the skin mediated SCTE (i.e. KLK5) into the active LL-37 peptide which plays an integral role in innate immunity. In rosacea patients, cathelicidin activation is elevated by increased TLR2 stimulation and increased KLK5 levels. This enhances levels of active LL-37 and irregular isoforms which significantly contribute to inflammation. (Bevins and Liu, 2007)

1.9 Management and Treatment

Rosacea therapy is targeted at symptomatic relief rather than disease treatment. Patient education regarding their symptoms, subtypes and trigger avoidance is an important element of rosacea management, along with skin care (Holmes & Steinhoff, 2017; Two *et al*., 2015b). The use of fragrance free and pH suitable soaps can alleviate agitated skin, for example burning sensation and stinging. The use of high factor sun protection with silicones has been shown to reduce transepidermal water loss and cosmetics with sun protection factor (SPF) has improved patient symptoms visually and psychologically (Holmes & Steinhoff, 2017; Barco & Alomar, 2008). Most pharmaceutical interventions include topical and oral antibiotics, some of which are approved by the food and drug administration (FDA) and others are off-label systemic treatments, as well as surgical applications. Alternative treatments involve targeting *Demodex* mites which can prove effective, natural remedies such as heat compression for ocular symptoms or home remedies such as cooled cucumber and yogurt application resulting in reduced oedema (Margalit *et al*., 2016; Powell, 2005). Some rosacea patients have shown low tolerance for topical steroid use with a common case of symptoms returning once treatment has ceased, an unfortunate characteristic of this relapse and remission skin disorder (Fujiwara *et al*., 2010; Crawford *et al*., 2004).

Topical treatments for rosacea typically include azelaic acid, metronidazole, benzoyl peroxide and erythromycin (Barco & Alomar, 2008; Gupta & Chaudhry, 2005). Metronidazole was first discovered in 1976 for the treatment of rosacea and is now the primary topical therapy since FDA approval in 1989 (Pye & Burton, 1976; Wolf & Del Rosso, 2007). Metronidazole works effectively as a combination therapy with therapies such as sun protection, with ivermectin to target *Demodex* mites or with the topical antibiotic of 10% sodium sulfacetamide and 5% sulfur lotion (Margalit *et al*., 2016; Barco & Alomar, 2008; Powell, 2005). MetroGel® is a 0.75% metronidazole gel with strong efficacy in rosacea treatment resulting in reduced inflammatory lesions of PPR and reduced erythema in ETR (Goldgar *et al*., 2009; Wolf & Del Rosso, 2007). Metronidazole has a specific mode of action unlike other topical treatments, whereby the drug inhibits reactive oxygen species (ROS) production and displays anti-inflammatory and antimicrobial properties (Holmes & Steinhoff, 2017; Two *et al*., 2015b). The efficacy of metronidazole gel was reviewed

in a large community-based study with 582 randomized subjects. Metronidazole gel (0.75%) was applied twice daily and evaluations were observed at 4, 8 and 12 weeks (Wolf & Del Rosso, 2007). At 12 weeks, the mean scores accounted for 25% reduction in itchiness, stinging and pain and improvements resulted in less embarrassment/ self-confidence (53%) and more social/leisure partaking (31%) (Wolf & Del Rosso, 2007).

Oral treatments for rosacea include tetracycline, macrolides, isotretinoin and metronidazole which are commonly used alone or in combination therapy with topical treatments (Holmes & Steinhoff, 2017; Barco & Alomar, 2008). Metronidazole and tetracycline gave similar clinical outcomes with the latter having a faster onset (Gupta & Chaudhry, 2005). Tetracycline is the most commonly prescribed medication for treatment of blepharitis in the US, which has similar symptoms to ocular rosacea (Geerling *et al*., 2011). Tetracycline was developed in 1948 as a systemic antibiotic and is best known for inhibiting inflammation, MMPs, KLK5 and targeting cellular process which are vital in rosacea progression such as angiogenesis, innate immune response factors and apoptosis (Holmes & Steinhoff, 2017; Margalit *et al*., 2016; Geerling *et al*., 2011).

Not many oral or topical therapies relieve telangiectasia, however procedural solutions such as pulse-dye laser, intense pulsed light treatment, flash lamp pumped dye and laser surgery have improved this secondary symptom (Gupta & Chaudhry, 2005; Powell, 2005). Similar surgical approaches are commonly used for moderate-severe phymatous rosacea also (Barco & Alomar, 2008; Powell, 2005). Beta-blockers are a type of systemic medication which reduce the presence of flushing and erythema on the skin surface (Two *et al*., 2015b; Powell, 2005). Ivermectin is an effective anti-parasitic drug that been shown to reduce the density of *Demodex* mites significantly after 6 and 12 weeks of 1% topical treatment (Schaller *et al*., 2017). Ivermectin also offers a beneficial dual role in the treatment of rosacea as it also plays an anti-inflammatory role. Ivermectin inhibits many cellular processes including the translocation of the transcription factor NF-κB and the reduction of inflammatory gene expression which downregulates IL-8, TNFα, TLR-2 and LL-37 (Schaller *et al*., 2017; Holmes & Steinhoff, 2017; Margalit *et al*., 2016). The discoverers of the mode of action of Ivermectin, William Campbell and Satoshi

Ōmura, jointly received the Nobel Prize in Physiology or Medicine for its beneficial contribution towards eradicating parasitic disease (Holmes & Steinhoff, 2017).

1.9.1 Ocular rosacea treatment

Demodex mites have been associated with the onset of dermal and ocular rosacea and the use of tea tree oil (TTO) is a common therapeutic avenue to target *Demodex* mites. TTO is an essential oil with antibacterial, anti-fungal and anti-inflammatory properties (Geerling *et al*., 2011; Gao *et al*., 2005). It's acaricide mode of action has been shown to reduce *Demodex* infestation of the skin (Margalit *et al*., 2016). However, in ocular rosacea a lid scrub of 50% TTO applied once weekly in combination with a daily TTO shampoo for the eyelid encourages migration of *Demodex* mites out from the eyelash follicle and has resulted in effective *Demodex* eradication (Gao *et al*., 2005).

Up to 50% of rosacea patients manifest ocular rosacea and the importance of eyelid hygiene can forestall symptoms (O'Reilly *et al*., 2012b; Powell, 2005). Artificial tears are treatment of choice for ocular symptoms such as dry eye and meibomian gland dysfunction as they lubricate the corneal surface of the eye and possibly enhance flushing out of toxins and debris residing on the surface (Geerling *et al*., 2011; Powell, 2005). Eye drops, sprays and ointments are also associated with ocular treatment, some of which are supplemented with tear film lipids (Geerling *et al*., 2011). Physical maintenance of the eyelid margin proved beneficial to some patients. For example, eyelid warm (40°C) towel compress onto closed eyelids for 15 minutes increased thickness of the tear lipid layer and infrared lamps have been shown to increase meibomian oil to the lid margin (Geerling *et al*., 2011). Many topical antibiotics such as metronidazole, fusidic acid and fluoroquinolones relieve ocular symptoms, the latter of which have minimal toxicity to the ocular surface and targets both Gram positive and Gram negative bacteria (McMahon *et al*., 2014; Geerling *et al*., 2011; Powell, 2005). Macrolides are effective antibiotics, for example erythromycin was the first oral antibiotic with a systemic effect to bacteria and successfully inhibit protein synthesis. The efficacy of erythromycin for ocular treatment is limited by its low aqueous solubility, however incorporating of the antibiotic into an ointment based treatment have proved effective (Geerling *et al*., 2011; Goldgar *et al*., 2009). The antibiotic doxycycline is used for the treatment of

ocular rosacea and displays anti-inflammatory properties with improvement in patient symptoms such as dryness, blurred vision and photosensitivity (Margalit *et al*., 2016; Powell, 2005). A broad range of topical, oral and surgical therapies exist for rosacea, with each treatment course focusing on patient symptoms rather than the disease.

1.10 Aims of this study

The aims of this research study were as follows:

1. To analyse the effect of temperature and culture medium on the growth and expression of stimulatory antigen of *B. oleronius*. Increased temperature may induce an inflammatory stress response and alter the bacterial protein expression, which may exacerbate rosacea patient symptoms.

2. To analyse the effect of oxidative stress on the growth, expression of stimulatory antigen and proteome in *B. oleronius.* Oxidative stress may disrupt cell homeostasis and trigger a significant outcome in bacterial protein expression, which could lead to tissue degradation and increased inflammation in rosacea patients.

3. To examine the potential of a therapeutic blocking agent for ocular rosacea, by targeting *B. oleronius* antigens prior to contact with the corneal surface. This study may prevent exacerbation of ocular symptoms and lead to an antimicrobial therapeutic for rosacea patients.

4. To assess the potential of a novel formulation to reduce the symptoms of erythematotelangiectatic rosacea and papulopustular rosacea. This novel approach may reduce erythema and improve the epithelial cell barrier with potential as a future treatment for dermal rosacea.

Chapter Two

Materials and Methods

2.1 General Chemicals and Reagents

All chemicals and reagents were of the highest purity and were purchased from Sigma Aldrich Chemical Company Ltd. (Dorset, UK) unless otherwise stated. Buffers were prepared using distilled H_2O, which was purified using a Millipore Milli-Q apparatus.

2.2 Sterilisation Procedures

All liquids were sterilised prior to use by autoclaving in a Systec 3170 ELV autoclave at 121°C and 15 lb/sq.in. for 15 minutes. Any chemicals unsuitable for autoclaving were filter-sterilised using a filter with a pore size of 0.2 μM (Sarstedt, Nümbrecht, Germany).

2.3 Statistical Analysis

All experiments were performed on three independent occasions in biological replicates and results are expressed as the mean ± SEM, unless otherwise stated. The statistical significance was assessed using GraphPad Prism version 6.0f for Mac OS X, GraphPad Software, San Diego California, USA, (www.graphpad.com). For all experimentation *p*-value of < 0.05 was deemed statistically significant.

2.4 Culture Media

2.4.1 Nutrient Agar

Nutrient agar (Scharlau) (28 g/L) was dissolved by stirring in dH_2O. This solution was autoclaved and allowed to cool before pouring into 9 cm petri dishes under sterile conditions. Plates were stored at 4°C until needed.

2.4.2 Nutrient broth

Nutrient broth (Oxoid) (13 g/L) was dissolved by stirring in distilled water (dH_2O). The solution was autoclaved and stored at room temperature until needed.

2.4.3 2XYT Broth

Tryptone (Oxoid) (16 g/L), yeast extract (Scharlau) (10 g/L) and NaCl (5 g/L) were dissolved in dH_2O. The solution was autoclaved and stored at room temperature until needed.

2.5 Culture Conditions

Cultures of *Bacillus oleronius* were maintained on nutrient agar plates and sub-cultured every 6-8 weeks using aseptic techniques (Lacey *et al.,* 2007; Delaney, 2004). Freshly sub-cultured plates were grown overnight at 30°C or 37°C depending on strain then stored at 4°C. Liquid cultures were inoculated with a loopful of bacteria from nutrient agar plates and grown to stationary phase in nutrient broth (100 ml) at 30°C under aerobic (shaking) conditions. For experiments involving an evaluation of the proteomic expression profile of the *B. oleronius* growth under varying environmental conditions, 1ml of culture was taken from an overnight culture and aseptically added to 100 ml of fresh nutrient broth (section 2.4.2) or 2XYT (section 2.4.3). *B. oleronius* was originally isolated from a *Demodex* mite and was identified by NCIMBs in Scotland (Delaney, 2004).

2.6 Phosphate Buffered Saline (PBS)

One PBS tablet (Oxoid) was dissolved in 100ml dH_2O and autoclaved at 121°C for 15 minutes. PBS was stored at room temperature.

2.7 *Bacillus* Lysis Buffer (pH 7.2)

Piperazine (20 mM) and NaCl (5 mM) were dissolved in dH_2O by stirring and the pH of the solution was adjusted to pH 7.2 before autoclaving. Triton X-100 (0.2% v/v) was added under sterile conditions and the buffer was stored at 4°C. Protease inhibitors (10 µg/ml each of Leupeptin, Pepstatin A, Aprotinin and TLCK) and 1% (v/v) phosphatase inhibitor cocktail 2 were added to the lysis buffer on the day of protein extraction.

2.8 Protein Extraction Protocol

2.8.1 Protein extraction from *Bacillus oleronius*

Liquid medium (100 ml) was inoculated with a loopful of bacterial culture, aseptically taken from a fresh plate and grown over night with shaking at 30ºC. This culture was then used to inoculate fresh media so the effect of varying environmental conditions on protein expression could be assessed. Cells were grown in nutrient broth (section 2.4.2) or 2XYT (section 2.4.3) at 30ºC or 37ºC, and with or without agitation. The effect of hydrogen peroxide on the bacterium was also examined by adding 10 mM H_2O_2 to 100 ml cultures.

B. oleronius cultures were grown to late stationary phase and cells were harvested by centrifugation at 3000 x *g* (g-force) for 15 minutes (Beckman GS-6 Centrifuge). The supernatant was discarded and cells were washed with sterile PBS (section 2.6) twice, and centrifuged at 3000 x *g* for 15 minutes at room temperature each time. Cells were re-suspended in lysis buffer and supplementary inhibitors (section 2.7) and stirred at 4ºC for 2 hours on a rotary wheel. The volume of lysis buffer used was dependent on the size of the cell pellet; approximately 1ml per 100ml of starting culture was used. Sonication was also employed as a method to extract proteins from the cell surface of the bacteria. Cell suspensions were sonicated with 3 x 10 second blasts using a soniprobe sonicator (Bandelin Sonopuls, HD 2200). Suspensions were stored on ice between sonications to avoid excessive overheating of the proteins.

Following treatment with lysis buffer or sonication, the protein suspension was obtained by centrifuging cells at 6000 x g for 2 minutes (Eppendorf Centrifuge 5418). The supernatant containing proteins was retained and the protein concentration was determined using Bradford protein assay (section 2.8.2). Protein samples were acetone precipitated (section 2.8.3) for 1D or 2D IEF SDS-PAGE or Q-exactive mass spectrometry (MS/MS) preparation (section 2.9, section 2.10 and section 2.14, respectively). Alternatively, 5X sample buffer (section 2.9.6) was added directly to the protein suspension which was boiled for 5 minutes at 95°C before storage at -20ºC until required.

2.8.2 Bradford assay for protein quantification

Sterile PBS was used to make a serial dilution of bovine serum albumin and this was used to make a range of standards (0.05 - 1.5 mg/ml). All samples used were diluted in sterile PBS. Bradford protein assay reagent (Bio-rad Laboratories) was diluted in ddH_20 (ratio 1:5). Sample (20µl) was placed in 1ml cuvette and 980µl of diluted Bradford protein assay reagent was added. The cuvettes were inverted and incubated for 5 minutes at room temperature before being read on a spectrophotometer (Eppendorf Biophotometer) at 595 nm to determine protein quantity.

2.8.3 Acetone precipitation of protein samples

Acetone precipitation was used to concentrate protein from a dilute sample and also to purify protein samples. The required volume of protein was calculated following Bradford assay quantification (section 2.8.2). The correct protein volume was aliquoted into fresh pre-chilled micro-centrifuge tubes and 100% (v/v) ice cold acetone was added to the tube at a ratio of 1:3 (sample volume: acetone). Protein was stored at -20ºC overnight and precipitated at 13,000 x *g* for 10 minutes to pellet protein. All protein pellets were placed upside down to air dry for 5 mins following removal of acetone before being prepared for SDS-PAGE (section 2.9) or Q-exactive MS (section 2.14).

2.9 Sodium Dodecyl Sulphate Gel Electrophoresis-Poly Acrylamide Gel Electrophoresis (SDS-PAGE)

2.9.1 Tris–HCl (1.5 M)

Tris-HCl (1.5 M) was prepared by dissolving 36.3g Trizma Base (Tris Base) in 200 ml deionised water and adjusted to pH 8.9 using HCl. Following pH adjustment 1.5 M Tris-HCl was filter sterilised through a 0.22µM cellulose filter (Millipore) and stored at 4ºC.

2.9.2 Tris-HCl (0.5 M)

Tris-HCl (0.5 M) was prepared by dissolving 12.1g Trizma Base in 200 ml deionised water and adjusted to pH 6.8 using HCl. Following pH adjustment 0.5 M Tris-HCl was filter sterilised through a 0.22µM filter (Millipore) and stored at 4ºC.

2.9.3 10% Sodium Dodecyl Sulphate (SDS)

Sodium dodecyl sulphate (10% w/v) was prepared by placing 5g SDS into a 50ml falcon and filling up to 50ml mark with deionised water and vortexing until all SDS had been solubilised. The solution was stored at room temperature.

2.9.4 10% Ammonium Persulphate (APS)

APS (10% w/v) was prepared by adding 0.1g APS into micro-centrifuge tube, filled up to 1ml with deionised water and vortexed briefly to achieve solubility. APS (10% w/v) stocks were frozen at -20ºC until required.

2.9.5 10X Electrode Running Buffer

Running buffer (10X) (electrode buffer), was prepared by dissolving Tris Base (30g/L), Glycine (144g/L) and SDS (10g/L) using distilled water filled up to 1000ml mark and the mixture was stirred until the solution was solubilised. Electrode running buffer (10X) stock was diluted to 1X concentration by making 1/10 dilution with distilled water when required.

2.9.6 5X Solubilisation Buffer for 1D SDS-PAGE

Solubilisation buffer was prepared by dissolving the constituents to solubility, as listed in Table 2.1.

Table 2.1 Constituents of 5X solubilisation buffer

Glycerol	8ml
Deionised water	4ml
SDS 10% (v/v)	1.6ml
Tris-HCl (0.5M)	1ml
Bromophenol Blue (0.5% w/v)	200µl
2-Mercaptoethanol	400µl

2.9.7 Separating gel composition (12.5%)

All glass plates (1.0mm) were cleaned thoroughly before use with 70% (v/v) ethanol. 1D and 2D IEF SDS-PAGE gels were made of acrylamide with 12% (v/v) Bis-acrylamide in all experiments and cast using Mini-Protean II gel casting apparatus. Table 2.2 list the volumes sufficient to make 2 gels.

Table 2.2 Constituents of separating gel for SDS-PAGE

1.5 M Tris-HCl (pH 8.9)	3ml
Deionised water	3.8ml
30% v/v Bis-Acrylamide	5ml
10% v/v SDS	120µl
10% v/v APS	50µl
TEMED	11.5µl

2.9.8 Stacking gel composition (5%)

The stacking gel was applied on top of the separating gel after setting. Combs were placed in the gel matrix before it set to create wells for sample loading. Table 2.3 list the volumes sufficient to cover 2 gels with separating stock.

Table 2.3 Constituents of stacking gel for SDS-PAGE

0.5 M Tris–HCl (pH 6.8)	630µl
Deionised water	3.4ml
30% v/v Bis-Acrylamide	830µl
10% v/v SDS	50µl
10% v/v APS	60µl
TEMED	6µl

2.9.9 1D SDS-PAGE sample loading and voltages

SDS-PAGE gels (12.5%) were immersed in 1X running buffer. Samples varied in volume and protein concentration depending on the experiment but were aliquoted using a sterile gel loading tip. The gels were electrophoresed at 40V initially and the voltage was increased to 60 V once the protein had travelled sufficiently through the stacking gel. Once the blue tracking dye had moved to the bottom of the gel, the gels were transferred to a clean staining dish.

2.10 2D IEF SDS-PAGE preparation and analysis

2.10.1 Isoelectric focussing (IEF) Buffer

The following constituents (Table 2.4) were added and dissolved in deionised water and stored in 1ml aliquots at -20ºC until required. Ampholytes (0.8%, v/v) and DTT (65 mM) were added to the defrosted aliquots on the day of use.

Table 2.4 Constituents of IEF buffer

Urea	8M
Triton X-100 (BDH)	1% (v/v)
CHAPS	4% (w/v)
Tris HCl	10mM
Thiourea	2mM

2.10.2 Equilibration buffer (pH 6.8)

The constituents of equilibration buffer (Table 2.5) were dissolved in deionised water followed adjustment to pH 6.8 and aliquoted in 40 ml volumes prior to storage at -20ºC. For equilibration, the buffer was modified as either reducing or alkylating. For reduction, DTT (0.01 g/ml) was added and dissolved thoroughly. For alkylation, IAA (0.025 g/ml) was dissolved thoroughly in the buffer.

Table 2.5 Constituents of Equilibration buffer

Tris-Base	50mM
Urea	6M
SDS	2% (w/v)
Glycerol	30% (v/v)

2.10.3 Agarose sealing solution

Agarose sealing solution (1% w/v) was prepared in advance and stored at room temperature. The solution was heated gently to melt the agarose when need and applied on top of IPG strips during 2D IEF SDS-PAGE.

Table 2.6 Constituents of agarose sealing solution (1% w/v)

Agarose 1% (w/v)	1g
1X running buffer	100ml
Bromophenol blue	0.5% (w/v)

2.10.4 2-Dimensional IEF Gel Electrophoresis

Protein was extracted from *B. oleronius* as described in section 2.8. Protein was adjusted to 200µg using Bradford protein assay (section 2.8.2) and acetone precipitated over night at -20ºC assay (section 2.8.3). The protein sample was centrifuged at 13000 x *g* for 10 mins and acetone was discarded allowing the pellet to air-dry. IEF buffer (section 2.10.1) (100µl) was added and vortexed for 5 minutes until the sample pellet was solubilized. A further 25µl of IEF buffer with a few grains of bromophenol blue was added to the sample. The sample was applied to a 7cm coffin (Immobiline DryStrip pH 4-7; G.E. Healthcare). Prior to isoelectric focusing the strips were covered in Plus One drystrip cover fluid (GE Healthcare). Focussing was performed on an Ettan IPGphor II (Amersham Biosciences, NJ, USA) (Figure 2.1) system using the programme described in Table 2.7.

Following IEF, IPG strips were transferred directly to equilibration buffer (section 2.10.2). Strips were initially equilibrated in 5 ml reducing equilibration buffer (DTT; 0.01 g/ml) for 15 min. Strips were transferred to 5ml of alkylation buffer (IAA; 0.025 g/ml) for 15 min. Following equilibration IPG strips were rinsed briefly in 1X electrode running buffer. Strips were placed on top of homogenous 12.5% SDS-PAGE gels (section 2.9.7) and sealed with 1% (w/v) agarose sealing solution (section 2.10.3) once hand hot.

Table 2.7 Isoelectric focusing programme used for 2D IEF SDS-PAGE

Time	Volts	Mode
8 Hours	50	Gradient
15 minutes	250	Gradient
2 hours	1000	Gradient
4 hours	4000	Gradient
4 hours	8000	Gradient
4 hours	8000	Hold

Figure 2.1 Isoelectric focusing Ettan IPGphor II used in 2D IEF SDS-PAGE

Coffins containing the IPG strips and samples are placed in coffins on the isoelectric focusing machine for the first dimension separation during 2-Dimensional IEF SDS-PAGE.

2.11 Staining of gels and analysis of differential expression of proteins

2.11.1 Colloidal Coomassie staining of gels

Gels were placed in fixing solution directly after electrophoresis and stored in a 13cm petri dish on a rocker at room temperature overnight. Following fixing, the gels were rinsed in ddH_20 to hydrate for an hour until returning to original size. Water was removed and colloidal stain solution added to the gels. To this, 0.1g of SERVA Blue G (SERVA) was added per gel. Gels were stained for 1.2 days. All stain was rinsed off and gels were washed in dH_2O before scanning using LabScan™ 6.0 (Epson Scanner 10000XL software).

Table 2.8 Colloidal Coomassie Fixing Solution

Ethanol	50% (v/v)
Phosphoric Acid	3% (v/v)
dH_2O	47% (v/v)

Table 2.9 Colloidal Coomassie Stain Solution

Methanol	34% (v/v)
Phosphoric acid	3% (v/v)
Ammonium Sulphate	17% (w/v)
Serva Blue G	0.1 g
Distilled water	4% (v/v)

2.11.2 Image J densitiometrical analysis of Western blots

Image J software was used to identity differential expression of immunobands in 1D Western blots. All blots were carried out on at least three separate occasions, densitometrical values for bands showing differential expression were the average of all replicates achieved using the Image J programme (version 1.50i).

2.11.3 Progenesis SameSpots software for analysis of 2-Dimensional IEF Gels

2D electrophoresis gel images (in triplicate) were analysed using Progenesis SameSpots software (Nonlinear Dynamics) in order to assess the fold change in protein expression in larvae subjected to different treatments. The level of differential expression was analysed by ANOVA with *p*-values of ≤ 0.05 considered statistically significant for changes in expression.

2.12 Identification of proteins from SDS-PAGE gels

2.12.1 Preparation for spot/band excision

All micro-centrifuge tubes were fresh from the bag or placed in a sealed container and autoclaved before use. Tips were autoclaved and cut to varied lengths for spot cutting and subsequently tips and all other utensils in contact with the gel, scalpels, and blunt needles were soaked in acetonitrile prior to use to eliminate keratin contamination.

2.12.2 Trypsin Digest of peptides from 1-Dimensional and 2-Dimensional IEF SDS-PAGE gels

Processing of bands and spots for LC-MS/MS/MS analysis was achieved by following the method of Shevchenko *et al*. (2006). Gel pieces were cut and transferred to sterile micro-centrifuge tubes using a scalpel when required to ensure full saturation of gel piece for de-staining and digestion process. Gel pieces were de-stained by addition of 100µl of (100 mM Ammonium bicarbonate: Acetonitrile 1:1) ratio and subsequent vortexing every 10-15 minutes (x3).

Acetonitrile (500µl) was added to dehydrate and shrink gel pieces to the point where they became white. Acetonitrile was removed and the samples were stored at -20ºC or processed further immediately. Tryptic digestion was achieved with the addition of approximately 20-30µl trypsin buffer (~10 ng/µl trypsin enzyme prepared in trypsin reconstitution buffer; 10 mM ammonium bicarbonate, 10% (v/v) acetonitrile). Samples were placed at 4ºC to prevent trypsin auto-digestion and to allow for the penetration of trypsin buffer into the gel piece. Gel pieces were checked after 30 minutes to ensure they were sufficiently covered or if more trypsin

buffer was required. Samples were rechecked after a further 30 minutes for adequate coverage of gel pieces. If required gel pieces were topped up with trypsin reconstitution buffer (10 mM ammonium bicarbonate/10% (v/v) acetonitrile) to prevent drying out. The samples were transferred to the 37ºC orbital incubator overnight.

Digested samples were centrifuged on a desk top Tomy centrifuge and the supernatant was transferred to clean micro-centrifuge tubes. The samples were lyophilised in a vacuum centrifuge and stored at -20ºC or immediately re-suspended in 20µl 0.1% (v/v) formic acid and sonicated for 5 minutes. All samples were filtered through 0.22µM cellulose acetate spin filter tubes (Spin-X®, Costar) and transferred to mass spectrometry vials. Analysis of digested peptides was achieved using an Agilent 6340 Ion Trap LC-MS/MS/MS using acetonitrile elution.

2.12.3 Bioinformatic analysis of peptide identification results

The fragmented protein samples were eluted by LC-MS/MS/MS (Agilent 6340 Ion Trap) which determines the relative charge to mass ratio from detected ionized particles. These data were analysed using the mascot search engine to identify the protein (www.matrixscience.com). MASCOT scores above 67 were deemed to have a significant match ($p < 0.05$). The mass error tolerance was 1 Da allowing for a maximum of no more than two missed cleavages. Verification of protein sequences was confirmed by using the BLAST-P analysis programme on the Uniprot (www.uniprot.org) and NCBI (www.ncbi.nlm.nih.gov) websites.

2.13 Western Blotting

2.13.1 10X Tris Buffered Saline (TBS) pH 7.6

Tris-HCl (0.5M, 78.8 g/L) and NaCl (1.5M, 87.66 g/L) were dissolved in 1L dH_2O followed by adjustment of pH to 7.6 with addition of NaOH. TBS (10X) was autoclaved and stored at room temperature. TBS (10X) stock 1X TBS-Tween by making a 1/10 dilution with dH_2O and adding in Tween-20 (0.05% v/v) by stirring. The 1X TBS-Tween was used as a wash buffer and used within two days of preparation.

2.13.2 Transfer Buffer

Transfer buffer was made up on the day by dissolving the constituents to solubility as listed in Table 2.10 for a 1L stock. Transfer buffer was stored at 4ºC to keep cold until needed.

Table 2.10 Constituents of transfer buffer

Tris Base	3.03g
Glycine	14.4g
Methanol	200ml
dH_2O	800ml

2.13.3 Blocking Buffer

Bovine serum albumin (BSA) (1% w/v) was dissolved in 1X TBS-Tween by stirring and was filter sterilised through a 0.45µM filter (Millipore) and stored at 4ºC until required.

2.13.4 Diaminobenzidine tetra-hydrochloride (DAB)

DAB was prepared fresh on the day of developing Western blot membranes. The constituents were dissolved and poured onto the membrane. Table 2.11 list the volumes sufficient to develop two membranes.

Table 2.11 Constituents of DAB

Tris-HCl (100 mM) (pH 7.6)	30ml
Hydrogen Peroxide (30% v/v)	25µl
DAB (10mg w/v)	0.02g

2.13.5 Western Blot Protocol

Extracted protein form *B. oleronius* was separated by 1D SDS-PAGE (section 2.9.9) and resolved proteins were transferred onto nitrocellulose membrane (Fisher Scientific) for Western blotting performed by electro-blotting using a wet blotter (Mini Trans-Blot Cell, Bio-Rad). Prior to transfer to Whatman filter paper, nitrocellulose membrane and sponge inserts were soaked in transfer buffer. The 'Western blot sandwhich' was assembled and placed into the transfer cassette as follows; black end of cassette, sponge insert, filter paper, nitrocellulose membrane, SDS-PAGE gel, filter paper, sponge insert and red end of the cassette (Figure 2.2). Gentle pressure was applied to the sandwhich to remove any air bubbles before being positioned into the wet transfer rig apparatus (Bio-Rad Laboratories). An ice cooling block was added to the rig and the blot sandwhich was submerged in cold transfer buffer (section 2.13.2) before transferring at 70 V and 400 mA for 70 minutes using a power-pac 300 (Bio-Rad Laboratories).

Following protein transfer, the nitrocellulose membrane was blocked for 1 hour at 4ºC on a rocker in blocking buffer (section 2.13.3) to inhibit non-specific binding. Blocking buffer was poured off and the membrane was incubated in primary antibody (Table 2.12) overnight at 4ºC on a rocker. The primary antibody was poured off (re-stored at -20ºC) and the membrane was washed with 1X TBS-Tween for 1 hour changing the wash buffer frequently (every 10-15 minutes). The membrane was incubated in the appropriate anti IgG-HRP labelled secondary antibody for 2 hours on a rocker at room temperature (Table 2.12) and the wash step was repeated again.

Some blots were also developed using diaminobenzidine tetra-hydrochloride (DAB), where the washed blot was incubated in the DAB solution (section 2.13.4) for 10 minutes followed by washing in dH_2O and allowed to air dry. Western blot

images were recorded using an ImageScanner™ III (GE Healthcare, Life Sciences) and acquired using LabScan™ 6.0 (Epson Scanner 10000XL software). Immuno-bands were quantified using Image J software (section 2.11.2).

Table 2.12 List of antibody dilutions

Antibody	Source	Alexa Fluor® Dilution	Company	Reference
Anti 62 kDa (*B. oleronius*) (Primary)	Rabbit	1:5000 (v/v)	Generated in DCU	Lacey *et al.,* (2007)
Anti-Rabbit IgG HRP-Linked (Secondary)	Donkey	1:1000 (v/v)	Sigma	McMahon *et al.,* (2015)

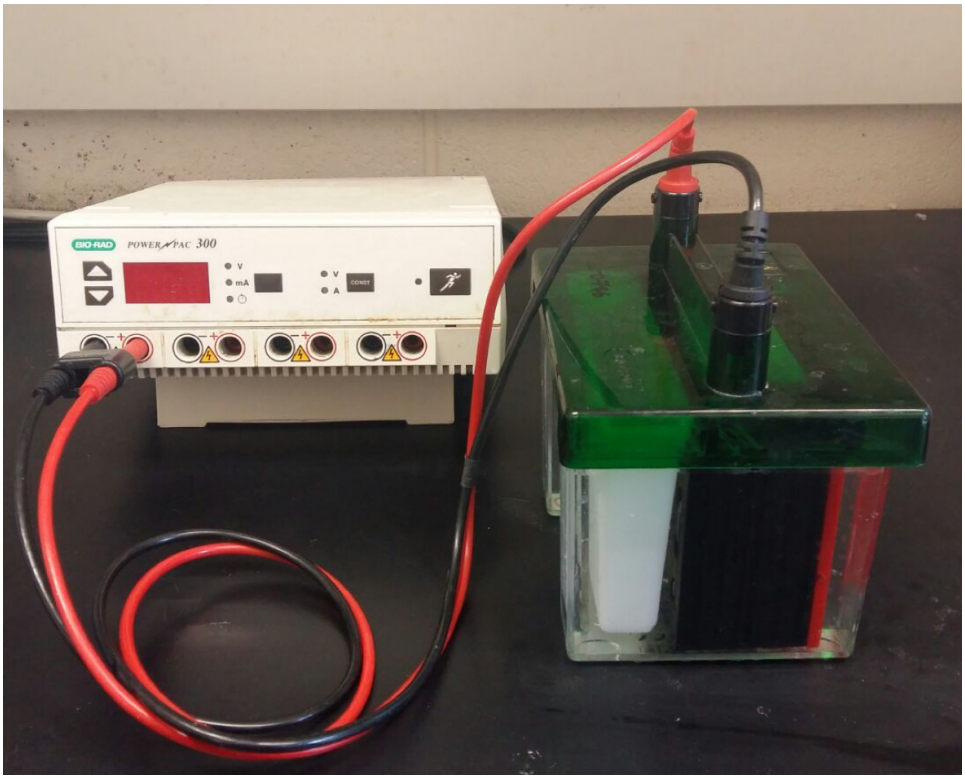

Figure 2.2 Western blot set-up with Mini Trans-blot cell by Bio-Rad.
The transfer rig apparatus contains the cassette with the 'Western blot sandwhich', an ice-block inserted alongside the cassette and the rig is filled with cold transfer buffer. The lid is connected to the power-pac 300 and the protein transfers from the cathode (black) to the anode (red).

2.14 In solution digest protocol for overnight peptide digestion for label free MS/MS proteomics

The list of buffers used for the in solution digestion of proteins in preparation for label free (LF-MS/MS) proteomics are presented below. Buffers were made fresh daily. Protease Max (Promega) was used in order for the trypsin (Promega) to digest the protein when using Urea and Thiourea. All water was deionised and was taken fresh before use from the deionised water dispenser.

Table 2.13 Sample resuspension buffer (pH8.0)

Urea	9.009g
Thiourea	3.806g
Tris-HCl	0.394g
ddH_20	25ml

Table 2.14 Ammonium bicarbonate (50 mM)

200 mM Ammonium bicarbonate		50 mM Ammonium bicarbonate	
Ammonium bicarbonate	0.394g	200 mM Ammonium bicarbonate	2.5ml
ddH_20	25ml	ddH_20	7.5ml

Table 2.15 Dithiothrietol (0.5 M)

DTT	0.077g
50mM Ammonium bicarbonate	1ml

Table 2.16 Idoacetamide (0.55 M)

Iodoacetamide	0.102g
50mM Ammonium bicarbonate	1ml

Table 2.17 ProteaseMAX solution and Trypsin solution

ProteaseMAX solution (1mg/100µl)		Trypsin solution (0.5µg/µl)	
PoroteaseMAX surfactant trypsin enhancer (Promega)	1mg	Sequence grade modified trypsin (Promega)	20µg
50mM Ammonium bicarbonate	100µL	Trypsin reconstitution buffer (Promega)	40µl

2.14.1 Protein preparation for label free MS/MS proteomics

Protein was extracted from control and treated cells as described in section 2.8. Protein concentration was corrected to 100µg using the Bradford protein assay (section 2.8.2) and acetone precipitated overnight (section 2.8.3). The samples were spun at 13000 x *g* for 10 minutes and allowed to air-dry. Protein was re-suspended in 25µl sample resuspension buffer (Table 2.13) and the sample was briefly vortexed to aid resuspension. The 50 mM ammonium bicarbonate (105µl) was added per sample (Table 2.14), followed by the addition of 1µl of 0.5M DTT (Table 2.15) and samples were incubated at 56ºC for 20 minutes. Samples were cooled at room temperature. The samples were alkylated by the addition of 2.7µl IAA (0.55 M) (Table 2.16) and incubated at room temperature in the dark for 15 minutes. The final solutions added to each sample were 1µl ProteaseMAX solution and 1µl trypsin solution (Table 2.17). The samples were wrapped in tinfoil and incubated at 37ºC in an orbital shaker for 24 hours. Protein enumeration was carried out using a Qubit fluorometer and the Qubit protein assay kit (Thermo Scientific). Protein concentrations for each sample determined by the Qubit protein assay were later used to adjust the samples to 1µg/µl just before they were loaded onto the Q-exactive MS.

2.15 Sample clean-up prior to loading on Q-exactive MS

The list of buffers for the sample clean-up to be used on Q-exactive MS using C18 spin columns (Thermo Scientific) are listed in Table 2.18. Buffers were made fresh directly before use. All water was deionised and was taken fresh before use from the deionised dispenser. The C18 columns are designed to trap only 30µg of protein and so is the final step of re-quantification before loading on the Q-exactive MS OrbiTrap. Care was taken to ensure the resin did not reach any flow through.

Table 2.18 Q-exactive MS clean-up buffers

Reagents	Sample buffer	Activation buffer	Equilibration Buffer	Wash Buffer	Elution buffer
TFA	20µl (2%)	-	25µl (0.5%)	25µl (0.5%)	-
Acetonitrile	200µl (20%)	2.5ml (50%)	250µl (5%)	250µl (5%)	700µl (70%)
ddH_2O	780µl (78%)	2.55ml (50%)	4.725ml (94.5%)	4.725ml (94.5%)	300µl (30%)

Digested protein samples (following digestion according to (section 2.14.1)) were briefly spun in a microfuge to collect any condensate, straight from the 37ºC incubator following overnight peptide digestion. TFA to a concentration of 0.75% (v/v) of the total volume of sample was added (approximately 0.75µl), vortexed briefly and incubated at room temperature for 5 minutes. The sample may appear cloudy at this stage but this is normal. Samples were spun at 13000 x *g* for 10 minutes to remove any debris that may have formed overnight, and the supernatant transferred to a fresh tube. Samples were mixed at a ratio (3 parts sample: 1 part sample buffer).

PierceTM C18 spin columns (Thermo Scientific) were tapped briefly to settle the resin, and the protective caps were removed from either end. Holes were pierced in the lid of sterile micro-centrifuge tubes to place C18 spin columns into (Figure

2.3). Resin was activated using 200µl of activation buffer, added to the top of the resin, and spun at 1500 x *g* for 1 minute. Flow through was discarded and the process repeated twice. Equilibration buffer (200µl) was added to the column, spun for 1 minute 1500 x *g* and the flow through discarded and repeated once more. Samples were loaded to the top of the resin in the C18 column, and a fresh receiver tube placed underneath. Tubes were spun at 1500 x *g* for 1 minute, flow-through collected, and placed back onto the resin. This was repeated three times to ensure complete peptide binding to the C18 resin. C18 columns were placed in a fresh receiver micro-centrifuge tube, and 200µl of wash buffer added. This was then spun at 1500 x *g* for 1 minute, flow through discarded, and the process repeated twice more to remove containments such as urea and ammonium bicarbonate. Column was placed over a fresh receiver tube, this time with the lid open and no hole pierced through the lid, and 20µl of elution buffer added to the top of the resin bed. The tubes were spun at 1500 x *g* for 1 minute and the flow-through untouched. This was repeated twice more to obtain a final volume of 60µl in the receiver micro-centrifuge tube, hence the cleaned peptide sample and the column can be disposed of. Samples were then dried down in a SpeedyVac and stored at -20ºC until running on the Q-exactive MS.

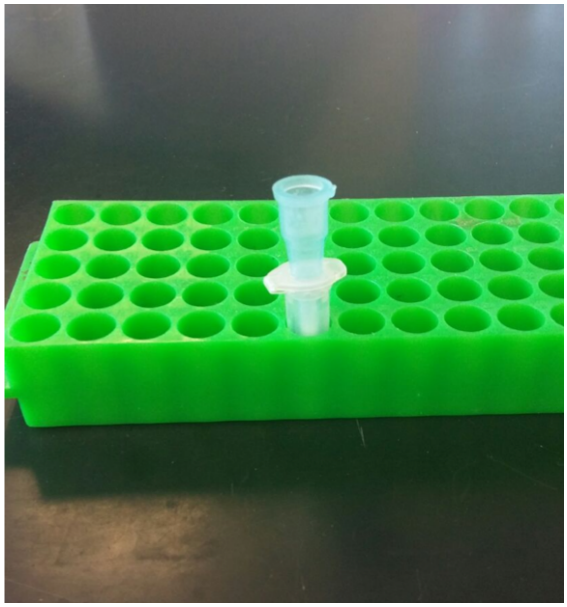

Figure 2.3 C18 spin column placed in 1.5ml micro-centrifuge tubes.
The lid of the micro-centrifuge tube is closed with a hole pierced in the top to comfortably fit the C18 spin column. This ensures the bottom part of the spin

column which contains the resin is kept away from any liquid during the clean-up process.

2.16 Preparation of sample prior to loading on Q-exactive MS

The protein concentration of each sample (from Qubit protein assay) was used to determine the volume of sample loading buffer needed to achieve peptide resuspension at a concentration of 1µg/µl. The samples were re-suspended in loading buffer (0.05% (v/v) TFA, 2% (v/v) Acetonitrile), vortexed for 30 seconds and placed in a water bath for sonication for 5 minutes. Samples were spun at 13000 x *g* for 5 minutes at room temperature to pellet any insoluble material and 30µl of the supernatant transferred to vials (VWR).

2.17 Parameters for running samples on Q-exactive MS

One microliter of peptide mix was eluted onto the Q-exactive MS, a high resolution accurate mass spectrometer connected to a Dionex Ultimate 3000 (RSLCnano) chromatography system. Peptides were separated by an increasing acetonitrile gradient on a Biobasic C18 Picofrit^{TM} column (100 mm length, 75 mm ID) using 180 minute reverse phase gradient at a flow rate of 250 ml/min. All data were acquired with the mass spectrometer operating in automatic data dependent switching mode. A high-resolution MS scan (300-2000 Dalton) was performed using the Orbitrap to select the 15 most intense ions prior to MS/MS.

2.18 Parameters for analysing quantitative results and statistical analysis

Protein identification from the MS/MS data was performed using the Andromeda search engine (Cox *et al*., 2011) in MaxQuant (version 1.2.2.5) (http://maxquant.org/) to correlate the bacterial data (*B. oleronius*) or human data (HEp-2 cells) against a database, depending on the experiment. The following search parameters were used: first search peptide tolerance of 20 ppm, second search peptide tolerance 4.5ppm with cysteine carbamidomethylation as a fixed modification and Nacetylation of protein and oxidation of methionine as variable modifications and a maximum of 2 missed cleavage sites allowed. False Discovery Rates (FDR) were set to 1% for both peptides and proteins and the FDR was

estimated following searches against a target-decoy database. Peptides with minimum length of seven amino acid length were considered for identification and proteins were only considered identified when more than one unique peptide for each protein was observed. Results processing, statistical analyses and graphics generation were conducted using Perseus (version 1.5.5.3).

LFQ intensities were $\log^2$ -transformed and ANOVA of significance and *t*-tests between the proteomes of control and treated samples was performed using a *p*-value less than 0.05 and significance was determined using FDR correction (Benjamini-Hochberg). Proteins that had non-existent values (indicative of absence or very low abundance in a sample) were included in the study only when they were completely absent from one group and present in at least three of the four replicates in the second group (referred to as qualitatively differentially abundant proteins). The Blast2GO suite of software tools was utilized to assign gene ontology terms (GO terms) relating to biological processes (BP), molecular function (MF) and cellular component (CC). Enzyme commission numbers and Kyoto Encyclopedia of Genes and Genomes (KEGG) pathway mapping was performed as part of the Blast2GO annotation pipeline.

2.19 Susceptibility assay for quantifying bacterial cell growth

Overnight liquid cultures of bacteria were prepared (section 2.5) and were read on a spectrophotometer (Eppendorf Biophotometer) at an optical density (OD) of OD_{600nm} to determine protein quantity. An OD of 0.1 estimated $1x10^6$ bacterial cells/ml. Fresh sterile media (100µl) was added to a 96-well plate (corning Incorporated Costar®) followed by the addition of the compound of interest (e.g. Oriel salt solution) with serial dilutions as required. Bacterial cells (100µl of $1x10^6$ cell/ml stock) were added to all 96 wells and the plates were incubated for 24 hours at 30ºC. The growth of each treatment was read at OD_{600nm} using a microplate reader (Boi-Tec® Synergy HT). The OD of each treated sample was compared to the control sample (i.e. with no compound of interest present) in order to determine the susceptibility of bacterial cell growth in the presence of the compound of interest.

2.20 Preparation of bacteria for confocal microscopy

B. oleronius was cultured overnight (section 2.5) at 30°C and 37°C. Cells were harvested by centrifugation at 3000 x *g* for 15 minutes and washed twice in PBS. Cells were fixed in 3.7% (v/v) formaldehyde for 10 minutes, washed twice, permeabilised in 2% (v/v) Triton X-100 for 10 minutes and washed twice. Cells were heat fixed at 37°C for 5 minutes and slides (Silane-Prep) were immersed three times in PBS before the cells were blocked for one hour with 1X Tris-buffered saline (TBS) Tween (0.05%, v/v) (pH 7.6) containing 1% (w/v) BSA. Slides were washed in PBS and incubated overnight at 4°C once primary antibody was added (Table 2.12). Slides were washed in 1X TBS Tween-20 three times and secondary antibody (1:500 Alexa Fluor® 594 anti-rabbit IgG or 1:1000 Alexa Fluor® 488 anti-rabbit IgG, Molecular Probes) was added for two hours in the dark at room temperature. Slides were washed once again, diamidino-2-phenylindole (DAPI) was added at room temperature for 10 minutes, slides were immersed in PBS and allowed to dry Following coverslip application and sealing. Cells were viewed using the Olympus FluoView 1000 confocal microscope (Version 3.0).

2.21 Fractionation and purification of *B. oleronius* antigen with Q-Sepharose™ Performance Beads and ÄKTA-FPLC

2.21.1 FPLC Binding buffer (pH 4.8)

Piperazine (20 mM) and 10 mM NaCl were dissolved in dH_2O, autoclaved and stored at 4ºC. The buffer was filtered through a 0.22µM disc before application to the ÄKTA FPLC.

2.21.2 FPLC Elution buffer (pH 4.8)

Piperazine (20 mM) and 1 M NaCl were dissolved in dH_2O, autoclaved and stored at 4ºC. The buffer was filtered through a 0.22µM disc before application to the ÄKTA FPLC.

Figure 2.4 ÄKTA-FPLC with attached column containing Q-Sepharose™ beads and *B. oleronius* protein sample

2.21.3 Protocol for *B. oleronius* protein purification using Q-Sepharose™ charge separation

B. oleronius was cultured and protein lysate was extracted (section 2.5) and filter sterilised using 0.45µM disc. The crude protein sample was inverted with washed Q-Sepharose™ beads at 4ºC overnight. The column attached to the ÄKTA and washed with binding buffer (section 2.21.1) before the sample/beads were inserted into the column. Binding buffer continued to be flushed through the column for 30 minutes (Figure 2.4). The elution buffer (section 2.21.2) was introduced through the column at a flowrate of 0.5ml/minute for 30 minutes and fractions were collected as the linear gradient increased. Once a 50:50 ratio between binding buffer and elution buffer was reached, fractions were collected for a further 30 minutes.

The elution buffer was set to 100% flowrate at 0.5ml/minute for 30 minutes. The fractions were collected and resolved by 1D SDS-PAGE (section 2.9) prior to Western blotting with anti-62 kDa rabbit antibody (section 2.13). The fractions containing the antigen of interest were pooled and filter concentrated using 3000 molecular weight Vivaspin®-20 filter columns (Viva products, GE Healthcare) at 3500 x *g* for 30 minutes. The concentrated sample was quantified using the Bradford method (section 2.8.2), acetone precipitated (section 2.8.3) and the pellet was re-suspended in sterile PBS to give a stock concentration of 200µg/ml. The antigen preparation was stored at -20ºC until required.

2.22 General HEp-2 cell culture methodology

2.22.1 HEp-2 cell line

HEp-2 cell line (ATCC CCL23, derived from an epidermoid carcinoma of the larynx) was obtained from the American Type Culture Collection (Maryland, USA). The HEp-2 cells were grown in 25cm^2 tissue culture flasks (Sarstedt) containing Eagles minimum essential medium (MEM) supplemented with 5% (v/v) foetal calf serum (FCS) and 2% (v/v) glutamine (GIBCO Laboratories) and incubated at 37ºC in a humidified atmosphere containing 5% CO_2. Cells were sub-cultured by trypsinisation every 3-5 days.

2.22.2 Sub-culturing HEp-2 cell line

Cell medium was poured into a waste bottle and 1 ml of trypsin solution (1ml Trypsin (GIBCO): 9ml PBS) was used to rinse out the remaining medium. The trypsin solution (5ml) was added into the 25cm^2 tissue culture flask and placed in an incubator at 37ºC, 5% CO_2 for 3-4 minutes. The flask was removed from the incubator and examined under an inverted microscope to ensure the successful dislodgement of HEp-2 cells from the flask surface into solution. MEM (5ml) was added to the flask to neutralise the trypsin solution and the cells were gently poured into a sterile tube and harvested by centrifugation at 1500 x *g* for 5 minutes. Medium was poured off and the pellet of cells was gently re-suspended in 4ml of pre-heated fresh culture medium. The cells were reseeded by pipetting 2ml of cells into a fresh 25cm^2 flask containing 5ml pre-heated MEM.

2.22.3 Cryopreservation of HEp-2 cell line in Liquid Nitrogen N_2

Cells were cultured to the exponential phase of growth (approximately 60% confluency) and harvested by trypsinization (section 2.22.2). Cryopreservation buffer (50% (v/v) MEM, 40% (v/v) FCS and 10% (v/v) DMSO) was prepared on the day, filter sterilised through a 0.22μM filter (Millipore) and stored on ice until needed. The HEp-2 pellet of cells was re-suspended in 1ml MEM medium and 1ml cryopreservation buffer was gently added drop-by-drop. The cell suspension was divided into two cryovials (Thermo Scientific) and stored at -80ºC overnight before being placed into a liquid N_2 tank for long term storage.

2.22.4 Recovery of HEp-2 cell line from Liquid N_2

The cells were recovered from liquid N_2 and the thawing process was performed quickly to promote cell viability. The cells were swiftly pipetted into a tube containing 9ml pre-warmed medium (section 2.22.1) and centrifuged at 1500 x *g* for 3 minutes. Supernatant was poured off and cell pellet was re-suspended in 5ml MEM and centrifuged once more. Medium was poured off and recovered cells were re-suspended in 1ml pre-warmed MEM prior to being pipetted into a 25 cm^2 tissue culture flask which contained 5ml pre-warmed MEM. Cells were incubated at 37ºC in a humidified atmosphere containing 5% CO_2 to attach overnight. Medium change was carried out the next day to remove unattached cells.

2.23 General hTCEpi cell culture methodology

2.23.1 hTCEpi cell line

Human telomerase-immortalized corneal epithelial cells (hTCEpi) (sourced from Tissue Engineering Lab, NICB, DCU) were maintained in Keratinocyte Basal Medium (KBM™)-Gold supplemented with KBM™-Gold SingleQuot™ kit containing growth factors (bovine pituitary extract (BPE), human epidermal growth factor (rhEGF), insulin, hydrocortisone, transferrin and epinephrine) (Lonza) hTCEpi cells were incubated at 37ºC in a humidified atmosphere containing 5% CO_2. Cells were sub-cultured by trypsinisation every 3-5 days depending on culture confluency.

2.23.2 Sub-culturing hTCEpi cell line

Cell medium was poured into a waste bottle and 2ml of trypsin solution (0.05% (v/v) trypsin and 0.02% (w/v) EDTA dissolved in PBS) was used to rinse out the remaining medium. The trypsin solution (2ml) was added into the 25cm^2 tissue culture flask and placed in an incubator at 37ºC, 5% CO_2 for 3-4 minutes. The flask was removed from the incubator and examined under an inverted microscope to ensure the successful dislodgement of hTCEpi cells from the flask surface into solution. KBM™-Gold medium (5ml) containing 10% (v/v) FCS was added to the flask to neutralise the trypsin solution and the cells were gently poured into a sterile tube and harvested by centrifugation at 1500 x *g* for 5 minutes. Medium was poured off and the pellet of cells was gently re-suspended in 1ml medium. Cells were added to 4ml medium and centrifuged at 1500 x *g* for 5 minutes. Medium was poured off and cells were re-suspended in 2ml pre-heated culture medium. The cells were reseeded by pipetting 1ml of cells into a fresh 25cm^2 flask containing 6ml KBM™-Gold medium.

2.23.3 Cryopreservation of HEp-2 cell line in Liquid Nitrogen N_2

Cells were cultured to the exponential phase of growth (approximately 60% confluency) and harvested by trypsinization (section 2.23.2). Cryopreservation buffer (40% (v/v) KBM, 40% (v/v) FCS and 20% (v/v) DMSO) was prepared on the day, filter sterilised through a 0.22μM filter (Millipore) and stored on ice until needed. The hTCEpi pellet of cells was re-suspended in 1ml KBM™-Gold medium and cells were enumerated to 1x10^6 cells/ml. A ratio (1:1) of hTCEpi cells to cryopreservation buffer was performed of which 1ml was transferred to each cryovial (Thermo Scientific) and stored at -80ºC overnight before being placed into a liquid N_2 tank for long term storage.

2.23.4 Recovery of hTCEpi cell line from Liquid N_2

The cells were recovered from liquid N_2 and the thawing process was performed quickly to promote cell viability. The cells were swiftly pipetted into a tube containing 9ml pre-warmed medium (section 2.23.1) and centrifuged at 1500 x *g* for 3 minutes. Supernatant was poured off and cell pellet was re-suspended in 5ml KBM™-Gold medium and centrifuged once more. Medium was poured off and recovered cells were re-suspended in 1ml pre-warmed KBM™-Gold medium prior

to being pipetted into a 25 cm^2 tissue culture flask which contained 5ml pre-warmed medium. Cells were incubated at 37ºC in a humidified atmosphere containing 5% CO_2 to attach overnight. Medium change was carried out the next day to remove unattached cells.

2.24 Acid phosphatase assay for determining toxicity on cell growth

Confluent cells were trypsinized, enumerated and used to seed 96-well plates (Corning Incorporated Costar®) at a density of $3x10^4$ cells/well in 100µl culture medium and cells were incubated overnight to attach. The compound of interest (e.g. mucin) was freshly prepared the next day and added to the 96-well plate (corning Incorporated Costar®) with serial dilutions as required. The positive control had 100µl culture medium added to have a total of 200µl per well. The plates were incubated at 37ºC and 5% CO_2 for 5-7 days prior to the quantification of cell growth. Following incubation, medium containing test compounds was removed from each well, and the attached cells were washed with PBS twice to three times. To each well, 100µl of acid phosphatase buffer (0.1 M sodium acetate, 0.1% (v/v) Triton-X 100, 10 mM p-nitrophenyl phosphate (pH 5.5)) was added and the plates were incubated at 37ºC and 5% CO_2 for 1.5 hours. The reaction was stopped with the addition of 50µl of 1M NaOH per well and colour development was assayed at 405nm using a microplate reader (Boi-Tec® Synergy HT). The percentage growth of cells with regard to the control cells in the presence of a compound of interest was determined.

2.25 qRT-PCR analysis of hTCEpi gene expression

2.25.1 RNA extraction from hTCEpi cells

hTCEpi cells were seeded (cells/well) into 6-well plates and incubated overnight to attach (section 2.23.2) before being exposed to purified *B. oleronius* 62 kDa antigen (section 2.21) for 72 hours. For RNA extraction, the 6-well plate was placed on ice, media was removed and 1ml Tri-Reagent was added per well. Wells were scraped with pipette filter tips and transferred to sterile Eppendorf tubes. Samples were kept on ice when possible and everything was treated with RNase-Zap.

In brief, 200µl chloroform was added per sample, inverted 10 times and stored at room temperature for 15 minutes. Samples were centrifuged at 16000 x *g* at 4ºC for 15 minutes. The top layer was transferred to a fresh tube and 500µl 2-propanol was added. The tube was inverted 10 times and stored at room temperature for 15 minutes. Samples were centrifuged at 16000 x *g* at 4ºC for 30 minutes. The supernatant was discarded and the pellet was washed in 750µl of 75% (v/v) ethanol and vortex for 10 seconds before being centrifuged at 16000 x *g* at 4ºC for 15 minutes. This wash step was repeated once more. The supernatant was removed and pellets were air-dried for 5 minutes. The pellet was re-suspended in 10µlnuclease-free water (Sigma LifeScience) and RNA concentration was determined using a NanoDrop spectrophotometer (ND-1000; Labtech International). RNA samples were stored at -80ºC or immediately used for cDNA synthesis.

2.25.2 cDNA synthesis

cDNA was synthesised according to the manufacturer's instructions using the high-capacity RNA-to-cDNA kit (Applied Biosystems). RNA was calculated to give a cDNA concentration of 2µg/20µl (i.e. 100ng/µl). RNA was added to the constituents of the RNA-to-cDNA kit which included 2X RT buffer, 20X RT enzyme buffer and nuclease-fee water to bring the total volume to 20µl. The samples were prepared and briefly centrifuged to spin contents down and remove any bubbles before reverse transcription. Samples were run in a cDNA synthesis programme using the cDNA thermocycler (T3 Thermocycler, Biometra) which involved three steps; incubation at 37ºC for 60 minutes, 95ºC for 5 minutes and 4ºC holding. cDNA was aliquoted and stored at -20ºC.

2.25.3 Quantitative Real-time polymerase chain reaction

The TaqMan® fast universal PCR master mix (2X) kit (Applied Biosystems) was used to prepare cDNA and primers for qPCR. Two master mixes were prepared on ice, the first contained 10µl, 2X TaqMan fast master mix, 1µl 20X TaqMan gene and 4µl nuclease-free water (sufficient for single reaction) and the second contained the 0.2µl [100ng/µl] cDNA and 4.8µl nuclease-free water (sufficient for single reaction). Amplification of IL-8, TNFα and IL-1β targets were performed using TaqMan gene expression assays (Hs00174103_ml, Hs00174128_ml and

Hs01555410_ml, respectively) on conjunction with the ABI 7500 fast real-time PCR thermal cycler (Applied Biosystems).

2.26 Wound healing assay

To test the effect of bacterial antigens on wound healing, HEp-2 cells ($1x10^6$ cells/well) and hTCEpi cells ($2x10^5$ cells/well) were cultured in 6 well plates and supplemented with MEM and KGM-2 medium respectively, until a confluent layer was achieved. A scratch wound the length of the well was made vertically across the cell layer using a 200µl pipette tip. The plate was washed with PBS to remove cell debris and 1ml cell medium was added per well. The antigen/blocking agents were prepared and incubated in 1ml aliquots at 37ºC for at least 1 hour, before being added into the well. The plates were wrapped in tinfoil and incubated at 37ºC and 5% CO_2 for 24, 48 and 72 hours. Media from each well was collected at each time-point (i.e. the cell secretome) and stored at -20ºC until required.

2.27 ELISA protocol to detect secreted cytokine expression levels

The effect of cytokine secretion on HEp-2 cells and hTCEpi cells was determined from the secretome of a 72-hour wound healing assay (section 2.26). The secretion levels of the expressed cytokines IL-8, TNFα, IL-1β and IL-6 were measured using commercial ELISA kits (Mabtech) according to the instructions given in the manufacturer's guidelines (Table 2.19) and all ELISAs were carried out in triplicate. The ELISAs were set up in 96-well plates with 100µl of coating antibody per well and stored overnight at 4ºC. Each of the coating antibodies were diluted in sterile PBS (pH 7.4).

The following day, wells were rinsed twice with 200µl per well of wash buffer (100ml PBS and (0.05% v/v) Tween). Plates were treated with 100µl incubation buffer per well (100ml PBS, (0.01% w/v) BSA and (0.05% v/v) Tween) and stored for 1 hour incubation at room temperature. Contents were removed and wells were washed five time with wash buffer (200µl per well). The HEp-2 and hTCEpi secretome samples were quantified using the Bradford method (section 2.8.2), prepared for ELISA and 100µl sample or standard was added per well. The

plates were incubated at room temperature for 2 hours. The contents were removed and the plates were rinsed five time with wash buffer as before. The detection antibody was prepared (Table 2.19) and 100µl added per well, incubated for 1 hour at room temperature. The contents were removed and the plates were rinsed five time with wash buffer as before, followed by the addition of 100µl per well streptavidin-HRP and plates were incubated for one hour at room temperature. Plates were rinsed five times with wash buffer (200µl per well) before 100µl per well of substrate solution was added, which in this case was 100% (v/v) TMB (3,3',5,5'-Tetramethylbenzindine, Moss, Inc.). The plate was stored for 15 minutes at room temperature and 100µl stop solution was added per well (0.5 M HCl) (Figure 2.5). Each ELISA plate was read at a specific absorbance wavelength according to the manufacturer's instructions using a microplate reader (Boi-Tec® Synergy HT).

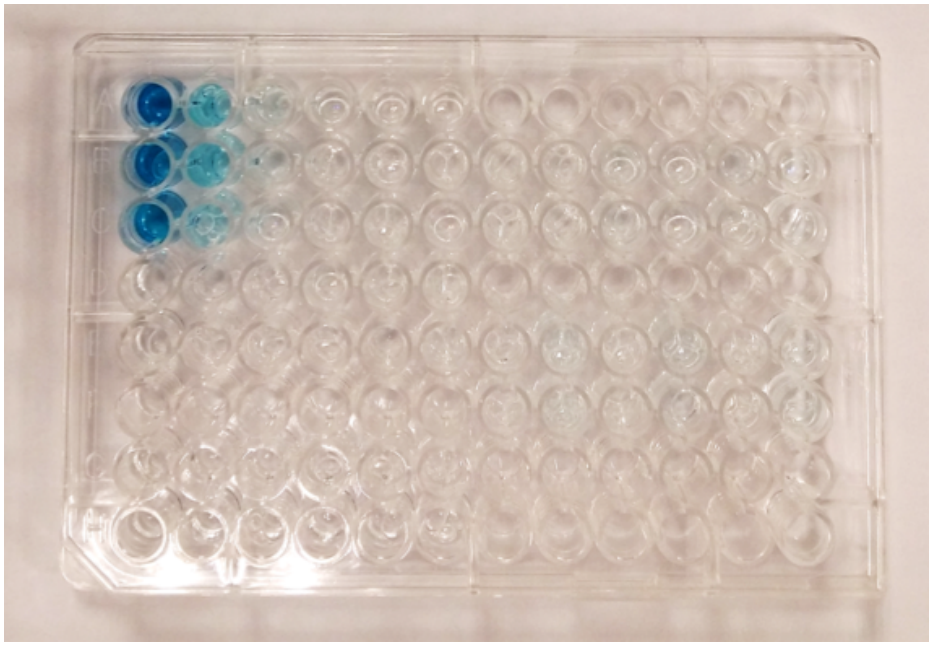

Figure 2.5 Example of ELISA plate with colour development following the addition of stop solution.

Table 2.19 ELISA buffers for detecting expression levels of cytokines

Cytokine Target	Product code	Capture Antibody Concentration	Detection Antibody Concentration	Enzyme Substrate
IL-8	3560-1H-6 (Mabtech)	mAb8H6 2µg/ml	MT8f19-biotin 1µg/ml	Streptavidin-HRP/TMB
TNFα	3510-1H-6 (Mabtech)	mAb TNF3/4 2µg/ml	mAb TNF5-biotin 1µg/ml	Streptavidin-HRP/TMB
IL-1β	3415-1H-6 (Mabtech)	mAb 1L1β-I 2µg/ml	mAb 1L1β-II-biotin 1µg/ml	Streptavidin-HRP/TMB
IL-6	3460-1H-6 (Mabtech)	mAb 13A5 0.5µg/ml	mAb 39C3-biotin 1µg/ml	Streptavidin-HRP/TMB

2.28 Pilot study for the comparison of Oriel Sea Salt on rosacea patient skin

Pilot studies were conducted under the supervision of Professor Ryszard Zaba at the Department of Clinical Dermatology, University of Medical Sciences, Poznan, Poland. Ethical approval was granted by the Ethics committee of the University of Medical Sciences, Poznan, Poland on July 30th 2015 (section 2.28.2) and January 30th 2016 (section 2.28.3). The trial was not registered with a trial database and patients were not given a choice between cream/gel formulation. No placebo was used but patients were compared before and after treatment. Patient recruitment was provided by volunteering patients attending the clinic. Permission for use of patient photographs was given to clinicians in Poland. For statistical basis, we aimed to have ten patients with one of the two subtypes (ETR or PPR), however this depended on numbers turning up to the clinic. My direct role was interpreting the data and carrying out statistical analysis of the study.

2.28.1 Parameters measured throughout patient pilot studies

Five parameters were measured throughout both pilot studies which included the level of erythema, melanin, sebum, transepidermal water loss (TEWL) and moisture. The erythema and melanin were evaluated on the basis of reflectance spectroscopy, whereby the redness is the difference between the melanin absorbance and the absorbance of the green filter, using the Colour Meter II (Cortex Technology). The sebum levels were determined using the probes of Cutometer

MPA 580. The TEWL level was evaluated using the Tewameter TM 300 (Courage-Khazaka) according to manufacturer's guidelines of the standardisation group of the European Society of Contact Dermatitis. A minimum of 20 measurements were recorded and expressed as a mean value in SI units (g/m2/h) with the normal range set between 0-25 g/m2/h. The moisture levels were evaluated by measuring the hydration of the stratum corneum (SC, Cornometry), aided by the Cornometer CM 825 (Courage-Khazaka). The basis for this measurement is that water has a dielectric constant of 81 and anything below this is classified as dry skin. A normal value of hydration here was accepted as a score higher than 40. Five measurements were recorded to give a mean value in accordance with manufacturer's guidelines.

2.28.2 Pilot Study One

Twenty patients with subtype one and/or two (ETR and PPR) participated in this pilot study. The average patient age of the trial was 47.85 years and the group consisted of 11 male and 9 female patients. Patients were instructed to apply Oriel sea salt cream or gel formulation onto their face twice to three times daily for 7 days. Patients were instructed not to apply other topical formulations to the face during this time. The concentration of the Oriel cream and Oriel gel used was 0.3% (w/v) and was prepared by Oriel Company. The parameters of each patient were measured before the trial commenced and after one week of treatment at the end of the trial (section 2.28.1).

2.28.3 Pilot Study Two

Ten patients with subtype one (ETR) and in some cases subtype two (PPR) participated in this pilot study. The average patient age of the trial was 48 years and the group consisted of 2 male and 8 female patients. Patients were instructed to apply Oriel sea salt cream onto the face twice to three times daily for 2 weeks. Patients were then instructed not to apply anything (including Oriel cream) to the face for two further weeks, in order to determine the prolonged effect of Oriel cream formulation on the skin. Patients were instructed not to apply any other topical formulations to the face during the 4 week period of the trial. The concentration of the Oriel cream used was 0.6% (w/v) and was prepared by Oriel Company. The parameters of each patient were measured before the trial commenced, after two weeks of treatment and after four weeks at the end of the trial (section 2.28.1).

Chapter Three

An Analysis of the Effect of Temperature on *Bacillus oleronius*

3.1 Introduction

Rosacea is an inflammatory dermatological condition with symptoms ranging from flushing, erythema, rhinophyma and the development of papules and pustules across the central region of the face (Jarmuda *et al*., 2012; Del Rosso, 2004). Rosacea patients often experience burning sensation and increased flushing in the face which is linked with the increased presence of blood vessels close to the skin surface (Yamasaki & Gallo, 2009; Guzman-Sanchez *et al*., 2007). This can result in vasodilation and telangiectasia, both prominent features of rosacea, which may contribute to an elevated skin temperature (Woo *et al*., 2016; Guzman-Sanchez *et al*., 2007). The condition may arise in patients who display a genetic predisposition associated with abnormal dermal immune responses and interplay with a variety of triggering factors including psychological, occupational or emotional states of rosacea patients (Woo *et al*., 2016; Wilkin *et al*., 2004). Many factors can induce rosacea, some of which expedite facial erythema and result in elevated facial temperature. Dietary triggers are commonly associated as flushing triggers for some rosacea patients, for example spicy foods, hot beverages and alcohol, which can induce vasodilation and edema (Guzman-Sanchez *et al*., 2007; Crawford *et al*., 2004; Wilkin, 1981).

Many organisms inhabit the skin microbiome, some of which live commensally and play a role in the pathogenesis of rosacea (Holmes, 2013). *Demodex* mites physically disrupt the skin barrier function and protrude through the skin resulting in papule and pustule development (Elston & Elston, 2014). *D. folliculorum* mites are present in higher densities of rosacea skin and harbour the bacterium associated with this inflammatory condition, *B. oleronius* (Woo *et al*., 2016; Jarmuda *et al*., 2012). Rosacea can be treated with a range of antibiotics (e.g. tetracycline; metronidazole) which clearing the skin of inflammation and symptoms, however cycles of remission and relapse are characteristic of a bacterial role in the condition (Margalit *et al*., 2016; Gupta & Chaudhry, 2005; Dahl *et al*., 1998).

The symptoms and trigger factors of rosacea increase the temperature of the skin which may induce a heat shock response in bacteria of the skin microbiome. Bacterial isolates from rosacea skin, such as *S. epidermidis*, have shown increased secretion of proteins in comparison to control isolates, and significantly more

proteins at 37°C than 30°C when cultured (Dahl *et al*., 2004). Rosacea skin has been shown to have increased blood flow and a lower pain threshold in response to heat when compared with control skin, thus rosacea patients have heightened facial flushing and burning sensations (Guzman-Sanchez *et al*., 2007). The skin of rosacea patients is at a raised temperature, due to the characteristic symptoms of the condition, including enhanced vasodilation of blood vessels and inflammation (Dahl *et al*., 2004). Inflammation is the first visible line of defence in the skin, represented by erythema on the central region of the face. *B. oleronius* antigens are immune-reactive in sera of most rosacea patients and are capable of activating neutrophils via the IP3 pathway (McMahon *et al*., 2016) leading to the secretion of MMP 9 and cathelicidin (O'Reilly *et al*., 2012a; Jarmuda *et al*., 2014). In particular, the 62 kDa protein which shares homology to the mammalian HSP GroEL, induces the strongest immune response in rosacea patients (Jarmuda *et al*., 2014; O'Reilly *et al*., 2012c).

Bacteria adapt to stress induced conditions in order to survive undesirable environments. Such adaption may be influenced by alteration in pH, temperature, salt stress or nutrient deprivation. It has been postulated that the elevated temperature of rosacea skin may affect the growth of *B. oleronius* and alter the production of the immune-stimulatory 62 kDa protein. The proteomic profile of *B. oleronius* was further studied to assess the level of protein abundance at 37°C in comparison to 30°C. The heat shock response is recognised in many bacteria and follows the upregulation of heat-induced regulons such as SigB and HrcA (Voigt *et al*., 2013). Temperature stressed conditions can produce mis-folding and denaturation of proteins which can be harmful to the skin. Classic heat shock proteins commonly upregulated include chaperones DnaK and GroEL which aid in the recovery of denatured proteins (Voigt *et al*., 2013; Periago *et al*., 2002). Elongation factor Tu is one of the most abundant bacterial proteins, which protects the cell against thermal stress and also plays a key role in ribosomal translation (Caldas *et al*., 1998; Pereira *et al*., 2015). Many elongation factors influence protein synthesis which is of key importance for the production of stress proteins and HSPs to help overcome heat stress. The production of stress related proteins such as 60 kDa chaperonin, putative phosphoesterase and universal stress protein can trigger the innate immune system leading to macrophage activation and neutrophil recruitment. Increased densities of

Demodex mites in rosacea introduce higher levels of *B. oleronius* into the pilosebaceous unit. Along with the higher skin temperature of rosacea patients, these cofactors may enhance the production of immune-stimulatory proteins by *B. oleronius*. Thus, promote excessive inflammation within the skin microbiome and exacerbate characteristic symptoms of the condition such as erythema and telangiectasia. Therefore, the aim of this research was to assess the effect of temperature on the cell density of *B. oleronius* over 72 hours, to measure the level of 62 kDa antigen expression and to investigate the proteomic differences of *B. oleronius* at these temperatures.

3.2 The effect of temperature on cell growth of *B. oleronius* over 72 hours

B. oleronius was grown in two different growth media, nutrient broth (NB) and 2X yeast tryptone broth (2XYT), as described in section 2.5. Cultures were grown at 30ºC and 37ºC for 72 hours. *B. oleronius* grew optimally in the minimal medium (NB) at 30ºC and reached the stationary phase of growth at 18 hours, while at 37ºC the culture failed to reach the stationary phase by 72 hours (Figure 3.1). In 2XYT cultures, *B. oleronius* grew optimally at 30ºC in comparison to 37ºC and cell density was higher in 2XYT medium in comparison to NB, as 2XYT is a more nutrient rich medium (Figure 3.2). Cells were grown for 72 hours until an OD between 1.5 and 2 was reached, where cell growth was recorded and compared. The difference in the rate of cell growth at 30ºC and 37ºC in 72 hours was statistically significant in NB ($p < 0.01$) and in 2XYT ($p < 0.05$). This may be due to the fact that *B. oleronius* is an environmental bacterium and prefers 30ºC rather than 37ºC.

3.3 The effect of temperature on the production of stimulatory 62 kDa antigen by *B. oleronius*

B. oleronius was cultured in NB and 2XYT at two different growth temperatures, 30ºC and 37ºC. As described in section 3.2, *B. oleronius* grows optimally at 30ºC in both growth media. Protein was extracted from each culture at 72 hours and 168 hours and resolved by 1D SDS-PAGE (Figure 3.3A) prior to Western blotting (section 2.13) using the anti-62 kDa rabbit antibody (Figure 3.3B). Densitometric analysis of 62 kDa expression was measured with Image J (section 2.11.2) to visualise the results obtained from Western blotting (Figure 3.4). The level of 62 kDa production remained consistent in 2XYT at 72 hours but reduced at 168 hours in the 37ºC culture (Figure 3.4). The level of stimulatory 62 kDa produced in NB at 72 hours was investigated further, as this was the primary growth medium throughout this research. This NB culture demonstrated statistically significant increased reactivity by the anti-62 antibody (1.65-fold increase) to proteins from the cells grown at 37ºC (Figure 3.5).

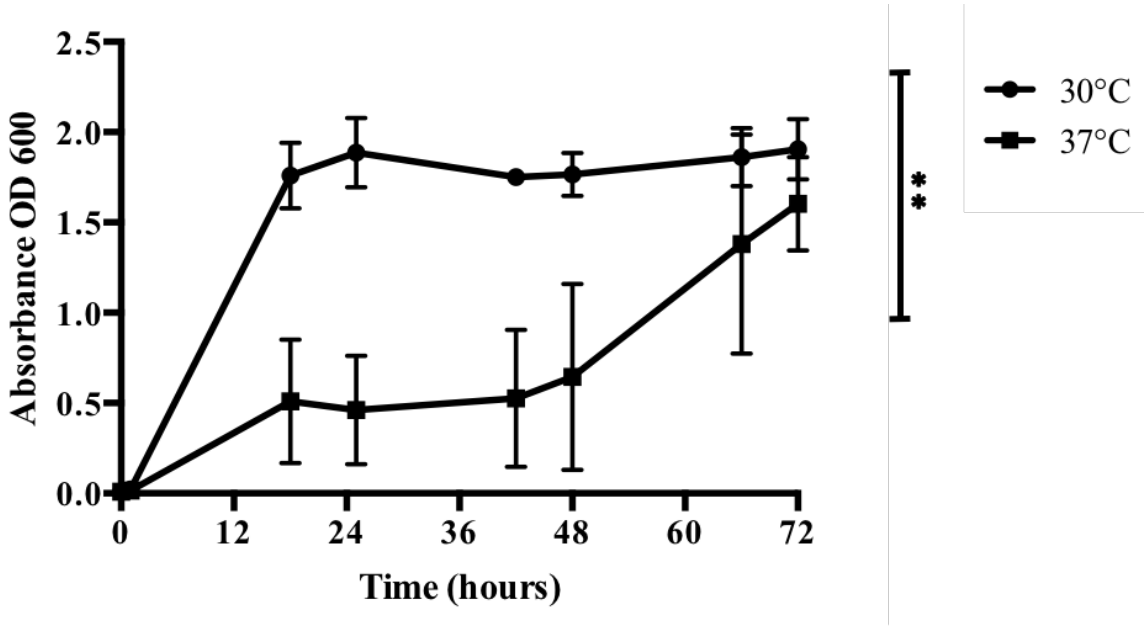

Figure 3.1 Growth of *Bacillus oleronius* in nutrient broth

Growth of *B. oleronius* for 72 hours cultured in nutrient broth at different temperatures. The optimal cell density is at 30°C. At 37°C the overall cell growth is significantly slower than at 30°C (**$p < 0.01$). All values are the mean ± SE of three independent determinations (n=3).

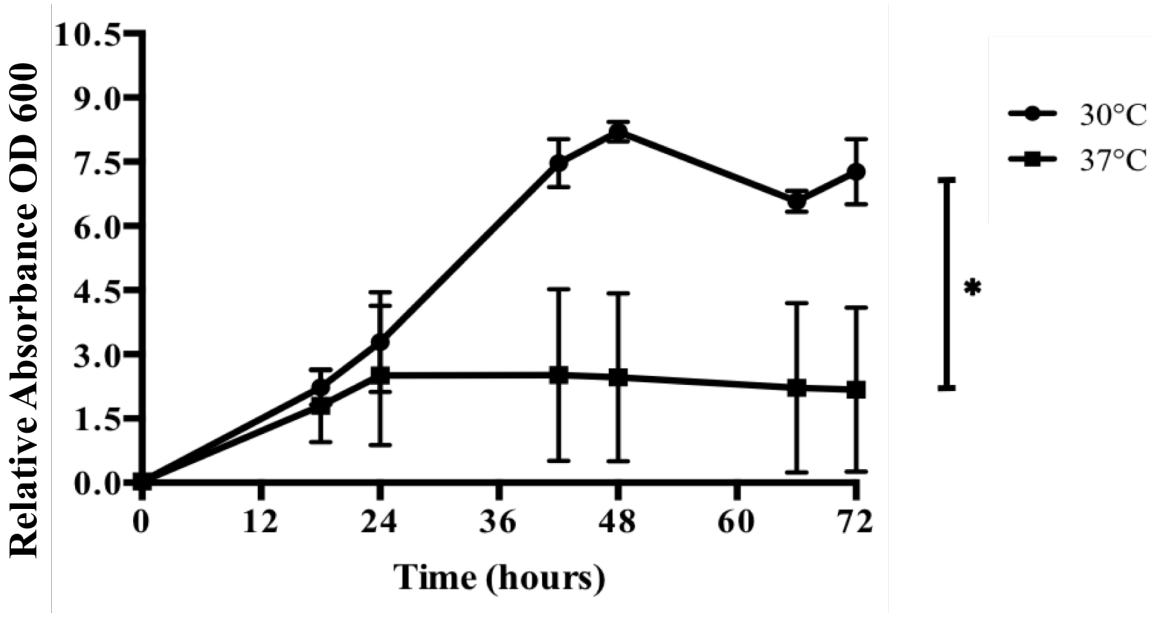

Figure 3.2 Growth of *Bacillus oleronius* in 2XYT medium

Growth of *B. oleronius* for 72 hours cultured in 2XYT medium at different temperatures. The optimal cell density is at 30°C. At 37°C cell growth is significantly slower than at 30°C (*$p < 0.05$). All values are the mean ± SE of three independent determinations (n=3).

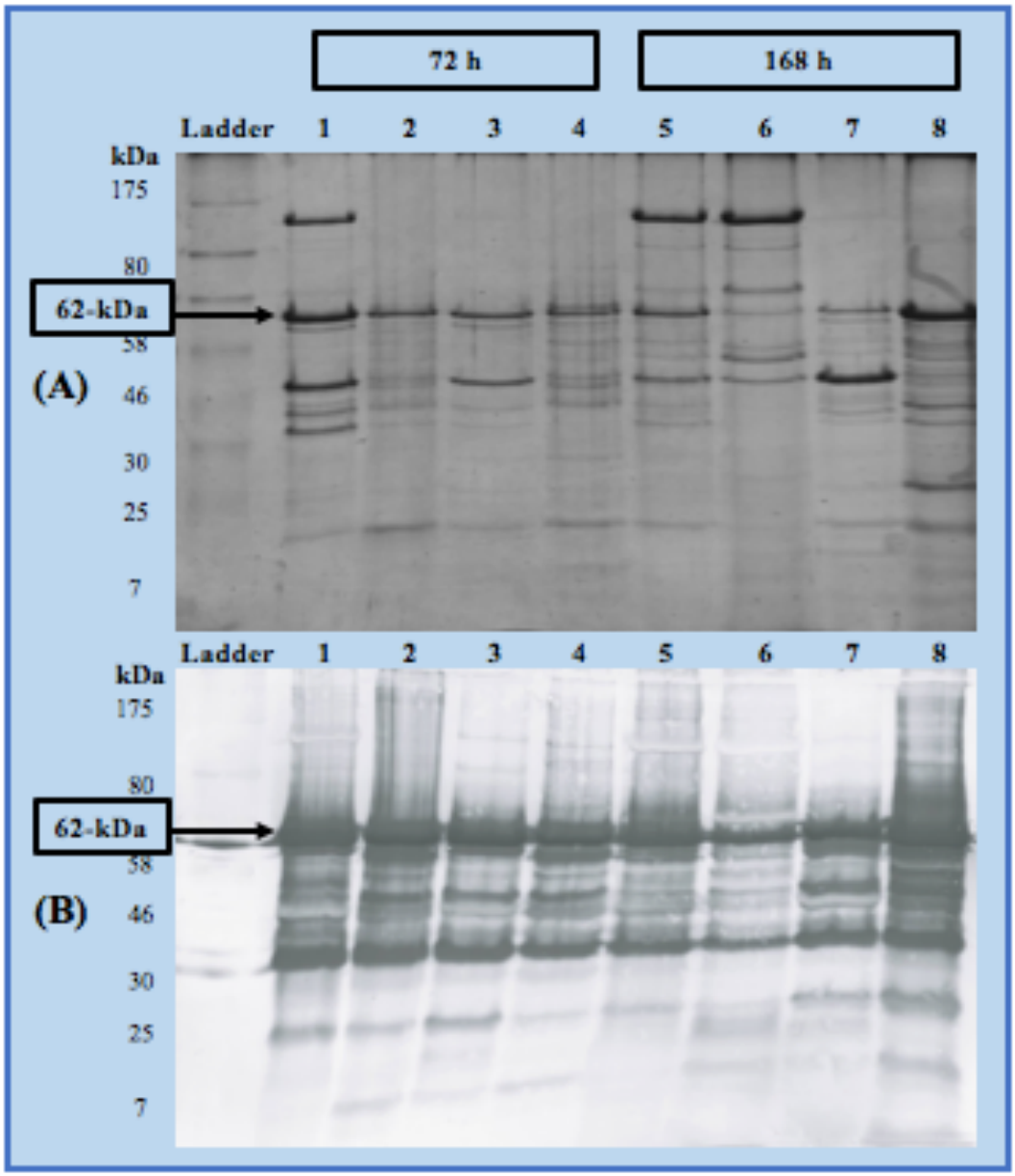

Figure 3.3 Representative Western blot measuring the expression of *B. oleronius* 62 kDa protein grown from cultures under temperature stressed environments

B. oleronius proteins resolved by SDS-PAGE (**A**) and Western blot analysed (**B**) with specific 62 kDa rabbit antibody. *B. oleronius* was cultured at two different temperatures in two different media and protein was expressed at 72 hours [1-4] and 168 hours [5-8]. 2XYT 30°C (1,5); 2XYT 37°C (2,6); NB 30°C (3,7); NB 37°C (4,8).

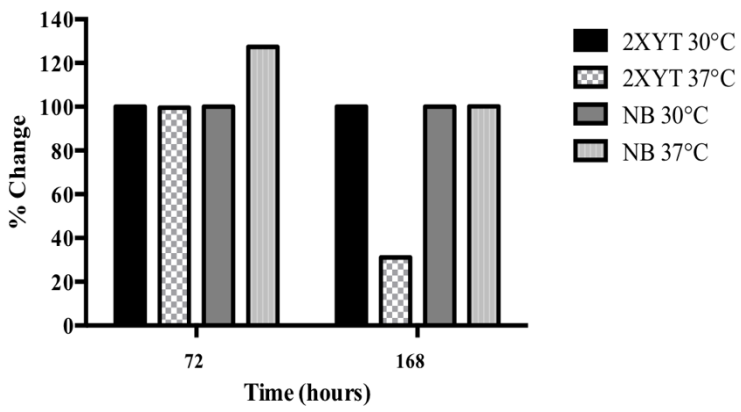

Figure 3.4 Level of 62 kDa *B. oleronius* antigen expression under temperature stressed culture conditions.

Representative Image J (version 1.50i) analysis of the level of 62 kDa antigen expressed by *B. oleronius*. In NB, the level of 62 kDa increased at 72 hours at 37°C compared to 30°C. In 2XYT, the 62 kDa level decreased at 168 hours at 37° compared to 30°C.

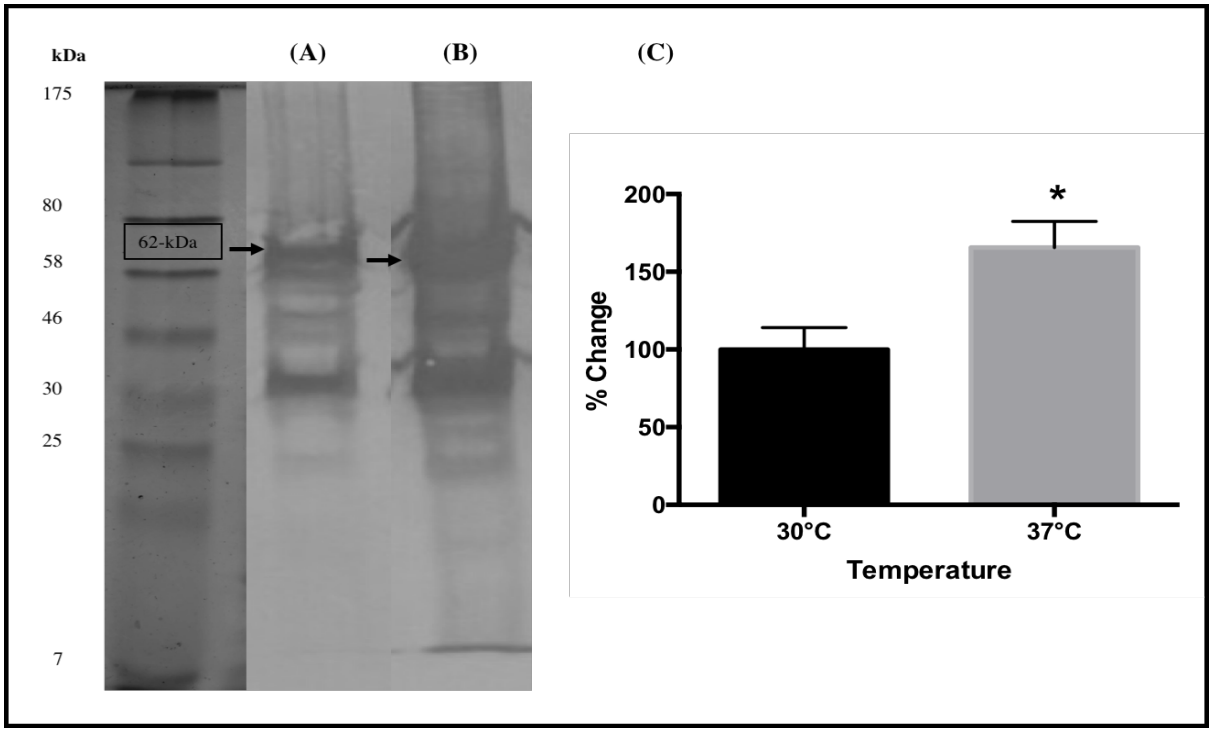

Figure 3.5 Western blot measuring the production of stimulatory 62 kDa antigen produced at 72 hours in nutrient broth culture

B. oleronius cultured in nutrient broth resolved by SDS-PAGE as described and Western blot analysed with anti-62 kDa rabbit antibody. An increase of the immune-reactive 62kDa is observed at 37°C **(B)** in comparison to expression at 30°C **(A)**. Image J analysis (version 1.50i) indicating significant 1.65-fold increase of reactive 62kDa at 37°C in comparison to 30°C ($p < 0.05$) **(C)** (n=3).

3.4 Investigating the effect of temperature on the production of *B. oleronius* antigen using confocal microscopy

Confocal microscopy was employed to visualize the presence of the 62kDa protein on the surface of *B. oleronius* cells grown at 30ºC or 37ºC in NB or 2XYT. DAPI was used to visualise the cells and two different fluorescent antibodies were utilised to visualise the 62 kDa expression as described in section 2.20. *B. oleronius* cultured in NB was fixed using Alexa Fluor® 594 anti-rabbit IgG to bind to the 62 kDa specific rabbit antibody. This gave a red fluorescence and the results displayed more of the stimulatory 62kDa antigen in *B. oleronius* grown at 37ºC (Figure 3.8) when compared against 30ºC (Figure 3.7). Alexa Fluor® 488 anti-rabbit IgG was employed for *B. oleronius* cultured in 2XYT, which produced a green fluorescence in the presence of 62 kDa antigen. The level of antigen visualised at 37ºC in 2XYT (Figure 3.10) was slightly increased in comparison to 30ºC (Figure 3.9) A representative image for all controls was used with Alexa Fluor® 488 anti-rabbit IgG (Figure 3.6).

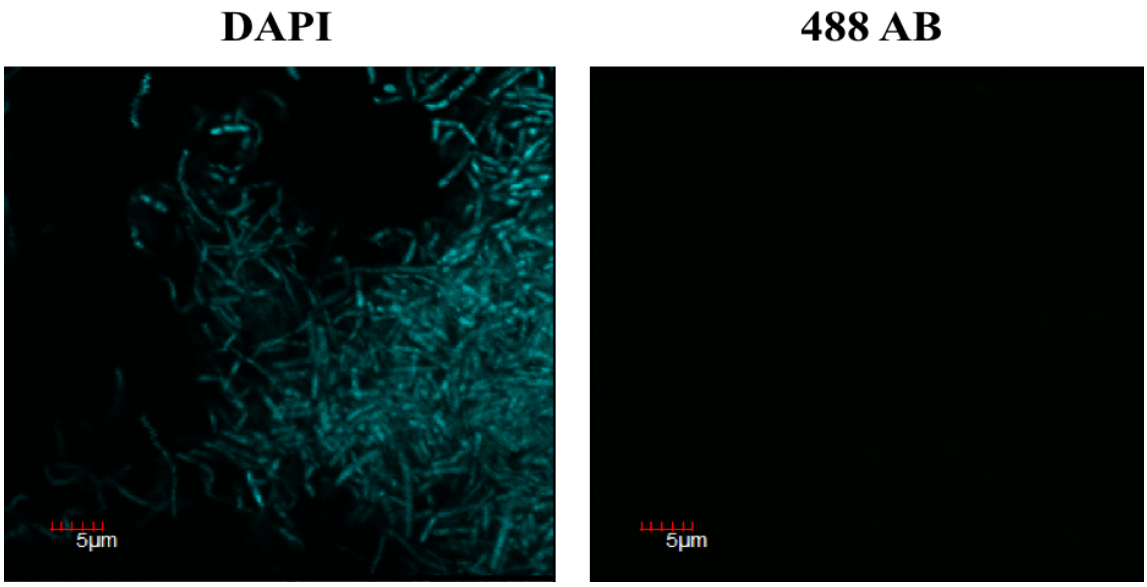

Figure 3.6 Confocal images of control sample antibody specific for *B. oleronius*
Representative confocal images of *B. oleronius* control samples were taken with Alexa Fluor® 488 fluorescent dye and a 60X objective. The control samples lacked the primary anti-62 kDa rabbit antibody. DAPI enabled visualisation of the cells and a successful negative control for antibody specific to the *B. oleronius* 62 kDa protein was applied. No green fluorescence can be visualised (488 AB) in the control image.

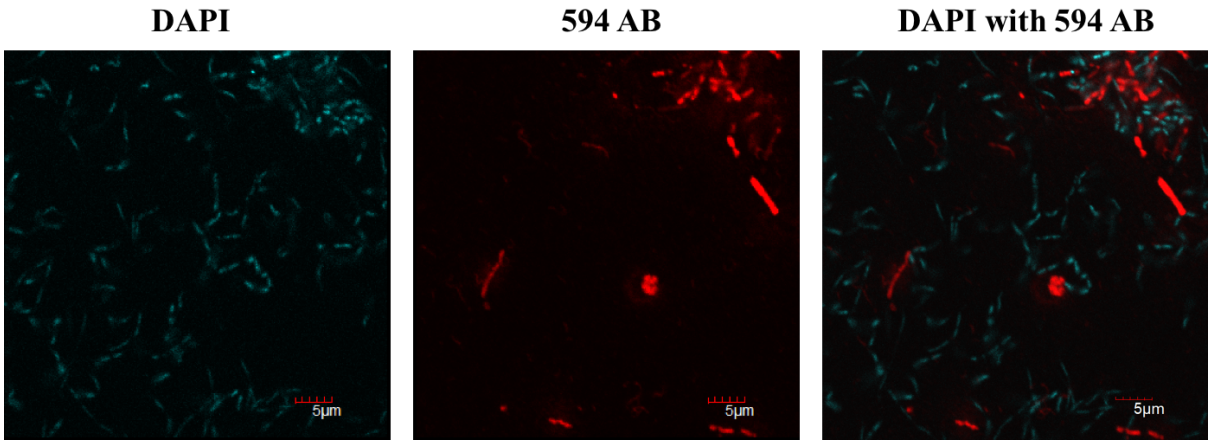

Figure 3.7 Confocal images of *B. oleronius* cultured in nutrient broth at 30°C
Images were taken with Alexa Fluor® 594 fluorescent dye and a 60X objective. DAPI enabled visualisation of the cells and the anti-62 kDa rabbit antibody (594 AB) gave a fluorescence in the presence of stimulatory *B. oleronius* 62 kDa antigen.

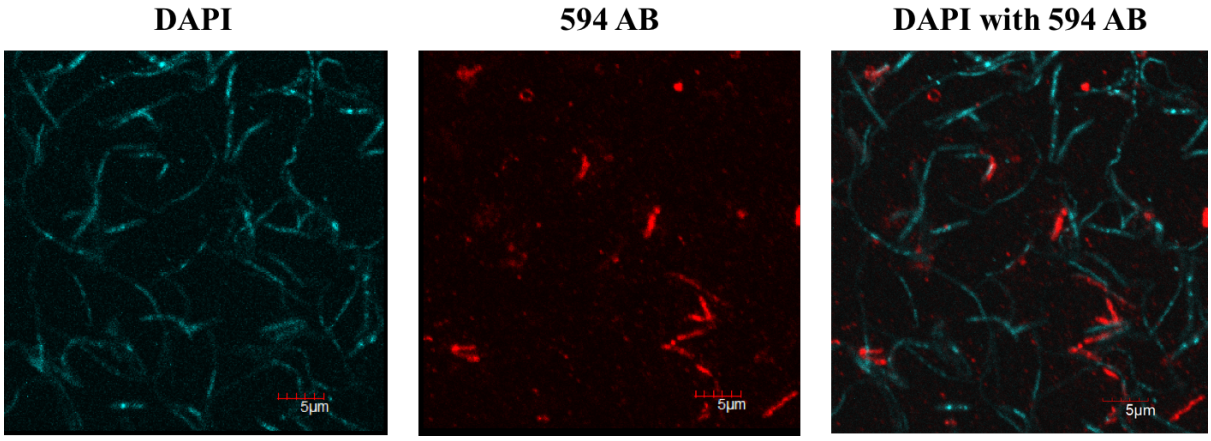

Figure 3.8 Confocal images of *B. oleronius* cultured in nutrient broth at 37°C
Images were taken with Alexa Fluor® 594 fluorescent dye and a 60X objective. DAPI enabled visualisation of the cells and the anti-62 kDa rabbit antibody (594 AB) gave a fluorescence in the presence of stimulatory *B. oleronius* 62 kDa antigen.

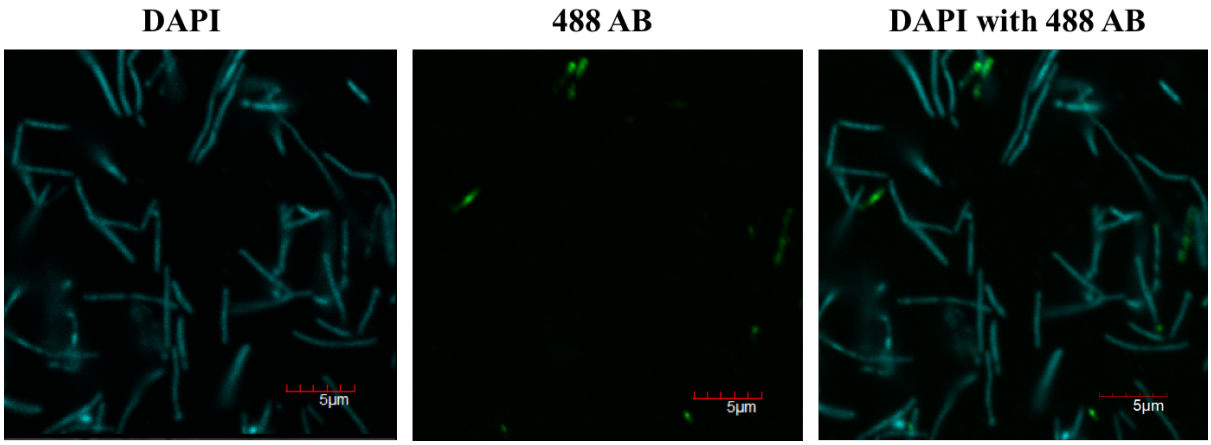

Figure 3.9 Confocal images of *B. oleronius* cultured in 2XYT medium at 30°C

Images were taken with Alexa Fluor® 488 fluorescent dye and a 60X objective. DAPI enabled visualisation of the cells and the anti-62 kDa rabbit antibody (488 AB) gave a fluorescence presence of stimulatory *B. oleronius* 62 kDa antigen.

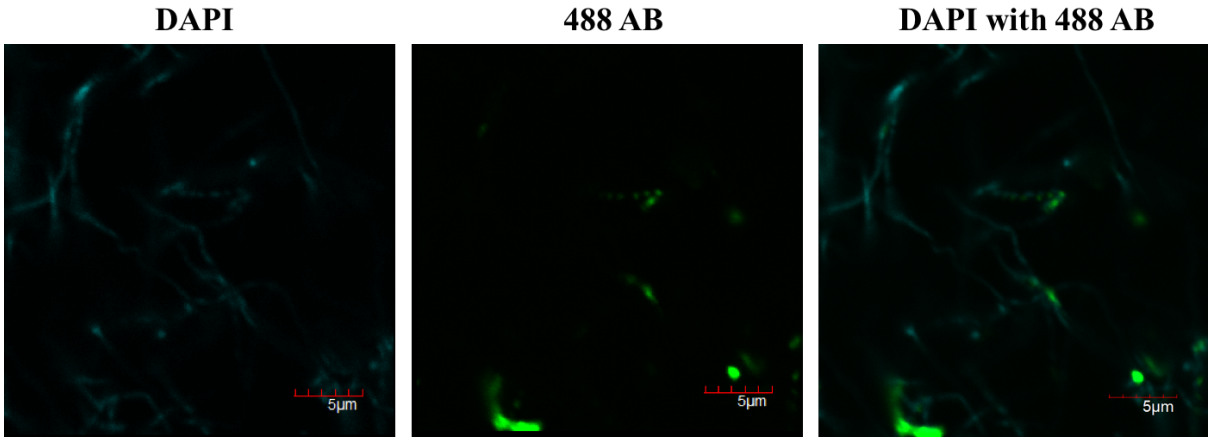

Figure 3.10 Confocal images of *B. oleronius* cultured in 2XYT medium at 37°C

Images were taken with Alexa Fluor® 488 fluorescent dye and a 60X objective. DAPI enabled visualisation of the cells and the anti-62 kDa rabbit antibody (488 AB) gave a fluorescence in the presence of stimulatory *B. oleronius* 62 kDa antigen.

3.5 A 2-Dimensional IEF SDS-PAGE investigation of the effect of temperature on the proteomic profile of *B. oleronius*

As previously observed, *B. oleronius* grows optimally at 30°C in comparison to 37°C in both NB and 2XYT (section 3.2). Growth temperature also influences the production of immune-stimulatory 62 kDa antigen in NB (section 3.3). Following this, the effect of temperature was further analysed using 2D IEF SDS-PAGE. *B. oleronius* was cultured in NB for 72 hours at 30°C and 37°C prior to protein extraction (200µg), which was resolved as described in section 2.10.4. Comparative analysis using Progenesis™ SameSpot software was employed to determine differential protein abundance between 30°C and 37°C. Spots of interest were excised and digested by LC-MS/MS (section 2.12).

A total of 11 spots (Figure 3.11) were identified as significantly abundant ($p < 0.05$) at 37°C in comparison to control temperature of 30°C, all of which had a fold change minimum of 1.4. Four proteins increased in abundance (Table 3.1), the largest of which was spot 9 (8.9 fold increase), identified as type I glyceraldehyde-3-phosphate dehydrogenase (GAPDH). Spot 1 was identified as arginase with a 3 fold increase. Spots 7 and 11 were identified as enolase (1.9 fold increase) and translational elongation factor Tu (EF-Tu; 4 fold increase) respectively, both of which were also identified with decreased abundances in Table 3.2. GAPDH and enolase are two enzymes involved in glycolysis and have also been associated with transcriptional regulation (Kim & Dang, 2005). Enolase is a member of thirty universally conserved proteins and in glycolysis, is responsible for the conversion of 2-phosphoglycerate to phosphoenolpyruvate (Commichau *et al*., 2009; Kim & Dang, 2005). Arginase (spot 1) hydrolyses L-arginine into L-ornithine and urea before further metabolism to polyamine production which contribute to cellular proliferation and regulate immune response (Duque-Correa *et al*., 2014; Pesce *et al*., 2009; Chen *et al*., 2004). EF-Tu (spot 11) increased 4 fold but was also found to decrease in abundance by 3.2 fold (Table 3.2). EF-Tu is mostly associated with protein synthesis in bacteria translation and is a member of the GTPase superfamily. EF-Tu binds to specific codon aminoacyl-tRNA and transports it to the corresponding aminoacyl site in the ribosome for translation (Schnicker *et al*., 2017; Pereira *et al*., 2015; Kuhle & Ficner, 2014; Caldas *et al*., 1998).

Seven spots identified were significantly decreased in abundance at 37°C in comparison to 30°C. Spots 2 and 6 were identified as the same protein, alanine dehydrogenase, with 6 fold and 5.5 fold decreases respectively (Figure 3.11). Alanine dehydrogenase is a metabolism protein and catalyses the conversion of L-alanine into ammonia and pyruvate (Moore & Leigh, 2005; Duché *et al*., 2002). Spot 5 was identified as beta-ketoacyl synthase (KAS) II (5.4 fold decrease), spot 2 was acetyl CoA, commonly referred to as thiolase (4.5 fold decrease) and spot 10 was identified as 2-Cys peroxiredoxin (2.2 fold decrease) (Table 3.2). KAS II is a condensing enzyme involved in the long chain elongation step of type II fatty acid biosynthesis in bacteria (Lai & Cronan, 2003; Marrakchi *et al*., 2002). Thiolase is also a condensing enzyme in fatty acid synthesis and generates acetyl-CoA (Soto *et al*., 2011; Fujita *et al*., 2007). 2-Cys peroxiredoxin is an important antioxidant protein which detoxifies H_2O_2 during oxidative stress. 2-Cys peroxiredoxin plays a biological role by protecting proteins from degradation, maintaining redox levels in the cell, and is most active during oxidative stress in the presence of H_2O_2 (Hall *et al*., 2009; Kalinina *et al*., 2008; Rhee *et al*., 2007). Spots 4 and 11 had the same identity, EF-Tu, with 3.2 fold decrease (Table 3.2) and 4 fold increase (Table 3.1) respectively. Similarly, spots 8 and 7 had the same identity, phosphopyruvate hydratase commonly referred to as enolase, with 3.6 fold decrease and 1.9 fold increase, respectively.

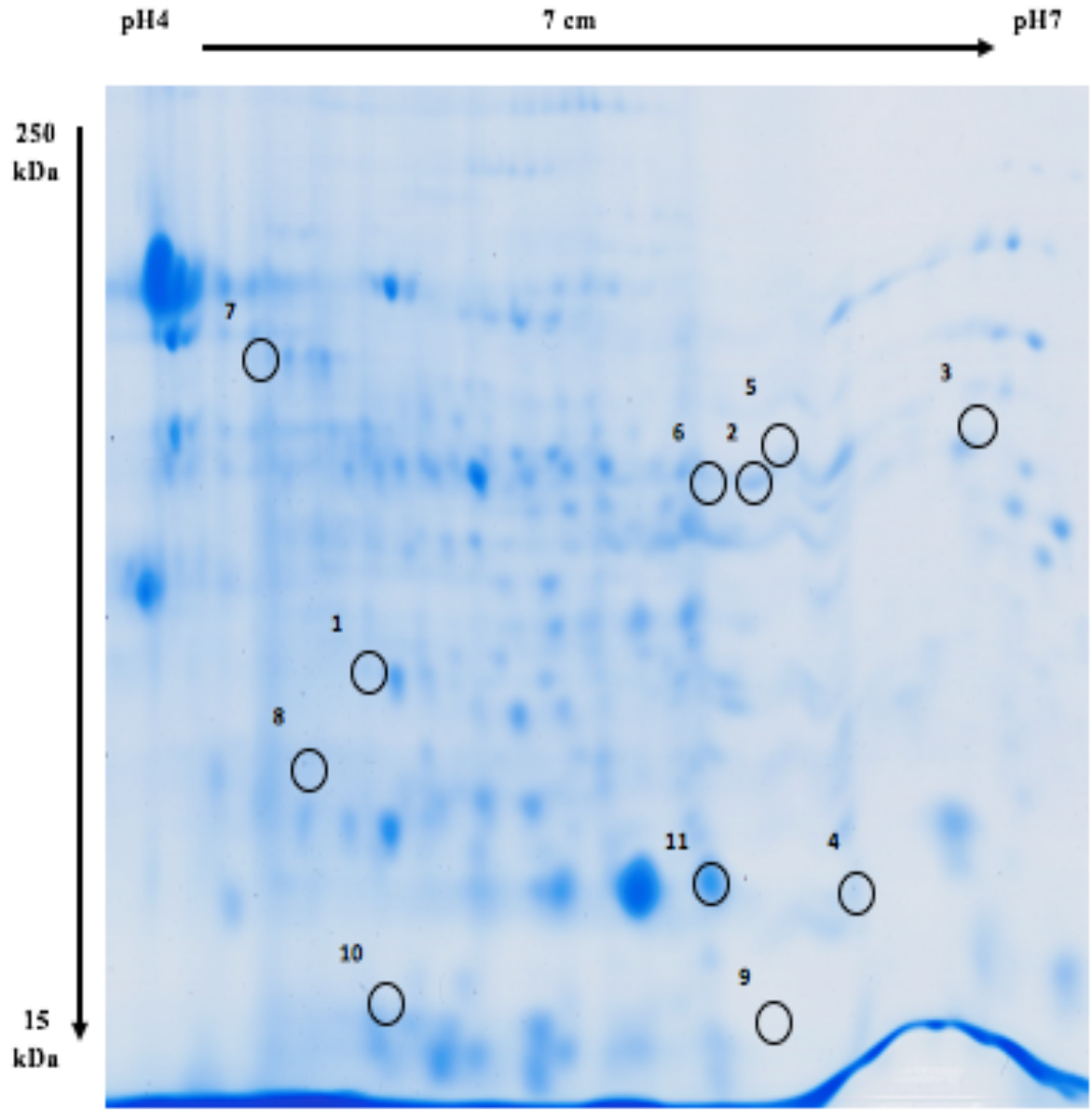

Figure 3.11 2-Dimensional IEF SDS-PAGE gel image displaying spots identified from *Bacillus oleronius* proteome

Representative gel image highlighting spots of interest from *B. oleronius* cultured at 30°C and 37°C. Comparative proteomic analysis was performed before excising and digesting proteins which were identified by LC-MS/MS (Tables 3.1 and 3.2).

Table 3.1 Protein identities of spots increased in *B. oleronius* proteomic profile at 37°C

Table of proteins that were identified from the comparative proteomic profile of *B. oleronius* cultured in nutrient broth for 72 hours at 30°C and 37°C. Identities listed in table were significantly increased ($p < 0.05$) in abundance at 37°C in comparison to 30°C. Selected spots shown in Figure 3.11.

Protein Spot and Identity	Mass (M_r)	p*I*	Coverage (%)	Score	Protein Identity	*p*-value	Fold change increased 37°C	Protein Function
1. Arginase	32099	4.76	11	164	WP_034765818.1	0.009	3	Amino acid transport and metabolism
7. Phosphopyruvate hydratase (Enolase)	46655	4.58	59	1278	WP_060672587.1	0.029	1.9	Energy metabolism; Glycolytic enzyme
9. Type I glyceraldehyde-3 – phosphate dehydrogenase	18986	5.76	8	119	WP_024770399.1	0.053	8.9	Carbohydrate transport and metabolism; Glycolytic enzyme; GAPDH
11. Translation elongation factor (Tu)	42689	5.78	3	97	OGH06529.1	0.059	4	GTP-binding translation factor; tRNA transport to ribosome

Table 3.2 Protein identities of spots decreased in *B. oleronius* proteomic profile at 37°C

Table of proteins that were identified from the comparative proteomic profile of *B. oleronius* cultured in nutrient broth for 72 hours at 30°C and 37°C. Identities listed in table were significantly decreased ($p < 0.05$) in abundance at 37°C in comparison to 30°C. Selected spots shown in Figure 3.11.

Protein Spot and Identity	Mass (M_r)	p*I*	Coverage (%)	Score	Protein Identity	*p*-value	Fold change decreased 37°C	Protein Function
2. Alanine dehydrogenase	39766	5.16	31	400	WP_0606 7 4981.1	0.011	6	Catalyzes NAD-dependent conversion to L-alanine
3. Acetyl-CoA acetyltransferase (Thioloase)	41391	5.6	29	351	WP_0606 7 2270.1	0.015	4.5	Catalytic role; Lipid transport and metabolism
4. Translation Elongation Factor Tu	42689	5.78	3	97	OGH 06529.1	0.019	3.2	GTP-binding translation factor; tRNA transport to ribosome
5. Beta-ketoacyl synthase II	44429	5.18	16	430	WP_06067 0277.1	0.023	5.4	Fatty acid biosynthesis
6. Alanine dehydrogenase	39766	5.16	46	662	WP_06067 4981.1	0.024	5.5	Catalyzes NAD-dependent conversion to L-alanine
8. Phosphopyruvate hydratase (Enolase)	46716	4.63	23	426	WP_06409 3004.1	0.052	3.6	Energy metabolism; Glycolytic enzyme
10. 2-Cys peroxiredoxin	18423	4.68	50	447	WP_03208 7344.1	0.057	2.2	Protective mechanism; Cell antioxidant

3.6 Comparative analysis of the effect of temperature on the proteomic profile of *Bacillus oleronius* using Label free MS/MS

An advanced study of the effect of temperature on the *B. oleronius* proteome has been made possible with advances in mass spectrometry-based proteomics. LF-MS/MS enables a quantitative examination at the relative change in protein abundances over multiple parameters a single mass spectrometry runs (Bantscheff *et al*., 2012). Here, LF-MS/MS was employed to identify the variations of protein expression in *B. oleronius* grown for 72 hours at 30°C and 37°C**.**

In total, 905 peptides were identified representing 900 proteins with two or more peptides and 560 proteins were determined to be differentially abundant with a fold change > 1.5 fold (ANOVA, $p < 0.05$) (Figure 3.13). Principal component analysis (PCA) was performed with normalized intensity values and resolved a clear difference in the proteomes (Figure 3.12A). All statistically significant proteins were visualised in a hierarchical cluster (Figure 3.12B), performed using Z-score normalized intensity values for differentially abundant proteins. At 37ºC, 506 proteins were found in higher abundance (426 non-imputated proteins and 80 imputated) (Table 3.3) and 54 proteins were found in lower abundance (9 non-imputated and 45 imputated) (Table 3.4) when compared against 30ºC. These proteins were statistically analysed following imputation of zero values using a number close to the lowest value of the range of proteins plus or minus standard deviation. (The proteins found in higher abundance continued from Table 3.3 are listed in Table A.31)

The protein showing the highest increase in abundance at 37ºC was alanine dehydrogenase with a fold change of 94.3 ($p < 0.05$) (Figure 3.13). Proteins identified at 37ºC with imputated values and higher abundances were phosphocarrier protein HPr (483.5 fold increase), putative phosphoesterase (385.5 fold increase), iron transporter FeoA (323.8 fold increase), cold-shock protein (260.2 fold increase), nucleoside diphosphate kinase (163.3 fold increase) (Table 3.3). The protein zinc metalloprotease was identified as the protein most decreased in abundance at 37ºC with a fold change of 19.3 ($p < 0.05$). Imputated proteins with a lowered abundance included ferredoxin (325.2 fold decrease), peptidase S8 (244.5 fold decrease),

protein prkA (57.2 fold decrease), stage IV sporulation protein A (33.4 fold decrease) and protein translocase subunit SecY (9.7 fold decrease) (Table 3.4).

The Blast2GO annotation software (www.blast2GO.com) was applied to group proteins together based on conserved gene ontology (GO) terms in order to identify pathways and processes potentially associated with temperature stress. GO terms were categorized by biological processes (BP; Figure 3.14), molecular function (MF; Figure 3.15) and cellular components (CC; Figure 3.16). The greatest change in protein proportion of BP were proteins labelled as cellular process (189 proteins in 30ºC; 562 proteins in 37ºC), single-organism process (151; 428) and metabolic process (194; 562). Only two GO categories were evident for MF associated proteins with an increase at 37ºC in both catalytic activity (176; 499) and binding (153; 469). Proteins grouped as CC with increased abundance at 37ºC were labelled under cell part (148 proteins in 30ºC; 444 proteins in 37ºC), macromolecular complex (59; 157) and cell (149; 445).

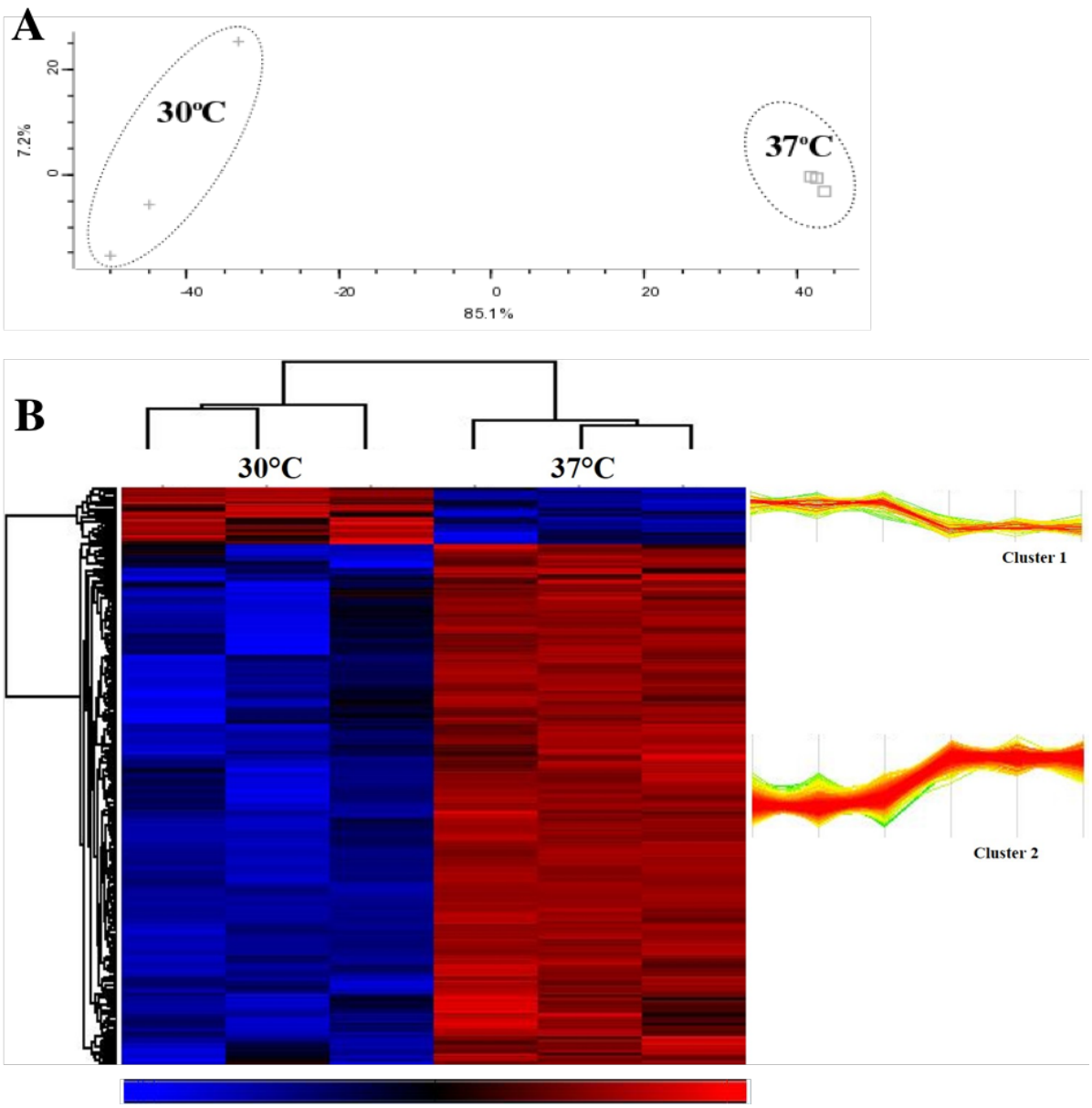

Figure 3.12 Label free MS/MS principal component analysis and hierarchical clustering of the quantitative differences in the proteomic profile of *B. oleronius* **(A)** Principal component analysis (PCA) of comparative temperature treatments included in label free quantification (LFQ). Dashed circles represent sample groups with three replicates per group. **(B)** This heat map represents the median protein expression values of all statistically significant differentially and uniquely detected proteins from *B. oleronius* proteomic profiles at 72 hours cultured at 30ºC and 37ºC. Hierarchical clusters resolved two distinct columns comprising the replicates from the original sample groups and cluster rows based on expression profile similarities. The red indicates high level of abundance and the blue indicates low level.

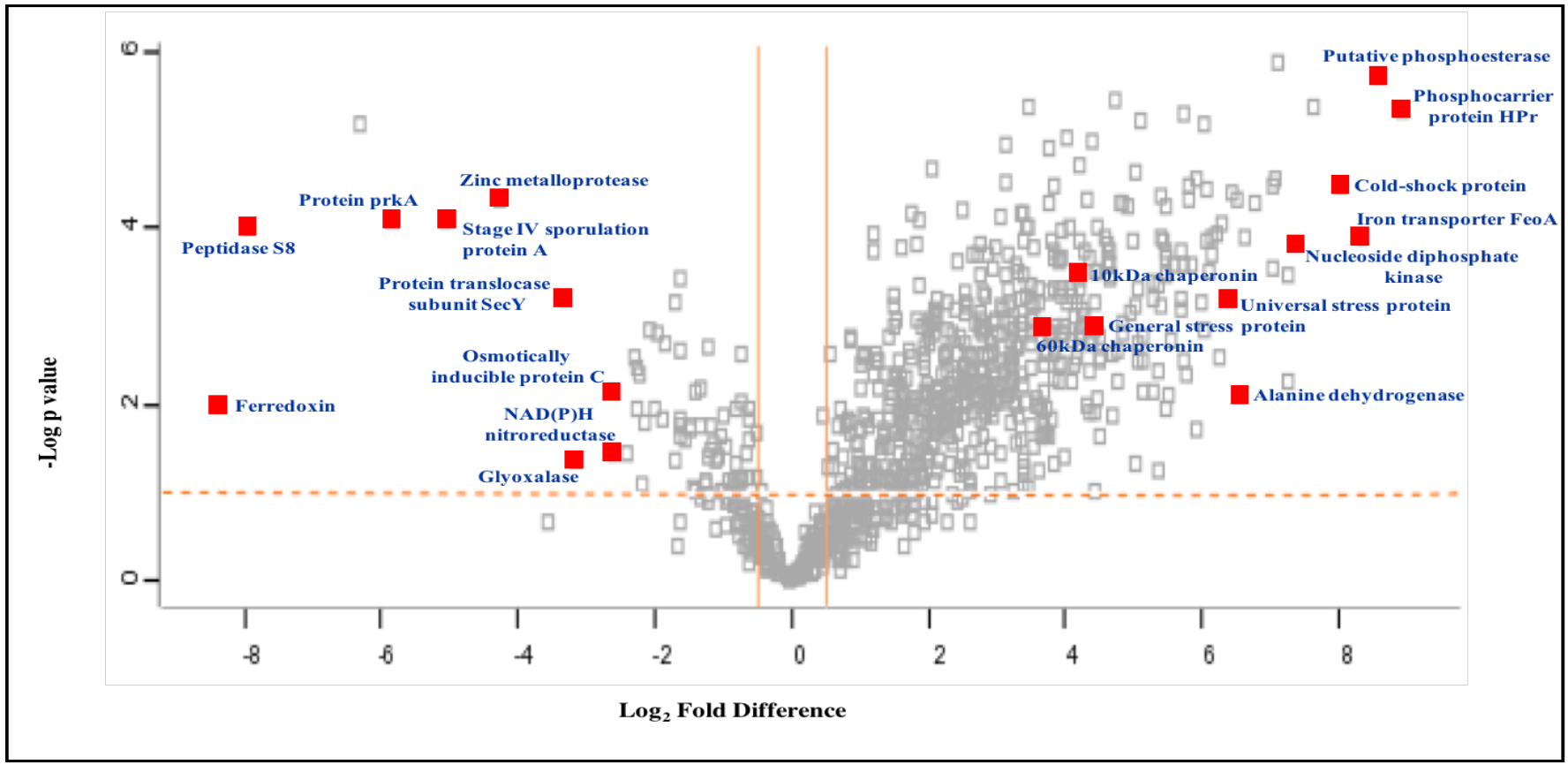

Figure 3.13 Volcano plot highlighting the twenty proteins most altered in abundance in *B. oleronius* when cultured at 37ºC versus 30ºC. Volcano plot showing the effect of temperature on protein abundance in *B. oleronius*. Protein intensity difference (-$\log_2$ mean intensity difference) and significance in differences (-log *p*-value) based on a two-sided *t*-test. Proteins above the dashed line are considered statistically significant ($p < 0.05$) and those to the right and left of the vertical lines indicate > 1.5 fold positive changes and fold negative changes at 37ºC respectively, versus control at 30ºC.

Table 3.3 Proteins identified at higher abundance in *B. oleronius* at 37ºC

Proteins that had over two matched peptides with a *t*-test probability < 0.5 and that were found to be differentially expressed at a 1.5 fold change were considered to be significantly higher in abundance at 37ºC. Table displays proteins with an increased fold difference >20.

Protein Annotation (* = non-imputated protein)	Peptides	Sequence Coverage %	PEP	Overall Intensity	Fold difference
Phosphocarrier protein HPr	13	98.9	3.39E-62	1.90E+11	483.5
Putative phosphoesterase	15	59.3	1.68E-172	1.01E+11	385.5
Iron transporter FeoA	9	57.8	9.09E-130	9.44E+10	323.8
Cold-shock protein	7	100	3.74E-76	8.26E+10	260.2
Nucleoside diphosphate kinase	16	75	5.23E-112	3.57E+10	163.3
Ethyl tert-butyl ether	7	40.2	0	2.84E+10	153.4
Cold-shock protein	11	100	5.91E-24	1.68E+11	150.8
Elongation factor Ts	29	57	1.67E-98	4.80E+10	139.0
Thiol-disulfide oxidoreductase	15	69.5	4.60E-65	2.67E+10	134.6
Phosphocarrier protein Chr	9	48.2	0	5.84E+10	131.5
Acetyl-CoA acetyltransferase	27	71.1	2.27E-175	2.18E+10	109.8
*Alanine dehydrogenase	29	80.1	4.30E-86	7.11E+10	94.3
Peroxiredoxin	9	67.1	0	2.53E+10	90.3
Peroxiredoxin	13	57.8	0	2.02E+10	85.9
Universal stress protein	10	54.7	1.79E-186	4.59E+10	84.0
Serine/threonine protein kinase	12	70.7	1.14E-188	1.60E+10	78.8
Iron ABC transporter ATP-binding protein	20	78.5	2.51E-38	2.11E+10	75.3
Cold-shock protein	5	97	1.01E-82	3.38E+10	74.2
Transition state regulator	11	77.4	5.08E-12	1.97E+10	71.0
ABC transporter substrate-binding protein	28	58.1	1.44E-199	1.78E+10	70.8
Nitrogen fixation	10	93.6	3.13E-232	3.86E+10	69.2
Carbonic anhydrase	8	45.9	2.30E-97	1.92E+10	67.7
Alkyl hydroperoxide reductase	17	71.7	6.41E-64	1.96E+10	67.3
50S ribosomal protein L11	9	46.8	1.35E-89	2.41E+10	65.7
XRE family transcriptional regulator	7	49.6	2.02E-198	1.40E+10	64.9
Flagellar basal body rod protein	4	14.9	6.40E-80	1.98E+10	63.8
Sugar ABC transporter substrate-binding protein	32	61.3	1.23E-98	8.06E+10	60.4

Branched-chain alpha-keto acid dehydrogenase subunit E2	25	62.9	0	2.09E+10	59.9
Translation initiation factor IF-1	7	88.9	1.01E-76	3.46E+10	57.9
Chemotaxis protein CheY	10	81.7	5.10E-42	1.61E+10	56.6
Malate dehydrogenase	15	58.3	7.68E-185	1.62E+10	56.0
ABC transporter substrate-binding protein	26	54.7	0	2.49E+10	54.0
Cytochrome C	34	73.4	1.27E-230	2.18E+10	53.3
Anti-sigma F factor antagonist	9	68.1	4.02E-28	1.55E+10	52.4
Penicillin-binding protein	41	45.3	8.87E-129	2.31E+10	51.6
*Ribosome-recycling factor	19	74.1	9.84E-121	6.74E+10	51.6
*Isocitrate dehydrogenase [NADP]	38	62.5	4.44E-109	4.83E+10	51.4
Anti-sigma factor antagonist	8	46.4	3.53E-167	1.38E+10	48.2
Probable transaldolase	18	71.4	4.45E-196	8.97E+09	46.7
ABC transporter substrate-binding protein	16	70.3	4.18E-90	3.85E+10	45.2
Sulfurtransferase	9	76.9	3.60E-280	1.43E+10	44.7
PTS cellobiose transporter subunit IIB	7	91.1	3.54E-151	1.87E+10	44.0
Ribose-phosphate pyrophosphokinase	14	60.2	5.98E-17	1.17E+10	44.0
GTP-sensing transcriptional pleiotropic repressor CodY	20	60.2	2.38E-227	1.51E+10	43.9
Cold-shock protein	4	60.6	7.57E-200	1.74E+10	43.8
Nucleoid-associated protein AM506_21130	9	68.9	3.22E-215	1.21E+10	43.4
Acyl--CoA ligase	30	59.6	2.27E-80	9.40E+09	42.3
*UPF0365 protein AM506_15965	24	70.6	0	3.83E+10	41.9
50S ribosomal protein L29	7	62.7	1.09E-130	1.26E+10	40.9
*Transcription elongation factor GreA	15	84.8	4.53E-304	3.37E+10	40.8
Cold-shock protein	4	60.6	7.09E-178	1.81E+10	39.4
*Clp protease ClpX	72	65.8	8.83E-227	6.02E+10	39.3
Cysteine synthase	17	52.8	4.79E-144	1.08E+10	39.0
50S ribosomal protein L10	17	78.3	3.37E-34	1.23E+10	35.4
*30S ribosomal protein S1	26	74.8	4.42E-189	2.79E+10	35.0
Bacterioferritin	12	65.5	0	2.45E+10	35.0
50S ribosomal protein L4	11	69.6	0	1.03E+10	33.8
3-hydroxybutyryl-CoA dehydrogenase	9	45.2	1.24E-163	9.92E+09	33.5
*Thioredoxin reductase	17	50.5	1.95E-138	1.18E+10	33.3
50S ribosomal protein L20	8	31.1	1.43E-131	1.38E+10	33.2
*Electron transfer flavoprotein subunit	25	87.2	0	7.15E+10	32.7

beta					
2-oxoisovalerate dehydrogenase	22	69.9	7.21E-119	1.20E+10	32.7
*Fructose-bisphosphate aldolase	25	81.1	1.18E-186	5.53E+10	32.5
Glutamate dehydrogenase	24	69.3	0	1.05E+10	31.4
50S ribosomal protein L6	10	45.8	6.23E-76	1.06E+10	31.0
50S ribosomal protein L25	11	47.5	0	6.28E+09	29.9
Cold-shock protein	7	70.4	5.52E-207	1.56E+10	28.5
Flagellin	9	11.9	0	1.08E+10	28.3
Alcohol dehydrogenase	9	39.1	1.85E-185	8.76E+09	28.3
UPF0358 protein AM506_01105	8	82.8	2.76E-36	8.47E+09	28.2
Enoyl-CoA hydratase	14	41	3.22E-208	8.76E+09	27.2
*Citrate synthase	29	71.8	1.88E-131	5.20E+10	27.1
Elongation factor P	4	20	2.28E-81	4.74E+09	26.3
*Protein RecA	31	86.1	5.10E-153	2.27E+10	26.0
Actin	27	65.1	2.33E-118	1.83E+10	25.9
Trehalose permease IIC protein	15	21	2.76E-238	5.35E+09	25.3
Lipoprotein	12	44.5	6.74E-66	8.99E+09	25.3
Ribonuclease J	26	64.1	6.26E-252	6.28E+09	24.9
*Enolase	33	94.4	2.59E-45	8.20E+10	24.9
Chemotaxis protein CheY	5	47.9	7.29E-244	1.05E+10	24.5
Putative phosphoesterase YjcG	5	11.7	0	7.75E+09	24.4
Peptide ABC transporter ATP-binding protein	22	58.2	2.11E-154	1.07E+10	24.4
NADH dehydrogenase	20	45.4	5.15E-180	8.18E+09	24.1
Cold-shock protein	4	92.3	2.31E-34	2.86E+10	22.9
Peptidylprolyl isomerase	26	50	3.47E-164	1.28E+10	22.6
*Serine dehydratase	22	75.1	6.41E-88	1.27E+10	22.6
Serine-protein kinase RsbW	10	72.9	2.25E-264	7.86E+09	22.6
Malate dehydrogenase	18	70.4	1.23E-80	4.96E+09	22.3
*4-hydroxyphenylpyruvate dioxygenase	34	83.3	1.58E-43	4.23E+10	22.0
Delta-aminolevulinic acid dehydratase	17	59.3	1.61E-75	4.90E+09	22.0
*Cyclodextrin-binding protein	20	50.1	3.39E-162	7.05E+10	21.8
General stress protein	16	82.8	2.54E-209	5.92E+09	21.7
Peptidyl-prolyl cis-trans isomerase	5	40	1.70E-153	8.81E+09	21.6
Protein hit	8	80	4.01E-114	1.33E+10	21.3
Methionine--tRNA ligase	36	49.2	5.66E-95	1.31E+10	21.0

Table 3.4 Proteins identified at lower abundance in *B. oleronius* at 37ºC

Proteins that had over two matched peptides with a *t*-test probability < 0.5 and that were found to be differentially expressed at a 1.5 fold change were considered to be significantly lower in abundance at 37ºC. Table displays all proteins with a decreased fold difference.

Protein Annotation (* = non-imputated protein)	Peptides	Sequence Coverage %	PEP	Overall Intensity	Fold difference
Ferredoxin	3	26.8	1.02E-22	1.70E+10	325.2
Peptidase S8	11	7.5	1.14E-72	1.66E+09	244.5
Protein prkA	9	19.2	1.33E-63	2.54E+08	57.2
Stage IV sporulation protein A	6	12.8	6.74E-22	1.13E+08	33.4
*Zinc metalloprotease	15	38.3	8.08E-177	1.72E+09	19.3
Protein translocase subunit SecY	4	7.9	2.47E-11	3.05E+08	9.7
Glyoxalase	4	39.2	4.87E-51	5.08E+08	9.0
*NAD(P)H nitroreductase	17	47.8	0	5.48E+10	6.1
*Osmotically inducible protein C	8	68.5	3.59E-194	1.67E+09	6.0
GMP synthase [glutamine-hydrolyzing]	6	14.2	1.94E-78	5.05E+07	5.4
ABC transporter ATP-binding protein	2	5.7	2.73E-22	6.07E+07	5.0
*Superoxide dismutase	13	79.7	0	3.57E+11	4.8
SAM-dependent methyltransferase	3	13.6	1.18E-16	8.63E+07	4.7
*Glutamine amidotransferase	8	64.2	1.47E-118	3.10E+09	4.5
Asparaginase	3	16.6	1.68E-41	9.32E+07	4.2
Thiamine pyrophosphokinase	3	16.3	6.09E-30	1.07E+08	4.0
*Oligoendopeptidase F	17	26.1	0	3.10E+09	3.9
Transcriptional regulator	3	26.8	1.22E-13	8.73E+07	3.7
Hydrolase	5	23	6.66E-57	1.07E+08	3.6
4-hydroxy-tetrahydrodipicolinate reductase	3	22.3	1.77E-20	8.26E+07	3.2
*Peptide deformylase	9	54.3	2.24E-189	1.31E+09	3.1
Segregation and condensation protein B	3	14.2	1.86E-07	8.30E+07	3.1
Energy-coupling factor transporter transmembrane protein EcfT	3	14.3	1.61E-06	9.12E+07	3.1
Glycerol-3-phosphate acyltransferase	1	7.3	8.78E-25	9.54E+07	3.1

Gluconeogenesis factor	3	13.8	5.68E-28	1.58E+08	2.9
Diguanylate phosphodiesterase	6	13	2.58E-19	1.13E+08	2.8
Alcohol dehydrogenase	4	13.7	5.46E-64	1.49E+08	2.8
SAM-dependent methyltransferase	4	12.6	8.63E-11	1.29E+08	2.7
Oxidoreductase	3	13	2.67E-61	1.22E+08	2.5
Peptide chain release factor 3	10	28.4	7.16E-72	1.53E+08	2.3
Elongation factor 4	10	21.3	1.12E-76	1.71E+08	2.3
Alkyl hydroperoxide reductase AhpD	3	30.6	3.52E-22	2.28E+08	2.3
*Pullulanase	4	7.4	1.53E-97	7.80E+07	2.3
GTPase Der	5	15.8	4.41E-102	1.64E+08	2.3
Aromatic amino acid aminotransferase	7	27.9	2.48E-73	1.79E+08	2.2
Glucose-1-phosphate adenylyltransferase	5	15.1	3.24E-68	2.09E+08	2.1
*Thioredoxin	8	64.4	4.03E-29	1.19E+10	2.0
Heme biosynthesis protein HemY	4	30	3.03E-35	1.74E+08	1.9
Beta-lactamase	6	20.1	6.28E-23	2.11E+08	1.8
Aminobenzoate synthetase	5	10.7	1.46E-20	1.36E+08	1.8
3-hydroxybutyrate dehydrogenase	6	28.3	2.04E-99	1.21E+08	1.7
NAD kinase	4	26.4	8.78E-41	2.41E+08	1.6
Enoyl-CoA hydratase	4	44.3	2.65E-43	2.50E+08	1.5
Diacetylchitobiose-6-phosphate hydrolase	6	18.5	1.66E-60	1.47E+08	1.5
Cytochrome D ubiquinol oxidase subunit I	3	6.5	2.41E-51	4.42E+08	1.5

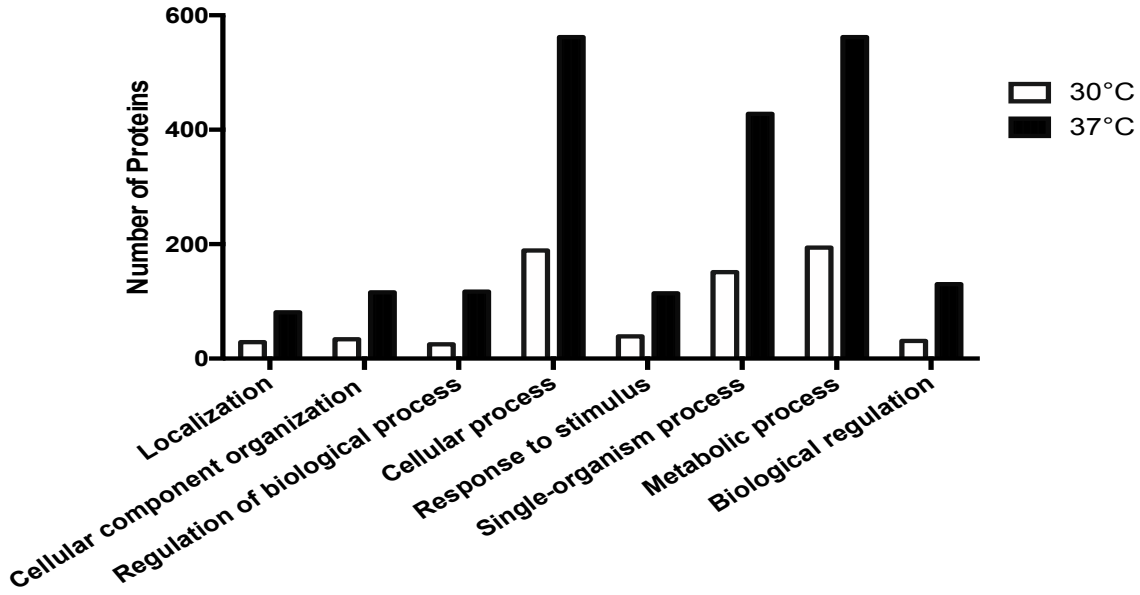

Figure 3.14 Biological Process Level 2 grouping of proteins found in *B. oleronius*

Comparative bar chart showing changes to the number of proteins involved in selected biological processes at level 2 ontology. Proteins based on percentage proportion of the total proteins found in the proteomic profile of *B. oleronius* affected by temperature.

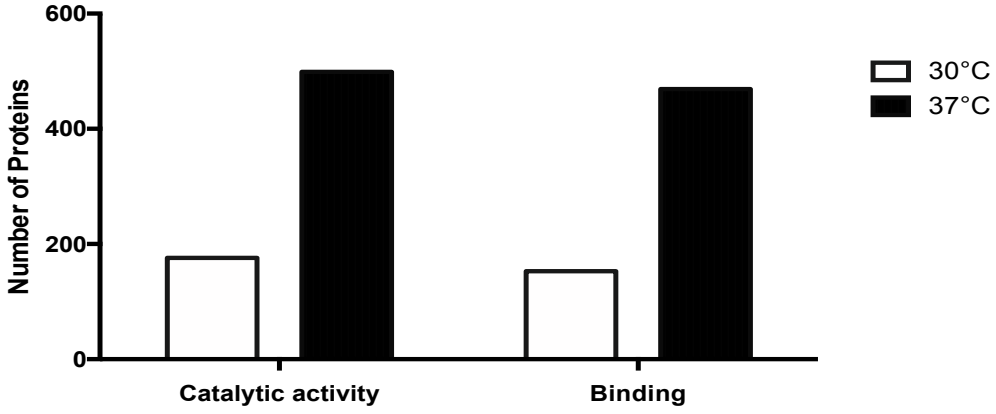

Figure 3.15 Molecular Function Level 2 grouping of proteins found in *B. oleronius*

Comparative bar chart showing changes to the number of proteins involved in selected molecular functions at level 2 ontology. Proteins based on percentage proportion of the total proteins found in the proteomic profile of *B. oleronius* affected by temperature.

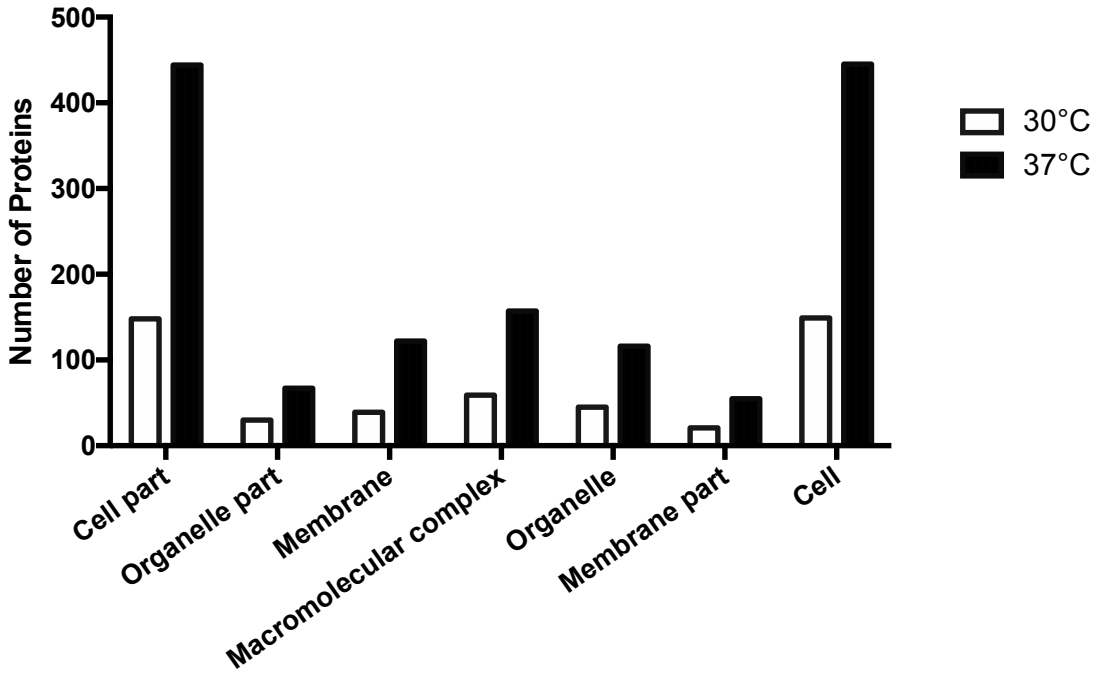

Figure 3.16 Cellular Component Level 2 grouping of proteins found in *B. oleronius*

Comparative bar chart showing changes to the number of proteins involved in selected cellular components at level 2 ontology. Proteins based on percentage proportion of the total proteins found in the proteomic profile of *B. oleronius* affected by temperature.

3.7 Discussion

The etiology of rosacea is not clearly defined and multiple factors may contribute to the onset, persistence and severity of the condition (Margalit *et al*., 2016; Gupta & Chaudhry, 2005). Genetic factors, microbial presence on the skin and immunological responses such as over protection of reactive oxygen species (ROS) may contribute to the appearance of symptoms (O'Reilly *et al*., 2012a; McMahon *et al*., 2014). The temperature of normal skin varies from 30-34ºC, while rosacea patients experience a higher skin temperature and burning sensation due to the vasodilation of blood vessels associated with the condition (Dahl *et al*., 2004; Guzman-Sanchez *et al*., 2007). A role for bacteria in the induction of rosacea has been suggested and a potential bacterial involvement may explain why antibiotics often lead to clearance of the condition (Jarmuda *et al*., 2012). Many microbes live commensally on the skin, however different conditions disrupt homeostasis which may trigger an immune response. The work presented here characterizes the effect of temperature on the abundance of immune stimulatory proteins by *B. oleronius*. It was hypothesized that the elevated skin temperature associated with this chronic dermatological condition may lead to an increase in the production of *B. oleronius* immunogenic proteins, thus heightening the cutaneous immune response.

The results presented here indicate that *B. oleronius* grows slower over 72 hours at 37ºC than at 30ºC in both NB media (Figure 3.1) and 2XYT media (Figure 3.2). The level of stimulatory 62 kDa antigen at 72 hours in 2XYT remains level (Figure 3.4) however, at 37ºC in NB the level of expression is increased by 1.65-fold ($p < 0.05$) (Figure 3.5). This was also observed using confocal microscopy, displayed by more of the immune-stimulatory 62 kDa antigen 37ºC (Figure 3.8) in comparison to 30ºC (Figure 3.7) in NB. The expression of 62 kDa antigen grown in 2XYT was very low in the medium and slightly increased at 37ºC (Figure 3.10) in comparison to 30ºC (Figure 3.9).

The effect of temperature on the proteomic profile of *B. oleronius* cultured in NB for 72 hours was analysed using 2D IEF SDS-PAGE. Selected proteins of interest that were significantly altered in abundance between 30ºC and 37ºC were compared (Figure 3.11). Arginase increased in abundance (3 fold increase; Table 3.1) and naturally competes for the same substrate L-arginine as nitric oxide

synthase, an enzyme required by macrophages for the production of cytokines in response to bacterial pathogenesis (Morris Jr., 2012; Pesce *et al*., 2009). Macrophages induced arginase expression in response to internal pathogens through the TLR pathway which leads to the production of polyamines (Duque-Correa *et al*., 2014; El Kasmi *et al*., 2008). Macrophages are the first line of defence and bacterial LPS can activate arginase-induced expression in macrophages which enhances angiogenesis and wound healing and also regulates the level of NO produced by inhibiting NOS from hydrolysing L-arginine (Buscher *et al*., 2017; El Kasmi *et al*., 2008; Gobert *et al*., 2002). The bacterium *H. pylori* has been associated with rosacea and also expresses arginase which can inhibit the NO-dependent apoptosis in macrophages, thus increasing the ability to survive (Holmes, 2013; Gobert *et al*., 2002). *B. oleronius* may increase the abundance of arginase in response to heat stress to overcome NO-dependent apoptosis induced by macrophages, promote angiogenesis, wound healing and enhance survival.

EF-Tu was identified with a 4 fold increase in abundance at 37ºC in comparison to 30ºC (spot 11), however this protein was identified once more (spot 4) with a 3.2 fold decrease (Figure 3.11). Further analysis of the *B. oleronius* proteome under increased temperature parameters revealed a number of translational elongation factors at 37ºC, all of which increased in abundance. For example, EF-Ts (139 fold increase), EF-GreA (40.8 fold increase) and EF-P (26.3 fold increase) (Table 3.3). EF-Tu is the most abundant bacterial protein and is a critical component bacterial translation, responsible for aminoacyl-tRNA binding and delivery to the correct aminoacyl site in the ribosome for protein synthesis (Pereira *et al*., 2015; Kuhle & Ficner, 2014). EF-Tu has also been associated with a dual role, the first in protein biosynthesis and the second in bacterial cell morphology, acting as a cytoplasmic protein. MreB is an actin-like protein required for cytoskeletal function and is responsible for the rod-shape cell of *B. subtilis* due to its helical filaments localising under the cell membrane. The eukaryotc version, EF-1A, has displayed similar structural roles via actin binding (Defeu Soufo *et al*., 2010; Dallo *et al*., 2002; Caldas *et al*., 1998). MreB and EF-Tu have been shown to interact previously in *E. coli* and EF-Tu has also been associated with the cell membrane under stressed conditions such as nutrient deprivation, immune system or tissue microenvironment (Pereira *et al*., 2015; Defeu Soufo *et al*., 2010; Dallo *et al*., 2002). GAPDH (8.9 fold

increase) is commonly referred to as a housekeeping protein, however it has many other role in biological processes such as apoptosis, phagocytosis and fusion Golgi transport (Das *et al*., 2016; Kim & Dang, 2005). However GAPDH has also been labelled a cytoplasmic protein similar to EF-Tu and is surface protein associated with fibronectin binding (Dallo *et al*., 2002). EF-Tu has a protective measure against thermal stress which involves protein refolding and protein renaturation, functioning similarly to bacterial molecular chaperones such GroEL (hsp60) and DnaK (hsp70) (Caldas *et al*., 1998).

The effect of temperature on *B. oleronius* led to increased abundance of other elongation factors (Table 3.3). EF-Ts plays a catalytic role by forming an exchange complex with inactive EF-Tu-GDP aminoacyl group to active form EF-Tu-GTP during bacterial protein synthesis (Wieden *et al*., 2002; Wittinghofer *et al*., 1983). EF-GreA is an important elongation factor during the RNA polymerase complex and has been with chaperone activity, similar to EF-Tu. EF-GreA has been shown to increase in many bacteria, for example *B. subtilis* and *E. coli*, during various stressful conditions to protect the cell against heat, salt or osmotic shock (Li *et al*., 2012; Srivastava *et al*., 2008; Stepanova *et al*., 2007). EF-P provides translational regulation during cell stress and monitors ribosomal activity when clusters of proline or glycine are introduced during protein synthesis (Doerfel & Rodnina, 2013; Zou *et al*., 2012). Both EF-P is positioned between the P (peptidyl tRNA) and the E (exiting tRNA) tRNA sites within the ribosome (Kumar *et al*., 2016; Zou *et al*., 2012).

A decrease in the abundance of condensing enzymes involved in fatty acid biosynthesis was observed during temperature stress (Table 3.2). KAS II (5.4 fold decrease; spot 5) has a similar 3D core structure to the enzyme thiolase (4.5 fold decrease; spot 3) and is responsible for initiating further elongation steps after the final stage of fatty acid synthesis is complete (Lai & Cronan, 2003; Marrakchi *et al*., 2002; Huang *et al*., 1998). KAS II has a condensing domain which consists of Cys and His residues while thiolase has a conserved Cyc-His region. Both of these enzymes share the ability to catalyse condensation reactions (Soto *et al*., 2011; Jiang *et al*., 2008).

Label-free MS/MS quantitative analysis identified a substantial number of proteins increased in abundance when *B. oleronius* was grown at 37ºC. Proteomic analysis revealed the increased abundance of many stress related proteins including phosphocarrier protein HPr (483.5 fold increase), putative phosphoesterase (385.5 fold increase), cold-shock protein (260.2 fold increase), universal stress protein (84.0 fold increase), general stress protein (21.7 fold increase), 10kDa chaperonin (18.1 fold increase) and 60 kDa chaperonin (12.6 fold increase) (Table 3.3; Table A3.1). This 60 kDa heat shock protein (HSP) is a member of the GroEL family. Stress proteins and HSPs are highly immunogenic and can act as an early trigger of the innate immune response by the recognition of macrophages (Horváth *et al*., 2008). *B. oleronius* 62 kDa antigen has been shown to recruit neutrophils to the site of infection which mediate the killing of phagocytosed pathogens (O'Reilly *et al*., 2012a). In healthy individuals, neutrophils induce an inflammatory cascade to target pathogens. The heightened immune response of rosacea patients highlights the abnormal activation of neutrophils which subsequently contributes to erythema and inflammation (McMahon *et al*., 2016). Neutrophil activation leads to the secretion of pro-inflammatory cytokines *in vivo* such as tumour necrosis factor (TNF-α) and IL-8, and also induces further neutrophil migration (Jarmuda *et al*., 2014; Holmes, 2013). The downstream effects of the innate immune defence lead to inflammation and tissue degradation in the vicinity of the sebaceous unit which is commonly seen in rosacea, particularly in cases of papulopustular rosacea where inflammation is localized at the site of papules and pustules (Jarmuda *et al*., 2012). Neutrophils also secrete matrix metalloprotease-9 (MMP-9) and cathelicidin, which degrade collagen and act as an antimicrobial (O'Reilly *et al*., 2012a).

The most significantly abundant protein at 37ºC was phosphocarrier protein HPr (483.5 fold increase) which is involved in the phosphotransferase system (PTS) responsible for the uptake of carbohydrates (Siebold *et al*., 2001). The phosphocarrier protein HPr is required by some Gram negative bacteria for virulence and the HPr regulon consists of many membrane-associated proteins which have been implicated in host interaction and stress response (Antunes *et al*., 2016). Iron transporter FeoA (323.8 fold increase) is involved in ferrous iron transport which is essential for bacterial virulence, however an overload of iron effectors has been

implicated with the inflammatory response (Wessling-Resnick, 2010; Cartron *et al*., 2006). It has been shown that rosacea patients are immune-reactive to the *B. oleronius* antigens; once the serum reactive antigens escape from the pilosebaceous unit, the innate immune system may be activated due to the presence of pathogenic foreign material. If the antigenic load reaches a critical level, this may induce an inflammatory cascade resulting in the erythemic symptoms of rosacea (Li *et al*., 2010; Lacey *et al*., 2009; Szkaradkiewicz *et al*., 2012).

The two proteins most significantly decreased in abundance were ferredoxin (325.2 fold) and peptidase S8 (244.5 fold) at 37ºC (Table 3.4). Ferredoxin is an iron sulfur protein from the flavoprotein superfamily and acts as one of two electron acceptors in the electron bifurcation mechanism (Peters *et al*., 2016; Seo *et al*., 2016; Mock *et al*., 2015). Most bacteria produce extracellular proteases at the stationary growth phase, however elevated growth temperature may act as a stress for *B. oleronius* and affect the production and transcription of proteases, such as peptidase S8. This protein is a subtilisin-like protease with catalytic mechanisms and biological activity (Liu *et al*., 2015; Morya *et al*., 2012; Di Cera, 2009). Protein prkA (57.2 fold) and stage IV protein A (33.4 fold) have key roles in bacterial sporulation and both are significantly reduced in abundance at 37ºC (Table 3.4). Protein prkA is a sigma^{E}-dependent sporulation protein functioning as a general marker protein for different stress factors (Tam *et al*., 2006). Although sporulation allows bacteria to survive during stress, it also creates an opportunity to remain dormant in environments that are temporarily undesirable. Lowered abundance of sporulation proteins at 37ºC inhibits *B. oleronius* from dormant protection during temperature stress. Stage IV protein A is involved with the development of the cortex and germ wall to form a peptidoglycan structure, all of which is essential for spore dormancy (Driks, 2002; Waites *et al*., 1970). Alanine dehydrogenase (Table 3.2) was identified twice in 2D IEF SDS-PAGE analysis (Figure 3.11) as spot 2 (5.5 fold decrease) and spot 6 (4.5 fold decrease) and is associated with sporulation and energy metabolism during stressed conditions such as heat shock (Moore & Leigh, 2005; Periago *et al*., 2002). However alanine dehydrogenase was identified as the most abundant protein in Table 3.3 (94.3 fold increase) at 37ºC. This protein is needed to for its catabolic function to promote cell growth when alanine is the only carbon or nitrogen source available (Moore & Leigh, 2005). The decreased abundance of sporulation proteins

and the overall increased abundance of alanine dehydrogenase may correlate with *B. oleronius* exiting the dormant phase of growth.

This work studied the proteomic changes of *B. oleronius* in response to elevated temperature and demonstrated increased abundance of proteins associated with stress responses, energy metabolism and biological processes. A similar increase of general stress proteins has been identified with *B. subtilis* in response to various stress and starvation conditions (Hecker & Völker, 2001). Importantly, at 37ºC a number of significant proteins were decreased in abundance (Table 3.4) resulting in reduced extracellular proteolytic activity and catalytic mechanisms (e.g. peptidase S8) as well as minimising the opportunity for sporulation (e.g. stage IV protein A). Elevated skin temperature in the face of rosacea patients can induce a stress response in *B. oleronius* once the bacterium comes into contact with the microenvironment of the skin. This thermal stress may lead to increased abundance of stress proteins as studied here, which activate macrophages and recruit neutrophils to the pilosebaceous unit. Pro-inflammatory cytokine production can provoke tissue damage, angiogenesis and exacerbate symptoms of this chronic dermatological condition.

Chapter Four

An Analysis of the Effect of Oxidative Stress on *Bacillus oleronius*

4.1 Introduction

Rosacea is a complex and chronic inflammatory disease with genetic, immunological and microbiological components (Margalit *et al*., 2016; Jarmuda *et al*., 2012). Changes in the immune status of the skin may make it susceptible to activation by external triggering factors (e.g. diet, medication, exposure to varying climates) , which in turn can influence endogenous conditions (e.g. lipids, sebum, sweat) (Holmes, 2013; Gupta & Chaudhry, 2005). Exposure to environmental triggers may exacerbate rosacea symptoms such as erythema, telangiectasia and corneal irritation. One study has highlighted the percentage of rosacea patients (n=1066) affected by external stimuli which include sun exposure (81%), hot weather (75%), wind (57%), strenuous exercise (56%) and alcohol consumption (52%) (Goldgar *et al*., 2009). Such factors can stimulate rosacea can induce oxidative stress, whereby the presence of active oxygen exceeds the cells tolerance (O'Reilly *et al*., 2012b; Cabiscol *et al*., 2000a).

UV radiation and other environmental factors can activate the first line of defence of the innate immune response, leading to the recruitment of neutrophils. *B. oleronius* has been implicated in the activation of neutrophils in rosacea (O'Reilly *et al*., 2012a). Neutrophils kill phagocytosed microorganisms by exposing the cells to reactive oxygen species (ROS) produced by the NAPDH oxidase complex (Hayes *et al*., 2011; Reeves *et al*., 2002; Roos *et al*., 2003). Neutrophil migration and killing mechanisms can cause tissue damage and induce inflammatory signalling pathways (O'Reilly *et al*., 2012a; Hayes *et al*., 2011). The most common ROS are superoxide (O_2^-), hydrogen peroxide (H_2O_2) and hydroxyl radical (OH^-).

Glycolysis leads to the breakdown of glucose into two pyruvates which feed into the citric acid cycle. Glycolysis can occur in the absence or presence of oxygen, however molecular oxygen is often used by microbes for respiration or oxidation to obtain energy in the form of ATP (Cabiscol *et al*., 2000a). Aerobic respiration and molecular oxygen can also lead to the ROS production via oxidation of O_2^- or H_2O_2 which can be harmful to bacterial cells (Fu *et al*., 2015). H_2O_2 is not a free radical but is more reactive than free molecular oxygen and is a product of O_2^- degraded by superoxide dismutase (Zhao & Drlica, 2014). Proteins exposed to ROS at the cellular

level can demonstrate amino acid modification which may disrupt protein structure and lead to disturbances in cellular metabolism (Cabiscol *et al*., 2000b).

Like almost all microbes, bacteria require iron for growth as well as many other functions such as oxygen activation, transport, proliferation and storage. The importance of iron homeostasis can be significantly interrupted by the presence of ROS, for example superoxide can affect iron-sulphur clusters (Van Acker & Coenye, 2017; Porcheron & Dozois, 2015). This results in ferrous iron (Fe^{2+}) becoming free to react with H_2O_2 and generate harmful hydroxyl radicals in a process referred to as the Fenton reaction (Van Acker & Coenye, 2017). DNA, lipids and proteins are directly targeted by hydroxyl radicals and damage can be deleterious to bacterial cells. OH^- can bind to polyunsaturated fatty acids and induce peroxidation of membrane lipids, which can directly impact membrane fluidity and membrane-bound protein function (Cabiscol *et al*., 2000b).

Neutrophils have adapted to employ the production of ROS in their killing mechanism to exploit the vulnerability of invading pathogens, such as *B. oleronius* in rosacea, to oxidative stress (Cabiscol *et al*., 2000b). The NADPH oxidase complex involves the production of O_2^- via redox reactions with molecular oxygen (Imlay, 2014; Roos *et al*., 2003). In order to combat neutrophils and the harmful effects of reactive H_2O_2 and Fe^{2+} in the Fenton system, bacteria have developed protective mechanisms from ROS. These include ROS-detoxifying enzymes such as superoxide dismutase (SOD), catalase and peroxidases, proteins such as glutaredoxin and thioredoxin and molecules such as glutathione (Fukai & Ushio-Fukai, 2011; Cabiscol *et al*., 2000b). SOD is responsible for degrading O_2^- to H_2O_2 and O_2, catalase and peroxidases then enzymatically degrade H_2O_2 and there is no known mechanism for detoxifying OH^- (Van Acker & Coenye, 2017; Imlay, 2015). Some bacterial species such as *E. coli*, have two catalases which degrade H_2O_2 to H_2O and O_2 (Cabiscol *et al*., 2000b). The importance of these ROS-scavenging enzymes has been highlighted in mutant species, resulting in DNA damage and iron damage, which prevented the bacteria from growing optimally (Imlay, 2015). The production of SOD, catalase and peroxidase enzymes is essential to suppress deleterious effects of the Fenton system (Zhao & Drlica, 2014).

Molecular oxygen has many advantages to the cell allowing aerobic respiration to yield large amounts of energy but oxic environments can lead to the production of ROS (Imlay, 2014). ROS in the presence of ferrous iron can impact the viability of bacterial cells (Fu *et al*., 2015). H_2O_2 can induce oxidative stress and this can result in damage to DNA, lipids and proteins (Van Acker & Coenye, 2017; Tretter & Adam-Vizi, 2000). ROS production can also be induced by neutrophils to kill invading bacterial pathogens, which can result in tissue degradation and inflammation, a key component associated with the chronic condition rosacea (Tisma *et al*., 2009). The aim of this Chapter was to assess the effect of static incubation conditions on the expression of 62 kDa antigen, an immune stimulatory protein produced by the strict aerobic bacterium, *B. oleronius*. Further work investigated the effect of oxidative stress induced by 10 mM H_2O_2 on the growth and proteomic profile of *B. oleronius*. The results highlighted the requirement of aerobic growth conditions for optimal expression of the 62 kDa protein. The abundance of proteins expressed by *B. oleronius* under oxidative stress was not greatly affected, however proteins grouped by associated functions were significant to note. Many glycolytic proteins increased in abundance under oxidative stress.

4.2 Investigating the effect of oxidative stress on the growth of *Bacillus oleronius*

B. oleronius was cultured in nutrient broth at 30°C for 72 hours with cell growth measured at various time points throughout (section 2.5). A concentration of 10 mM H_2O_2 was added to the culture from the beginning (0 hours) and also at the late stationary phase of growth (44 hours). The control sample of *B. oleronius* grew as normal at 30°C and reached stationary phase at 18 hours (Figure 4.1).
B. oleronius did not grow when H_2O_2 was present from the start due to the undesirable growth conditions caused from H_2O_2, indicative of oxidative stress. The control and the 10 mM H_2O_2 treatment added at 44 hours, displayed similar growth curves in that the lag phase was completed in the first 24 hours, followed by the stationary phase of growth and the final decline phase began after 40 hours. The third treatment consisted of *B. oleronius* cultures grown with 10 mM H_2O_2 added at 44 hours during the latter end of the stationary phase of growth. This did not significantly affect the growth as the lag phase of growth was reached in the first 24 hours (Figure 4.1).

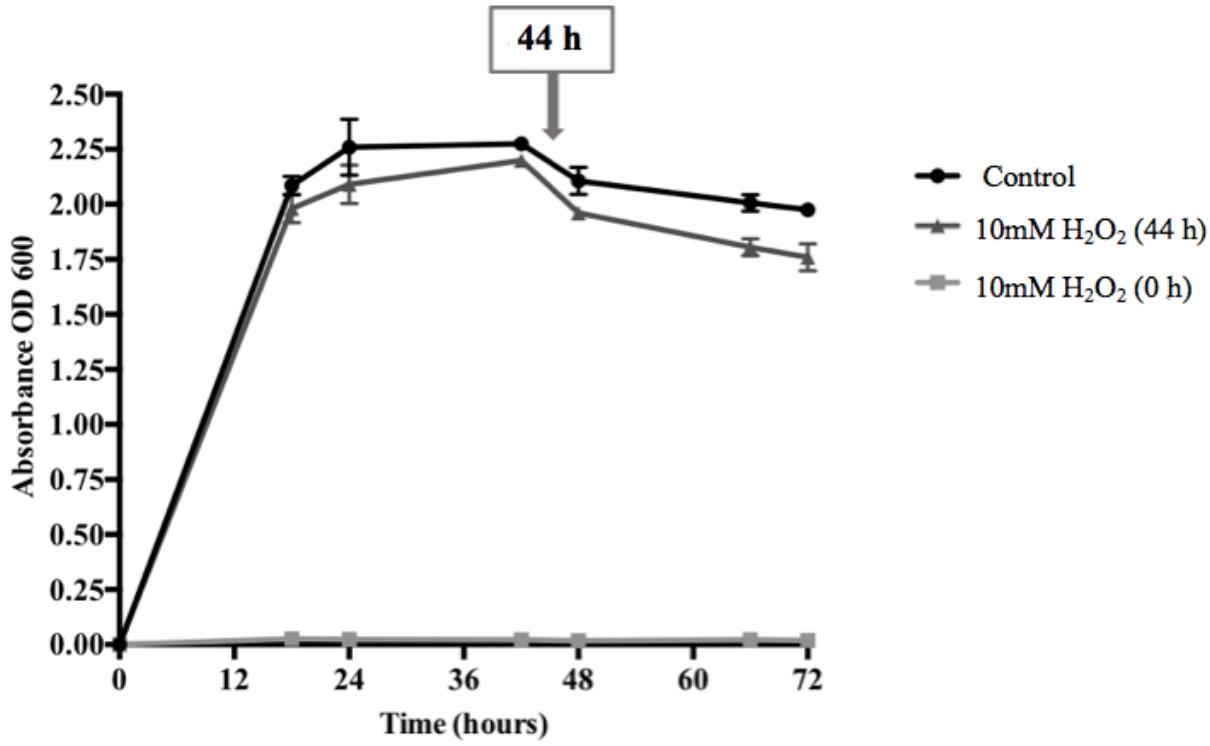

Figure 4.1 Growth of *B. oleronius* in the presence of 10 mM H_2O_2

Effect of oxidative stress on the growth of *B. oleronius* cultured at 30°C in nutrient broth in the presence of 10 mM H_2O_2. No growth occurred when cultured in nutrient broth and 10 mM H_2O_2 from the beginning (0 hour). No statistically significant decline in growth at 44 hours once 10 mM H_2O_2 was introduced to culturing in comparison to control. All treatment values are the mean ± SE of three independent determinations.

4.3 Investigating the effect of aerobic and static incubation growth conditions on the production of stimulatory 62 kDa antigen by *B. oleronius*

As shown in section 3.2, the optimal growth conditions for *B. oleronius* cultures are in NB at 30°C under aerobic (shaking) conditions. This facilitates a dense stationary phase of growth with the expression of the immune-reactive 62 kDa antigen by *B. oleronius* (Figure 3.5). This section analysed the requirement of oxygen for growth and for *B. oleronius* to express the 62 kDa protein.

B. oleronius cultures were grown in NB for 72 hours at 200 rpm (aerobic) or under static incubation conditions (static) at 30°C. The secretome and protein lysate were extracted and prepared for 1-D SDS-PAGE and for Western blotting with the anti-62 kDa rabbit antibody, as described in sections 2.9 and 2.13. The results highlight the lowered levels of protein abundance by 1-D SDS-PAGE (Figure 4.2A) and 62 kDa expression measured by Western blotting (Figure 4.2B) in static conditions compared with aerobic growth conditions. The level of protein abundance is similarly lowered for lysate samples (Figure 4.3A), however the expression of 62 kDa is less abundant as visualised by Western blot (Figure 4.3.B). Densitometric analysis of 62 kDa expression was obtained with Image J (section 2.11.2) and resulted in a statistically significant ($p < 0.05$) decrease of 62 kDa expression in the lysate samples grown under static conditions (Figure 4.4) compared to aerobic. The level of expression was also decreased in the secretome of static cultures (Figure 4.4) compared with aerobic, however not significantly.

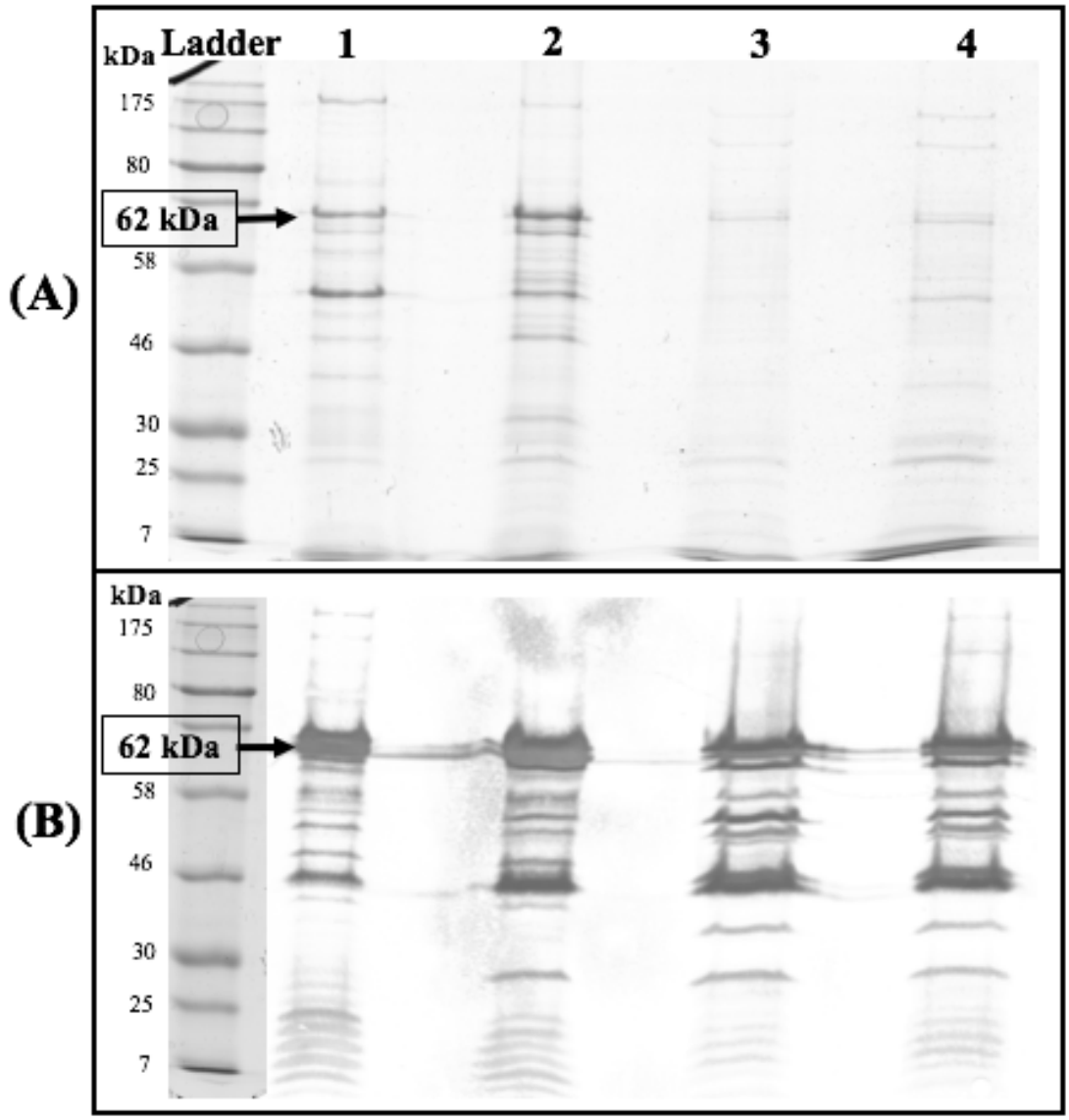

Figure 4.2 Representative 1-Dimensional SDS-PAGE and Western blot measuring the expression of *B. oleronius* 62 kDa protein found in secretome samples

(A) 1-D SDS-PAGE gel of protein extracted from the secretome of *B. oleronius* cultured for 72 hours under aerobic or static growth conditions. Decreased 62 kDa production can be visualised in static treatments (lanes 3 and 4) versus aerobic conditions (1 and 2). **(B)** Western blot analysis of anti-62 kDa conjugate carried out after (A). Slight decrease in expression under static conditions. Layout of lanes: protein ladder; aerobic replicate (1,2); static replicate (3,4). Both experiments were carried out on three independent occasions.

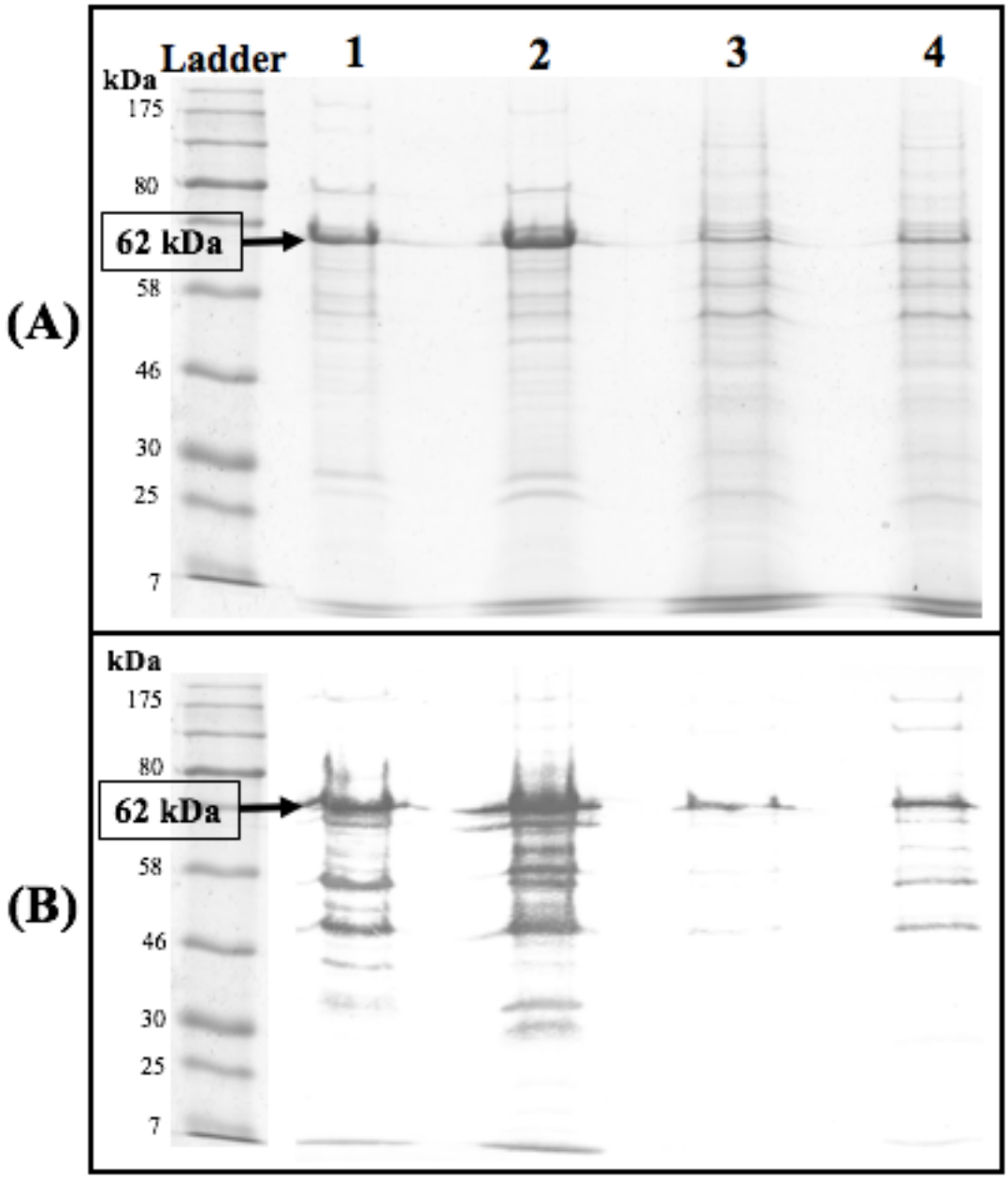

Figure 4.3 Representative 1-Dimensional SDS-PAGE and Western blot measuring the expression of *B. oleronius* 62 kDa protein found in lysate samples **(A)** 1-D SDS-PAGE gel of protein extracted from lysate of *B. oleronius* cultured for 72 hours under aerobic or static growth conditions. Decreased 62 kDa production can be visualised in static treatments (lanes 3 and 4) versus aerobic conditions (1 and 2). **(B)** Western blot analysis of anti-62 kDa conjugate carried out after (A). Visible decrease in expression of 62 kDa under static conditions (3 and 4) compared with aerobic. Layout of lanes: protein ladder; aerobic replicate (1,2); static replicate (3,4). Both experiments were carried out on three independent occasions.

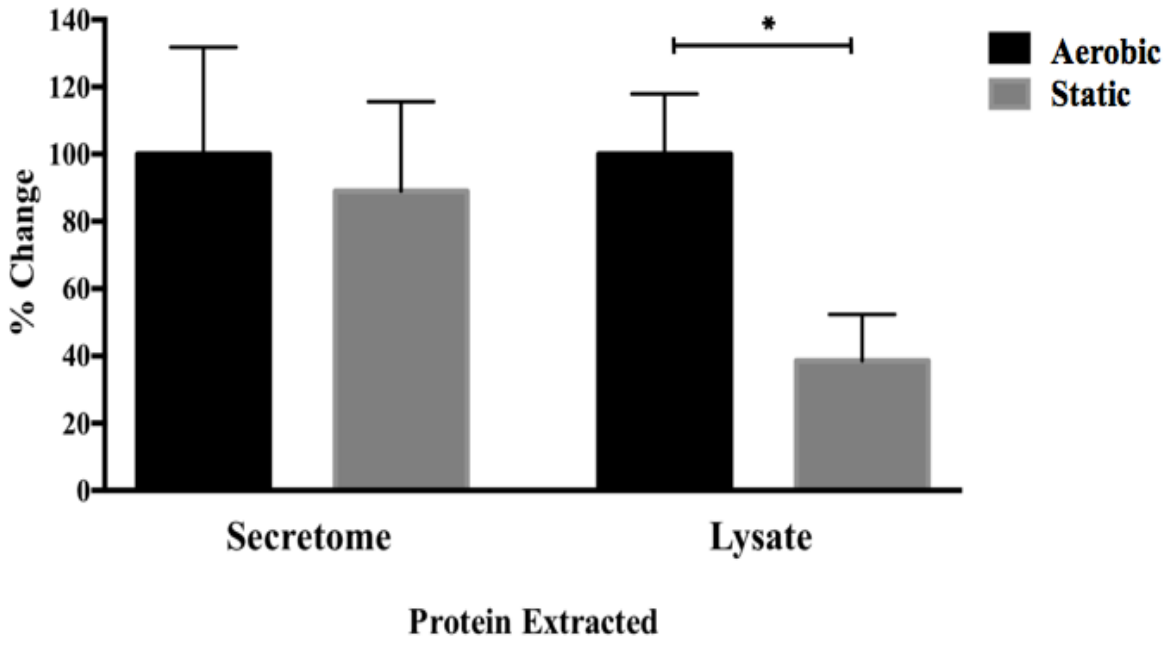

Figure 4.4 Densitometric analysis of stimulatory 62 kDa antigen expressed in aerobic or static incubation conditions

B. oleronius was cultured in NB at 30°C for 72 hours in aerobic conditions or static incubation conditions as described. Protein extracted from culture secretome and cell lysate was Western blotted with anti-62 kDa rabbit antibody and densitometry analysis was performed with Image J (version 1.50i). The expression of 62 kDa decreased slightly under static conditions in the secretome but significantly ($p < 0.05$) decreased in the lysate in comparison to aerobic conditions. All values are the mean ± SE of three independent determinations.

4.4 A 2-Dimensional IEF SDS-PAGE investigation of the effect of oxidative stress on proteomic profile of *B. oleronius*

From the results in section 4.2, it is clear that *B. oleronius* growth during 72 hours is unaffected following the introduction of 10 mM H_2O_2 at 44 hours (Figure 4.1). The effect of oxidative stress was further examined by 2D IEF SDS-PAGE. All cultures were incubated for 48 hours under aerobic conditions with 10 mM H_2O_2 added to treated cultures four hours prior to protein extraction (section 2.5).

The induction of oxidative stress, by the presence of 10 mM H_2O_2, resulted a change in the abundance of 19 proteins (Figure 4.5), determined using Progenesis^{TM} SameSpot software (section 2.11.3) to analyse differential expression between the control and treated *B. oleronius* proteomes. Spots of interest were excised and digested by LC-MS/MS. A total of 5 proteins were significantly increased in abundance in 10 mM H_2O_2 treated cultures ($p < 0.05$), all with a minimum of 1.7 fold change (Table 4.1). Spot 1 was identified as glycerol-3-phosphate dehydrogenase/oxidase, commonly referred to as GAPDH, with the highest increase of 2.5 fold. Spot 15 was identified as glucose-6-phosphate isomerase (GPI) and has a 1.7 fold increase in stressed cells. Spots 1 and 15 are both glycolytic enzymes, involved in the biochemical pathway glycolysis. GPI plays a crucial role in the primary phase of glycolysis by catalysing the interconversion of D-glucose-6-phosephate to D-fructose-6-phospate (Zong *et al*., 2015; Commichau *et al*., 2009). GAPDH is a key regulator of glycolysis and facilitates the NAD^+ dependent oxidation of glyceraldehyde-3-phosphate to 1, 3-biphosphoglycerate (Das *et al*., 2016; Kim & Dang, 2005).

Fourteen spots of interest were significantly decreased in abundance in cells treated with H_2O_2 (Table 4.2). Spots 7-9 were identified as the same protein, phophopyruvate hydratase, with a decrease of 4.1 fold. This protein is also referred to as enolase and is involved in the catalytic conversion of 2-phosphoglycerate (2PG) to phosphoenolpyruvate (PEP) in glycolysis (Kim & Dang, 2005). Enolase is one of thirty proteins conserved universally in all organisms and it has been postulated that enolase plays a physiological role in mRNA destabilisation in response to metabolic stress, which may prevent the build-up of glucose-6-phosphate (Morita *et al*., 2004; Commichau *et al*., 2009). Spot 12 was identified as

BMP family ABC transporter substrate-binding protein with the largest decrease at 5.3 fold. ABC (ATP binding cassette) transporters are found in all organisms and play a physiological role in bacteria for the transport and uptake of nutrients (Higgins, 2001). ABC proteins bind to peptide substrates on the extracytoplasmic receptor for translocation across the cytoplasmic membrane (Borezee *et al*., 2000). Acyl-CoA dehydrogenase was identified three times (spots 10, 13 and 18) with a maximum decrease of 4.3 fold (Table 4.2). The bacterial short chain of acyl-CoA dehydrogenase is a homotetramer with oxidase activity and is the first enzyme of fatty acid degradation in the β-oxidation cycle (Borezee *et al*., 2000; Battaile *et al*., 2002). Superoxide dismutase (spot 2) and serine protease (spot 4) decreased in abundance by 2.8 fold and 2.7 fold respectively. Superoxide dismutase serves as a protective functioning enzyme against reactive oxygen species (ROS) and degrades superoxide (O_2^-) (Van Acker & Coenye, 2017; Zhao & Drlica, 2014). Serine proteases are enzymes produced by most *Bacillus* species and play a role in biological processes. Serine proteases are typically endoproteases which catalyze the hydrolysis of peptide bonds, an activity shown to be repressed under stressful conditions (Liu *et al*., 2015; Morya *et al*., 2012; Di Cera, 2009).

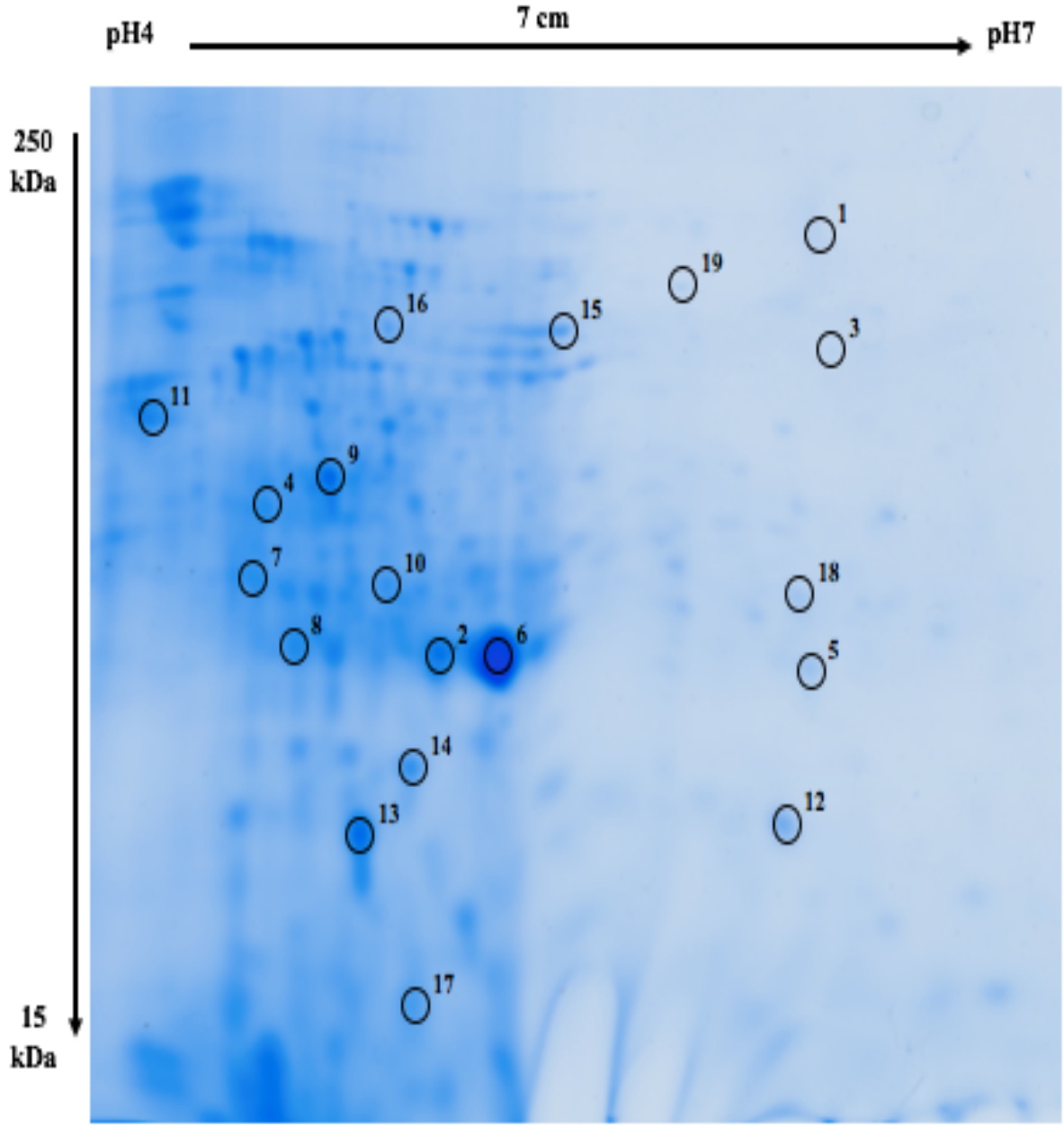

Figure 4.5 2-Dimensional IEF SDS-PAGE gel image displaying spots identified from the proteome of *Bacillus oleronius*

Representative gel image highlighting spots of interest from *B. oleronius* cultured for 4 hours under oxidative stress. Comparative proteomic analysis against control was performed before excising and digesting proteins which were identified by LC-MS/MS (Tables 4.1 and 4.2). All 2D gels were replicated on three independent occasions.

Table 4.1 Identities of spots increased in abundance in *B. oleronius* proteomic profile

Table of proteins that were identified from the comparative proteomic profile of *B. oleronius* cultured for 48 hours with the addition of 10 mM H_2O_2 at 44 hours versus without H_2O_2 (control). Identities listed in table were significantly increased ($p < 0.05$) in abundance in H_2O_2 treatments in comparison to controls. Selected spots shown in Figure 4.5.

Protein Spot and Identity	**Mass (M_r)**	**p*I***	**Coverage (%)**	**Score**	**Protein Identity**	***p*-value**	**Fold change increased H_2O_2**	**Protein Function**
1. Glycerol-3- phosphate dehydrogenase/ oxidase	61787	6.54	13	413	WP_0606 72058.1	7.475 e-005	2.5	GAPDH; Glycolysis; Housekeeping protein
3. ATP synthase subunit alpha	54724	6.01	15	504	WP_0347 65162.1	4.425 e-004	1.8	Peptide metabolism and transport
15. Glucose-6-phosphate isomerase	50130	5.02	7	184	WP_0606 73113.1	0.013	1.7	Glycolyic enzyme; Cell motility
16. 1-pyrroline-5 – carboxylate dehydrogenase	59898	4.89	10	371	WP_0606 74847.1	0.015	2.1	Energy production; Detoxification
19. Tetratriopeptide protein	23405	9.08	5	90	WP_0671 11612.1	0.047	2.5	Pilus stability; Pilus biogenesis

Table 4.2 Identities of spots decreased in abundance in *B. oleronius* proteomic profile

Table of proteins that were identified from the comparative proteomic profile of *B. oleronius* cultured for 48 hours with the addition of 10 mM H_2O_2 at 44 hours versus without H_2O_2 (control). Identities listed in table were significantly decreased ($p < 0.05$) in abundance in H_2O_2 treatments in comparison to controls. Selected spots shown in Figure 4.5.

Protein Spot and Identity	**Mass (M_r)**	**p*I***	**Coverage (%)**	**Score**	**Protein Identity**	***p*-value**	**Fold change increased H_2O_2**	**Protein Function**
2. Superoxide dismutase	22352	5.15	15	168	WP_034757581.1	4.425 e-004	2.8	ROS-detoxifying enzyme
4. Serine protease	34685	4.57	12	176	WP_060671537.1	0.001	2.7	Endoproteases; Polypeptide hydrolysis
5. Methionyl-tRNA formyltransferase, partial	12209	9.63	11	75	OSB07512.1	0.004	4.6	Translation; Biogenesis
6. 1-pyrroline-5-carboxylate dehydrogenase	59898	4.89	11	370	WP_060674847.1	0.004	3.2	Energy production; Detoxification
7. Phospho-pyruvate hydratase	46684	4.62	13	377	WP_034764211.1	0.005	2.7	Enolase; Glycolytic enzyme; Catalytic role
8. Phospho-pyruvate hydratase	46684	4.62	10	273	WP_034764211.1	0.005	4.1	Enolase; Glycolytic enzyme; Catalytic role

9. Phospho-pyruvate hydratase	46684	4.62	19	434	WP_0347 64211.1	0.007	2.5	Enolase; Glycolytic enzyme; Catalytic role
10. Acyl-CoA dehydrogenase	41636	5.21	7	194	WP_0580 06765.1	0.007	1.7	Lipid transport and metabolism; Oxidase activity
11. BMP family ABC transporter substrate-binding protein	39040	4.63	32	636	WP_0347 60098.1	0.008	2.3	ABC membrane substrate; Nutrient uptake
12. BMP family ABC transporter substrate-binding protein	39040	4.63	14	312	WP_0347 60098.1	0.009	5.3	ABC membrane substrate; Nutrient uptake
13. Acyl-CoA dehydrogenase	41809	5.21	5	179	WP_0068 37446.1	0.011	4.3	Lipid transport and metabolism; Oxidase activity
14. Aconitate hydratase 1	99299	5.04	2	193	WP_0292 81102.1	0.012	2.0	TCA cycle; Energy metabolism
17. Aldo/keto reductase	31673	5.23	15	260	WP_0347 63147.1	0.016	2.6	Oxidoreductase; Secondary metabolite synthesis
18. Acyl-CoA dehydrogenase	41636	5.21	7	166	WP+0580 06765.1	0.021	2.3	Lipid transport and metabolism; Oxidase activity

4.5 Comparative analysis of the effect of oxidative stress on the proteomic profile of *Bacillus oleronius* using Label Free MS/MS

Label free MS/MS quantitative proteomics was performed on cell lysate from *B. oleronius* cultured in NB at 30°C for 48 hours, with the addition of 10 mM H_2O_2 at 44 hours in treated cultures. LF-MS/MS enables a quantitative examination at the relative change in protein abundances over multiple parameters at single mass spectrometry runs (Bantscheff *et al*., 2012). PCA was performed with normalised intensity values (n=4) and resolved a clear difference in the proteomes (Figure 4.6A). All statistically significant proteins were visualised in a hierarchical cluster (Figure 4.6B) performed using Z-score normalised intensity values for differentially abundant proteins.

In total, 373 peptides were identified, representing 371 proteins with two or more peptides and 103 of these proteins were identified as differentially abundant with a fold change > 1.5 fold (ANOVA, $p < 0.05$) (Figure 4.7). When compared against control samples, 10 mM H_2O_2 treatments had 58 protein in higher abundance, 25 of which were imputated and 33 non-imputated (Table 4.3). A total of 45 proteins were found in lower abundance of which 10 proteins were imputated and 35 non-imputated (Table 4.4). These proteins were statistically analysed following imputation of zero values using a number close to the lowest value of the range of proteins ± standard deviation.

The protein with the highest increase in abundance in H_2O_2 treated samples was glutamate-1-semialdehyde 2,1-aminomutase (GSA-AM) with a 4.5 fold increase (Table 4.3). This protein is involved in the synthesis of δ-aminolevulinate acid (ALA), the universal precursor of all tetrapyrroles (Grimm, 1990). ALA plays a role in the biosynthesis of oxygen- carrying and electron-carrying porphyrins, for example heme, cobalamin and chlorophylls. GAS-AM is involved in the final step of ALA synthesis where it catalyses the transamination of GSA to ALA (Lüer *et al*., 2005; Murakami *et al*., 1993). Proteins identified with imputated values and higher abundances in H_2O_2 samples included dihydrolipoyl dehydrogenase (19.4 fold), uncharacterised UPF0473 protein (8.6 fold) and citrate synthase (8.3 fold) (Table 4.3). Dihydrolipoyl (dihydrolipamide) dehydrogenase consists of two subunits, a Flavin adenine dinucleotide (FAD) and a redox-active disulphide subunit (Dietrichs

et al., 1990)**.** This FAD-containing protein is the third member of the complex which catalyses the conversion of α-ketoglutarate (α-KGDH) to succinyl-CoA and pyruvate (PDH) to acetyl-CoA (Cabiscol *et al*., 2000a; Dietrichs & Remmer Andreesen, 1990). Citrate synthase is a bifunctional enzyme involved in the methylcitric acid cycle and has been used to identify bacterial species due to its phenotypical cellular fatty acid composition (Joblet *et al*., 1995; Reddick *et al*., 2017). Other proteins of interest that increased in abundance as a result of oxidative stress included ferrochelatase (7.5 fold increase), peroxiredoxin (7.4 fold increase) and thioredoxin (5.4 fold increase) (Figure 4.7).

The protein with the lowest abundance following H_2O_2 treatment ($p < 0.05$) was catalase-peroxidase with a 3-fold decrease (Table 4.4). This family of proteins is encoded by *katG* and is responsible for the reduction of H_2O_2 to H_2O and O_2 (Fukai & Ushio-Fukai, 2011; Imlay, 2014). Under oxidative stress H_2O_2 can become involved in the Fenton reaction which produces harmful hydroxyl radicals. However, with the ROS-detoxifying functions of catalases and peroxidases, the Fenton reaction can be suppressed (Zhao & Drlica, 2014; Van Acker & Coenye, 2017). Imputated proteins with a lower abundance included oligopeptide transport ATP-binding protein OppF (6.5 fold decrease), uncharacterized UPF0342 protein (6.4 fold decrease) and 3-hydroxyacyl CoA dehydrogenase (2.6 fold decrease). Other non-imputed proteins that were lowered in abundance included deoxyribose-phosphate aldolase (2.8 fold decrease) and peptidylprolyl isomerase (2.8 fold decrease) (Figure 4.7). The ATP-binding protein OppF is a member of the ATP-binding cassette (ABC) which was also found to be decreased in 2D IEF SDS-PAGE analysis in section 4.4 (Figure 4.5; spot 12) (Borezee *et al*., 2000). ABC transporters are highly conserved and function in ATP hydrolysis as well as bacterial virulence (Linton & Higgins, 1998). Oligopeptide transport systems such as the Opp system in *B. subtilis*, have been associated with extracellular signalling required for bacterial sporulation and survival (Borezee *et al*., 2000). A decrease in the ABC transporter substrate as seen here, may be to conserve energy and ATP hydrolysis by *B. oleronius* during oxidative stress.

The Blast2GO annotation software was employed to identify pathways and processes associated with oxidative stress. Level 3 GO terms were categorized into BP (Figure 4.8), MF (Figure 4.9) and CC (Figure 4.10). Subsequently, the total number of differential abundant proteins displayed no major significant differences within the B2G analysis of the entire proteome (357 protein in control and 371 proteins in H_2O_2). The most abundant proteins associated with BP were proteins involved in organic substance metabolic processes (198 proteins in control; 207 proteins in 10 mM H_2O_2), primary metabolic processes (187; 195) and cellular metabolic processes (182; 189) respectively (Figure 4.8). Proteins in MF increased slightly in H_2O_2 samples, mainly in heterocyclic- and organic cyclic-compound binding (133; 136) and ion binding (130; 133) (Figure 4.9). The two processes in which the most abundant proteins were involved in CC were intracellular part (120; 123) and intracellular (123; 126) (Figure 4.10). Further B2G analysis at level 3 GO was employed to differentially identify pathways and processes between statistically significant ($p < 0.05$) proteins increased and decreased in abundance in H_2O_2 treatments compared with control. These were categorized as before, BP (Figure 4.11), MF (Figure 4.12) and CC (Figure 4.13). The greatest change of protein proportion in BP were proteins labelled in organic substance metabolic pathways (25 proteins in increased abundance; 37 proteins in decreased abundance), primary metabolic process (25; 34), cellular metabolic process (27; 34), single-organism metabolic process (16; 33) and cellular component organization (4; 28) (Figure 4.11). The MF GO analysis had more proteins involved from the increased abundance data than decreased abundance (Figure 4.12). The most variable categories included heterocyclic compound binding (24 increased; 4 decreased), oxidoreductase activity (16; 7), ion binding (25; 12), organic cyclic compound binding (24; 15) and small molecule binding (14; 6). Fewer GO categories were involved in CC with less differences between increased and decreased protein abundance. Intracellular part (21; 15) and intracellular (23; 15) display the most variance in statistically significant data, with non-membrane bound organelle and intracellular organelle showing no difference in abundance (Figure 4.13).

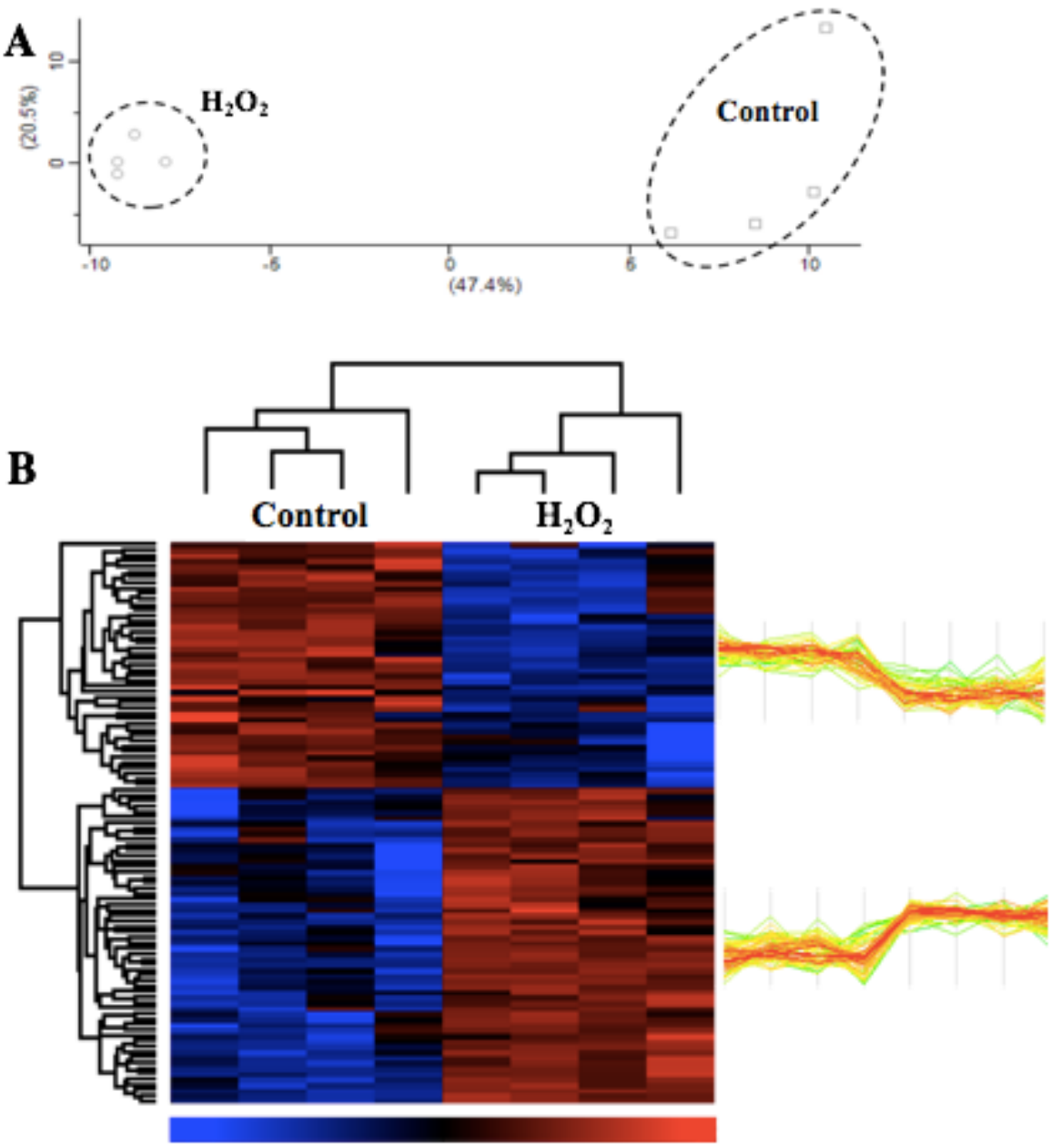

Figure 4.6 Label free MS/MS principal component analysis and hierarchical clustering of the quantitative differences in the proteomic profile of *B. oleronius* **(A)** PCA of comparative oxidative stress included in LFQ. Dashed circles represent sample groups with four replicates per group. **(B)** Heat map represents the median protein expression values of all statistically significant differentially and uniquely detected proteins from *B. oleronius* proteomic profiles at 48 hours untouched (control) and with the addition of oxidative stress at 44 hours (10 mM H_2O_2). Hierarchical clusters resolved by two distinct columns comprising the replicates from the original sample groups and cluster rows based on expression profile similarities. Red indicates high abundance, blue indicates low abundance.

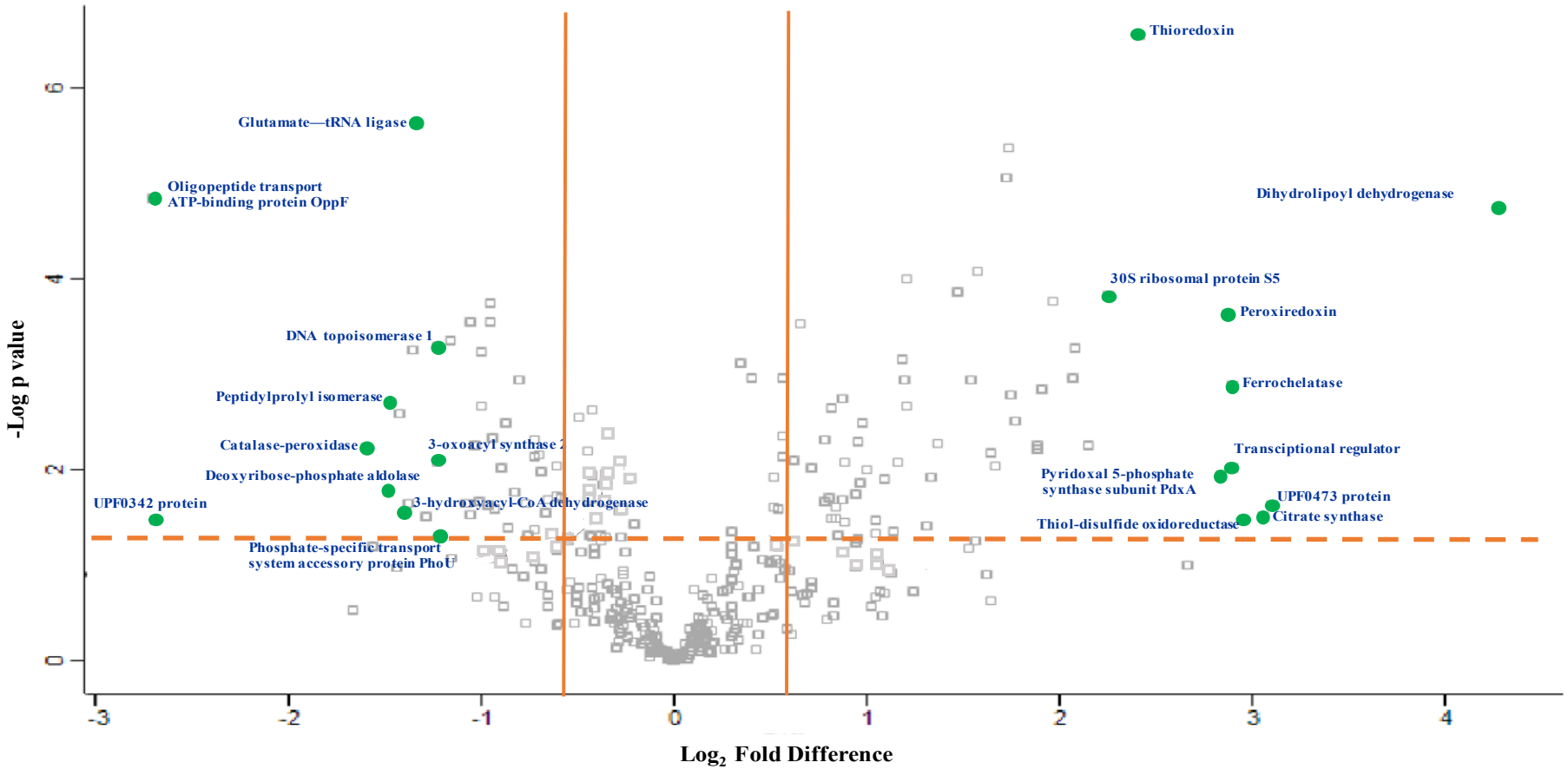

Figure 4.7 Volcano plot highlighting the twenty proteins most altered in abundance in *B. oleronius* when cultured under oxidative stress

Volcano plot showing the effect of oxidative stress on protein abundance in *B. oleronius*. Protein intensity difference (-$\log_2$ mean intensity difference) and significance in differences (-log *p*-value) based on a two-sided *t*-test. Proteins above the dashed line are considered statistically significant ($p < 0.05$) and those to the right and left of the vertical lines indicate > 1.5 fold positive changes and fold negative changes in 10 mM H_2O_2 respectively, versus control with no H_2O_2.

Table 4.3 Proteins identified at higher levels of abundance in *B. oleronius* treated with 10 mM H_2O_2 for 4 hours

Proteins that had over two matched peptides with a *t*-test probability < 0.5 and that were found to be differentially expressed at a 1.5 fold change were considered to be significantly higher in abundance in *B oleronius* cultured with 10 mM H_2O_2 at 44 hours. Table displays all 55 proteins with an increased fold difference.

Protein Annotation (* = non-imputated protein)	Peptides	Sequence Coverage %	Overall Intensity	Fold difference
Dihydrolipoyl dehydrogenase	5	14.9	9.98E+08	19.4
UPF0473 protein AM506_03120	2	28.1	8.20E+08	8.6
Citrate synthase	14	28.8	2.56E+09	8.3
Thiol-disulfide oxidoreductase	3	14.6	1.14E+09	7.7
Ferrochelatase	5	13.5	7.17E+08	7.5
Transcriptional regulator	4	15.1	4.08E+08	7.4
Peroxiredoxin	5	44.9	5.51E+08	7.4
Pyridoxal 5-phosphate synthase subunit PdxS	7	28	1.65E+09	7.1
Thioredoxin	3	24.8	4.00E+08	5.4
30S ribosomal protein S5	3	13.3	3.19E+08	4.8
* Glutamate-1-semialdehyde 2,1-aminomutase	4	14.7	2.40E+08	4.5
UDP-3-O-(3-hydroxymyristoyl) glucosamine N-acyltransferase	3	13.1	1.69E+08	4.3
Putative heme-dependent peroxidase	3	6.5	2.57E+08	4.2
*Fructose-bisphosphate aldolase	8	37.2	1.21E+09	3.9
UvrABC system protein B	5	10.6	1.84E+08	3.8
*Ornithine aminotransferase	10	29.7	1.66E+09	3.7
Biotin carboxylase	3	10	4.30E+08	3.7
Oxidoreductase	2	17.3	4.35E+08	3.4
Serine protease	6	25.9	9.90E+07	3.4
*Chemotaxis protein CheY	6	28.9	6.94E+08	3.3
*S-adenosylmethionine synthase	9	37.2	5.22E+08	3.3
Probable glycine dehydrogenase (decarboxylating) subunit 2	3	8	3.72E+08	3.2
*NADPH dehydrogenase	5	18.3	4.34E+08	3.1
*Site-determining protein	7	28.1	2.06E+08	3.0
*30S ribosomal protein S3	7	28.4	8.07E+08	2.9

Ribonucleoside-diphosphate reductase subunit beta	5	10.7	1.17E+08	2.8
Ribonuclease J	8	18.9	2.63E+08	2.5
Bifunctional protein GlmU	4	10.9	3.00E+08	2.5
*Elongation factor Tu	13	41.4	3.56E+10	2.3
2-C-methyl-D-erythritol 2,4-cyclodiphosphate synthase	5	46.8	1.34E+08	2.3
*Translation initiation factor IF-2	6	7.2	4.35E+08	2.3
*Peptidase M28	5	13.3	1.75E+09	2.3
Inositol monophosphatase	5	28.3	9.96E+07	2.2
Acetyl-CoA carboxylase	5	16.2	4.97E+08	2.2
Glucose-6-phosphate isomerase	5	14.9	3.39E+08	2.1
Thymidylate synthase	4	29.2	2.65E+08	2.1
NADPH-dependent 7-cyano-7-deazaguanine reductase	4	38.2	1.64E+08	2.1
*Dihydrolipoyllysine-residue succinyltransferase component of 2-oxoglutarate dehydrogenase complex	10	26.6	3.51E+09	2.0
Glutamate dehydrogenase	4	16.2	1.97E+08	1.9
*Transcriptional regulator	12	36.9	2.32E+09	1.9
Methylmalonyl-CoA mutase	14	13.2	2.30E+08	1.9
*Cysteine protease	7	54.4	4.28E+09	1.9
Ribonuclease J	3	9.9	1.44E+08	1.9
*Ferredoxin	5	47.2	1.20E+09	1.8
*Bacitracin ABC transporter ATP-binding protein	8	25.3	1.19E+09	1.8
*Alanine dehydrogenase	8	23.7	3.25E+09	1.8
Aspartate aminotransferase	4	15.7	1.59E+08	1.8
Glyoxalase	2	16.5	9.04E+07	1.8
*Aspartyl/glutamyl-tRNA(Asn/Gln) amidotransferase subunit B	10	25.8	2.69E+08	1.8
*Phosphoenolpyruvate carboxykinase [ATP]	9	17.4	3.05E+09	1.8
*Isocitrate dehydrogenase [NADP]	11	21.5	1.18E+09	1.7
*NonF	7	40.1	2.27E+09	1.7
*Leucine dehydrogenase	11	45.2	2.03E+09	1.6
*Glyoxal reductase	7	27.9	9.09E+08	1.6
*Aldo/keto reductase	3	14.6	8.12E+08	1.5

Table 4.4 Proteins identified at lower levels of abundance in *B. oleronius* treated with 10 mM H_2O_2 for 4 hours

Proteins that had over two matched peptides with a *t*-test probability < 0.5 and that were found to be differentially expressed at a 1.5 fold change were considered to be significantly lower in abundance in *B oleronius* cultured with 10 mM H_2O_2 at 44 hours. Table displays all 45 proteins with a decreased fold difference.

Protein Annotation (* = non-imputated protein)	Peptides	Sequence Coverage %	Overall Intensity	Fold difference
Oligopeptide transport ATP-binding protein OppF	3	13.1	4.11E+08	6.5
UPF0342 protein AM506_02645	4	31.6	6.18E+08	6.4
*Catalase-peroxidase	8	13.8	9.56E+08	3.0
*Deoxyribose-phosphate aldolase	4	24.2	1.00E+09	2.8
*Peptidylprolyl isomerase	7	25.8	1.32E+08	2.8
3-hydroxyacyl-CoA dehydrogenase	8	10.7	3.50E+08	2.6
*Glutamate--tRNA ligase	5	14.8	5.85E+08	2.5
DNA topoisomerase 1	6	13.3	1.68E+08	2.3
*3-oxoacyl-[acyl-carrier-protein] synthase 2	6	9.4	5.29E+08	2.3
Phosphate-specific transport system accessory protein PhoU	3	12.8	1.22E+08	2.3
*6-phosphogluconate dehydrogenase, decarboxylating	11	28.8	1.74E+09	2.2
*Elongation factor Ts	12	32.8	1.32E+09	2.1
*4-hydroxyphenylpyruvate dioxygenase	16	39.4	5.89E+09	2.1
C4-dicarboxylate ABC transporter	4	5.4	9.35E+07	2.1
*50S ribosomal protein L3	4	15.8	9.32E+08	2.0
*Fur family transcriptional regulator	3	21.7	1.22E+09	2.0
*Acyl--CoA ligase	11	18.8	1.15E+09	2.0
*Cell cycle protein GpsB	3	33	3.33E+08	2.0
*Methylmalonate semialdehyde dehydrogenase [acylating]	4	16.4	2.05E+08	2.0
*ABC transporter ATP-binding protein	8	18.2	3.67E+08	1.9
*Fructose-bisphosphate aldolase class 1	6	18.9	9.47E+08	1.9
*Short-chain dehydrogenase	4	12.1	3.87E+08	1.9
Proline dehydrogenase	3	11.5	1.11E+08	1.9
*DNA gyrase subunit A	13	14.9	5.94E+08	1.9

*RNA polymerase sigma factor SigA	5	25.8	3.74E+08	1.8
*Acetoin utilization protein AcuB	4	20.5	5.67E+08	1.8
*Glycine--tRNA ligase	7	25.8	8.92E+08	1.8
*Glycine cleavage system H protein	4	39.4	6.26E+09	1.7
*Fe-S cluster assembly protein SufB	7	21.1	8.32E+08	1.7
Stage III sporulation protein AH	4	23.4	1.63E+08	1.7
*Ribonuclease Y	18	31	1.59E+09	1.7
*Foldase protein PrsA	8	30	8.72E+08	1.6
*Branched-chain alpha-keto acid dehydrogenase subunit E2	13	26.7	4.57E+09	1.6
*Sporulation protein	3	11.6	1.42E+08	1.6
*Serine hydroxymethyltransferase	11	26.9	2.29E+09	1.6
*Probable manganese-dependent inorganic pyrophosphatase	5	21.8	9.83E+08	1.5
*Fumarate hydratase	10	21.6	9.06E+08	1.5
*Cold-shock protein	2	66.2	6.06E+09	1.5

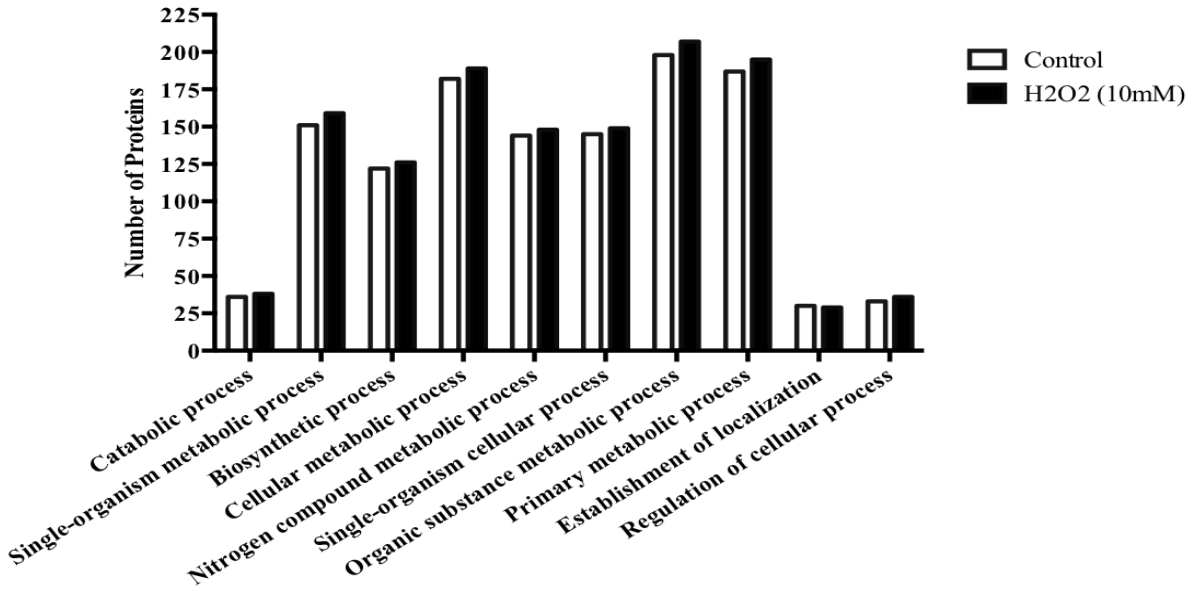

Figure 4.8 Biological Process Level 3 of proteins found in *B. oleronius*

Comparative bar chart showing changes to the number of proteins involved in selected biological processes at level 3 ontology. Proteins based on percentage proportion of the total proteins found in the proteomic profile of *B. oleronius* affected by oxidative stress.

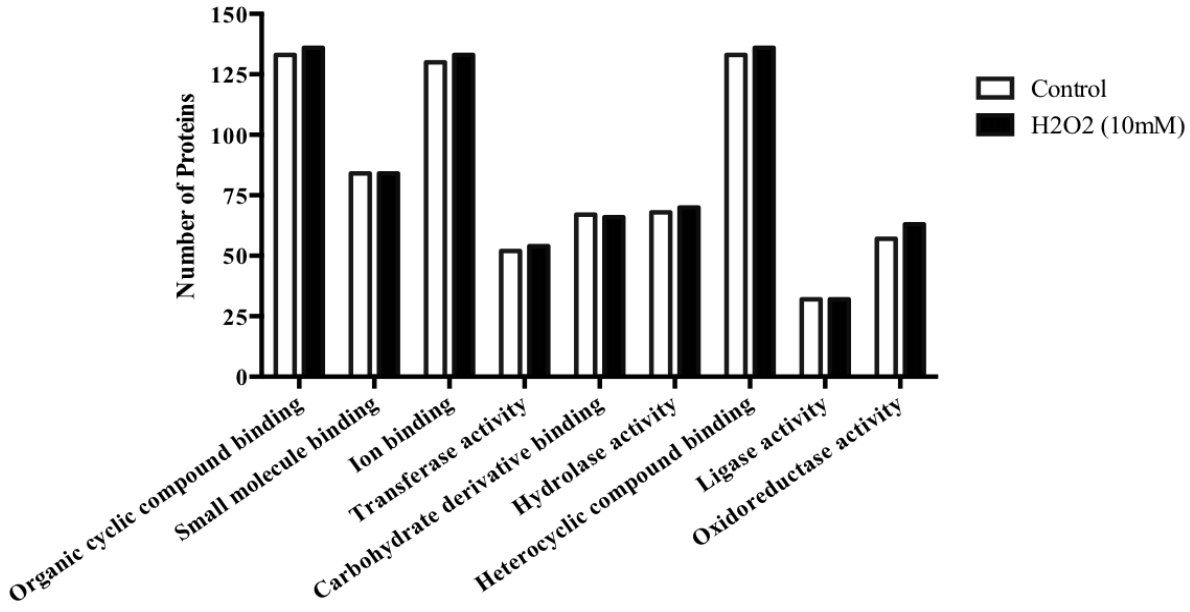

Figure 4.9 Molecular Function Level 3 of proteins found in *B oleronius*

Comparative bar chart showing changes to the number of proteins involved in selected molecular functions at level 3 ontology. Proteins based on percentage proportion of the total proteins found in the proteomic profile of *B. oleronius* affected by oxidative stress.

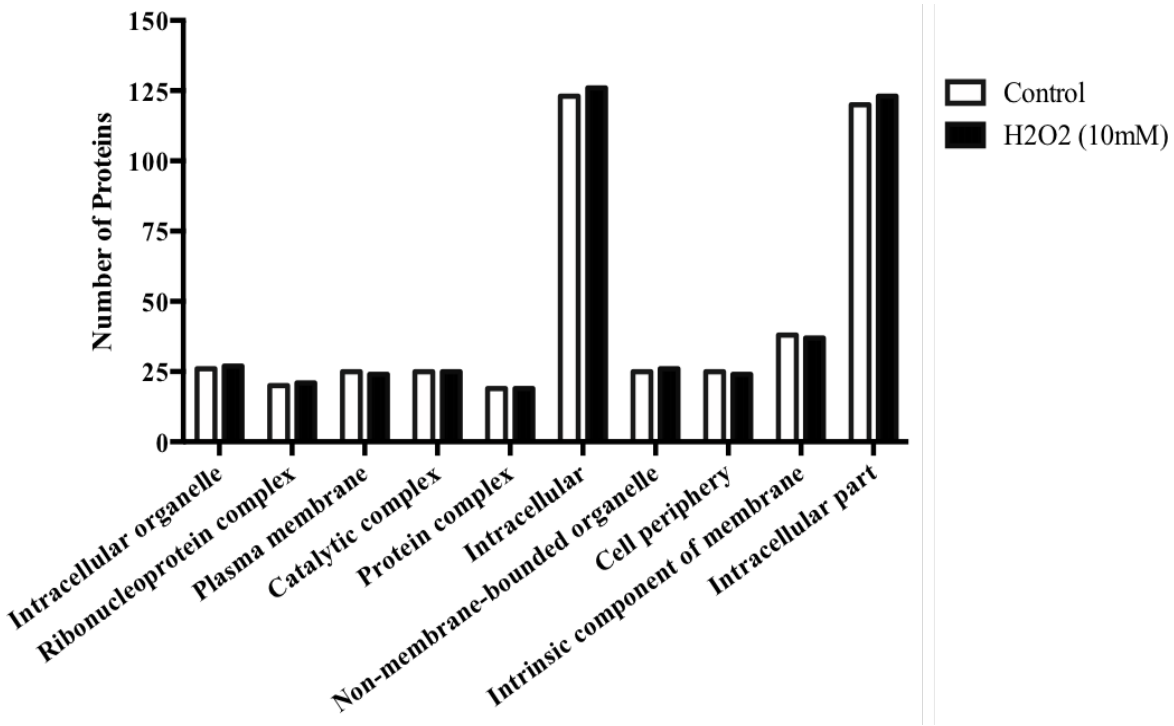

Figure 4.10 Cellular Components Level 3 of proteins found in *B. oleronius*

Comparative bar chart showing changes to the number of proteins involved in selected cellular components at level 3 ontology. Proteins based on percentage proportion of the total proteins found in the proteomic profile of *B. oleronius* affected by oxidative stress.

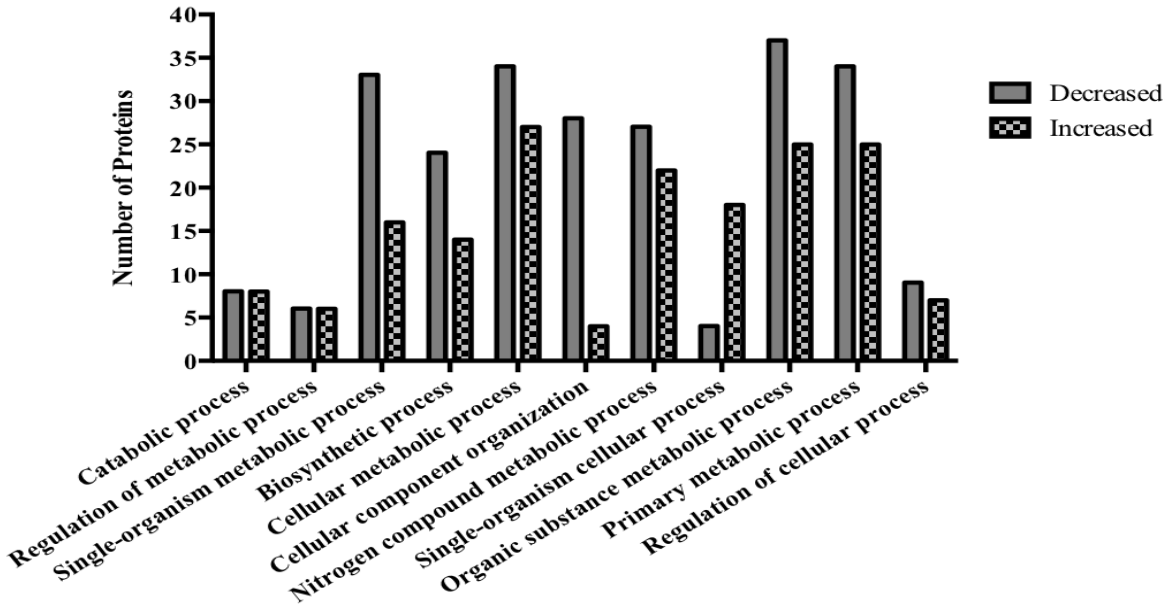

Figure 4.11 Biological Process Level 3 of altered proteins found in *B. oleronius*

Comparative bar chart showing the changes to the number of proteins involved in selected biological processes at level 3 ontology. Proteins based on percentage proportion of the statistically significant proteins increased or decreased in abundance found in the proteomic profile of *B. oleronius* affected by oxidative stress.

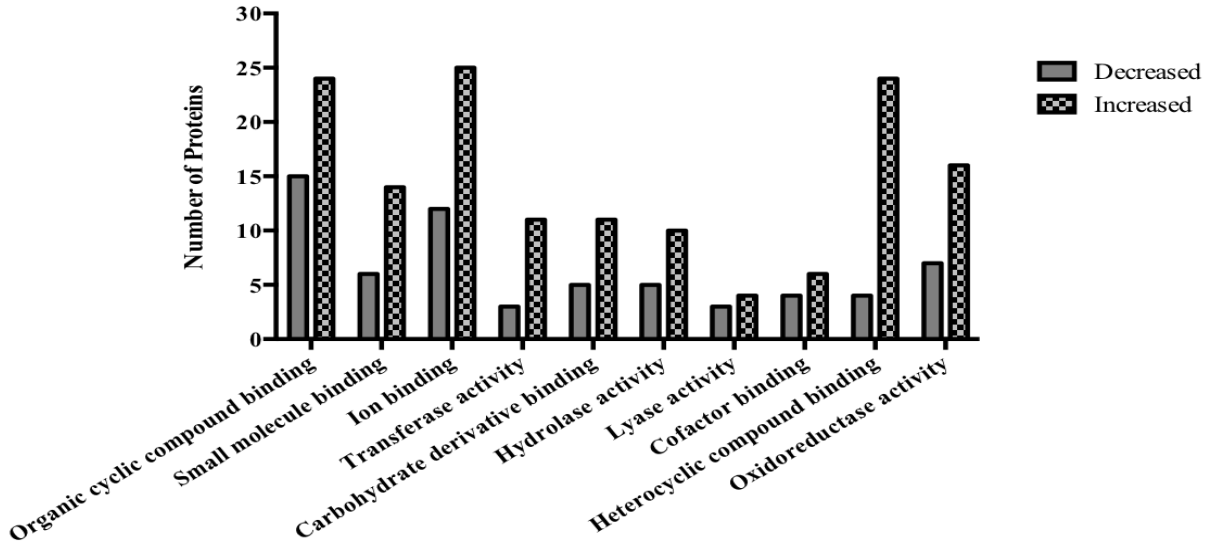

Figure 4.12 Molecular Function Level 3 of altered proteins in *B. oleronius*

Comparative bar chart showing the changes to the number of proteins involved in selected molecular functions at level 3 ontology. Proteins based on percentage proportion of the statistically significant proteins increased or decreased in abundance found in the proteomic profile of *B. oleronius* affected by oxidative stress.

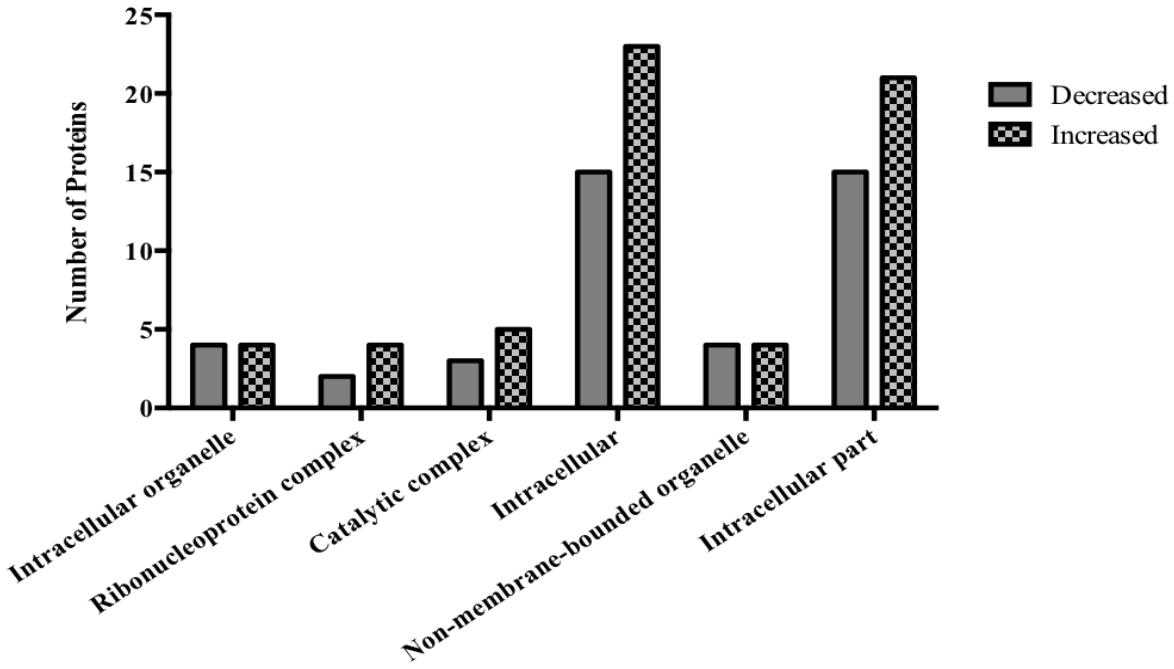

Figure 4.13 Cellular Component Level 3 of altered proteins in *B. oleronius*

Comparative bar chart showing the changes to the number of proteins involved in selected cellular components at level 3 ontology. Proteins based on percentage proportion of the statistically significant proteins increased or decreased in abundance found in the proteomic profile of *B. oleronius* affected by oxidative stress.

4.6 Discussion

B. oleronius has been extracted from the digestive tract of a *Demodex* mite and is believed to be an endosymbiont of *Demodex* mites which flourish on the skin of the face and eyelashes (Lacey *et al*., 2007). *Demodex* infestation is significantly higher in the skin of rosacea patients than healthy controls, thus once *Demodex* mites die and rupture, it releases higher levels than normal of *B. oleronius* into the pilosebaceous unit (Zhao *et al*., 2017; Szkaradkiewicz *et al*., 2012). Many external factors can influence the onset of rosacea, such as emotional stress, alcohol consumption, UV radiation and exposure to high temperature (Yamasaki & Gallo, 2011; Goldgar *et al*., 2009). Many immune factors are also implicated with the onset, such as toll-like receptor (TLR) stimulation, antimicrobial peptide, cytokine and cathelicidin release which all regulate inflammation (McMahon *et al*., 2016; Margalit *et al*., 2016). A number of triggers, as well as the exposure of bacterial antigens leaked from *Demodex* mites, can activate the innate immune response leading to the induction of neutrophil activation and recruitment (Jarmuda *et al*., 2014; Hayes *et al*., 2011). Neutrophils are effector cells that mediate the killing of engulfed pathogens such as *B. oleronius*, which can often lead to inflammation (Hayes *et al*., 2011). Bacteria have adapted defence mechanisms to overcome neutrophil mechanisms and oxidative stress, including detoxifying enzymes such as superoxide dismutase, catalase and peroxidases (Fukai & Ushio-Fukai, 2011; Roos *et al*., 2003).

The presence of molecular oxygen with H_2O_2 or free ferrous iron can be toxic to bacterial cells and induce oxidative stress leading to the development of harmful hydroxyl radicals. *B. oleronius* has been shown to increase the production of immune stimulatory 62 kDa protein under stressed conditions (O'Reilly *et al*., 2012c; McMahon *et al*., 2016). The level of *B. oleronius* 62 kDa expression in the presence and absence of oxygen was investigated over 72 hours in both the secretome (Figure 4.2) and the cell lysate (Figure 4.3). The level of 62 kDa abundance in secretome remained consistent between aerobic and static cultures which was visualised via Western blot (Figure 4.2B) and quantitatively measured using Image J (Figure 4.4). However the difference in 62 kDa expression was significantly lower in abundance in lysate from statically grown cells (Figure 4.4). This implies that *B. oleronius* grown under static incubation conditions secretes most

of the 62 kDa protein into the surrounding environment. Aerobic condition at 30°C is optimal for *B. oleronius* growth (Section 3.2) and expression of 62 kDa protein (Figure 4.4).

Bacteria have adapted defence mechanisms when they encounter stressful conditions such as temperature shift, oxidative stress or neutrophil attack. The transition of *B. oleronius* from the digestive tract of *Demodex* into the host environment may impact the bacterial cell in many ways. *B. oleronius* alters protein expression to overcome the impact of ROS produced by neutrophils and the level of oxidative stress induced by trigger factors of rosacea such as UV radiation or toxic levels of ROS (McMahon *et al*., 2016; Fukai & Ushio-Fukai, 2011). To measure the effect of oxidative stress on *B. oleronius* growth and proteome, 10 mM H_2O_2 was used as described in section 4.2. *B. oleronius* in the presence of the ROS at 0 hours from culture commencement, resulted in no growth as the levels were too toxic (Figure 4.1). However the bacterium was capable of maintaining growth following exposure to oxidative stress. In order to understand how *B. oleronius* can do this, the proteomic profile was investigated to highlight any processes or pathways or proteomic patterns that could lead to the tolerance and survival of *B. oleronius* under oxidative stress.

Many glycolytic proteins increased in abundance in cultures treated with 10 mM H_2O_2, compared with controls. Glycerol-3-phosphate dehydrodenase/oxidase (GAPDH) and glucose-6-phosphate isomerase (GPI) increased 2.5 fold and 1.7 fold respectively following 2D IEF SDS-PAGE analysis (Table 4.1). Fructose-biphosphate aldolase (FBP) and GPI increased 3. 9 fold and 2.1 fold respectively following Q-exactive MS analysis (Table 4.3). Glycolysis is an ancient biochemical pathway that can occur in the presence of oxygen or anaerobically, to yield energy and play an important role in metabolism (Commichau *et al*., 2009). Glycolysis is a key pathway of the respiration cycle and has two phases; the priming phase, also referred to as the preparatory phase which uses energy (ATP) to convert glucose to fructose-1,6-biphosphate and the second phase also referred to as the payoff phase which results in a net energy yield and the further breakdown of fructose-1,6-biphosphate to pyruvate (Commichau *et al*., 2009; Kim & Dang, 2005). GPI was identified in both 2D and Q-exactive MS studies, and is the second glycolytic

enzyme involved in the priming phase of glycolysis (Zong *et al*., 2015). FBP is the first enzyme involved in the payoff phase and is responsible for the conversion of fructose-1,6-biphosphate to glyceraldehyde-3-phosphate, which in turn is oxidised by GAPDH to 1,3-biphosphoglycerate (Schürmann & Sprenger, 2001; Dandekar *et al*., 1999). GPI and GAPDH have multiple non-glycolytic roles. GPI is a recognised cytokine, growth factor, and also functions in cell motility and invasion (Zong *et al*., 2015; Kim & Dang, 2005). GAPDH catalyses reactions involved in Krebs Cycle, transcriptional regulation role and is also associated with cellular functions such as phagocytosis and apoptosis (Das *et al*., 2016; Kim & Dang, 2005; Commichau *et al*., 2009).

A number of proteins were increased in abundance in response to oxidative stress including peroxiredoxin (7.4 fold increase), thioredoxin (5.4 fold increase), oxidoreductase (3.4 fold increase), NADPH dehydrogenase (3.1 fold increase), glutamate dehydrogenase (1.9 fold increase), glyoxalase (1.8 fold increase) and isocitrate dehydrogenase (NADP) (1.7 fold increase) (Table 4.3). The thioredoxin system is a protective mechanism in bacteria against oxidative stress whereby NADPH is reduced by thioredoxin reductase into thioredoxin (Kováryová & Kollárová, 2008; Cabiscol *et al*., 2000a). Peroxiredoxin and thioredoxin are cell anti-oxidants which maintain the redox conditions of the cell by sequestering reactive molecular oxygen (Van Acker & Coenye, 2017; Kalinina *et al*., 2008). Glutamate dehydrogenase plays a role in stress-induced carbonylation and is the enzyme involved in the conversion of glutamate to the amino acid glutamine, which is an integral metabolite in bacterial physiology (Nyström, 2005; Tanous *et al*., 2002; Meers *et al*., 1970). H_2O_2-induced oxidative stress requires a high yield of NADPH which can be sourced from the glycolysis pathway during the reaction catalysed by GAPDH (Kim & Dang, 2005; Grabowska & Chelstowska, 2003). Oxidoreductase (3.4 fold increase) is a catalyst enzymes for electron transfer, dihydrolipoamide dehydrogenase (19.4 fold increase; Figure 4.7) belongs to the family of oxidoreductase (3.4 fold increase), an electron transfer catalyst enzyme (Ezraty *et al*., 2017; Dietrichs & Remmer Andreesen, 1990). Oxidoreductase family members also include thioredoxin reductase and glutathione reductase, all of which consist of a flavin adenine dinucleotide (FAD) subunit and an active redox-disulfide subunit. The FAD containing subunits are involved in the α-KGDH and PDH complexes,

which can sometimes be limited during oxidative stress caused by ROS (Ezraty *et al*., 2017; Tretter & Adam-Vizi, 2000; Dietrichs *et al*., 1990). An increase in NADPH dehydrogenase (3.1 fold) may be necessary for the upkeep of the α-KGDH and PDH complexes and is also associated with some bacterial oxidoreductase enzymes (Liao *et al*., 2013; Maruyama *et al*., 2003; Rasmusson *et al*., 1999). Oxidative stress induced by ROS can disrupt the reducing environment of the cytosol which can impact protein folding which is termed "disulphide stress". Glutathione and NADPH play a crucial role in scavenging molecular oxygen, with glutathione acting as an electron donor (Van Acker & Coenye, 2017; Cabiscol *et al*., 2000b). Glyoxalase (1.8 fold increase) is detoxifying enzyme and converts glutathione to *S*-D-lactoylglutathione which controls an element of efflux pumps in the cell (Suttisansanee & Honek, 2011; Suttisansanee *et al*., 2011; Cabiscol *et al*., 2000b).

H_2O_2 is a small uncharged molecule and that can competently pass through the membranes, thus initiating oxidative stress. SOD, catalase and peroxidases are required by bacteria to survive this oxidative stress. Without these detoxifying enzymes, H_2O_2 can react with molecular oxygen, iron-sulphur dehydratases or ferrous iron in the Fenton system and generate more harmful hydroxyl radicals (Imlay, 2014; Zhao & Drlica, 2014). Both SOD (Table 4.1; Spot 2) and catalase (Table 4.4) have decreased in abundance after four hours of 10 mM H_2O_2 exposure, 2.8 fold and 3.0 fold respectively. Catalase and peroxidases are important ROS-detoxifying enzymes that degrade H_2O_2. However, the requirement for these antioxidant enzymes at 48 hours may no longer be necessary, hence their decrease in abundance.

A number of iron associated proteins were altered in abundance under oxidative stressed conditions. Iron is an essential component for bacterial growth, however the presence of free iron can be potentially toxic to the cells as it can react with H_2O_2 in the Fenton system. The iron related proteins included ferrochelatase (7.5 fold increase), ferredoxin (1.8 fold increase), Fur family transcriptional regulator (2 fold decrease) and Fe-S cluster assembly protein (1.7 fold decrease) (Table 4.3; Table 4.4). Ferredoxin is an iron-sulfur protein and an electron donor that plays a role in energy metabolism and is also required in some redox reactions such

as the NADPH-ferredoxin oxidoreductase complex to restore NADPH levels (Imlay, 2014; Buckel & Thauer, 2013). Iron is the substrate of ferrocheletase, which catalyzes free iron in the heme biosynthesis pathway (Qi & O'Brian, 2002). Iron deficiency is common in a nutritionally stressed environment thus iron homeostasis must be tightly regulated to prevent the detrimental effects of iron redox reactions and the development of hydroxyl radicals. Such an iron regulator is the ferric uptake regulator, also known as Fur (Porcheron & Dozois, 2015; Becerra *et al*., 2014; Fillat, 2014). Fur can have a negative influence on iron availability during iron-rich conditions and may be inactivated to regain normal iron levels (Porcheron & Dozois, 2015). The iron response regulator (Irr) protein negatively regulates the *hemB* gene which encodes ALA, the universal precursor of all tetrapyrroles (Qi & O'Brian, 2002; Grimm, 1990). Ferrochelatase inactivates Irr in the presence of iron, which prevents the accumulation of iron and suppresses the Fenton reaction (Imlay, 2015; Qi & O'Brian, 2002). SOD and catalase protect the cell from oxidative stress and prevent ROS reacting with ferrous iron or molecular oxygen. For example, SOD targets superoxide and prevents the development of hydroxyl radicals by inactivating Fe-S (iron-sulfur) clusters which contain enzymes like aconitase and fumerase, thus preventing DNA damage (Fukai & Ushio-Fukai, 2011). During oxidative stress, the requirement for Fe-S cluster assembly protein and the Fur regulator are both decreased in abundance with ferrochelatase and ferredoxin increased. This may represent the control of iron homeostasis and prevent the formation of harmful hydroxyl radicals via the Fenton reaction.

As outlined previously, there was no significant difference in the abundance of proteins within the B2G analysis of the entire proteome of 10 mM H_2O_2 compared to control (357 proteins in control and 371 proteins in H_2O_2) (section 4.5). This was also reflected in the volcano data, which represents only statistically significant ($p < 0.05$) abundances in H_2O_2 treated cells (58 increased and 45 decreased proteins), compared to the control (Figure 4.6B). The volcano data were investigated further to identify pathways and processes using B2G analysis at Level 3 GO. This resulted in a concise measurement of the differential involvement of proteins altered in abundance in the three Level 3 GO categories. Proteins found to be higher in abundance in H_2O_2 treated cells were found to be more involved in MF (Figure 4.12)

and CC (Figure 4.13) than proteins lower in abundance, whereas proteins lowered in abundance were associated with BP (Figure 4.11).

In summary, rosacea is an inflammatory condition associated with the production of ROS induced by neutrophils and environmental trigger factors such a UV radiation (Imlay, 2015; Tisma *et al*., 2009; Reeves *et al*., 2002). The increased density of *Demodex* mites can create more tissue damage than normal as well as the mite exoskeleton stimulating the TLR-2 pathway (Margalit *et al*., 2016). The more *Demodex* present, the more *Bacillus* leak into the pilosebaceous unit thus exposing *Bacillus* to the innate immune response within the skin. This can contribute to the excessive exposure of pathogen-associated molecular patterns (PAMPs), danger-associated molecular patterns (DAMPs) and neutrophil stimulation, all of which regulate inflammation (Ezraty *et al*., 2017; Margalit *et al*., 2016). Oxidative stress can induce detrimental effects on the cell but bacteria have adapted to overcome this stress and escape ROS damage. H_2O_2 was used to measure the effect of oxidative stress on the *B. oleronius* proteomic profile, with many glycolytic proteins increased in abundance for energy metabolism and protection (Ling *et al*., 2004). Iron homeostasis is an important element for bacterial growth and survival within the cell and iron proteins must be tightly monitored and regulated (Porcheron & Dozois, 2015). NADPH is a key reducing agent for cellular pathways and scavenges potentially harmful reactive molecular oxygen during oxidative stress (Van Acker & Coenye, 2017; Cabiscol *et al*., 2000b). Some proteins were decreased in abundance, which may prove crucial to cell survival by keeping iron and cellular stress proteins at a normal range. *B. oleronius* proteins activate key members of the host immune response, resulting in neutrophil recruitment and the induction of oxidative stress. This can result in the altered abundance of *B. oleronius* proteins which may further provoke the host inflammatory response and lead to the exacerbation of existing rosacea symptoms.

Chapter Five

Investigation of the Potential Use of Selected Blocking Agents for Preventing *B. oleronius* protein-host cell interactions

5.1 Introduction

Antimicrobial agents inhibit or kill microorganisms such as bacteria, fungi and parasites (Jenssen *et al*., 2006). Antibiotics display bactericidal and bacteriostatic properties towards bacteria with a toxic concentration, by targeting bacterial components that humans lack (e.g. cell wall) or binding with a higher affinity to bacterial components that share human homologs (Xu *et al*., 2013; Woo *et al*., 2003). Topical and oral antibiotics are the mainstay of rosacea treatment due to their antibacterial and in some cases anti-inflammatory roles, and range from broad functioning therapies (e.g. tetracycline) to specific targeting drugs (e.g. metronidazole) (Holmes & Steinhoff, 2017; Two *et al*., 2015b). Antimicrobials also display bactericidal properties however their bacteriostatic role will be focused on for the purposes of this research. *B. oleronius* antigens may be leaked from dead *Demodex* mites within the pilosebaceous unit of the skin and eyelashes and rosacea patients have displayed immune-reactivity to *B. oleronius* antigens (Jarmuda *et al*., 2014; McMahon *et al*., 2014; Lacey *et al*., 2007). This research focused attention on potential agents that have the ability to bind to *B. oleronius* proteins and block their interaction with the skin or corneal surfaces in the treatment of dermal and ocular rosacea, respectively.

Three different agents were used to target the *B. oleronius* 62 kDa antigen; bovine serum albumin (BSA), anti-62 kDa rabbit antibody and mucin (type I-S). Each was examined for their capabilities as blocking agents alone and in combination, with the aim to inhibit *B. oleronius* antigen interaction with the epithelial surface, as potential treatments for dermal and ocular rosacea. Serum albumins bind to internal (e.g. fatty acids, hormones, amino acids) and external (e.g. drug molecules, nutrients) molecules and transport them to the desired tissue (Marković *et al*., 2018; Mathew & Kuriakose, 2013). BSA is one of the most studied serum albumins and is a model protein for the interaction between protein and ligand binding (Minic *et al*., 2018; Żurawska-Płaksej *et al*., 2018). BSA is a globular protein consisting of 583 amino acids with seventeen disulphide bridges that contribute to three homologous domains (I, II and III), each of which has two further subdomains (A and B) (Minic *et al*., 2018; Mathew & Kuriakose, 2013). Most importantly, BSA shares strong homology with human serum albumin, making it an

important model protein for ligand binding *in vitro* (Żurawska-Płaksej *et al*., 2018; Dawoud Bani-Yaseen, 2011).

Antibodies can be used as molecular tools for the detection, purification and identification of specific membrane molecules (Noble & Weisberg, 2005; Mason & Williams, 1980). Antibodies have been utilized clinically in vaccines for influenza and also in drugs such as infliximab, an anti-TNF antibody which targets TNF in rheumatoid arthritis (Bongartz *et al*., 2006; Goodwin *et al*., 2006). The use of anti-62 kDa rabbit antibody to target the stimulatory antigen in rosacea patients may be a potential therapeutic for rosacea patients.

In the eye, mucins are secreted from goblet cells, corneal and conjunctival epithelia and from lacrimal glands which provide tear fluid and antimicrobial components to the ocular surface (Gipson, 2016; Mantelli & Argüeso, 2008; Gipson, 2004). Mucins have the potential to bind to penetrating pathogens and clear the ocular surface of such dangers, all the while supplying the mucosal epithelia with anti-adhesive properties and a protective barrier (Mantelli & Argüeso, 2008). The mucosal cells secrete mucins, highly glycosylated glycoproteins which form the central component of the wet-surface epithelium and serve multiple physiological roles (Gipson, 2004; Khanvilkar *et al*., 2001). Mucins coat the cornea and conjunctiva and form the dense glycocalyx at the epithelium-tear film interface (Albertsmeyer *et al*., 2010; Gipson, 2004). A total of 19 mucin gene products have been reported to date in humans, all of which contribute to homeostasis of the mucosal epithelium barrier on the body (Sandberg *et al*., 2009; Mantelli & Argüeso, 2008). Mucins are classified into two categories, membrane-associated mucins (MAMs) and secretory mucins. The ocular surface contains 11 MAMs and 7 secreted mucins (Mantelli & Argüeso, 2008). MUC1, MUC4 and MUC16 are three MAMs expressed at the ocular epithelium and contribute to the tear-film interface (Albertsmeyer *et al*., 2010; Gipson, 2004). Mucins are secreted by mucous glands below the epithelial surface and by specialized goblet cells which are intercalated with the internal mucosal epithelium (Gipson, 2016; Khanvilkar *et al*., 2001). Goblet cells in the conjunctiva secrete the gel-forming mucin MUC5AC, one of the most prominent ocular mucins along with the three MAMs (Mantelli & Argüeso, 2008).

Mucins play a particularly important role in coating the wet-surfaced epithelia, such as the eye, whereby they protect the eye from invading pathogens and allergens, form an apical epithelial barrier and regulate lubrication and water retention across the ocular surface (Sandberg *et al*., 2009; Mantelli & Argüeso, 2008; Gipson, 2004). The capturing ability of mucins in conjunction with their viscoelasticity and reputation in coating epithelial surfaces, suggests their potential as adhesive decoys by inhibiting *B. oleronius* antigens as they come into contact with the ocular surface. The eye is protected from eyelashes, the eyebrow and forehead above and the cheek and nose at the sides. This makes it more difficult to access and cleanse the eye region daily (Lacey *et al*., 2009). If a blocking agent successfully inhibits *B. oleronius* proteins interacting with the corneal surface, it may be possible in future studies to create a synergy between blocking agents targeting the *Bacillus* proteins and antimicrobial agents targeting *Demodex* mites.

5.2 Purification of the *B. oleronius* 62 kDa antigen by ÄKTA-FPLC

It has previously been shown that rosacea patients show immune-reactivity to *B. oleronius* proteins, particularly the 62 kDa and 83 kDa antigens, in ETR, ocular rosacea and PPR (O'Reilly *et al*., 2012c; Li *et al*., 2010; Lacey *et al*., 2007). Lacey *et al.* generated the anti-62 kDa antibody in rabbits (Lacey *et al*., 2007). The immune-stimulatory 62 kDa antigen was purified by fast performance liquid chromatography (FPLC) and used in assays with human laryngeal epithelial (HEp-2) cells and human telomerase-immortalized corneal epithelial (hTCEpi) cells.

Multiple cultures of *B. oleronius* were grown aerobically in NB at 30°C for 72 hours to maximise the amount of crude lysate extracted, as described in section 2.5. The crude lysate preparation was resolved by 1D SDS-PAGE and Western blotted with anti-62 kDa rabbit antibody to access the presence of the antigen of interest. Following crude preparation, the pure *B. oleronius* protein was fractioned using Q-Sepharose™ high performance beads and the ÄKTA-FPLC. Fractionation was performed using the ÄKTA Purifier 100 system (Amersham Biosciences) and a Q-Sepharose column, monitored by the Unicorn 5.01 programme. The column was prepared and equilibrated before use. The crude lysate was inverted with the Q-Sepharose beads in a binding buffer (section 2.21.3) prior to loading onto the column. It has previously been stated that *B. oleronius* proteins bind favourably to the positively charged beads, hence the prior inversion (Lacey *et al*., 2007). The beads and protein sample were inserted onto the prepared column and loaded up to the ÄKTA system. Fractionation of the *B. oleronius* lysate from the Q-Sepharose beads began with an elution buffer (section 2.21.3), by pumping an increasing saline gradient using the ÄKTA-FPLC (Figure 5.1). Fractions of the "pure" proteins were assembled by the fraction collector and stored for the next phase of pure protein preparation i.e. pooling of fractionated pure protein preparations and measuring the level and presence of 62 kDa antigen by Western Blotting (section 2.13.5).

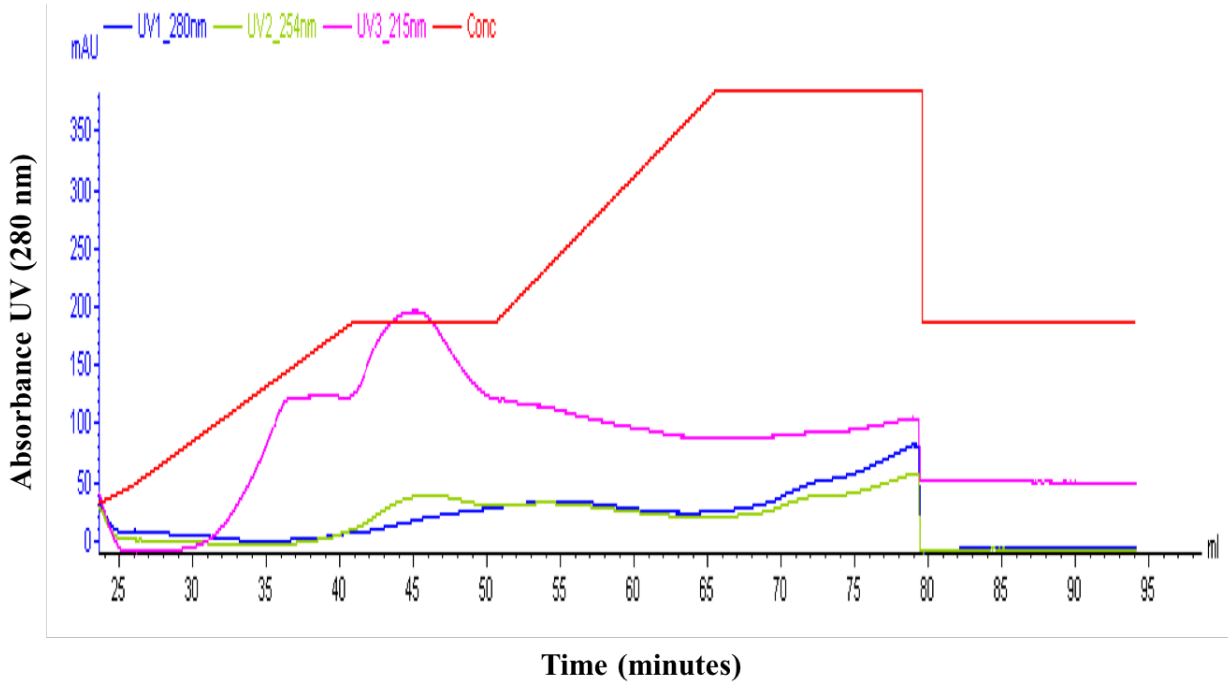

Figure 5.1 Chromatograph from ÄKTA-FPLC fractionation of *B. oleronius* protein preparation

Chromatograph of *B. oleronius* protein from crude lysate during fractionation using the ÄKTA system in FPLC. Blue line represents UV 280nm absorbance reading, which is the protein being eluted from the column. The red line represents the concentration which is the salt gradient and elution of protein sample preparations off the column and into the fraction collector.

5.2.1 SDS-PAGE and Western blot analysis of 'pure' *B. oleronius* FPLC fractions

B. oleronius sample preparations 1-70 that were fractionated using ÄKTA-FPLC were resolved by 1D SDS-PAGE to determine the presence of the protein of interest, i.e. the 62 kDa antigen. Sample preparations 37-45 and 46-53 had the 62 kDa protein present (Figure 5.2) and were Western blotted to confirm antigen presence (Figure 5.3). The two sets of fractionated sample preparations were pooled together to form two sets of pooled pure protein. The newly pooled pure proteins, 37-45 and 46-53, were resolved by 1D SDS-PAGE with crude protein and Western blotted (Figure 5.4). Anti-62 kDa rabbit antibody was used to detect the level of 62 kDa protein, the antigen most immune-reactive in rosacea patient serum.

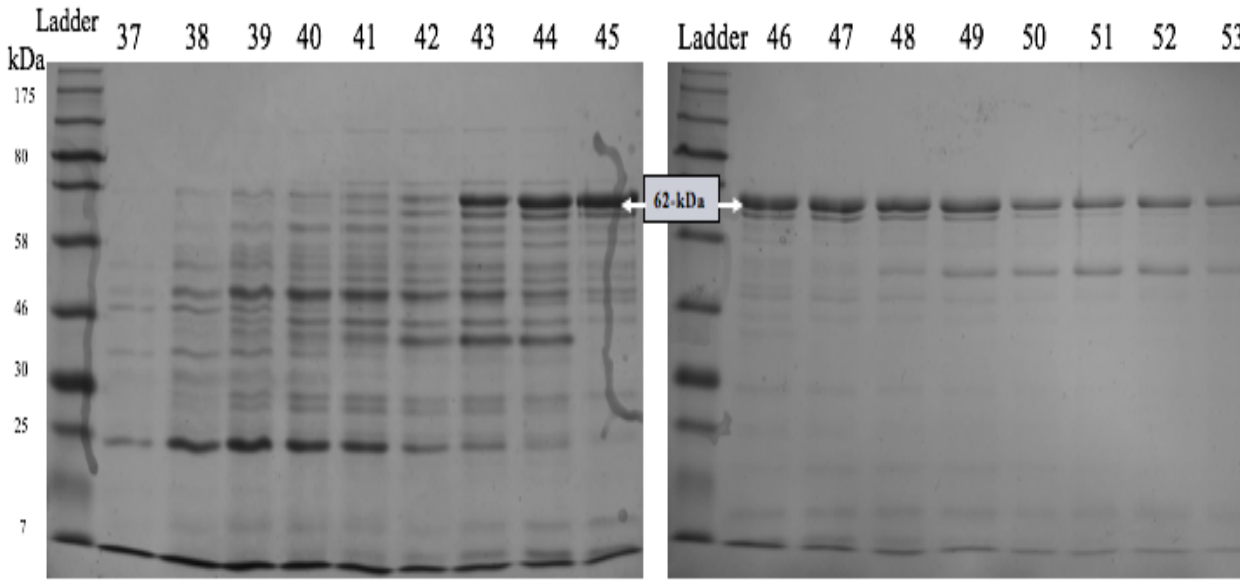

Figure 5.2 Representative 1D SDS-PAGE of sample protein preparations collected from ÄKTA-FPLC fractions

Purified *B. oleronius* protein samples were eluted from the Q-Sepharose™ column during ÄKTA-FPLC. Collected fractions 37-45 (left) and (46-53) were resolved by 1D SDS-PAGE.

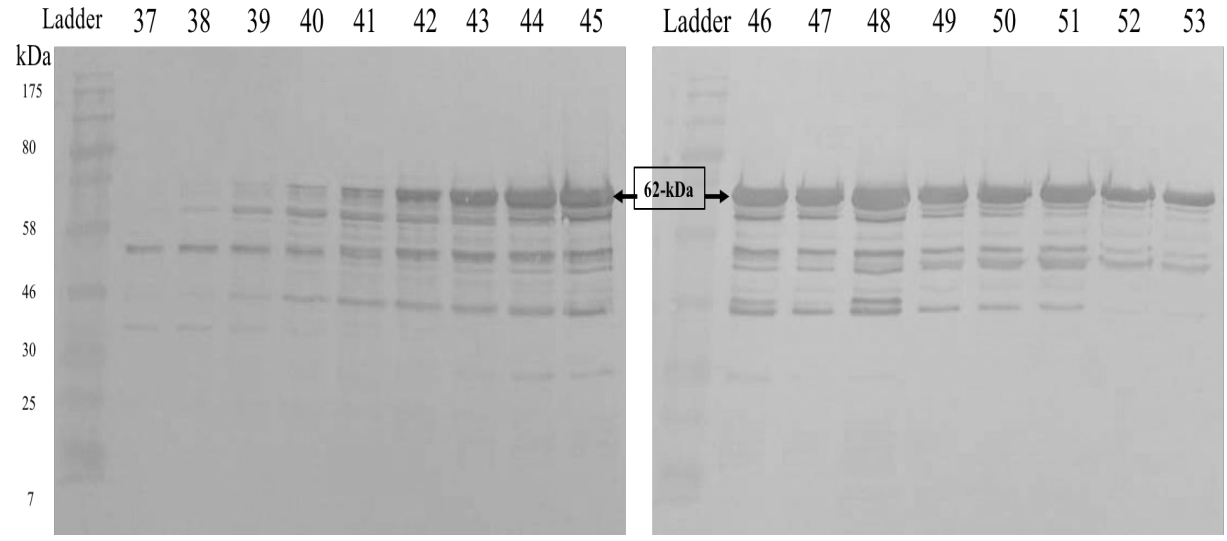

Figure 5.3 Representative Western blot of sample protein preparations collected from ÄKTA-FPLC fractions

Purified *B. oleronius* protein samples fractionated using ÄKTA-FPLC were Western blotted using *B. oleronius* anti-62 kDa rabbit antibody. Collected fractions 37-45 (left) and 46-53 (right) display higher levels of the 62 kDa antigen from fraction 42-53.

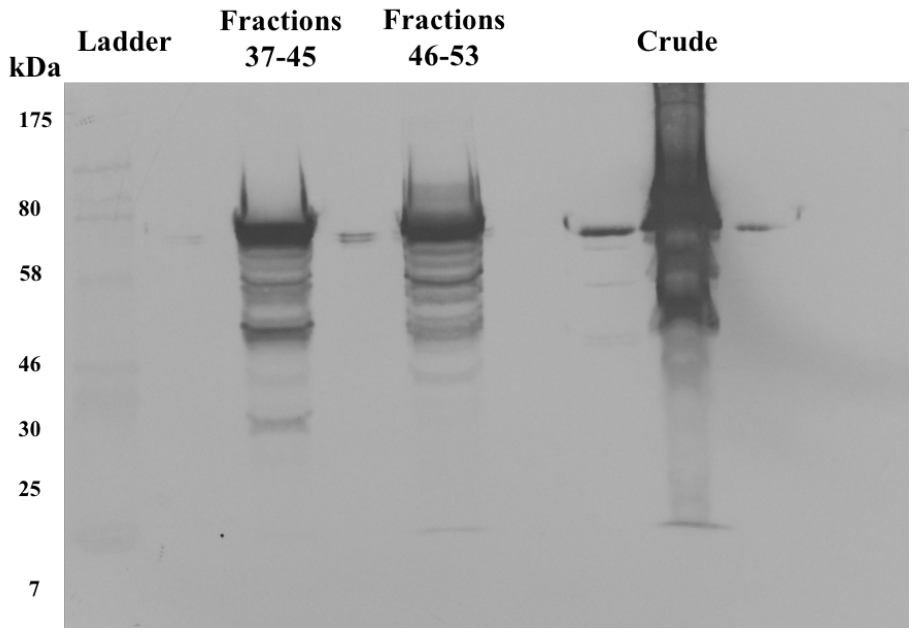

Figure 5.4 Representative Western Blot of *B. oleronius* 'pure' and crude protein
Western blot of pooled sample preparations eluted from Q-Sepharose™ beads using ÄKTA-FPLC. Pure *B. oleronius* protein is represented by the pooling of fraction 37-45 and 46-53. The level of 62 kDa antigen was clarified and compared between *B. oleronius* pure protein (pooled fractions) and crude protein lysate (not fractionated) using anti-62 kDa rabbit antibody.

5.3 Effect of purified 62 kDa *B. oleronius* antigen on human cell proliferation

As previously described, the *B. oleronius* 62 kDa antigen is immune-reactive with rosacea patient serum. The 62 kDa has been successfully fractionated and purified for human cell assays throughout this research. HEp-2 and hTCEpi cells were chosen as dermal and ocular cell line representatives, respectively. HEp-2 cells have previously been used an epithelial cell culture model and were used as a dermal representative throughout this research to gain an insight to the general cellular response of different measured parameters such as temperature, and protein expression and cytokine expression (Martínez *et al.,* 2009). The pure *Bacillus* antigen as isolated from section 5.2, was exposed to both cell line in lowering concentrations to determine the effect on proliferation and toxicity.

HEp-2 cells were grown in MEM media and prepared for an acid phosphatase assay. Media and lowering concentrations of 62 kDa antigen, starting at 6 µg/ml, were added to the wells followed by the HEp-2 cells ($3x10^4$ cells/well) and stored for 5-7 days before being assessed (section 2.24). Cell growth was inhibited the most when cells were exposed to the highest concentration of antigen (6 µg/ml) with growth reaching 71% in comparison to control cells (Figure 5.5). HEp-2 cell growth was affected by lowering concentrations of 62 kDa antigen exposure and reached levels over 100% after 0.188 µg/ml and lower.

hTCEpi cells were grown in KBM-Gold basal medium and seeded ($2x10^4$ cells/well) for a proliferation assay as described in section 2.33.2. Cells were incubated and attached overnight prior to the addition of fresh medium and lowering concentrations of *Bacillus* antigen. Cells were stored for 72 hours (Figure 5.6) and 144 hours (Figure 5.7), after which cell proliferation was enumerated to determine the effect of 62 kDa antigen on hTCEpi cell growth. A representative image was taken of hTCEpi cells at 72 hours to visually compare the number of cells present in a portion of the well (Figure 5.8). The highest concentration of antigen (6 µg/ml), inhibited hTCEpi cell growth at 72 hours (74.2%) and at 144 hours (83.3% in comparison to the control cells. The cells exposed to 6 µg/ml antigen were significantly lower in number in comparison to 0.2 µg/ml at 72 hours ($p < 0.001$) and at 144 hours ($p < 0.05$). This latter concentration of 0.2 µg/ml had no effect on hTCEpi cell growth at either time point.

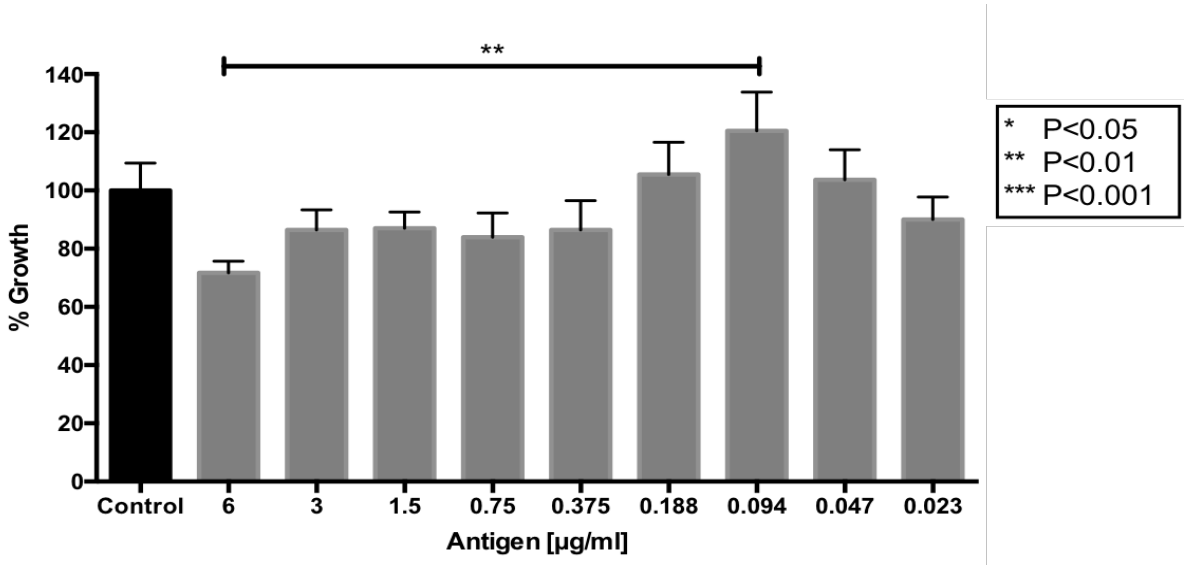

Figure 5.5 HEp-2 cells exposed to *B. oleronius* 62 kDa antigen.

The effect of *B. oleronius* 62 kDa antigen on HEp-2 cell growth as visualized by acid phosphatase assay. The highest concentration of antigen 6 µg/ml inhibited HEp-2 cell growth in comparison to the control. All values are the mean ± SE of three independent determinations.

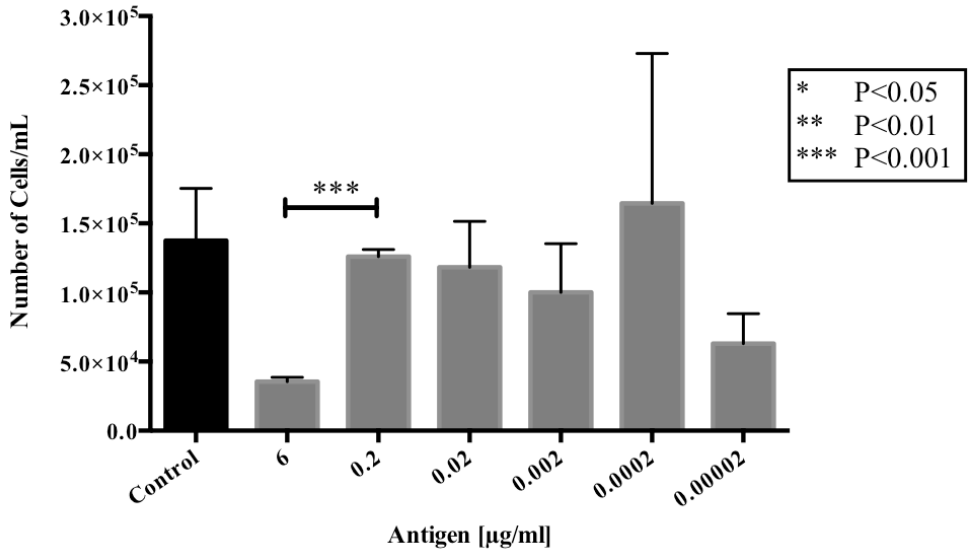

Figure 5.6 hTCEpi cells exposed to *B. oleronius* 62 kDa protein for 72 hours.

hTCEpi cells were exposed to 62 kDa antigen at 6 µg/ml and lower consecutive concentrations of the antigen for 72 hours in a proliferation assay. The 6 µg/ml antigen inhibited cell growth. All values are the mean ± SE of three independent determinations.

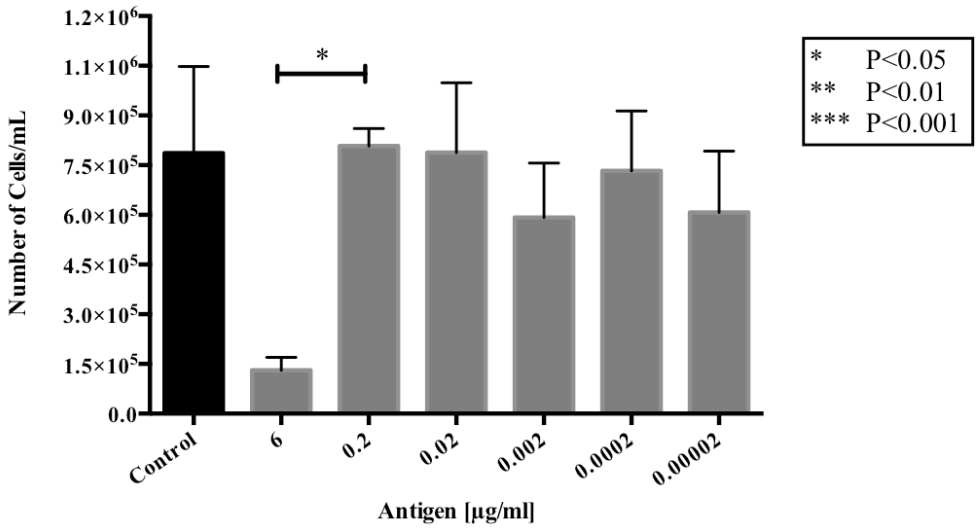

Figure 5.7 hTCEpi cells exposed to *B. oleronius* 62 kDa protein for 144 hours. hTCEpi cells exposed to pure 62 kDa antigen for 144 hours in a proliferation assay. The 6 µg/ml antigen inhibited cell growth and was significantly lower than 0.2 µg/ml antigen. All values are the mean ± SE of three independent determinations.

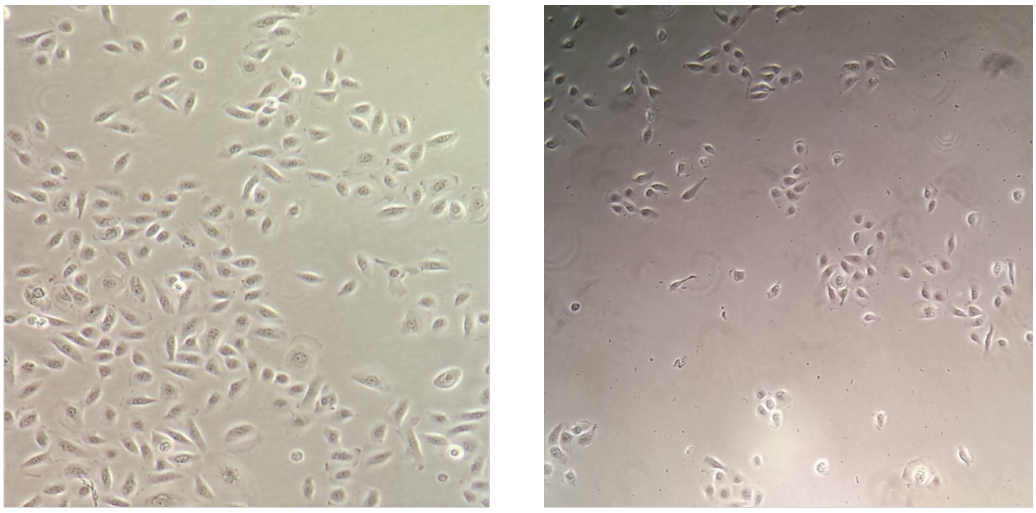

Figure 5.8 hTCEpi cells exposed to *B. oleronius* 62 kDa protein at 72 hours. Representative image of hTCEpi control cells (0 µg/ml), in comparison to cells exposed to the inhibitory antigen concentration of 6 µg/ml. A reduced number of cells is visible in the 6 µg/ml well at 72 hours. Image taken at x100 magnification. (Image author's own)

5.3.1 The effect of *B. oleronius* antigen on hTCEpi gene expression

Rosacea patients have previously shown serum immunoreactivity to *B. oleronius* proteins and a correlation has been established between this sensitivity and *Demodex* infestation in the eyelash follicle (Jarmuda *et al*., 2014; O'Reilly *et al*., 2012b; Lacey *et al*., 2007). A correlation between patient serum immunoreactivity and ocular *Demodex* infestation has been established (Li *et al*., 2010).

Pure *B. oleronius* 62 kDa protein was exposed to hTCEpi cells for 72 hours and 6 µg/ml antigen significantly inhibited cell proliferation (Figure 5.6). Following from this, an enzyme-linked immunosorbent assay (ELISA) was carried out to investigate the effect of *Bacillus* antigen on cytokine expression in hTCEpi cells. The cytokines included IL-1β, IL-8 and TNFα, all of which are pro-inflammatory cytokines associated with rosacea. The hTCEpi cells were exposed to 62 kDa antigen for 72 hours and quantitative real-time polymerase chain reaction (qRT-PCR) analysis was carried out (section 2.25) to measure the level of gene expression in hTCEpi cells.

IL-1β gene expression increased the most in hTCEpi cells exposed to antigen at 2 µg/ml (Figure 5.9). As the level of antigen decreased (1/10 dilution), the rate of IL-1β gene expression also decreased and leveled out when antigen concentrations were very dilute. IL-8 gene expression significantly increased following hTCEpi exposure to 2 µg/ml antigen ($p < 0.001$) in comparison to the control cells 0 µg/ml and remained high at 0.2 µg/ml antigen exposure also (Figure 5.10). hTCEpi cells exposed to 2 µg/ml antigen resulted in significant upregulation of TNFα gene expression ($p < 0.001$) and no other concentration of antigen had an effect on TNFα gene expression (Figure 5.11).

The results displayed here indicate that hTCEpi cells are sensitive to pure *B. oleronius* 62 kDa antigen, resulting in the upregulation of genes associated with pro-inflammatory mediators. In ocular rosacea, this may lead to inflammation of the eyelids, disrupt corneal homeostasis and possibly exacerbate ocular symptoms.

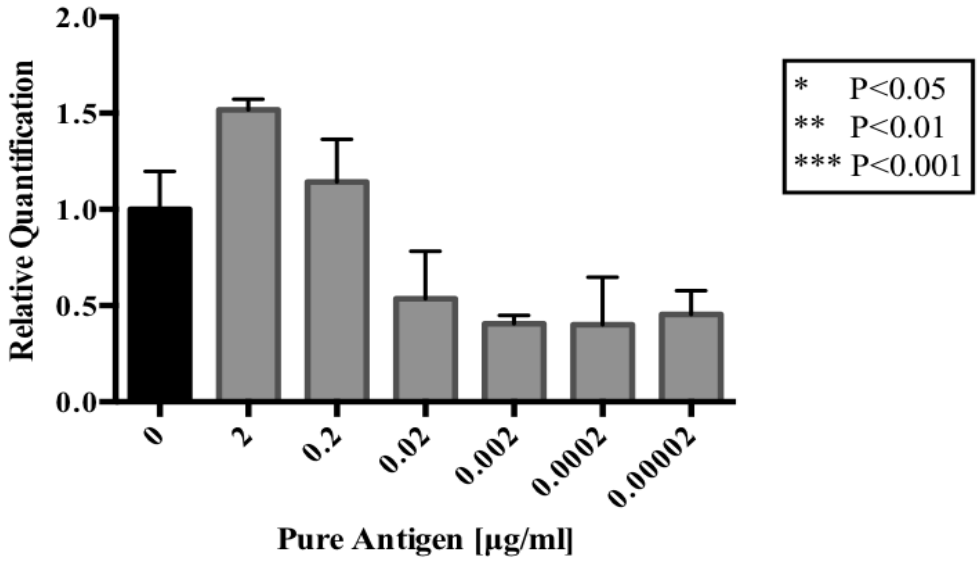

Figure 5.9 Effect of pure *B. oleronius* antigen exposure on IL-1β gene expression in hTCEpi cells as measured by qRT-PCR.

hTCEpi were cells exposed to 62 kDa antigen for 72 hours. Cells exposed to antigen 2 µg/ml and 0.2 µg/ml demonstrated increased IL-1β gene expression in comparison to control cells.

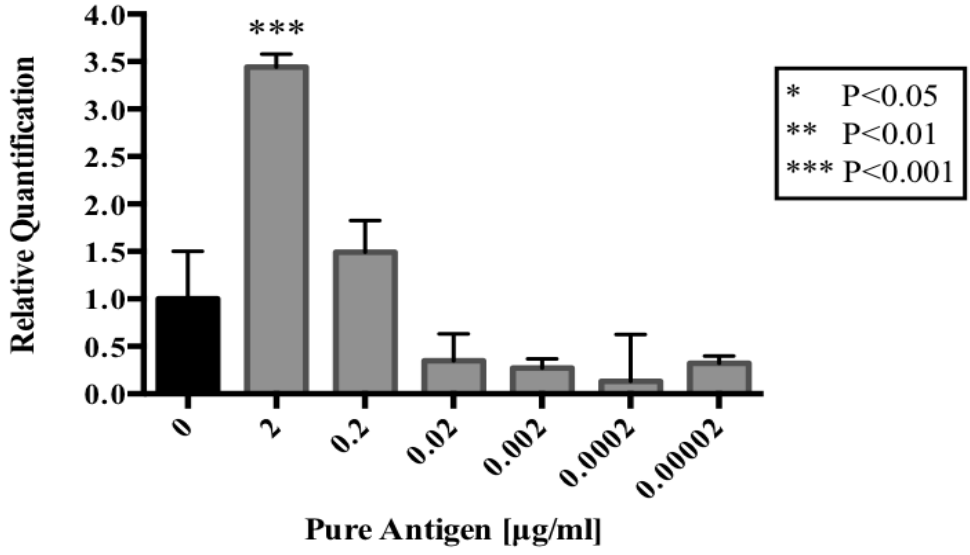

Figure 5.10 Effect of pure *B. oleronius* antigen exposure on IL-8 gene expression in hTCEpi cells as measured by qRT-PCR.

hTCEpi were cells exposed to 62 kDa antigen for 72 hours. Cells exposed to antigen 2 µg/ml and 0.2 µg/ml demonstrated increased IL-8 gene expression in comparison to control cells.

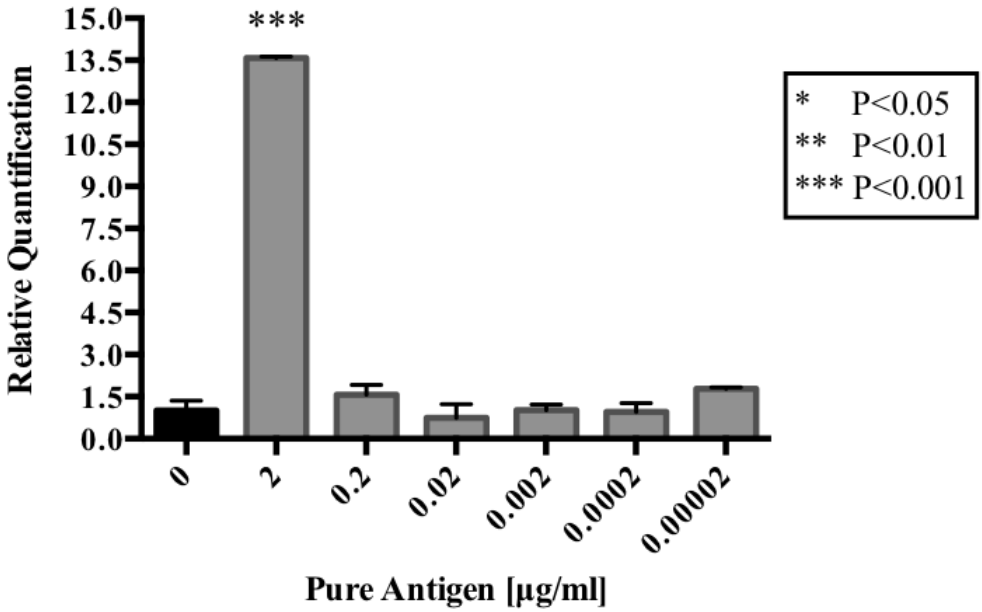

Figure 5.11 Effect of pure *B. oleronius* antigen exposure on TNF*α* gene expression in hTCEpi cells as measured by qRT-PCR.

hTCEpi were cells exposed to 62 kDa antigen for 72 hours. Cells exposed to antigen 2 µg/ml demonstrated in the significant increase of TNF*α* gene expression in comparison to control cells ($p < 0.001$).

5.4 Determining the toxicity of potential blocking agents to human cells

Three separate agents were investigated to measure their capabilities as potential blocking agents for capturing *B. oleronius* proteins, such as the 62 kDa antigen, and inhibiting their effect on the dermal or ocular surface. In rosacea, these blocking agents may have the potential to act as decoys for the 62 kDa antigen, therefore preventing the interaction between the antigen and the rosacea patient epithelium, which can induce an innate immune response and inflammation. The three agents examined are mucin, BSA and anti-62 kDa rabbit antibody (antibody).

The toxicity of each blocking agent to HEp-2 cells and hTCEpi cells was assessed and visualized by acid phosphatase assay (section 2.24). HEp-2 cells and hTCEpi cells were exposed to mucin in concentrations ranging from 0.5 mg/ml to 0.0039 mg/ml. In HEp-2 cells there was a statistically significant difference between all concentrations of mucin and the control ($p < 0.01$) (Figure 5.12). From this assay, the chosen working concentration of mucin in HEp-2 cells was 0.0625 mg/ml. The effect of mucin on hTCEpi cell growth was quite different to HEp-2 cells. No concentration of mucin was statistically different to the control and overall, hTCEpi cell growth increased following exposure to mucin (Figure 5.13). The working concentration of mucin chosen from this assay was 0.0625 mg/ml or less.

BSA toxicity was investigated in HEp-2 cells (Figure 5.14) and in hTCEpi cells (Figure 5.15). BSA concentration started at 1 mg/ml for hTCEpi cells and then ranged from 0.5 mg/ml to 0.002 mg/ml in both cell lines. BSA was not toxic to HEp-2 cells. Moreover, the level of HEp-2 growth remained consistent with the control and a working concentration of BSA was established for HEp-2 cells at 0.0625 mg/ml. hTCEpi cells exposed to BSA had reduced growth to 60% in comparison to the control at 1 mg/ml. No toxicity was observed from 0.5 mg/ml of BSA onwards and remained consistent with control levels. The same working concentration of BSA was established for hTCEpi cells at 0.0625 mg/ml.

Anti-62 kDa rabbit antibody was the final blocking agent that HEp-2 cells (Figure 5.16) and hTCEpi cells (Figure 5.17) were exposed to in order to determine toxicity levels. This primary anti-62 kDa rabbit antibody was prepared in a working dilution of 1/5000 *in vitro*. Therefore, the detection range of antibody exposed to HEp-2 cells and hTCEpi cells was from 1/20K (i.e. one in twenty-thousand) to 1/5.12m (i.e. one in five point twelve million). The first two dilutions of antibody significantly reduced HEp-2 cell growth ($p < 0.01$). All other concentrations of antibody did not or minimally affect HEp-2 cells and a working dilution of 1/160K was determined for future work with HEp-2 cells. Antibody was significantly toxic to hTCEpi cells at 1/20K, 1/40K and 1/80K ($p < 0.001$). As the concentration of antibody decreased, the level of toxicity to hTCEpi cells decreased. The same working concentration of 1/160K was chosen for future hTCEpi work. Although the 1/160K did inhibit the growth of hTCEpi cells, this concentration was chosen as this is a polyclonal antibody (Lacey *et al*., 2007) and may bind to other *B. oleronius* antigens and inhibit corneal cell proliferation somewhat in ocular rosacea patients.

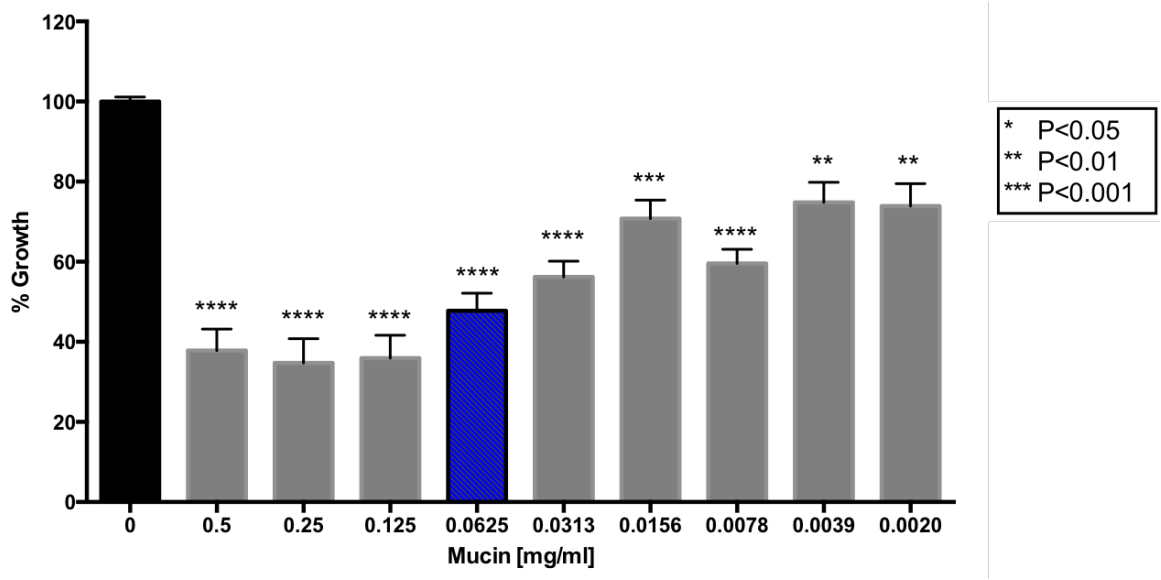

Figure 5.12 Toxicity of mucin to HEp-2 cells.

HEp-2 cells were exposed to mucin to determine levels of toxicity. The chosen working concentration of mucin with HEp-2 cells was 0.0625 mg/ml (blue column). All values are the mean ± SE of three independent determinations.

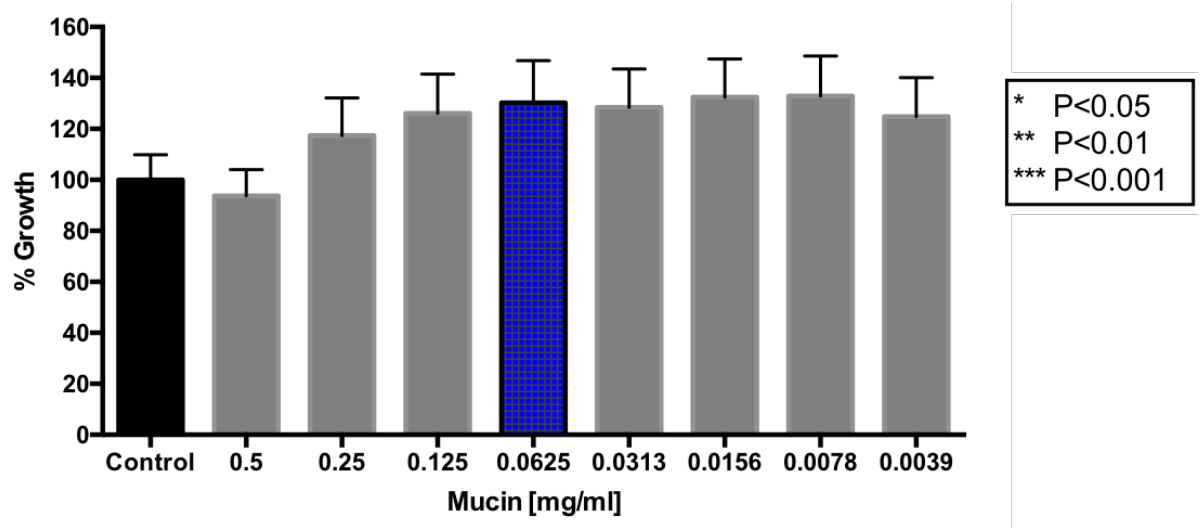

Figure 5.13 Toxicity of mucin to hTCEpi cells.

hTCEpi cells were exposed to mucin to determine levels of toxicity. The chosen working concentration of mucin with hTCEpi cells was 0.0625 mg/ml (blue column). All values are the mean ± SE of three independent determinations.

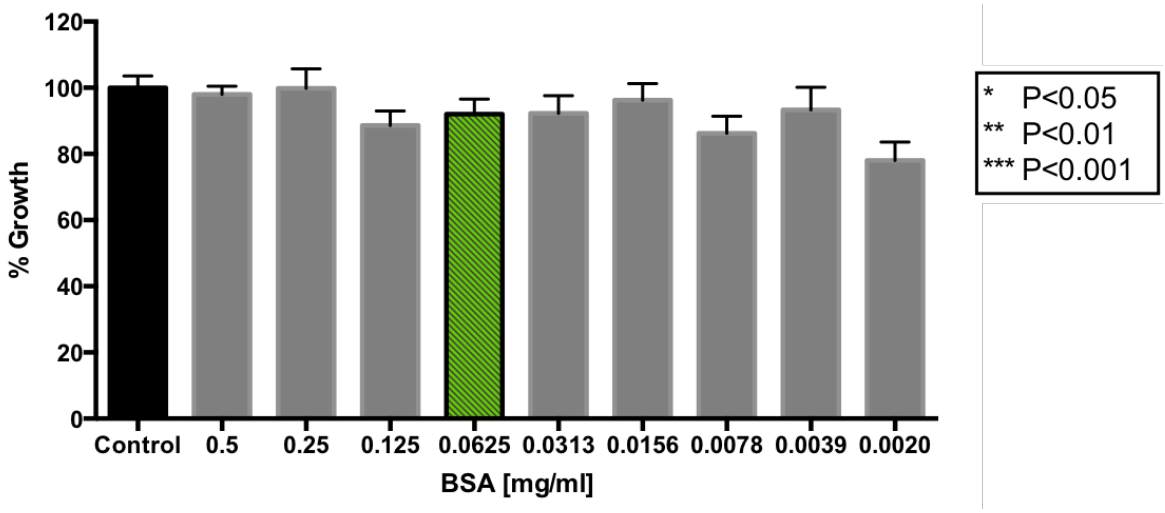

Figure 5.14 Toxicity of BSA to HEp-2 cells.

HEp-2 cells were exposed to BSA to determine levels of toxicity. The chosen working concentration of BSA with HEp-2 cells was 0.0625 mg/ml (green column). All values are the mean ± SE of three independent determinations.

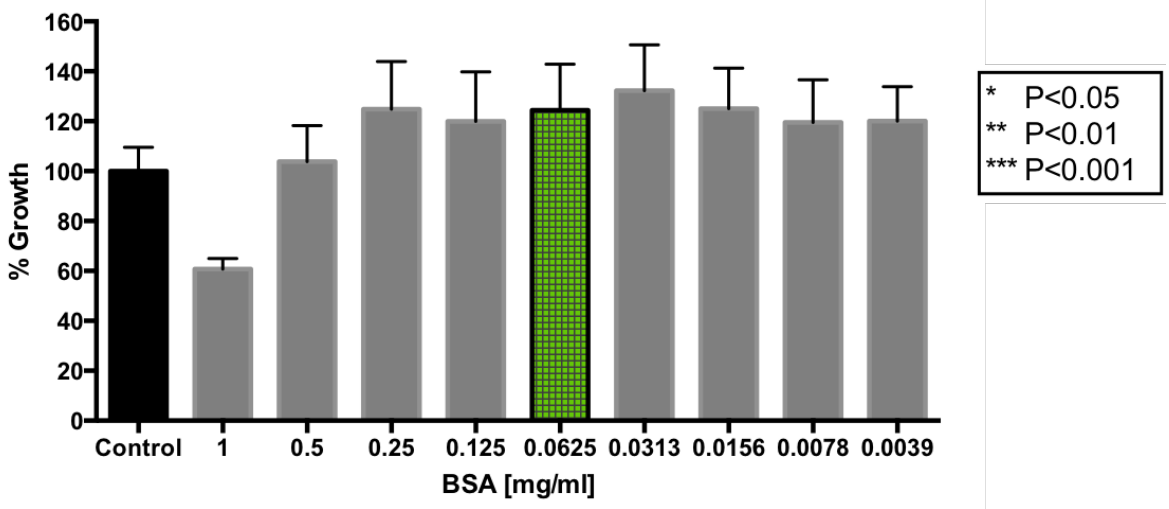

Figure 5.15 Toxicity of BSA to hTCEpi cells.

hTCEpi cells were exposed to BSA to determine levels of toxicity. The chosen working concentration of BSA with hTCEpi cells was 0.0625 mg/ml (green column). All values are the mean ± SE of three independent determinations.

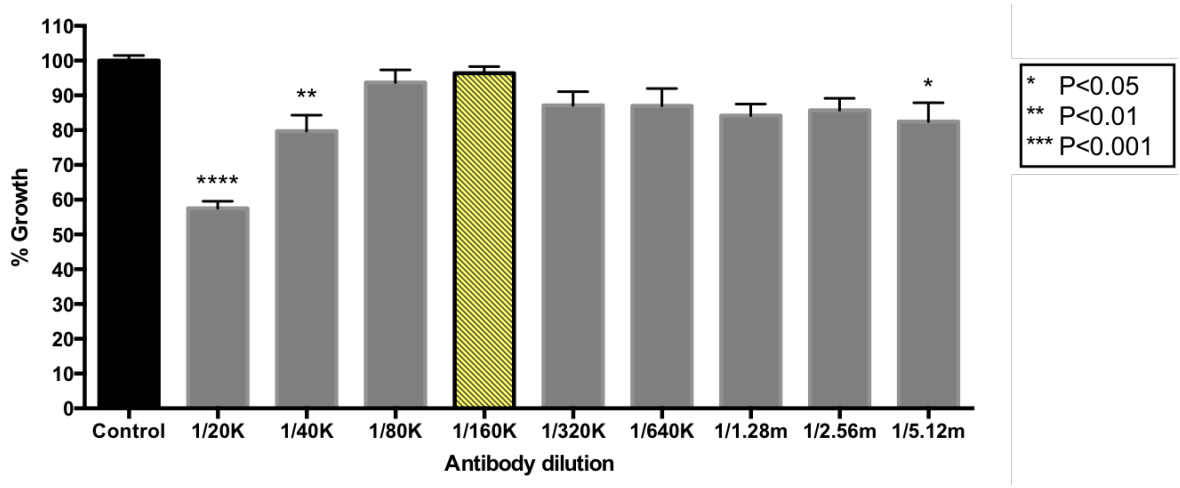

Figure 5.16 Toxicity of anti-62 kDa rabbit antibody to HEp-2 cells.

HEp-2 cells were exposed to dilutions of antibody to determine levels of toxicity. The chosen dilution of antibody with HEp-2 cells was 1/160K (yellow column). All values are the mean ± SE of three independent determinations.

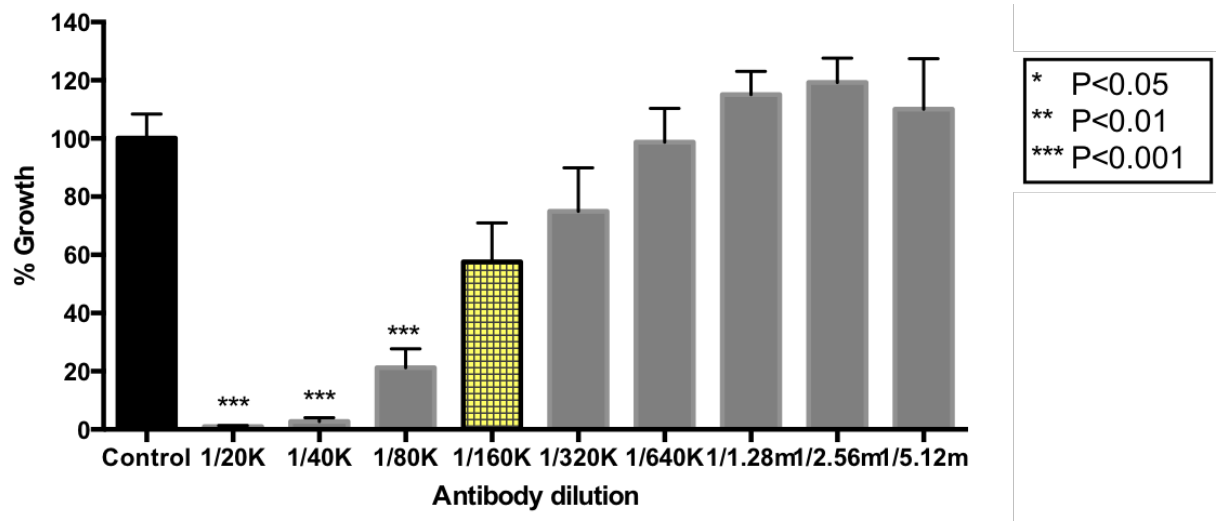

Figure 5.17 Toxicity of anti-62 kDa rabbit antibody to hTCEpi cells.

hTCEpi cells were exposed to dilutions of antibody to determine levels of toxicity. The chosen dilution of antibody with hTCEpi cells was 1/160K (yellow column). All values are the mean ± SE of three independent determinations.

5.5 The effect of potential blocking agents on human cell proliferation alone and in combination

The toxicity of mucin, BSA and antibody were determined on HEp-2 cells and hTCEpi cells. Following the toxicity results (section 5.4), working concentrations of each potential blocking agents were determined; mucin and BSA concentrations were 0.0625 mg/ml for both HEp-2 and hTCEpi cells. The chosen antibody dilution was 1/160K for HEp-2 and hTCEpi cells. The effect of these concentrations alone and in combination with antigen on HEp-2 and hTCEpi cell proliferation was determined.

The blocking abilities of these agents was investigated alone and in combination with the *B. oleronius* 62 kDa antigen in the case of HEp-2 cells (Figure 5.18). HEp-2 cells were grown in MEM media and seeded ($2x10^5$ cells/well) for a 72-hour proliferation assay (section 2.23). Cells were incubated and attached overnight prior to the addition of fresh medium (control), 3 µg/ml pure 62 kDa antigen, designated concentrations of mucin, BSA, antibody and the combination of latter agents with the 3 µg/ml antigen. HEp-2 cell growth significantly decreased in antigen exposed cells (53.8%) in comparison to control cells ($p < 0.01$), thus highlighting the inhibitory effect of *B. oleronius* antigen on HEp-2 proliferation. The blocking agents alone (blue columns) reduced cell numbers in comparison to the control but not to any statistically significant values. For the combination effect, each blocking agent was incubated with antigen for at least one hour prior to cell exposure. The combined effect of the blocking agent-antigen complex (yellow columns) resulted in a significant increase in HEp-2 cell proliferation in comparison to the control ($p < 0.001$). This combined result displays the potential of mucin, BSA and antibody successfully binding to or capturing the 62 kDa antigen and preventing the decreased cell proliferation as seen with the antigen alone (red column) (Figure 5.18).

The mucin was the most effective at blocking the antigen and counteracted the effect of antigen exposure on HEp2 cells in comparison to the control. This led to further proliferation assays in HEp-2 cells and hTCEpi cells, with just mucin as a potential blocking agent. The proliferation assays were set up as previously stated for 72 hours, with the mucin and antigen incubated together for at least one hour prior to HEp-2 cell exposure (section 2.23). In HEp-2 cells exposed to antigen (3 µg/ml) cell proliferation significantly decreased (51.6%) when compared with the control ($p < 0.05$) (Figure 5.19). Mucin (0.0625 mg/ml) exposed to HEp-2 cells did not inhibit cell proliferation. The combination of mucin in the presence of antigen exposed to HEp-2 cells matched the proliferation rate of the control cells, thus the mucin may be blocking the interaction of *B. oleronius* 62 kDa antigen with the host cell and restored normal growth.

The growth of hTCEpi cells exposed to antigen 3 µg/ml reduced by 25% in comparison to the control (Figure 5.20). The mucin had no effect on cell proliferation at 0.0625 mg/ml. However, the combination of mucin and antigen significantly reduced hTCEpi cell proliferation in comparison to the control ($p < 0.001$). However, the combination of mucin and antigen did not restore the proliferation rate to normal level. The mucin and antigen combination significantly reduced hTCEpi cell proliferation by 75% in comparison to the control ($p < 0.001$). This particular concentration of mucin may have been too high, for hTCEpi cells, to work effectively as a blocking agent.

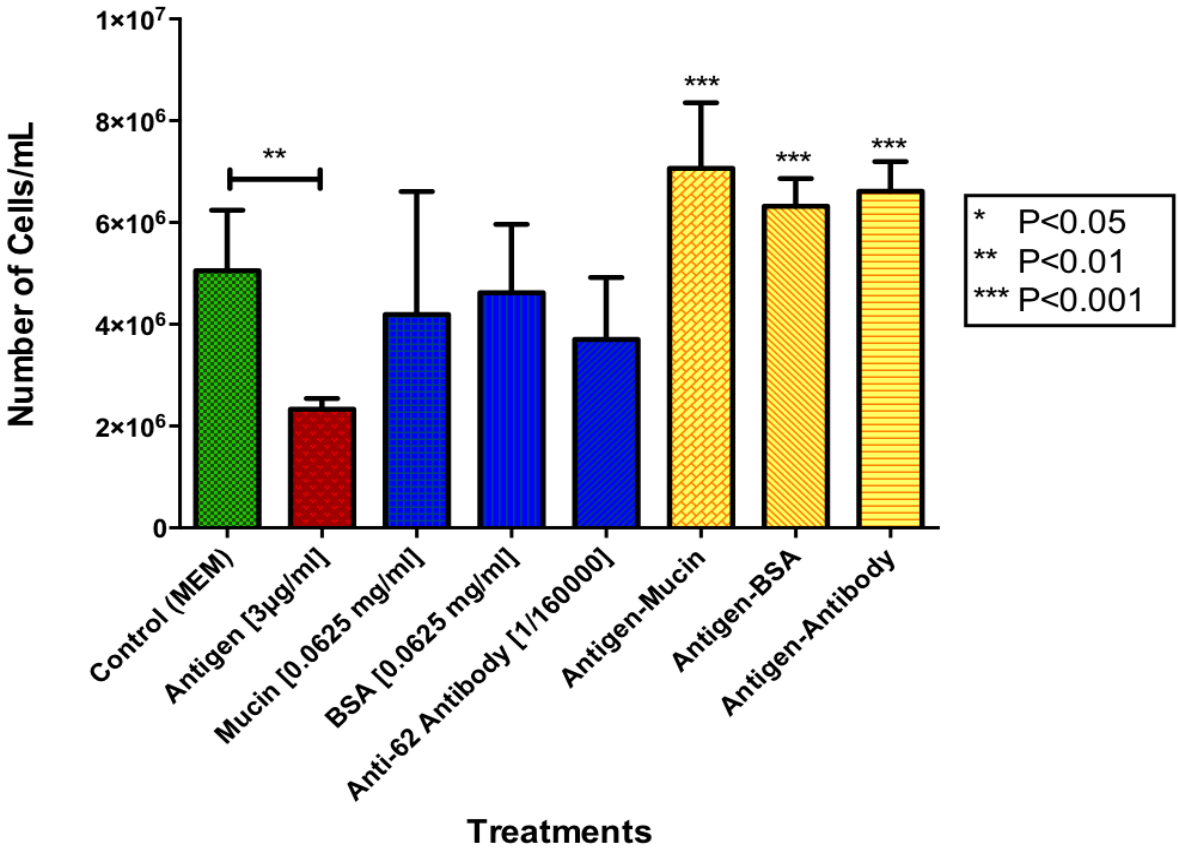

Figure 5.18 HEp-2 cell proliferation in the presence of three potential blocking agents alone and in combination with *B. oleronius* 62 kDa antigen.

The *B. oleronius* pure 62 kDa antigen (red column) significantly reduced HEp-2 cell proliferation. The effect of each blocking agent in the presence of the antigen (yellow columns) counteracts this inhibitory effect and may be indicative of the potential of each as a blocking agent against 62 kDa antigen in rosacea.

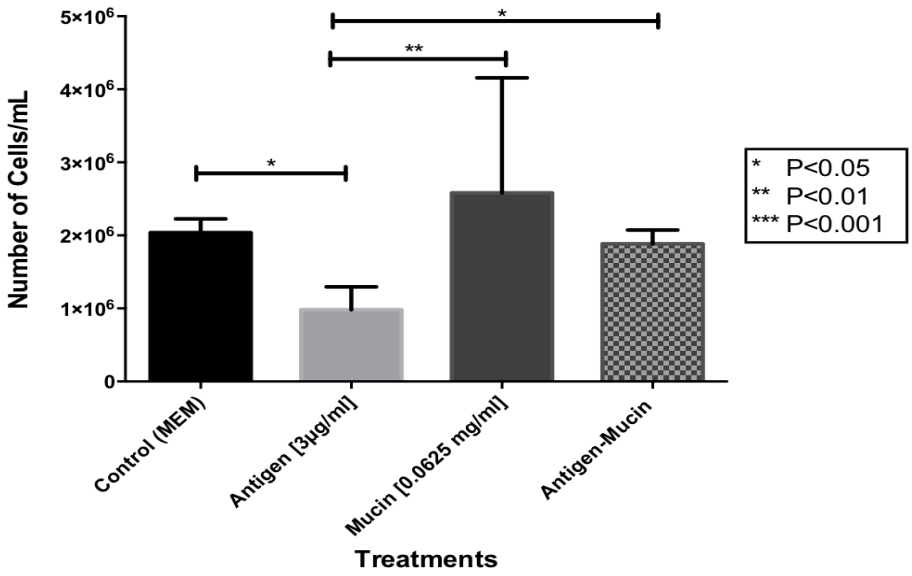

Figure 5.19 The effect of mucin as a blocking agent against *B. oleronius* 62 kDa antigen in HEp-2 cell proliferation at 72 hours.

Antigen (3 µg/ml) significantly reduced HEp-2 cell proliferation. This inhibitory effect was counteracted when antigen was in the presence of mucin 0.0625 mg/ml, restoring cell growth to normal level.

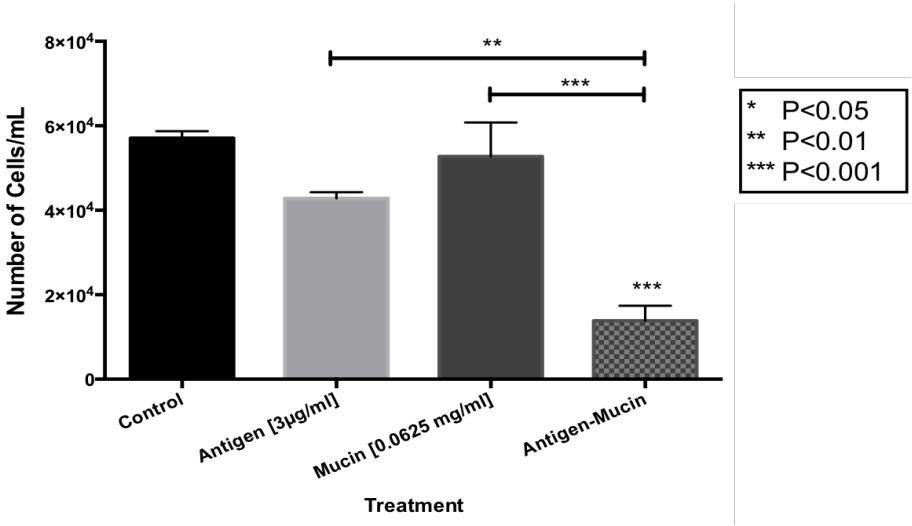

Figure 5.20 The effect of mucin as a blocking agent against *B. oleronius* 62 kDa antigen in hTCEpi cell proliferation at 72 hours.

Antigen 3 µg/ml reduced hTCEpi cell growth after 72 hours. The addition of mucin 0.0625 mg/ml in the presence of antigen, enhanced this inhibitory effect on cell proliferation and at this concentration, mucin did not block the effect of antigen on hTCEpi cells.

5.6 The effect of *B. oleronius* protein on wound healing in human cells

The effect of *B. oleronius* 62 kDa antigen on the wound healing response of HEp-2 cells and hTCEpi cells was investigated. Mucin was used as a potential blocking agent in combination with the antigen to observe its function in the wound healing response. Cells were grown to confluency in 6 well culture plates, scratched once to create the wound and components were added into the wells along with culture medium (section 2.26). The mucin was incubated in the presence of antigen at least one hour prior to cell exposure.

HEp-2 cells were seeded ($1x10^6$ cells/well) and two concentrations of antigen were investigated (6 µg/ml and 2 µg/ml) alone or in combination with mucin 0.0313 mg/ml (Figure 5.21). The cell image at the top is a photo taken just after healthy confluent cells were scratched to create a wound at 0 hours. HEp-2 cells were incubated for 72 hours and photos were taken to visualize the effect of pure 62 kDa antigen and the blocking agent mucin on the wound healing response. The results displayed HEp-2 cells in the control and mucin 0.0313 mg/ml migrating towards the center of the wound to heal and close the wound. Cells exposed to the lower concentration of antigen 2 µg/ml migrated more towards the wound than 6 µg/ml antigen, the latter of which displayed less movement towards the edge of the wound in response to healing or closing in the wound. The addition of mucin in combination with antigen resulted in cells migrating towards to lining of the wound.

Scratch assays with hTCEpi cells were seeded ($2x10^5$ cells/well) and grown to confluency (section 2.26). One concentration of antigen (3 µg/ml) was applied for the wound healing response in hTCEpi cells and two concentrations of mucin 0.0625 mg/ml and 0.313 mg/ml (Figure 5.22). The top photo was taken at 0 hours immediately after cells were wounded and all other photos were taken at 24 hours following hTCEpi exposure. Cells exposed to antigen migrate more towards the wound in a healing response that the control cells. hTCEpi cells exposed to both mucins independently had a similar wound healing response to the control cells. The addition of mucin (0.0625 mg/ml and 0.0313 mg/ml) in combination with the antigen proved the most effective at healing the artificial wound, however this may be the result of uncontrolled growth in the presence of antigen.

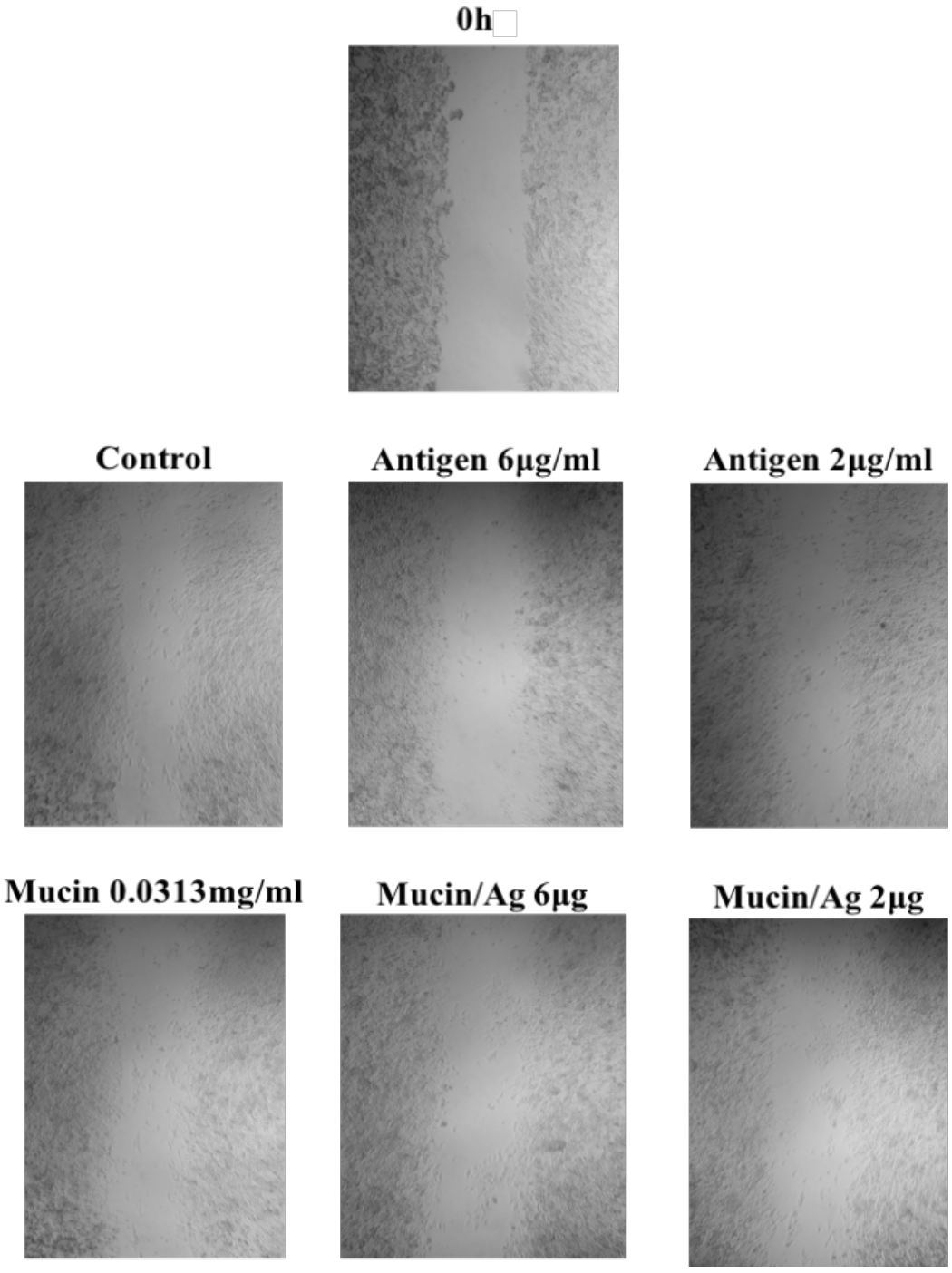

Figure 5.21 The effect of potential blocking agent mucin and *B. oleronius* proteins on the healing of a scratch wound at 72 hours in HEp-2 cells.
Confluent layers of HEp-2 cells were wounded and the healing response was observed after 72 hours. Mucin 0.0313 mg/ml in combination with antigen 2 µg/ml cells displayed more healing properties and migration towards the wound than the higher concentration of antigen 6 µg/ml. Representative set of results from one of two independent replicates. Images taken at x100 magnification.

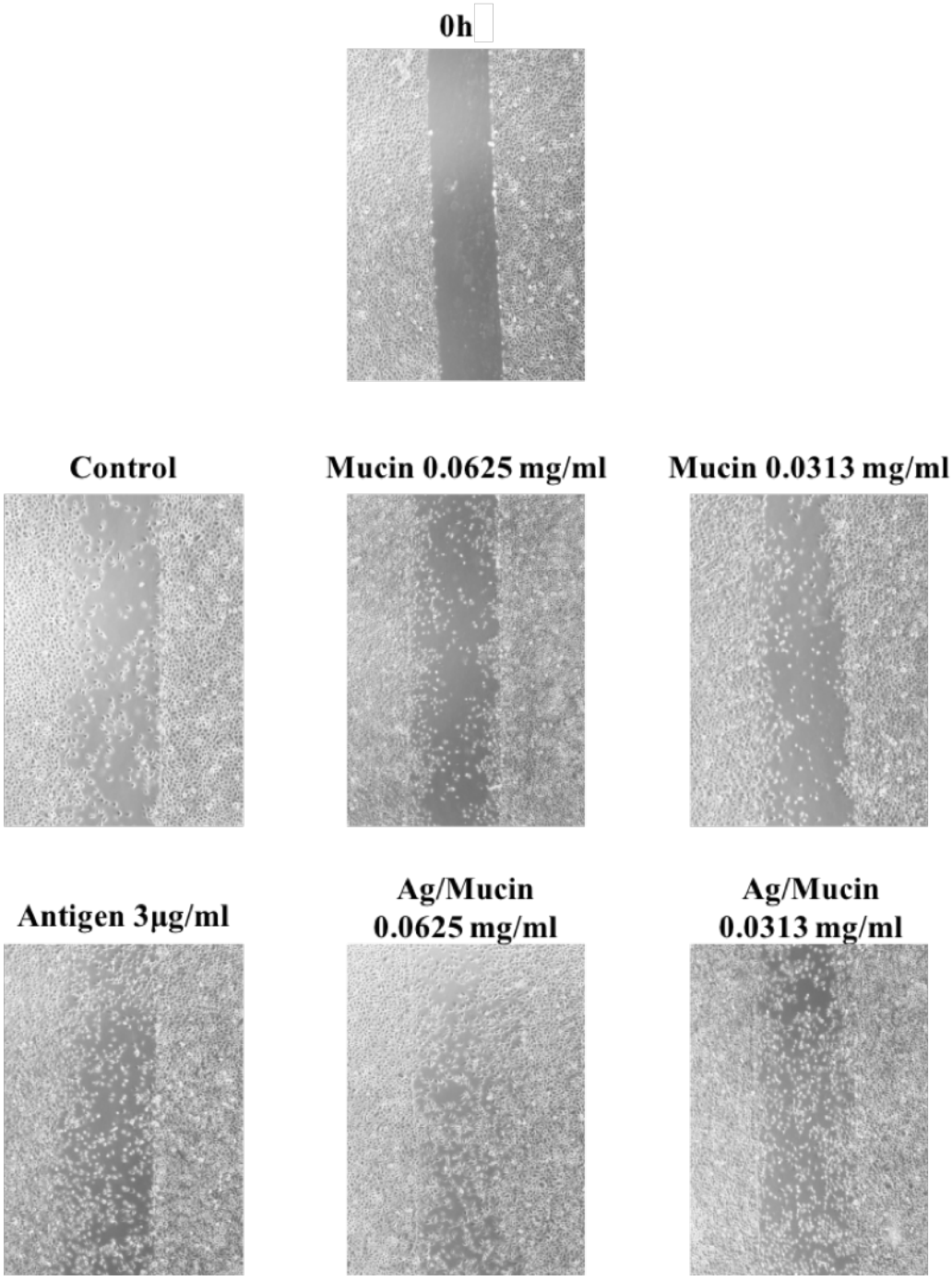

Figure 5.22 The effect of potential blocking agent mucin and *B. oleronius* proteins on the healing of a scratch wound at 24 hours in hTCEpi cells.
Confluent layers of hTCEpi cells were wounded and the healing response was observed after 24 hours. Antigen 3 µg/ml treated cultures displayed more growth than the control, which was further enhanced in the presence of mucin. Representative set of results from one of two independent replicates. Images taken at x100 magnification.

5.6.1 The effect of *B. oleronius* protein on cytokine expression in response to wound healing in human cells

Neutrophils are activated and recruited to a site of injury or infection which leads to the secretion of pro-inflammatory cytokines such as IL-8 and TNFα (Jarmuda *et al*., 2014; Holmes, 2013). The downstream effect of the innate immune response to such injuries can be induction the production of pro-inflammatory cytokines. Following on from the wound healing assay (section 5.6), HEp-2 and hTCEpi cell secretome was collected after 72 hours and applied to an ELISA assay (section 2.27). The cytokines investigated were IL-8, IL-1β, IL-6 and TNFα, all of which are associated with rosacea and play pro-inflammatory roles.

The effect of cytokine production on HEp-2 cells in a wound healing response was observed (Figure 5.23). Two antigen concentrations (6 µg/ml and 2 µg/ml) and one mucin concentration (0.0313 mg/ml) were exposed to HEp-2 cells alone and in combination. The level of IL-8 cytokine significantly increased in comparison to the control when exposed to antigen (6 µg/ml) and mucin-antigen (6 µg/ml) combinations ($p < 0.05$). The mucin had some blocking effect on the antigen in the cases of IL-6 and TNFα cytokine production in comparison to elevated levels of antigen.

In hTCEpi cells, one concentration of purified 62 kDa antigen (3 µg/ml) was exposed to cells as well as two concentrations of the potential blocking agent mucin (0.0625 mg/ml and 0.0313 mg/ml) (Figure 5.24). No significant changes in cytokine production were observed however, the level of IL-8 increased in hTCEpi cells exposed to antigen (3 µg/ml) in comparison to control cells. Experiments were carried out in a minimum of two independent replicates for HEp-2 cells and hTCEpi cells, representing an indication of cytokine secretome from cells during the wound healing response.

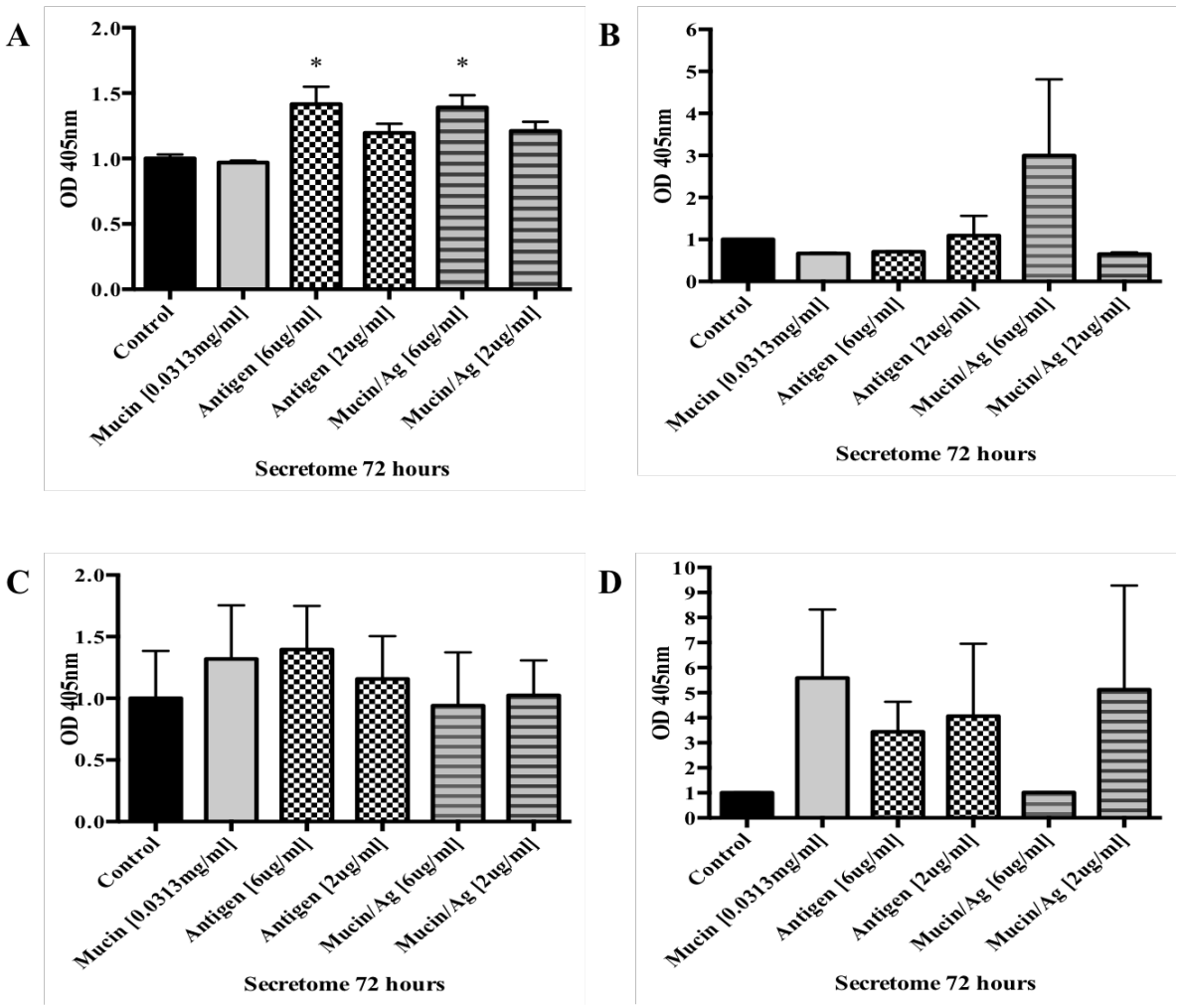

Figure 5.23 The effect of *B. oleronius* protein exposure on cytokine expression during a wound healing response at 72 hours in HEp-2 cells.

HEp-2 cells were exposed to *B. oleronius* 62 kDa antigen and potential blocking agent mucin following a scratch wound assay for 72 hours. Cell secretome was investigated for the presence of pro-inflammatory associated cytokines including (**A**) IL-8, (**B**) TNFα, (**C**) IL-6 and (**D**) IL-1β. All values are the mean ± SE of two independent determinations.

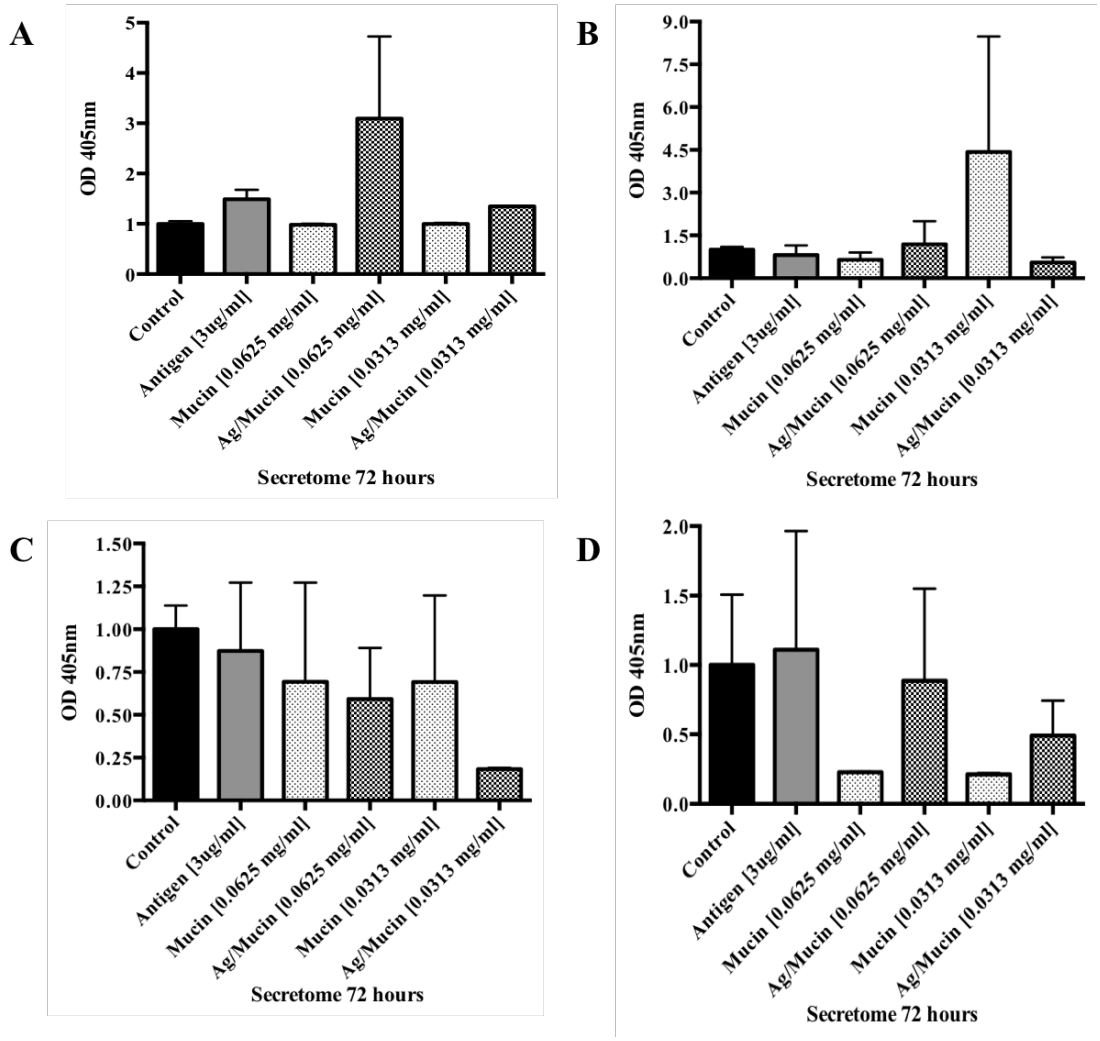

Figure 5.24 The effect of *B. oleronius* protein exposure on cytokine expression during a wound healing response at 72 hours in hTCEpi cells.

hTCEpi cells were exposed to *B. oleronius* 62 kDa antigen and potential blocking agent mucin following a scratch wound assay for 72 hours. Cell secretome was investigated for the presence of pro-inflammatory associated cytokines including (**A**) IL-8, (**B**) TNFα, (**C**) IL-6 and (**D**) IL-1β. All values are the mean ± SE of two independent determinations.

5.7 Discussion

Demodex mites are normal residents of the skin however there is an increased density of *Demodex* mites in the face of rosacea patients compared to healthy individuals (McMahon *et al*., 2014; Bonnar *et al*., 1993). *B. oleronius* is a bacterium associated with this chronic inflammatory condition and has been isolated from the digestive tract of a *Demodex* mite extracted from the face of papulopustular rosacea patient (Lacey *et al.,* 2007; Delaney, 2004). The connection between *Demodex* and *B. oleronius* in the pilosebaceous unit may contribute to the symptoms experienced in all four subtypes of the condition. Almost 50% of rosacea patients manifest ocular symptoms which can be uncomfortable and irritating for patients, for example blurred vision, itchiness and foreign body sensation (Tan & Berg, 2013; O'Reilly *et al*., 2012b). The treatment for ocular rosacea ranges from the use of oral and topical antibiotics, some of which have the dual role of antibacterial and anti-inflammatory properties (McMahon *et al*., 2014; Gupta & Chaudhry, 2005).

Artificial tears are the mainstay management of ocular rosacea as they lubricate the corneal surface of the eye and possibly lead to the flushing out and clearance of debris and toxins present on the ocular surface (Geerling *et al*., 2011; Powell, 2005). Eye drops, sprays and ointments are also common in ocular treatment, some of which are supplemented with tear film lipids or antibiotics (Geerling *et al*., 2011). The potential use of blocking agents for the prevention of *B. oleronius* protein-host cell interactions were investigated. The three agents chosen were BSA, anti-62 kDa rabbit antibody and mucin. The approach considered was to analyze the binding and capturing abilities of these blocking agents with the *B. oleronius* antigens as they approach the corneal surface from the lash follicle in ocular rosacea. If the agents can inhibit the *B. oleronius* protein-cell surface interaction in rosacea patients, it may lead to the relief of symptoms and act as a potential treatment. The delivery of the blocking agent to the corneal surface may be in the form of an eye drop, an acceptable method in the treatment and management of ocular rosacea.

It has previously been shown that rosacea patients are immune-sensitive to the *B. oleronius* antigens which was purified from crude protein using the ÄKTA-FPLC (Figure 5.1) (Jarmuda *et al*., 2014; O'Reilly *et al*., 2012b; Lacey *et al*., 2007). The *B. oleronius* 62 kDa antigen was applied to cells assays throughout this research. The fraction samples eluted from the Q-Sepharose column were collected and resolved on 1D SDS-PAGE followed by Western blotting with anti-62 kDa rabbit antibody (Figures 5.2 and 5.3). Fractions with the most 62 kDa antigen reactivity were pooled together to comprise pure 62 kDa antigen. The *B. oleronius* pure fractions and original crude protein was re-analyzed via Western blot and displayed intensified bands of 62 kDa protein (Figure 5.4). The pure 62 kDa antigen was then exposed to HEp-2 cells and hTCEpi cells to determine the effect of this antigen on cell growth. At a concentration of 6 µg/ml the growth of HEp-2 cells decreased by 29% in comparison to the control (Figure 5.5). Normal cell growth was restored when HEp-2 cells were exposed to 0.188 µg/ml antigen dose and below. The hTCEpi cells exposed to 6 µg/ml antigen were decreased by 74.2% and 83.3% in cultures of 72 hours and 144 hours respectively (Figures 5.6 and 5.7). In both hTCEpi proliferation assays, normal growth was restored in the presence of 0.2 µg/ml antigen. The exposure of HEp-2 cells and hTCEpi cells to the 6 µg/ml pure 62 kDa antigen represents the inhibitory effect of the antigen on cell growth. condition. This can be visualized in hTCEpi cells after 72 hours of exposure to the 6 µg/ml antigen dose (Figure 5.8).

Neutrophil recruitment has been demonstrated previously when exposed to *B. oleronius* proteins, which led to the production to cytokines (Jarmuda *et al*., 2012; O'Reilly *et al*., 2012a). The increased expression of pro-inflammatory cytokines such as IL-8 leads to further recruitment of neutrophils, all of which may contribute the chronic inflammation and tissue degradation that is characteristic of rosacea patients (McMahon *et al*., 2014; Jarmuda *et al*., 2012). The level of genes encoding these inflammatory mediators were investigated in hTCEpi cells exposed to the 62 kDa antigen (section 5.3.1). hTCEpi cells displayed increased gene expression of IL-1β, IL-8 and TNFα respectively, following exposure of 2 µg/ml antigen dose. As the *B. oleronius* antigen comes into contact with the ocular surface, pro-inflammatory gene expression may be upregulated and may lead to the production of cytokines which exacerbate ocular symptoms in rosacea.

In order to potentially inhibit this protein-host interaction, three blocking agents were investigated. HEp-2 cells and hTCEpi cells exposed to each blocking agents to determine levels of toxicity. Mucin (Type I-S) induced a significant reduction of growth in HEp-2 cells but encouraged hTCEpi cell growth (Figures 5.12 and 5.13). Mucins are glycoproteins secreted by the mucosal epithelium which adapts to surrounding environments and shield underlying tissues from exogenous damage (Linden *et al*., 2008; Khanvilkar *et al*., 2001). Serum albumins are the most abundant proteins in the blood plasma of all vertebrates and are known as carrier proteins, responsible for binding to compounds and transporting them into the bloodstream to the targeted tissue (Żurawska-Płaksej *et al*., 2018; Dawoud Bani-Yaseen, 2011). BSA displayed no toxicity to HEp-2 cells or hTCEpi cells at the chosen concentration of 0.0625 mg/ml (Figures 5.14 and 5.15). The anti-62 kDa rabbit antibody binds to the 62 kDa antigen and induced some significant reduction in HEp-2 and hTCEpi cell growth (Figures 5.16 and 5.17). The antibody dilution of 1/160K was chosen which did not display any toxicity in HEp-2 cells and some toxicity in hTCEpi cells. The use of antibodies to detect and identify antigens are efficient molecular tools and may have the potential to block the 62 kDa antigen as a rosacea treatment.

To measure the efficacy of these potential blocking agents, proliferation assays were performed in HEp-2 cells, with the blocking agents alone and in combination with the 62 kDa antigen (Figure 5.18). The antigen significantly reduced cell growth ($p < 0.01$) in comparison to the control. The blocking agents alone displayed minimal toxicity to HEp-2 cells. Each blocking agent was incubated with the antigen prior to cell exposure with the potential to bind to the 62 kDa antigen and inhibit or block it form interacting successfully with the host cells. HEp-2 cells exposed to the blocking agents and antigen combination, resulted in significant restoration of cell growth, more than the control. Antigen alone (3 µg/ml dose) inhibited growth by 54% while the blocking agents in combination the antigen counteracted this effect. Mucin increased cell proliferation by 40%, BSA by 25% and antibody by 31%, indicating the capability to capture or block the effect of 62 kDa antigen with the host cell interaction. The mucin displayed the strongest blocking ability and so further assays were performed to test the blocking potential of mucin against 62 kDa antigen. This capability was observed once again in HEp-2

cells with the mucin and antigen combination restoring HEp-2 cell growth to the same as the control (Figure 5.19). However, when hTCEpi cells were exposed to the mucin-antigen complex, cell growth was reduced by 75.8% ($p < 0.001$). It may be the case that mucin facilitated the antigen-host interaction rather than blocking the 62 kDa antigen in the hTCEpi cells. In the eye, mucins have the potential to capture pathogenic components and invading microorganisms and clear the ocular surface of such dangers (Mantelli & Argüeso, 2008). hTCEpi cells are incubated for 72 hours in a 6 well plate and it is possible that the mucin had nowhere to clear the bound 62 kDa antigen to without causing damage and further decreased in cell proliferation. For this reason, the blocking agent was assessed in various ways, with some results indicating potential.

The effect of the *B. oleronius* antigen on wound healing and cytokine secretion was analysed with HEp-2 cells and hTCEpi cells (section 5.6). HEp-2 cells were exposed to antigen (6 µg/ml and 2 µg/ml) and mucin (0.0313 mg/ml) alone and in combination to investigate the cell response to a superficial wound. HEp-2 cells exposed to the mucin alone and in combination with the antigen displayed similar growth to the control, as cells migrated from the edge of the scratch wound towards closing and healing the wound (Figure 5.21). The cells exposed to the 2 µg/ml antigen dose displayed some of these migratory properties also however the 6 µg/ml antigen dose had fewer cells at the lining of the wound and some cell growth in the middle of the scratch wound. This displays the blocking potential of mucin against the inhibitory effect of wound healing in cells exposed to *B. oleronius* antigen. The secretome from the scratch wound assays were collected and the level of pro-inflammatory cytokines were measured (Figure 5.23). The secretion of IL-8 was significantly increased in HEp-2 cells exposed to 6 µg/ml alone and in combination with mucin. This indicates that although mucin may block the damaging effect of the 62 kDa antigen, it has no impact on the level of IL-8 cytokine secreted from the HEp-2 cells. However, the level of IL-6 and IL-1β cytokine production increased in HEp-2 cells exposed to 6 µg/ml antigen but decreased back to control level when in the presence of mucin, indicating a reduction in the inflammatory side effects of antigen exposure.

The hTCEpi cells were visualized 24 hours after the scratch wound and a 0-hour image was used once again as a reference point (Figure 2.22). hTCEpi cells exposed to mucin (0.0625 mg/ml and 0.0313 mg/ml) alone and in combination with 3 µg/ml antigen dose. The mucin treated cells displayed growth from the lining of the wound inwards to heal the wound, similar to the control. hTCEpi cells exposed to the antigen displayed a higher migration of cells around the edge of the scratch wound but also dispersed throughout the middle of the wound. Cells exposed to the combination of mucin and antigen displayed more growth than the control and the antigen alone. This result correlates with the proliferation assay (Figure 5.20), whereby mucin at this particular concentration may enhance the damaging effect of the antigen. Although the wound is healing, it may be the case that cells are growing rapidly an unregulated matter in response to antigen stimulation. The secretome from the scratch wound assay was collected after 72 hours and cytokine expression was measured using ELISA (Figure 2.24). Antigen stimulated IL-8 and IL-1β cytokine production slightly in hTCEpi cells. It is possible that the level of cytokines produced at 72 hours had little to no alteration in abundance, as at 24 hours the wells with mucin and antigen combination displayed growth that almost fully covered the scratch wound.

In severe cases of ocular rosacea corneal ulcers may develop and if symptoms persist this may result in blindness (McMahon *et al*., 2014). A similar pathology to corneal ulcers has been demonstrated in hTCEpi cells following exposure to *B. oleronius* sera reactive proteins (O'Reilly *et al*., 2012b). The hTCEpi cells in that case displayed increased migration of cells into the area of the wound rather than growth from the lining of the wound as in control cells (O'Reilly *et al*., 2012b). A similar result was observed with hTCEpi cells in the scratch wound assay. It is possible that corneal epithelial cells are more sensitive to the concentration of mucin and the binding effect of mucin to the antigen may enhance dysregulated growth and contribute to corneal damage and ulcer-like growth.

In summary, the potential use of blocking agents targeting *B. oleronius* 62 kDa antigen was evaluated. These preliminary results provided an insight into BSA, anti-62 kDa rabbit antibody and mucin as blocking agents by preventing the 62 kDa antigen and host cell interactions. The mucin displayed the most potential and the

whole body and corneal surface is also lined with the protective mucosal epithelium which naturally secretes mucins (Gipson, 2016; Mantelli & Argüeso, 2008; Khanvilkar *et al*., 2001). One important functional characteristic of mucins is their viscoelasticity ability, which help serve pathogen binding and protective roles (Khanvilkar *et al*., 2001). For example, *Pseudomonas aeruginosa* invading the corneal surface has previously been blocked and penetration was prevented based on mucin binding to and clearing the pathogen from the ocular region (Mantelli & Argüeso, 2008; Pier, 1994). This limiting effect of pathogen entry by mucins and their "sticky" binding nature has also been observed in HEp-2 and hTCEpi cell results presented here. Mucins are at the interface of the epithelia layer of the eye and tear-fluid, and may have the potential, following extensive future studies, as blocking agents that could bind and inhibit *B. oleronius* protein contact with the cornea surface in rosacea.

Chapter Six

Biological and Clinical Evaluation of a Novel Salt Based Formulation for the Treatment of Symptoms of Dermal Rosacea

6.1 Introduction

The treatment and management of the chronic inflammatory condition rosacea is often approached by targeting symptomatic relief in individual patients rather the disease itself. Simple alterations in everyday life can help to reduce the persistence of rosacea symptoms by avoiding certain trigger factors such as spicy foods or specific medication, wearing high sun protection factor on a daily basis or using fragrance free and pH suitable soaps (Holmes & Steinhoff, 2017; Barco & Alomar, 2008). Most rosacea patients require to antibiotic treatments that can be applied topically to the face or orally consumed. Antibiotics such as metronidazole, tetracycline and erythromycin all contribute to alleviating symptoms such as inflammation, chronic erythema and ocular symptoms. Some antibiotics have a dual role, in that they have anti-bacterial and anti-inflammatory properties, for example metronidazole gel (Holmes & Steinhoff, 2017; Two *et al.,* 2015b).

The potential of a novel therapeutic for the symptomatic relief of rosacea subtypes one and two, ETR and PPR respectively, were investigated. This novel compound is naturally sourced off the East coast of Ireland and is Oriel Marine Mineral Complex. Working in collaboration with the Oriel Company, the anti-inflammatory potential of this natural and unique product was reviewed. The Oriel product is a type of sea salt that previously displayed anti-inflammatory effects on keratinocyte cells and has induced increased cell adhesion and endothelial cell growth (Previous Study, Oriel Company; Personal communication).

The use of salt as a therapeutic agent is strongly associated with respiratory disease. Inhalation of hypertonic saline has proved beneficial in treating acute respiratory distress syndrome (ARDS), cystic fibrosis and asthma (Artigas *et al*., 2017; Elkins *et al*., 2006; Gibson *et al*., 2001). Overproduction of an inflammatory respiratory response is characteristic of ARDS, which leads to pulmonary inflammation and oedema (Artigas *et al*., 2017). Treatment for ARDS is a similar approach to rosacea treatment, in that the target is to relieve patient symptoms and reduced inflammatory mediators in lung tissue in this case. ARDS patients and cystic fibrosis patients have positively responded to hypertonic saline (HS) treatment ranging between 3% and 14% (Artigas *et al*., 2017; Elkins *et al*., 2006). Treatments for both of the respiratory conditions consisted of nebulized HS which produced

results similar to mucolytic agents, whereby mucociliary clearance improved (Furnari *et al*., 2012; Elkins *et al*., 2006). In these conditions, mucus tends to be more viscous than normal individuals and coughing can help remove the mucus build-up (Artigas *et al*., 2017). Overall, nebulized HS or HS inhaled with the use of a bronchodilator benefited patients as the saline treatment improved lung function, improved sputum transport and mucociliary clearance as previously mentioned, and also resulted in fewer exacerbations in the case of cystic fibrosis patients (Artigas *et al*., 2017; Donaldson *et al*., 2006; Elkins *et al*., 2006).

Rosacea and perioral dermatitis share many similarities in that the aetiology and pathogenesis of each condition is unknown, a role for trigger factors influence the onset of symptoms, both conditions feature a granulomatous variant and patients often suffer with similar symptoms such as sensitive skin (Dirschka *et al*., 2004). Patients suffering from either of these two separate conditions experience burning and stinging sensation in their skin, particularly after applying moisturizers or facial creams that may result in the skin feeling tight and dry (Dirschka *et al*., 2004). This dryness, particularly in rosacea patients, is a sign of roughness and scaling in the skin which is due to lack of hydration (Elkins *et al*., 2006; Dirschka *et al*., 2004). Patients with psoriasis have benefited from bathing in a 5% Dead Sea salt solution resulting with improved hydration of the skin and reduction of roughness and redness (Proksch *et al*., 2005). Improved hydration in the airways of cystic fibrosis patients was also a short term result of HS inhalation along with transport of sputum and improved quality of life for patients (Furnari *et al*., 2012; Elkins *et al*., 2006).

Corticosteroids are anti-inflammation agents that are sometimes misused in the management of perioral dermatitis and rosacea, which can induce the onset of trigger factors and symptoms. Budesonide is a corticosteroid used to treat asthma and a single does has improved inflammation and hyper-responsiveness in the airways of patients (Hashemian *et al*., 2018; Dirschka *et al*., 2004; Gibson *et al*., 2001). Patients with asthma displayed 2.2 fold improvement in the airways in response to HS following treatment with budesonide (Gibson *et al*., 2001). Budesonide dissolved and prepared in a saline solution has also proved effective at treating patients with chronic obstructive pulmonary disease (COPD). Nebulized budesonide reduced lung inflammation and inflammatory mediators such as IL-8 and

IL-6 cytokine expression in COPD (Hashemian *et al*., 2018). Nebulization of HS is a safe and inexpensive treatment for respiratory conditions with results including the reduction of lung injury, reduced MMP activity and decreased expression of pro-inflammatory cytokines, all of which contribute to the anti-inflammatory efficacy of HS inhalation (Artigas *et al*., 2017; Wohlauer *et al*., 2012; Elkins *et al*., 2006).

The application of saline products onto the skin have improved hydration levels and transepidermal water loss (TEWL) in the case of psoriasis treatment with Dead Sea salt solution (Proksch *et al*., 2005). This treatment improved skin integrity as a result of increased TEWL, leaving the skin of patients feeling less dry and more moisturised, hydrated and with improved elasticity (Proksch *et al*., 2005). The use of saline instillation in wound cleansing has displayed additional therapeutic benefits when used in combination with negative pressure wound therapy (Leung *et al*., 2010). Wounds are typically cleansed with non-toxic solutions such as water or salt to aid the removal of debris, prevent the accumulation of cellular products in the wound bed and also to remove the possibility of bacterial infection (Leung *et al*., 2010). The application of saline in wound dressing is desirable as it does not induce tissue damage or influence normal bacteria present in the skin (Leung *et al*., 2010). Dead Sea salt application to the skin was well tolerated by patients with sensitive skin and indicated early signs of wound healing (Proksch *et al*., 2005). The level of TEWL improved following Dead Sea salt treatment and this indirectly played a role in the reduction of pathogen penetration through the skin as the skin barrier function was strengthen and improved (Proksch *et al*., 2005). Treating the skin with Oriel salt solution may display similar improvement in skin barrier function and possibly inhibit the interaction of *B. oleronius* with the skin surface or alternatively, Oriel salt solution may possess similar anti-inflammatory properties to the Dead Sea salt solution.

There is great potential for the use of saline therapeutics in dermal and pulmonary therapies. Based on these treatment efficacies and the anti-inflammatory effect of Oriel salt solution in keratinocytes, this research focuses on the collaboration with Oriel Company to determine the efficacy of Oriel salt solution in the treatment of dermal rosacea.

6.2 Determining the toxicity of Oriel salt and NaCl on human cell growth

The Oriel sea salt solution and sodium chloride (NaCl) were each dissolved in PBS. HEp-2 cells and hTCEpi cells were exposed to both solutions to determine the effect on cell proliferation and toxicity. HEp-2 cells were grown in MEM, hTCEpi cells were grown in KBM-Gold basal medium and results were visualized by an acid phosphatase assay (section 2.24).

HEp-2 cells were seeded ($3x10^4$ cells/well) and incubated for 5-7 days before being assessed. HEp-2 cells were exposed to Oriel (Figure 6.1) and NaCl (Figure 6.2) in concentrations ranging from 50 mg/ml to 0.195 mg/ml. The higher concentrations of Oriel were toxic to HEp-2 cells and significantly inhibited cell growth to 29.3% when exposed to 6.25 mg/ml Oriel ($p < 0.001$). HEp-2 cells exposed to a concentration of 3.125 mg/ml Oriel or lower did not inhibit cell growth significantly and were not found to be toxic. The effect of NaCl on HEp-2 cell growth was similar to Oriel, in that cell growth was inhibited significantly when cells were exposed up to 6.25 mg/ml, which had percentage growth of 49.3% in comparison to the control ($p < 0.01$). HEp-2 cells exposed to concentrations of NaCl lower than 3.125 experienced no growth inhibition.

hTCEpi cells exposed to concentrations of 50 mg/ml to 3.125 mg/ml of Oriel (Figure 6.3) and NaCl (Figure 6.4) resulted in significant inhibition of cell proliferation ($p < 0.001$). hTCEpi cells exposed to 3.125 mg/ml Oriel were inhibited by 25% and hTCEpi cells exposed to 3.125 mg/ml NaCl were inhibited by 39%. The effect of Oriel and NaCl on hTCEpi cells exposed to concentrations lower than 1.563 mg/ml did not inhibited growth. The rate of cell proliferation increased as the concentrations of Oriel or NaCl decreased. For example, hTCEpi cells exposed to 1.563 mg/ml Oriel dose or NaCl dose showed growth of 96% and 89% respectively.

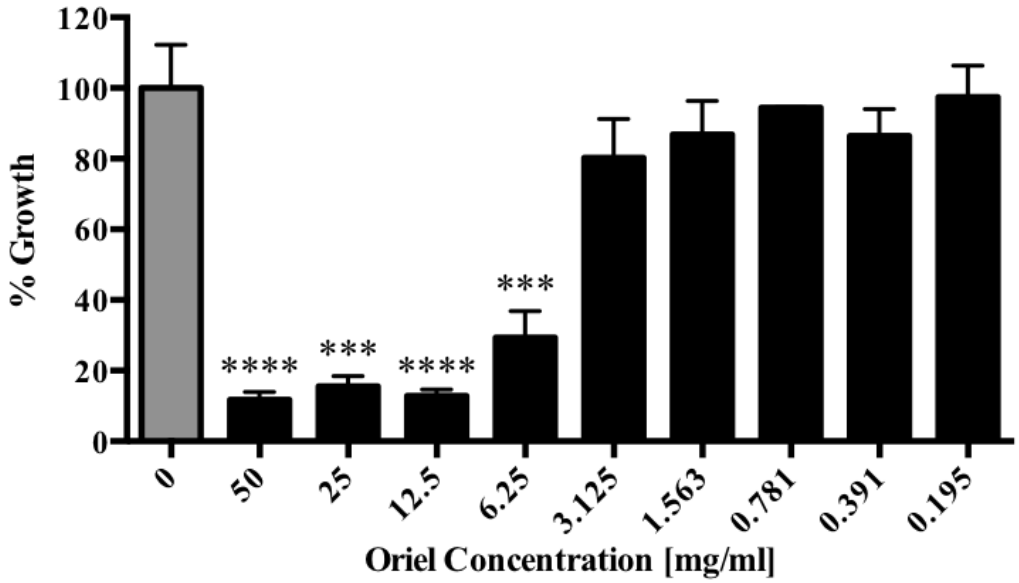

Figure 6.1 Growth of HEp-2 cells exposed to Oriel salt solution

The effect of Oriel on HEp-2 cell growth as visualized by acid phosphatase assay. HEp-2 cells exposed up to 6.25 mg/ml Oriel dose significantly inhibited cell growth ($p < 0.001$). HEp-2 cells exposed to Oriel below the concentration of 3.125 mg/ml inhibited growth by 20% or less.

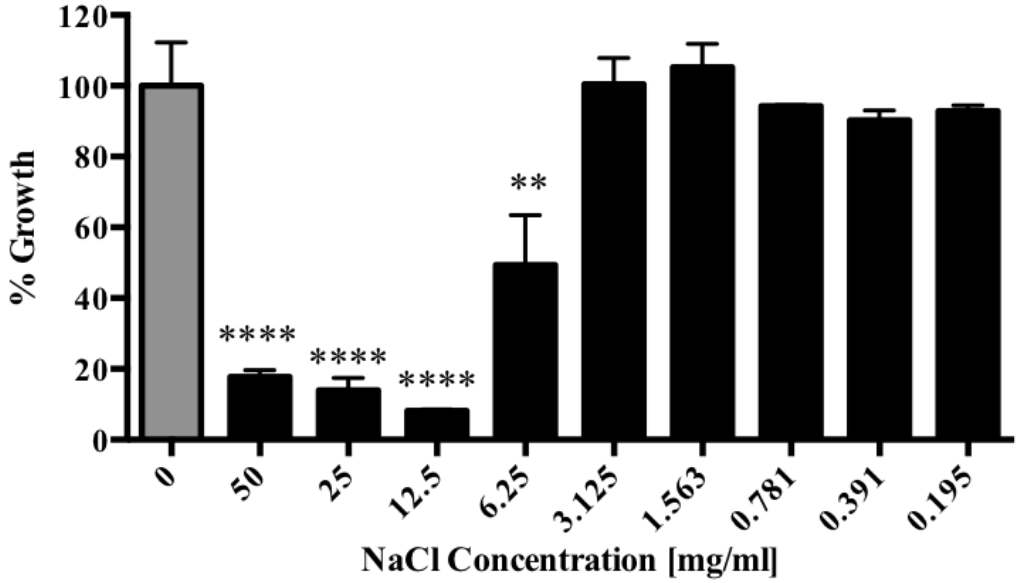

Figure 6.2 Growth of HEp-2 cells exposed to NaCl solution

The effect of NaCl on HEp-2 cell growth as visualized by acid phosphatase assay. HEp-2 cells exposed to 6.25 mg/ml NaCl were significantly inhibited ($p < 0.01$). There was no toxic effect on cell growth of 3.125 mg/ml NaCl or below.

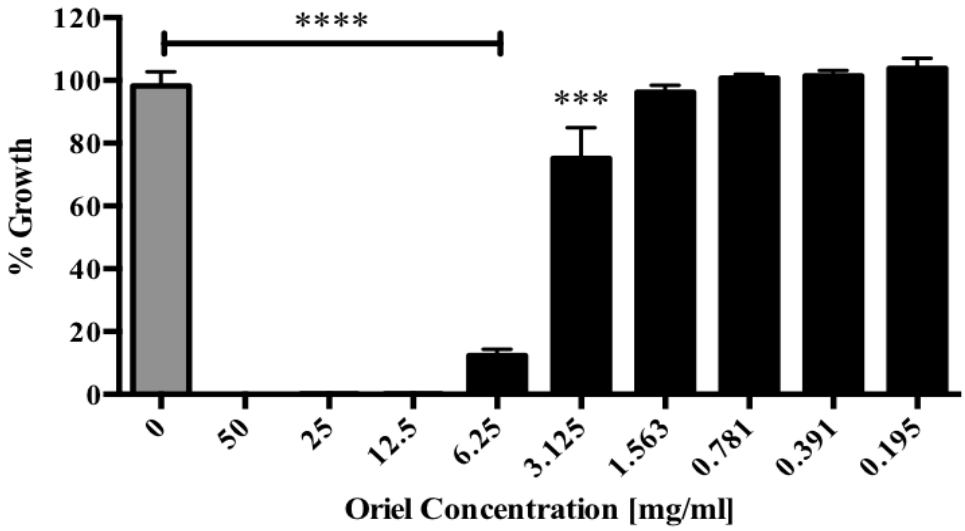

Figure 6.3 Growth of hTCEpi cells exposed to Oriel salt solution

The effect of Oriel on hTCEpi cell growth as visualized by acid phosphatase assay. hTCEpi cells exposed to Oriel above 3.125 mg/ml were found to be toxic and inhibited cell growth by more than 25% ($p < 0.001$). No toxic effect was observed on hTCEpi cells exposed to 1.563 mg/ml Oriel does or lower.

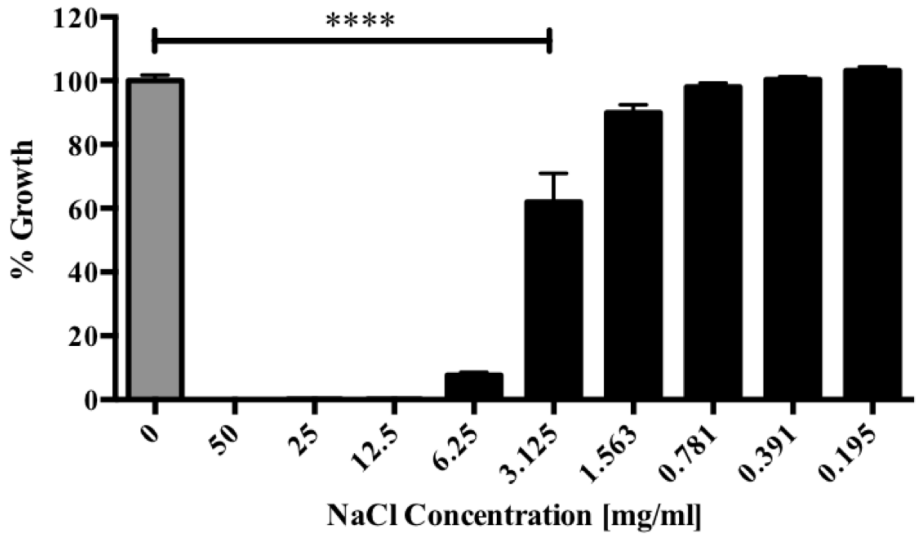

Figure 6.4 Growth of hTCEpi cells exposed to NaCl solution

The effect of NaCl on hTCEpi cell growth as visualized by acid phosphatase assay. Concentrations of NaCl above 3.125 mg/ml were found to be toxic to hTCEpi cell growth ($p < 0.001$). hTCEpi cells exposed to 3.125 mg/ml NaCl showed significantly reduced cell growth. hTCEpi cells exposed to NaCl below the concentration of 1.563 mg/ml only inhibited growth by 10% or less.

6.2.1 Effect of Oriel salt solution and NaCl on HEp-2 cell proliferation

The Oriel salt solution may have the potential as a facial application to reduce inflammation in ETR and PPR therapy. In order to assess the effect of Oriel product on the face, the HEp-2 cell line was chosen as a dermal representative. HEp-2 cells were grown in MEM media and prepared for a 72 hour proliferation assay. HEp-2 cells were seeded ($4.3x10^5$ cells/well) and incubated overnight to attach, followed by the addition of fresh medium and Oriel or NaCl at two concentrations, 3.12 mg/ml and 0.78 mg/ml (section 2.22).

HEp-2 cells exposed to 3.12 mg/ml Oriel salt had significantly decreased proliferation by 63% ($p < 0.01$). The 0.78 mg/ml Oriel dose was not as inhibitory with cell proliferation but growth was still significantly reduced ($p < 0.05$). A similar difference in cell proliferation was observed with NaCl exposure. HEp-2 cells exposed to 3.12 mg/ml NaCl resulted in significant reduction in proliferation by 65.5% ($p < 0.001$), however the 0.78 mg/ml dose resulted in a 21% reduction in comparison to the control.

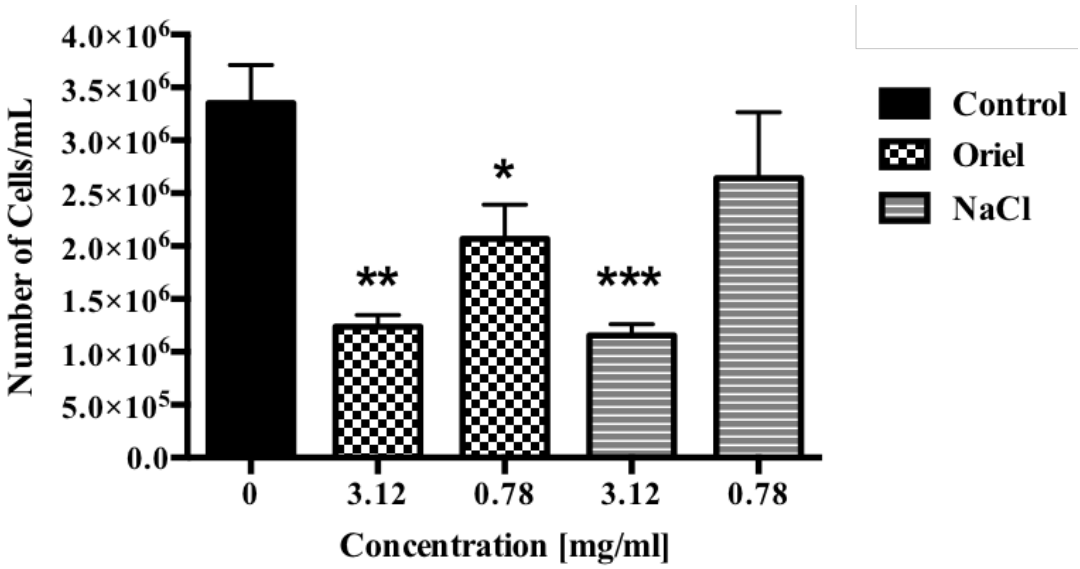

Figure 6.5 HEp-2 cells exposed to Oriel and NaCl for 72 hours.

HEp-2 cells exposed to two concentrations of Oriel and NaCl in a proliferation assay. The 3.12 mg/ml doses of Oriel and NaCl significantly reduced cell growth ($p < 0.01$). HEp-2 cells exposed to Oriel at 0.78 mg/ml resulted in a significant decrease in cell growth ($p < 0.05$) and cells exposed to NaCl at 0.78 mg/ml had some decreased growth in comparison to the control. All values are the mean ± SE of three independent determinations.

6.3 Comparative analysis of the effect of Oriel salt on the proteomic profile of HEp-2 cells using Label free MS/MS

Label free MS/MS quantitative proteomics was performed on cell lysate from HEp-2 cells exposed to 0.78 mg/ml Oriel for 48 hours. LF-MS/MS enables a quantitative examination at the relative change in protein abundances over multiple parameters at single mass spectrometry runs (Bantscheff *et al.,* 2012). Here, LF-MS/MS was employed to identify the variations of protein expression in HEp-2 cells exposed to Oriel in comparison to control (medium only). PCA was performed with normalised intensity values (n=3) and resolved a clear difference in the proteomes (Figure 6.6A). All statistically significant proteins were visualised in a hierarchical cluster performed using Z-score normalised intensity values for differentially abundant proteins (Figure 6.6B).

In total, 1905 peptides were identified, representing 1901 proteins with two or more peptides and 9 proteins were determined to be differentially abundant with a fold change > 1.5 fold (ANOVA, $p < 0.05$) (Figure 6.7). In HEp-2 cells exposed to Oriel salt solution for 48 hours, five proteins were found in higher abundance, one of which was not imputated and four proteins were found to be lower in abundance, all of which were imputated (Table 6.1) when compared against HEp-2 cells exposed to MEM medium only. These proteins were statistically analysed following imputation of zero values using a number close to the lowest value of the range of proteins plus or minus standard deviation. The volcano data (Figure 6.7) displays four statistically significant proteins that were decreased in abundance including microtubule-associated protein (8 fold decrease), Golgi resident protein (2.4 fold decrease), 2-oxoisovalerate dehydrogenase subunit beta (2.3 fold decrease) and THO complex subunit 2 (1.6 fold decrease). Five proteins were significantly increased in abundance including aldo-keto reductase family (1.5 fold increase), ran-binding protein 3 (2.1 fold increase), DNA excision repair protein (3.9 fold increase), SEC23-interacting protein (4.8 fold increase) and thioredoxin mitochondrial (1.7 fold increase).

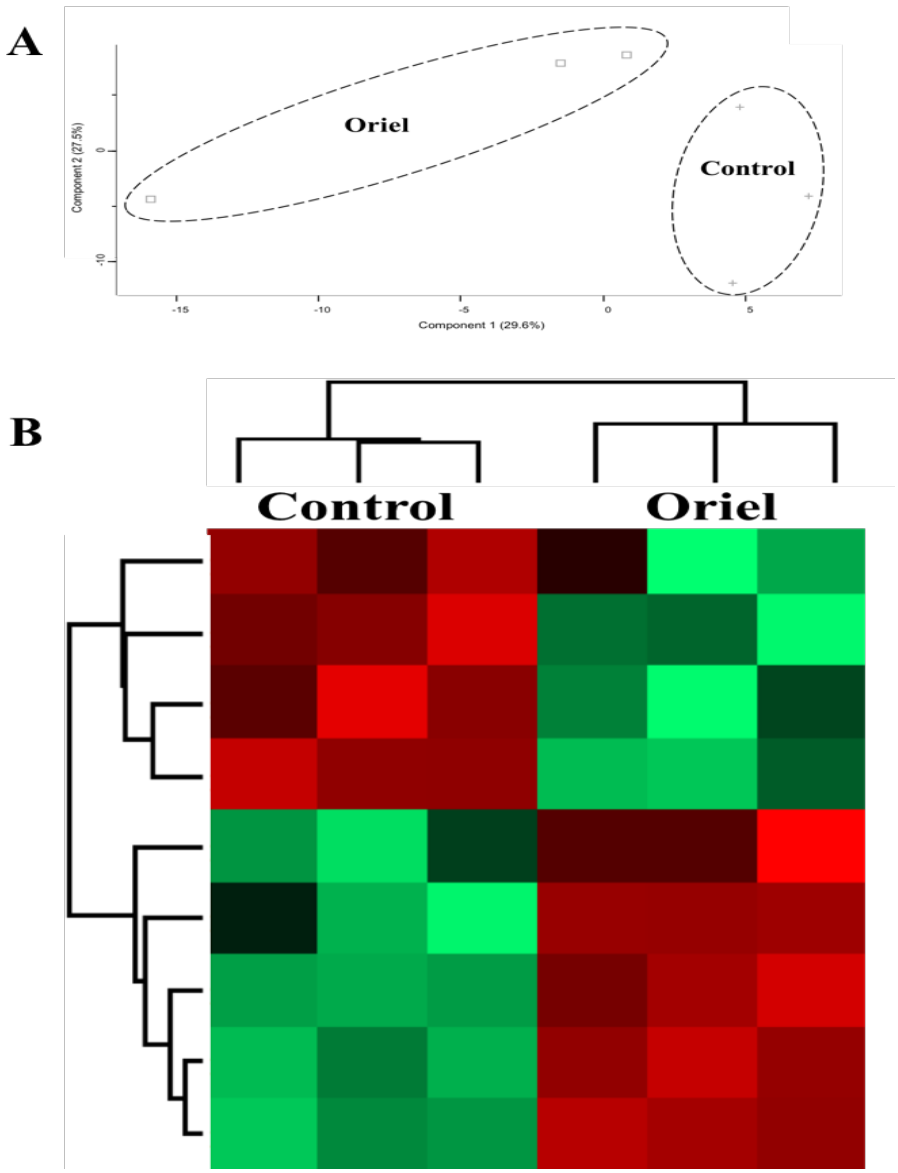

Figure 6.6 Label free MS/MS principal component analysis and hierarchical clustering of the quantitative differences in the proteomic profile of HEp-2 cells **(A)** Principal component analysis (PCA) of comparative HEp-2 cell treatments included in label free quantification (LFQ). Dashed circles represent sample groups with three replicates per group. **(B)** This heat map represents the median protein expression values of all statistically significant differentially and uniquely detected proteins from HEp-2 cell proteomic profiles at 48 hours. Hierarchical clusters resolved two distinct columns comprising the replicates from the original sample groups and cluster rows based on expression profile similarities. The red indicates high level of abundance and the green indicates low level.

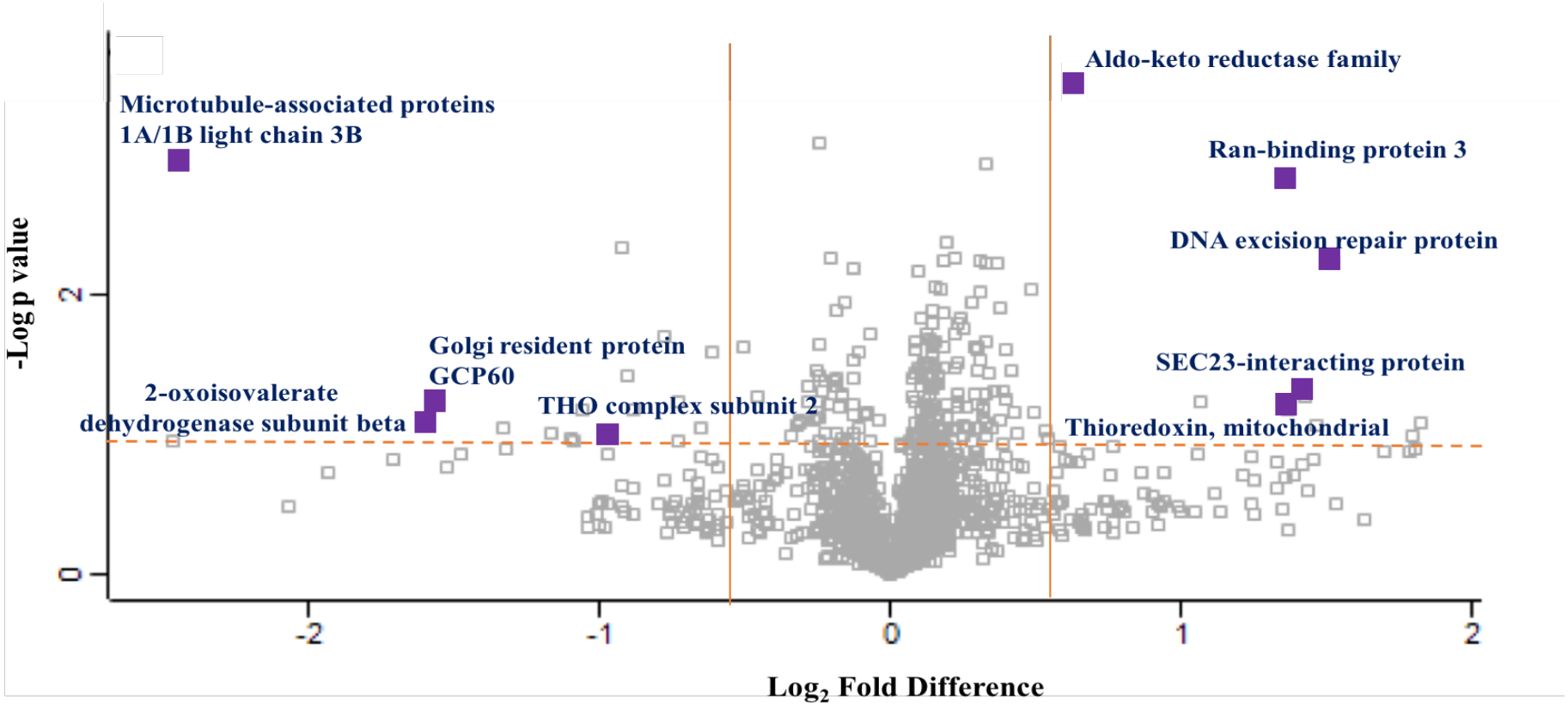

Figure 6.7 Volcano plot highlighting the proteins altered in abundance in HEp-2 cells exposed to Oriel solution

Volcano plot showing the effect of Oriel exposure on protein abundance in HEp-2 cells. Protein intensity difference (log_2 mean intensity difference) and significance in differences (-log *p*-value) based on a two-sided *t*-test. Proteins above the dashed line are considered statistically significant ($p < 0.05$) and those to the right and left of the vertical lines indicate > 1.5-fold negative changes (left) and fold positive changes (right) in HEp-2 cells exposed to Oriel respectively, versus control.

Table 6.1 Proteins identified at higher and lower abundances in HEp-2 cells exposed to Oriel salt solution

Proteins that had over two matched peptides with a *t*-test probability < 0.5 and that were found to be differentially expressed at a 1.5 fold change were considered to be significantly altered in abundance in Oriel treated HEp-2 cells. Table displays proteins with an increased and decreased fold difference.

Protein Annotation (* = non-imputated)	Peptides	Sequence Coverage (%)	PEP	Overall Intensity	Fold difference
SEC23-interacting protein	13	21.9	4.14E-87	5.15E+08	+ 4.8 increase
DNA excision repair protein ERCC-6	2	1.7	1.41E-07	2.36E+08	+ 3.9 increase
Ran-binding protein 3	6	14.8	1.02E-25	3.33E+08	+ 2.1 increase
Thioredoxin, mitochondrial	3	32.5	4.56E-25	1.77E+08	+ 1.7 increase
*Aldo-keto reductase family 1 member C1	21	79.3	2.11E-282	1.45E+10	+ 1.5 increase
Microtubule-associated proteins 1A/1B light chain 3B	4	32.8	3.00E-14	2.68E+08	- 8.0 decrease
Golgi resident protein GCP60	9	28.8	1.44E-120	3.98E+08	- 2.4 decrease
2-oxoisovalerate dehydrogenase subunit beta, mitochondrial	3	13.8	3.35E-08	1.87E+08	- 2.3 decrease
THO complex subunit 2	7	6.7	2.12E-19	1.60E+08	- 1.6 decrease

6.4 Effect of Oriel salt and NaCl on bacterial cell growth

A susceptibility assay was carried out to assess anti-bacterial properties of Oriel, and NaCl as a comparison, on bacterial cell density by measuring the OD. Antibiotics used to treat rosacea sometimes play a dual role in targeting bacteria, but also have anti-inflammatory roles. The Oriel salt solution has displayed anti-inflammatory properties in keratinocytes previously, thus potential antibacterial properties were examined here. Understanding the effect of Oriel on *B. oleronius* cell density is an important factor as this bacterium is associated with rosacea. *B. oleronius, E. coli* and *S. aureus* were all exposed to Oriel and NaCl in a susceptibility assay to measure the effect of each salt solution on bacterial cell growth. Overnight cultures of the bacteria were grown aerobically in nutrient broth at 30ºC 200 rpm and incubated for 24 hours (section 2.19).

Exposure of *B. oleronius* to Oriel significantly enhanced cell density in comparison to control samples which were set at 100%. The maximum cell density reached 179% when exposed to 12.5 mg/ml Oriel ($p < 0.001$) and the minimum at 105% when exposed to 0.195 mg/ml Oriel ($p < 0.01$), in comparison to the control (Figure 6.8). *B. oleronius* grown in the presence of NaCl ranging from 50 mg/ml to 6.25 mg/ml had significantly decreased cell density with the most reduction at 34.7% when exposed to 25 mg/ml ($p < 0.001$) (Figure 6.9). *B. oleronius* exposed to 3.125 mg/ml NaCl and lower resulted in growth matching the control and above.

E. coli exposed to Oriel (Figure 6.10) and NaCl (Figure 6.11) displayed similar results in that concentrations of either salt solution at 25 mg/ml or lower resulted in no significant change from the control and cell denisty remained consistent with the control. The growth of *E. coli* exposed to 50 mg/ml Oriel or NaCl was significantly less than the control ($p < 0.05$). *S. aureus* exposed to Oriel (Figure 6.12) and NaCl (Figure 6.13) displayed similar results. Oriel concentrations of 50 mg/ml and 25 mg/ml enhanced *S. aureus* cell density significantly to 115% and 106% respectively ($p < 0.05$). *S. aureus* cell density was significantly reduced in the presence of Oriel ranging from 12.5 mg/ml to 1.563 mg/ml ($p < 0.001$). *S. aureus* cell density was enhanced when exposed to 50 mg/ml NaCl and significantly reduced when exposed to 705 and 68% when exposed to 12.5 mg/ml and 6.25 mg/ml respectively ($p < 0.01$).

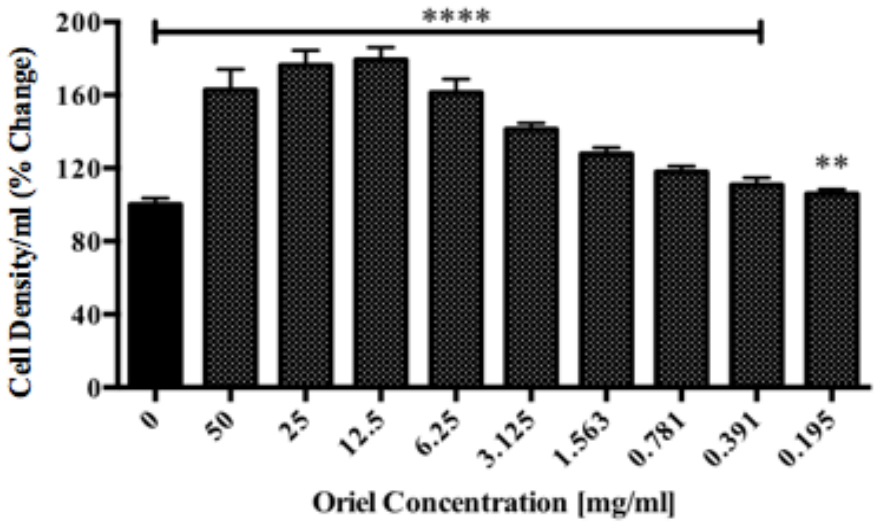

Figure 6.8 The effect of Oriel salt solution on *B. oleronius* cell density.
Susceptibility assay of *B. oleronius* exposed to Oriel for 24 hours to determine the effect on cell density. Results measured cell density as a percentage change of all treated samples in comparison to the control sample (0 mg/ml; 100%). Oriel had a significant effect on *B. oleronius* cell density in comparison to the control ($p < 0.01$). All values are the mean ± SE of three independent determinations.

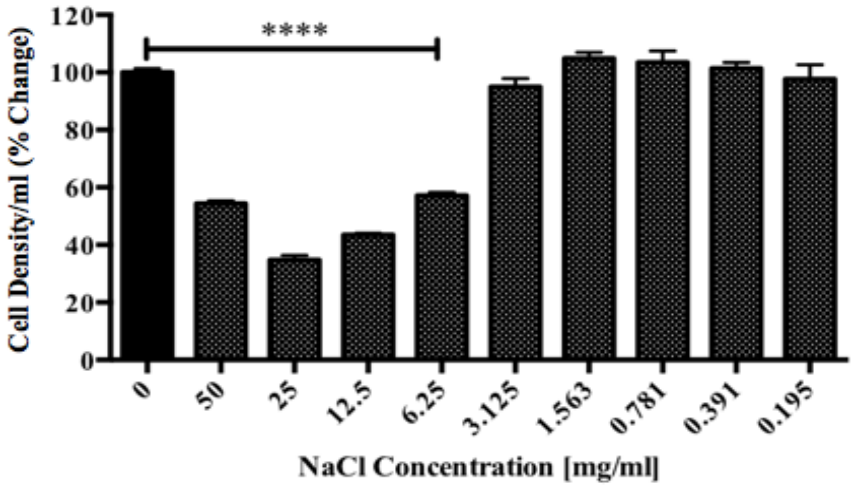

Figure 6.9 The effect of NaCl on *B. oleronius* cell density.
Susceptibility assay of *B. oleronius* exposed to NaCl for 24 hours to determine effect on cell density. Results measured cell density as a percentage change of all treated samples in comparison to the control sample (0 mg/ml; 100%). NaCl significantly reduced *B. oleronius* cell density when exposed to 6.25 mg/ml or higher doses ($p < 0.001$). Cell density was unaffected when cells were exposed to 3.125 mg/ml NaCl or lower. All values are the mean ± SE of three independent determinations.

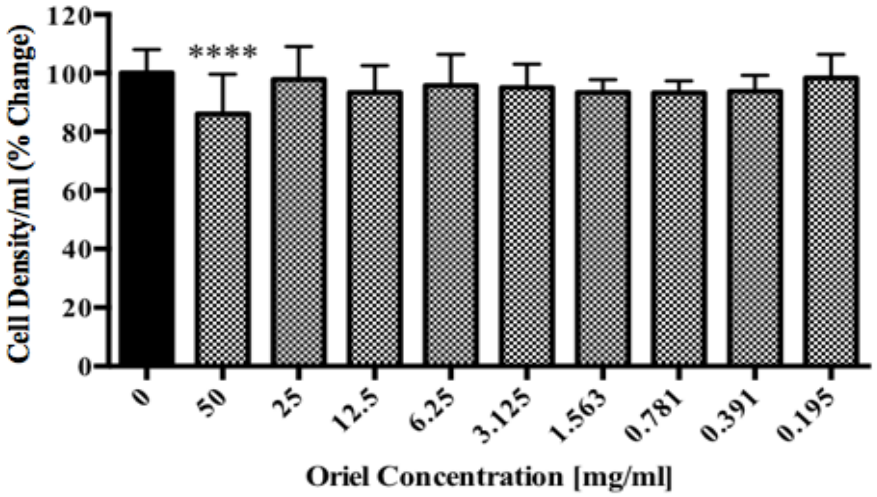

Figure 6.10 The effect of Oriel salt solution on *E. coli* cell density.

Susceptibility assay of *E. coli* exposed to Oriel for 24 hours to determine effect on cell density. Results measured cell density as a percentage change of all treated samples in comparison to the control sample (0 mg/ml; 100%). *E. coli* cell density was significantly reduced when exposed to 50 mg/ml Oriel dose ($p < 0.001$). All values are the mean ± SE of three independent determinations.

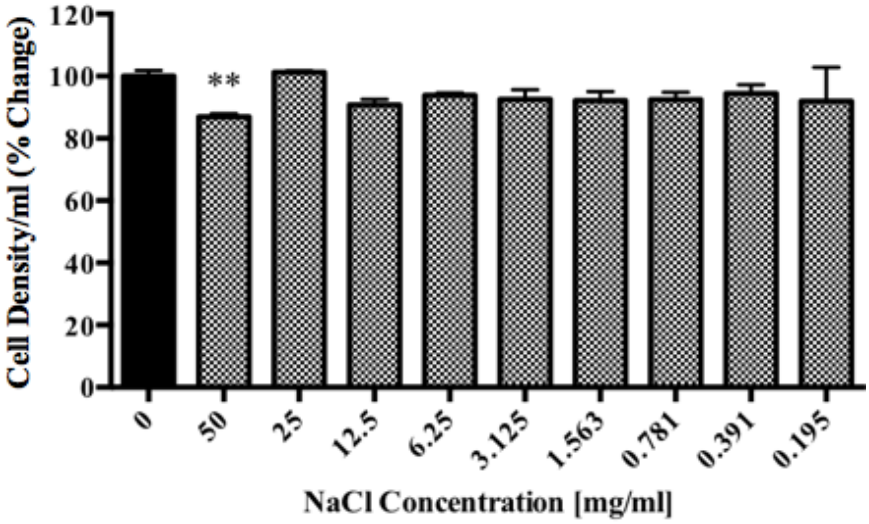

Figure 6.11 The effect of NaCl on *E. coli* cell density.

Susceptibility assay of *E. coli* exposed to NaCl for 24 hours to determine effect on cell density. Results measured cell density as a percentage change of all treated samples in comparison to the control sample (0 mg/ml; 100%). *E. coli* cell density was significantly reduced when exposed to 50 mg/ml Oriel dose ($p < 0.01$). All values are the mean ± SE of three independent determinations.

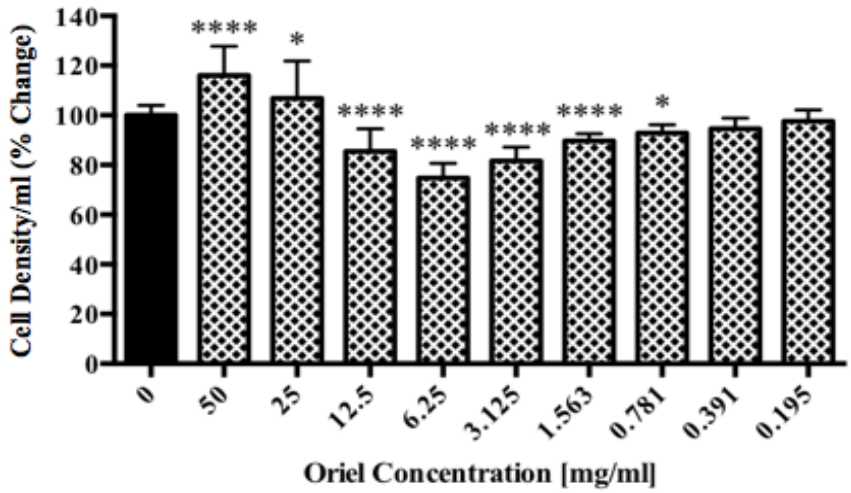

Figure 6.12 The effect of Oriel salt solution on *S. aureus* cell density.

Susceptibility assay of *S. aureus* exposed to Oriel for 24 hours to determine effect on cell density. Results measured cell density as a percentage change of all treated samples in comparison to the control sample (0 mg/ml; 100%). *S. aureus* cell density significantly increased when exposed to 50 mg/ml and 25 mg/ml Oriel dose and significantly decreased when exposed from 12.5 mg/ml to 1.563 mg/ml ($p < 0.05$). All values are the mean ± SE of three independent determinations.

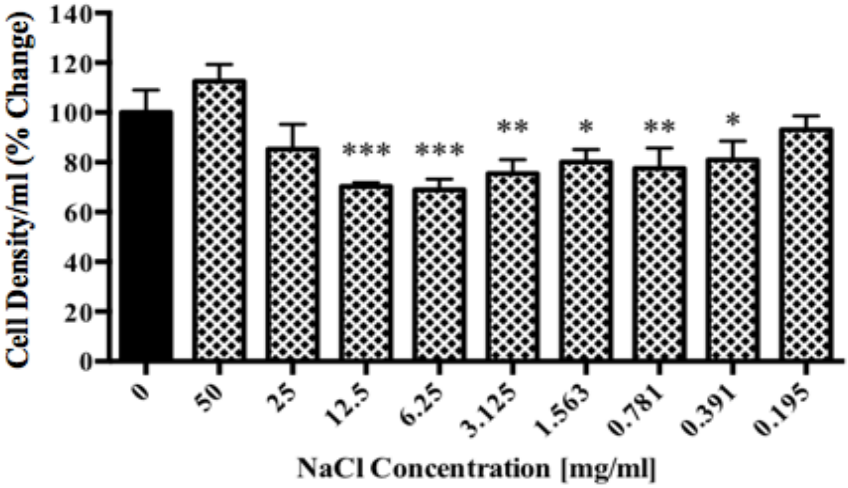

Figure 6.13 The effect of NaCl on *S. aureus* cell density.

Susceptibility assay of *S. aureus* exposed to Oriel for 24 hours to determine on cell density. Results measured cell density as a percentage change of all treated samples in comparison to the control sample (0 mg/ml; 100%). *S. aureus* cell density significantly reduced in comparison to control when exposed to 12.5 mg/ml and 6.25 mg/ml ($p < 0.001$). All values are the mean ± SE of three independent determinations.

6.5 The effect of different Oriel formulations at inhibiting bacterial cell growth on an agar plate

Three different formulations of the Oriel product were supplied by Oriel Company. The first formulation consisted of 1% Oriel in solution, dissolved in nutrient broth. The second and third were cream and gel formulations. An overnight culture of the bacteria was grown in nutrient broth and spread onto nutrient agar to set up for an inhibition assay (section 2.5). A well was created in the agar and one of the three Oriel products was inserted per well. *B. oleronius* was grown at 30ºC and *S. aureus* was grown at 37ºC for 72 hours in the presence of each formulation and the zones of growth inhibition were measured.

The agar plates with *B. oleronius* and *S. aureus* cultures displayed no zones of inhibition with the Oriel in solution (Figure 6.14A). Neither bacteria was sensitive to the solution formulation and grew as normal. A representative image of the agar plate with *B. oleronius* displays the largest zone of growth inhibition to be the gel formulation (Figure 6.14C). *B. oleronius* did not grow around the well containing the Oriel gel with an average area of 1357 mm^2. The cream formulation did result in some inhibition of *B. oleronius* growth with an average area of 341 mm^2 (Figure 6.14B). Each zone of inhibition was measured for *B. oleronius* and *S. aureus* after 72 hours (Figure 6.15) and displayed that the gel formulation was most effective at inhibiting *B. oleronius* and *S. aureus* growth. The gel formulation was significantly more inhibitory than the cream formulation ($p < 0.01$). *S. aureus* was more sensitive to the gel as the zone of inhibition was 941 mm^2 in comparison to the cream, which had a zone of 381 mm^2 (Figure 6.15).

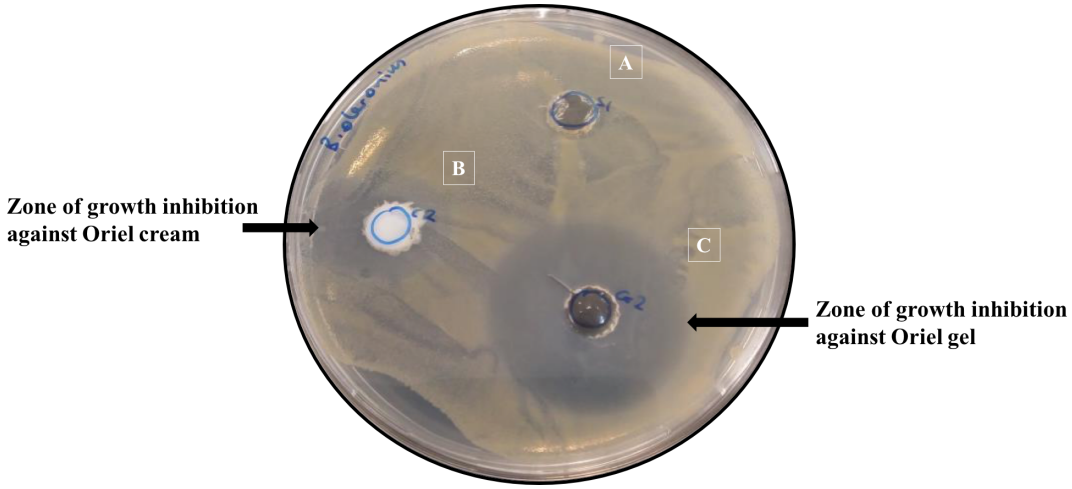

Figure 6.14 *B. oleronius* zones of growth inhibition in response to Oriel

B. oleronius grown on nutrient agar plate in the presence of three different Oriel formulations supplied by Oriel Company. **(A)** Oriel in solution, **(B)** Oriel in a cream format and **(C)** Oriel in a gel format. Zones of inhibition were measured where no growth occurred surrounding the area of Oriel formulations. The gel formulation was the most effective at inhibiting *B. oleronius* growth.

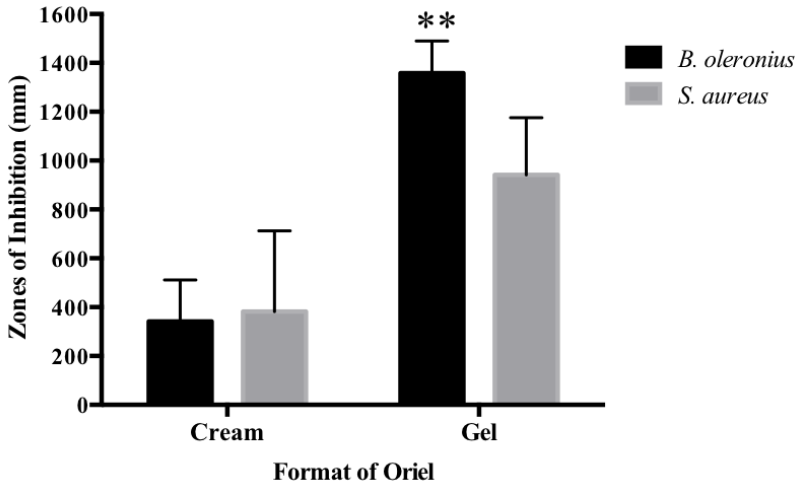

Figure 6.15 *B. oleronius* and *S. aureus* zones of inhibition measured in response to Oriel formulations

The gel formulation of Oriel was significantly more effective at inhibiting *B. oleronius* growth than the cream formulation on the nutrient agar plate ($p < 0.01$). This was similarly seen in *S. aureus* growth inhibition with the gel being more effective than the cream formulation. All values are the mean ± SE of three independent determinations.

6.6 Oriel salt as a potential treatment for symptomatic relief of ETR and PPR – Pilot study One

Following the results presented previously, Oriel has displayed little toxicity or inhibition of growth to HEp-2 cells and hTCEpi cells. Previous work with keratinocytes showed the anti-inflammatory potential of Oriel salt (Previous study, Oriel Company; Personal communication). In some formulations, Oriel inhibits the growth of *B. oleronius*, the bacterium associated with rosacea. The Oriel Company have previously worked with keratinocytes in a private study. Keratinocytes exposed to various concentrations of Oriel product resulted in the promotion of endothelial cell growth and the promotion of cell adhesion and cell spreading. Their results also revealed an anti-inflammatory role for Oriel, when the product was applied topically to the skin, the role of recovery increased.

As a result of Oriel Company's private study and the results thus far, a pilot study was established in collaboration with Professor Ryszard Zaba, Dr. Adriana Polanska and Dr. Aleksandra Dańczak-Pazdrowska, University of Medical Sciences, Poland (section 2.28). Twenty rosacea patients with subtype one (ETR) and/or subtype two (PPR) participated in the pilot study. Patients were provided with a cream or gel formulation (no choice was provided) and instructed to apply the formulation to the face twice to three times daily for one week. Patients were not given a placebo and were also instructed not to use other forms of topical treatment throughout the study. The concentration of Oriel applied to the face was 0.3% (w/v).

Five parameters were measured in each patient before and after the treatment. These consisted of erythema, melanin, sebum, transepidermal water loss (TEWL) and moisture. The average age of the patient group was 47.85 years old and the group consisted of 9 female patients and 11 male patients. The overall average score of each parameter was measured before and after treatment (Table 6.2). The average level of erythema remained almost unchanged and melanin levels did not change after treatment. Average sebum levels and TEWL levels decreased and average moisture levels increased following treatment. (The remainder of data excluded from this pilot study is listed in Table A6.1 and patient photos excluded are presented from Figure A6.1 to Figure A6.7 inclusive).

The level of erythema decreased slightly after one week of Oriel application (4.2% reduction). The erythema levels were observed from each patient (Figure 6.16) as the average erythema levels do not correlate with the visual improvement and reduction of erythema in patient skin. The technique or method to measure facial erythema may need to be altered or changed to obtain the levels of erythema in more detail. Although the average erythema levels do not greatly reduce after treatment, some individual patients did display reduced scores (Figure 6.16). For example, patients 4, 7, 8 and 13 all showed reductions in erythema. Most patients had no change in erythema score and some experienced an increase in erythema scores. Although the scores presented here are low on average, patient erythema did improve on the face one week after treatment which can be seen in patient photos (Figure 6.21). The level of melanin on average did not change after treatment in ETR patients or PPR patients (Figure 6.17).

Sebum is one of the food sources of *Demodex* mites which are strongly associated with rosacea. The correlation in *Demodex* density and rosacea has been established and *B. oleronius* has previously been isolated from a *Demodex* mite extracted from the face of PPR patient (Jarmuda *et al.,* 2012; Li *et al.,* 2010; Delaney, 2004). The sebum levels in ETR and PPR patients decreased following one week of treatment with Oriel application (Figure 6.18).

Levels of TEWL decreased following one week of Oriel application (Figure 6.19) and moisture levels increased (Figure 6.20). These two parameters correlate with one another; as the TEWL decreased, the skin epithelial barrier is improved and strengthened. Thus the level of moisture within the skin is enhanced by this barrier function and moisture levels increase in patient skin. Patients 4, 15 and 19 displayed improved symptoms of subtypes one and two on the face after one week of treatment with Oriel (Figures 6.21, 6.22 and 6.23). The erythema (E), melanin (ML), sebum (S), transepidermal water loss (WL) and moisture (MO) scores are displayed before and after treatment to compare each patients' symptoms individually.

Table 6.2 The mean results from pilot study one after one week of treatment with Oriel cream or gel application to the face (n=20).

Parameter	Before	After
Erythema	23.8	22.8
Melanin	39.9	39.9
Sebum	103.2	66.3
TEWL	17.3	12.2
Moisture	36.5	49.5

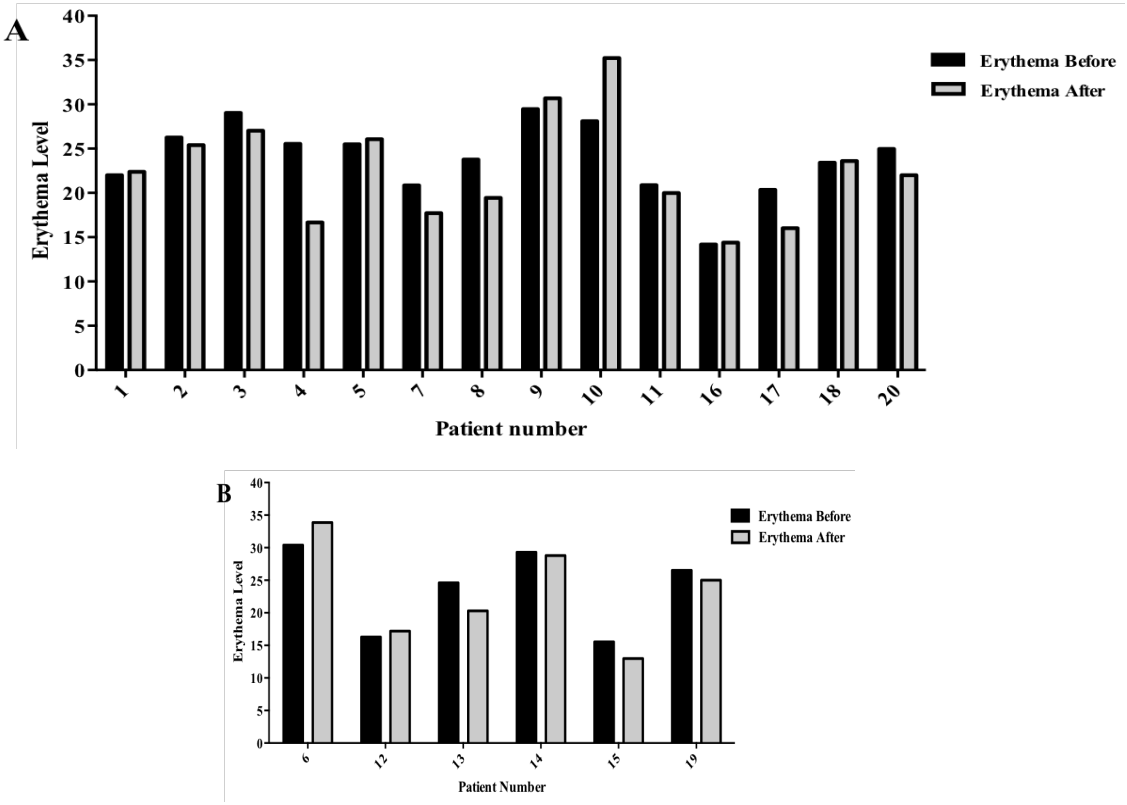

Figure 6.16 Erythema levels before and after one week of Oriel facial application

The levels of facial erythema of each individual participant before and after one week of Oriel product was applied to the face. Some patients experienced reductions in erythema (e.g. Patient 4), some had no change (e.g. Patient 18) and few experienced an increase in erythema (e.g. Patient 6) post treatment. **(A)** ETR patients (n=14) and **(B)** PPR patients (n=6).

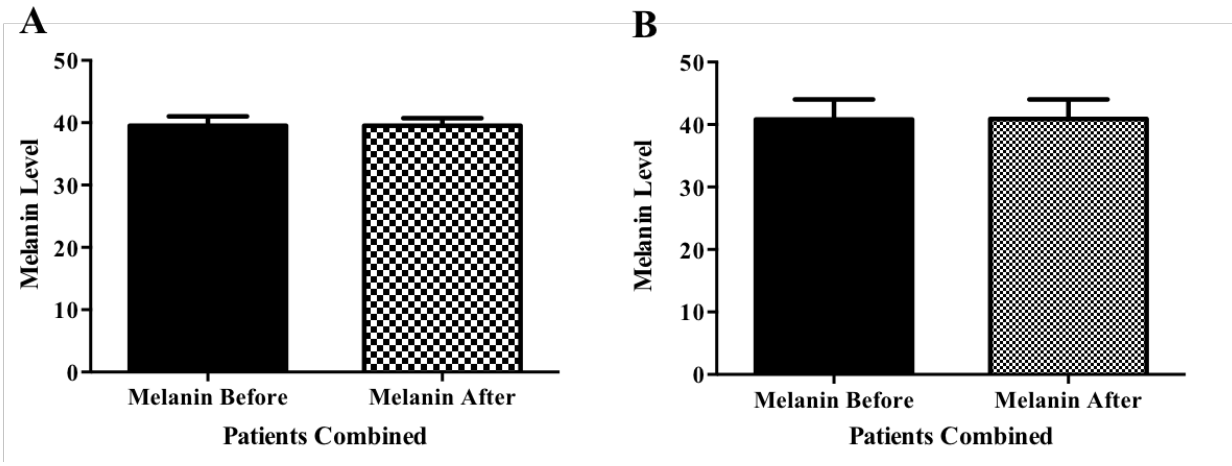

Figure 6.17 Melanin levels before and after one week of Oriel facial application

The levels of melanin were measured before treatment and one week post treatment. The average levels of melanin remained unchanged in ETR patients **(A)** and PPR patients **(B)** (ETR, n=14; PPP, n=6).

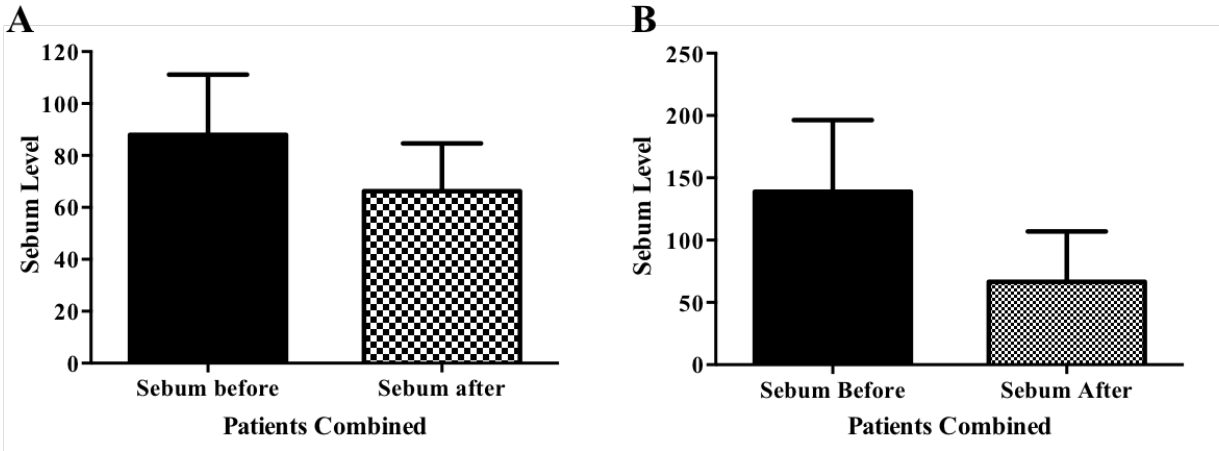

Figure 6.18 Sebum levels before and after one week of Oriel facial application

The average levels of sebum decreased after one week of treatment in ETR patients **(A)** and PPR patients **(B)**. PPR participants had the highest level of reduction in sebum levels in comparison to the ETR participants (ETR, n=14; PPP, n=6).

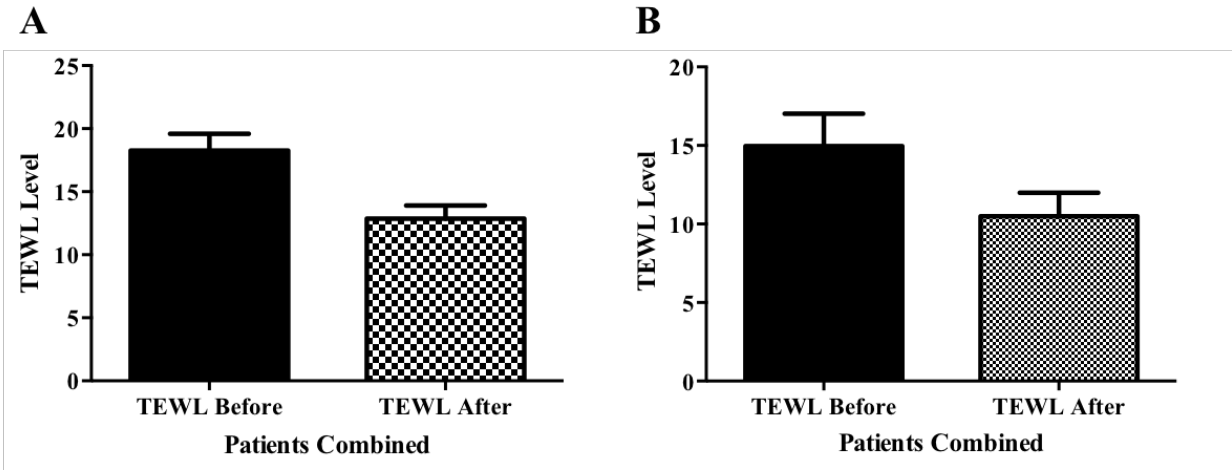

Figure 6.19 TEWL levels before and after one week of Oriel facial application

The average levels of transepidermal water loss (TEWL) decreased one week after treatment in both ETR patients **(A)** and PPR patients **(B)**. This may benefit the patient skin by improving the epithelial skin barrier of the face and prevent the amount of water loss from the skin (ETR, n=14; PPP, n=6).

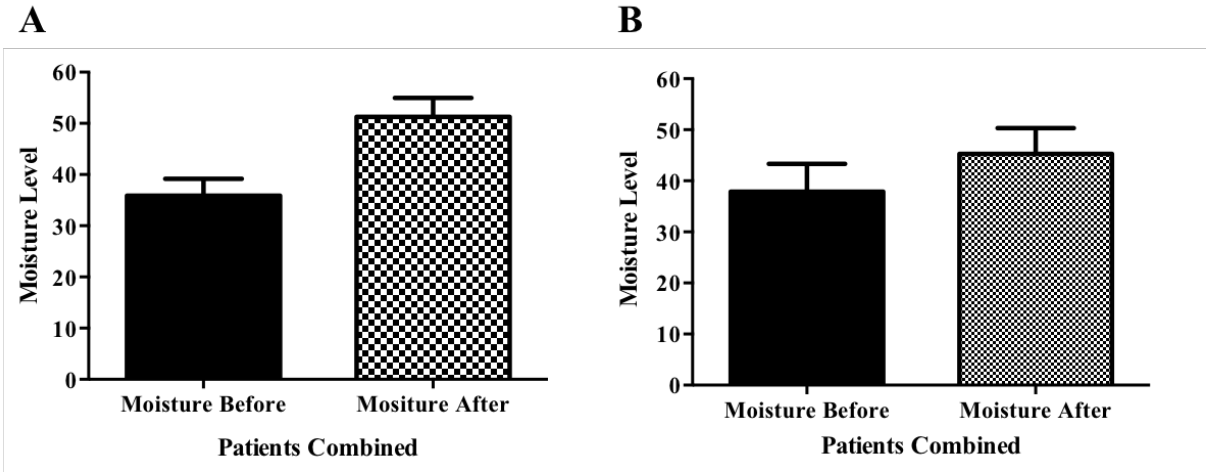

Figure 6.20 Moisture levels before and after one week of Oriel facial application

The average levels of moisture improved after one week of treatment. ETR patients **(A)** had the most increase in moisture after treatment followed by the PPR patients **(B)** (ETR, n=14; PPP, n=6).

Before

E Score: 25.55

ML Score: 40.6

S Score: 3

WL Score: 13.5

MO Score: 25.8

After

E Score: 16.6

ML Score: 41

S Score: 26

WL Score: 9.7

MO Score: 42.5

Figure 6.21 Effect of Oriel application on face of patient four after one week of treatment.

Patient four, female, aged 51 years old presented with subtype one, ETR. Erythema score reduced by 8.95 and reduction in facial redness is noticeable from the 'after' photo. TEWL score decreased by 3.8. Melanin, sebum and moisture all increased one week after treatment.

Figure 6.22 Effect of Oriel application on face of patient fifteen after one week of treatment.

Patient fifteen, female, aged 56 years old presented with subtypes one and two, ETR and PPR. Erythema score reduced by 2.55 with visual reduction in papules and pustules and also the bed of erythema on the forehead in the 'after' photo. Melanin, sebum and TEWL scores all decreased post treatment and moisture increased.

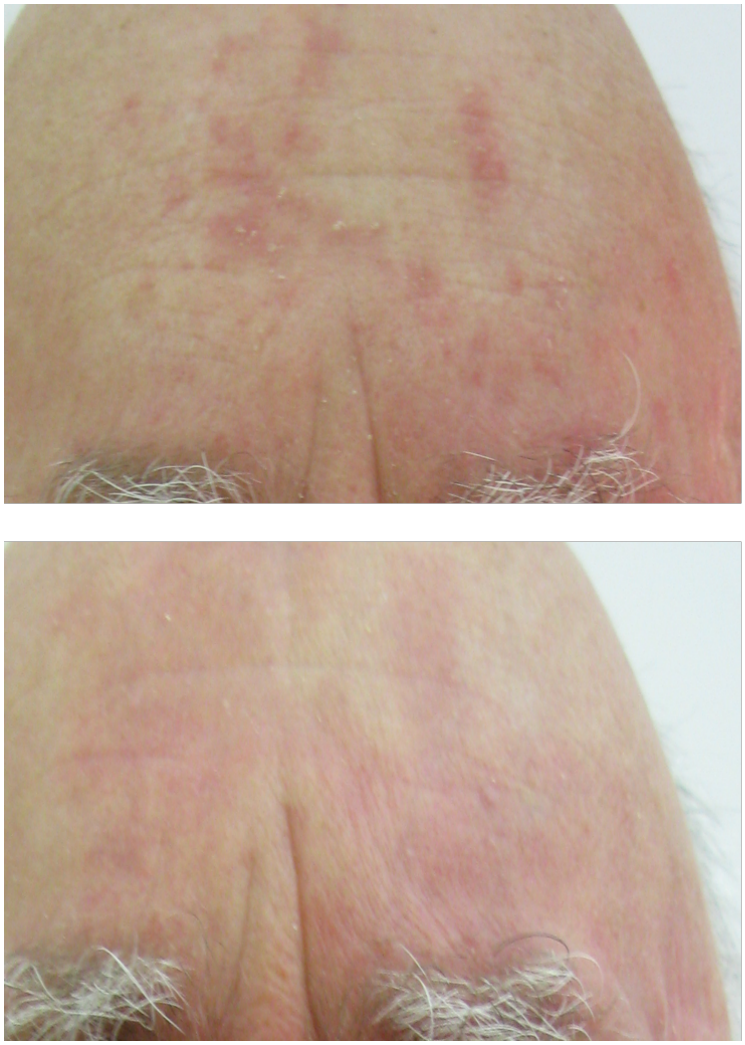

Figure 6.23 Effect of Oriel application on face of patient nineteen after one week of treatment.

Patient nineteen, male, aged 67 years old presented with subtypes one and two, ETR and PPR. Erythema score reduced by 1.53 with visual clearance of papules and pustules on the forehead following one week of Oriel application. Melanin, sebum and TEWL scores all decreased post treatment and moisture increased.

6.7 Oriel salt as a potential treatment for symptomatic relief of ETR and PPR – Pilot study Two

Results from the first pilot study with Oriel cream or gel formulation showed some reduced facial erythema, reduced the average sebum level and improved the level of moisture in the face which correlates with the decreased TEWL level in some cases (Table 6.2). A second pilot study was conducted with the cream formulation only. Ten rosacea patients participated in the trial and were instructed to apply the cream to the face twice to three times daily for two weeks. Patients were then instructed not to apply any topical therapy to the face for another two weeks post-treatment (section 2.28.3). Thus, the same five parameters were measured at the beginning of trial commencement (0 weeks), at the end of cream application (after 2 weeks) and once more at the end of the trial (after 4 weeks). The concentration of the cream applied to the face was doubled in comparison to first pilot study, from 0.3% to 0.6%, as was the treatment time from one week to two weeks. The two weeks post-treatment was to measure the prolonged effect of the Oriel treatment after application ceased. The average age of the patient group was 48 years old and the group consisted of 8 female patients and 2 male patients. (The remainder of data excluded from this pilot study is listed in Table A6.2 and patient photos excluded are presented from Figure A6.8 to Figure A6.14 inclusive)

The level of erythema was observed in each of the ten patients individually to demonstrate patient-to-patient scores (Figure 6.24). Most patients displayed a similar declining pattern in erythema levels from before treatment to the end of treatment after four weeks. For example, patients A, E and I. Patient G was the only patient not to show change following treatment after two weeks, thus no prolonged effect was expected. On average, the level of erythema throughout the group of ten rosacea patient participants was reduced after two weeks of Oriel application and a significant prolonged effect followed after four weeks in comparison to before ($p < 0.05$) (Figure 6.25).

The effect of Oriel cream on the level of melanin is similar to the results from the first pilot study. Oriel application to the face for two weeks, followed by two further weeks of no application did not affect melanin levels overall. A small reduction after four weeks was observed but not a substantial reduction (Figure

6.26). The average level of sebum reduced by 5-fold after two weeks of Oriel cream application (Figure 6.27). A prolonged effect was measured, resulting in decreased levels in sebum in comparison to the start of the trial. After four weeks the average sebum level of rosacea patients was reduced by 1.5-fold. The sebum results represent nine out of ten patient values.

Application of Oriel cream improved barrier function as the average TEWL levels reduced after two weeks and this result was maintained after four weeks. This demonstrates a prolonged effect of Oriel cream on TEWL level and skin barrier function (Figure 6.28). The average level of moisture within the skin on the face of rosacea patients increased after two weeks of Oriel cream application (Figure 6.29). After four weeks the level of moisture reduced to a score similar to the beginning of the trial. This may be the result of no cream application to the face, however the level after four weeks is slightly higher than it was at the beginning.

Ten rosacea patients participated in the trial, with photos taken before treatment, two weeks after Oriel application and four weeks from the beginning of the trial to determine any prolonged effects of the treatment. Patients E, G and H displayed reduced levels of facial erythema and other criteria, with their individual scores listed two weeks and four weeks from the beginning of the trial to demonstrate patient-to-patient symptomatic relief (Figures 6.30, 6.31 and 6.32).

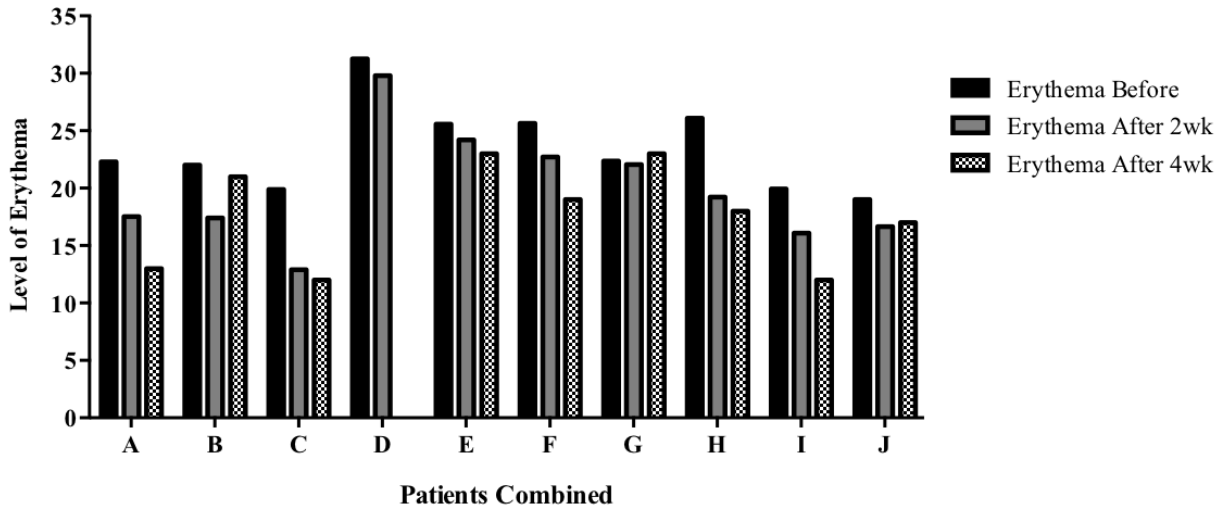

Figure 6.24 Erythema levels before, during and after Oriel cream facial application

The levels of facial erythema of the ten individual participants before treatment, two weeks after Oriel application and after four weeks from the beginning of the trial. A similar declining pattern of erythema levels is displayed in most patients over the three measurements.

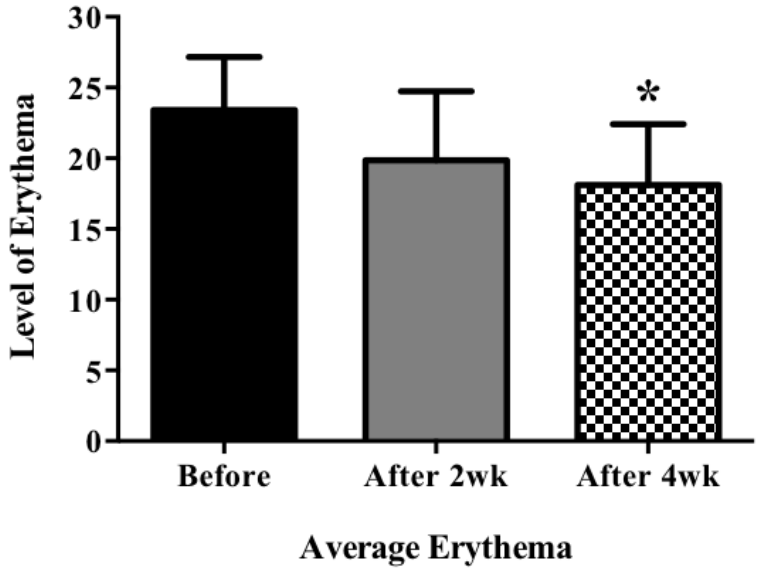

Figure 6.25 Average erythema levels before and after Oriel cream application

The level of erythema decreased after two weeks of applying Oriel cream to the face and the prolonged effect of erythema levels was maintained, with significant reduction after four weeks in comparison to before treatment ($p < 0.05$) (n=10).

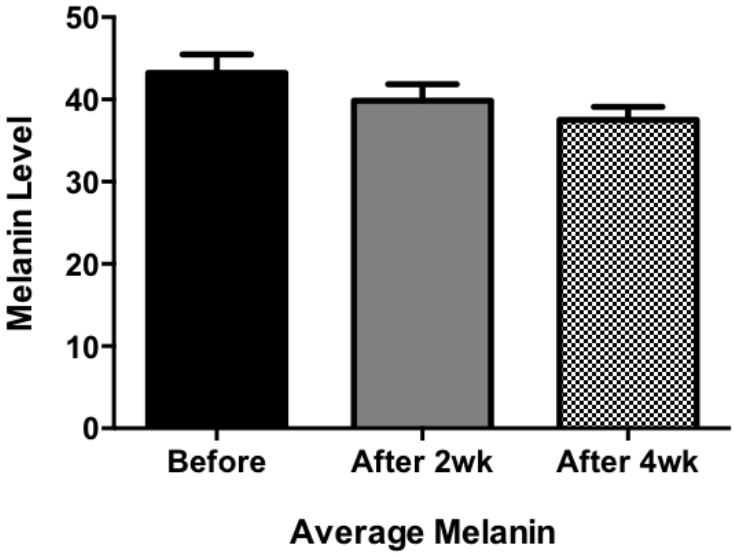

Figure 6.26 Average melanin levels before and after Oriel cream application
Oriel cream application resulted in minimal reduction of melanin levels and the prolonged effect after four weeks was further reduced in comparison to before treatment (n=10).

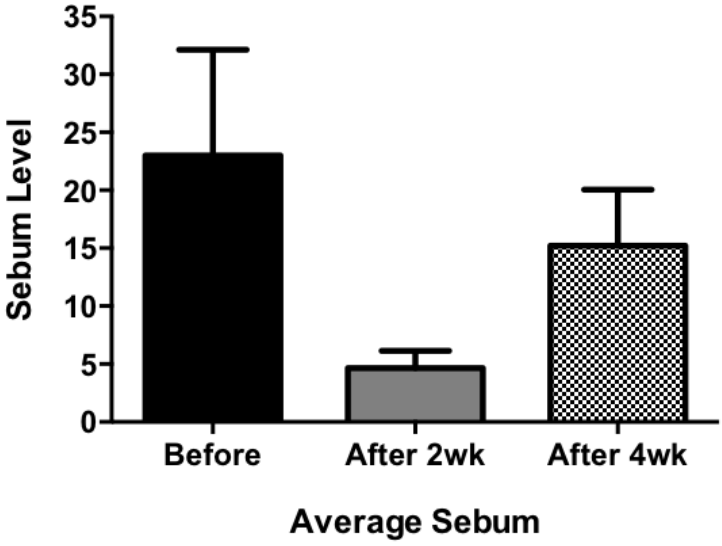

Figure 6.27 Average sebum levels before and after Oriel cream application
The sebum level reduced by almost 5-fold two weeks after Oriel application. The prolonged effect without application at four weeks showed lower levels of erythema in comparison to control treatment (n=9).

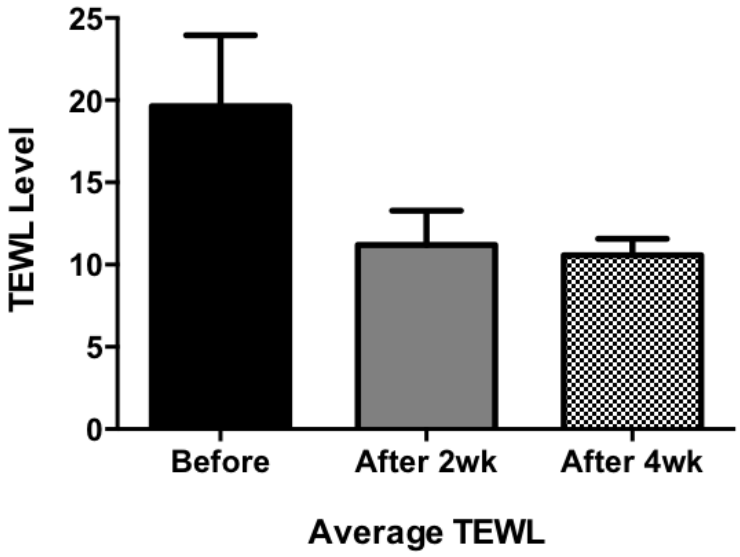

Figure 6.28 Average TEWL levels before and after Oriel cream application
The average level of transepidermal water loss (TEWL) in nine participants was measured two weeks after treatment and four weeks from the beginning. TEWL reduced by 50% and remained at this level following Oriel application (n=10).

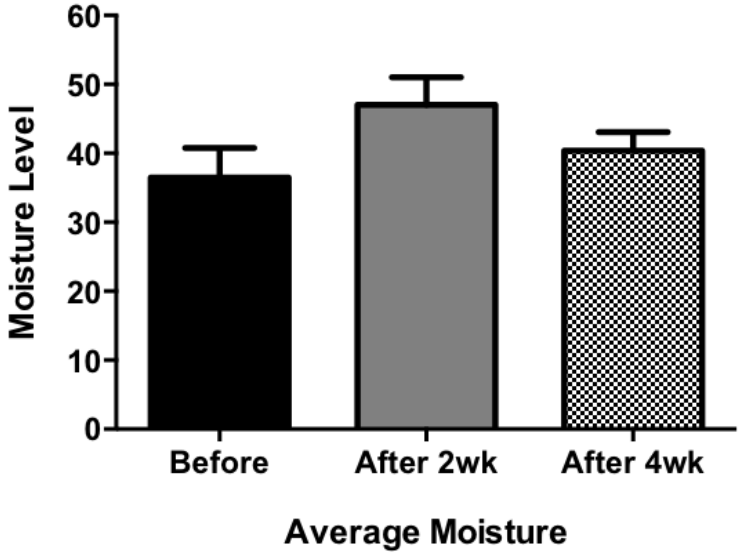

Figure 6.29 Average moisture levels before and after Oriel cream application
The average moisture levels in ten rosacea patients increased two weeks after Oriel cream application to the face. The cream had no prolonged effect on moisture levels as displayed after four weeks (n=10).

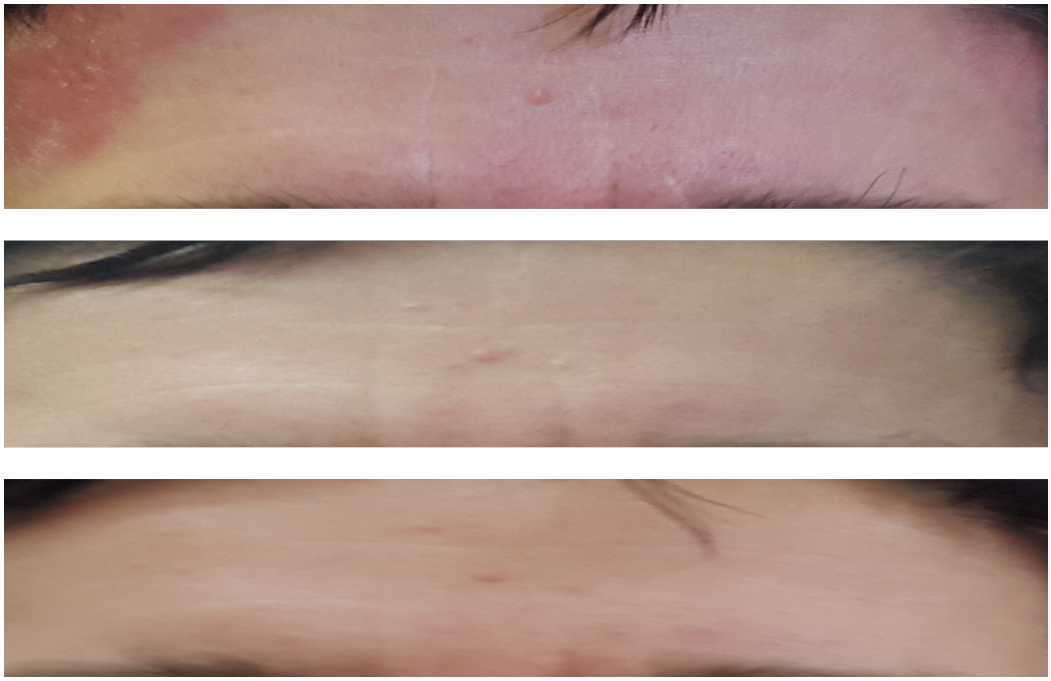

Scores	Before	After (2 weeks)	After (4 weeks)
Erythema	25.57	24.21	23.93
Melanin	42.2	38.4	42.17
Sebum	18	4	19
TEWL	13.2	6.7	7.8
Moisture	22.6	36.9	28

Figure 6.30 Effect of Oriel application before and after treatment in patient E. Patient E, female, aged 42 years old presented with subtype one rosacea, ETR. Erythema score reduced however the photos display the reduction in erythema on the forehead two weeks after treatment in comparison to before. The prolonged effect of the cream was also maintained as seen after four weeks in comparison to before. The level of melanin and sebum decreased after two weeks but increased close to the original score after four weeks. TEWL reduced after two and four weeks in comparison to the control. The moisture level reduced after two weeks but increased above the original level, possibly due to no Oriel cream being applied to the face.

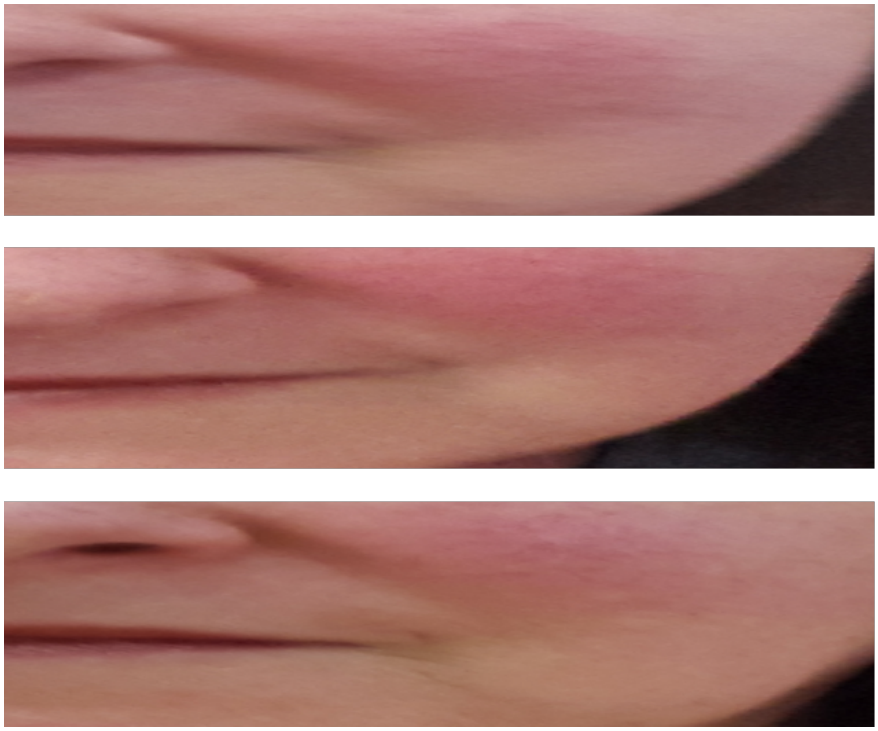

Scores	Before	After (2 weeks)	After (4 weeks)
Erythema	22.35	22.05	23.03
Melanin	45.16	43.37	45.01
Sebum	34	0	45
TEWL	13.3	8	6.1
Moisture	42.4	57.03	41.07

Figure 6.31 Effect of Oriel application before and after treatment in patient G. Patient G, female, aged 60 years old presented with subtype one rosacea, ETR. Erythema levels and melanin levels remained close to the original scores before treatment. A small reduction in facial erythema can be noted in the image four weeks after treatment, with redness appearing less intense. Sebum levels decreased to zero in comparison to before and no prolonged effect of Oriel cream was observed. TEWL level decreased two weeks and four weeks after treatment and the moisture level increased after two weeks of cream application but retreated to scores before treatment.

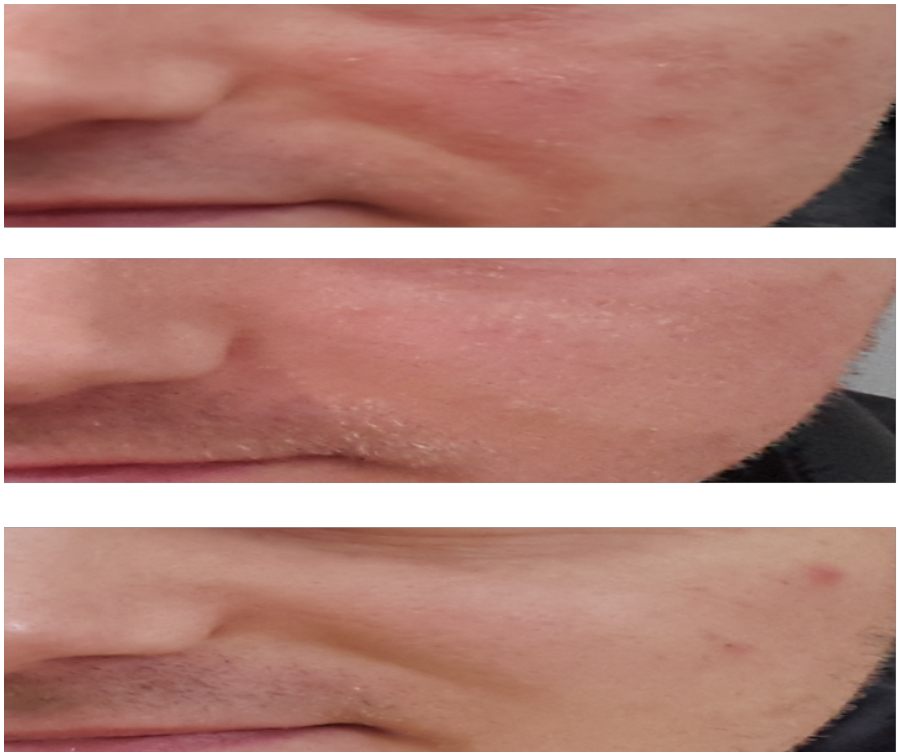

Scores	Before	After (2 weeks)	After (4 weeks)
Erythema	26.1	19.23	18.9
Melanin	40.88	37.57	34.71
TEWL	38.8	26.8	12.3
Moisture	7.1	29.01	31

Figure 6.32 Effect of Oriel application before and after treatment in patient H. Patient H, male, aged 38 years old presented with subtypes one rosacea and two, ETR and PPR. Erythema levels reduced after two weeks of Oriel application and a prolonged effect of Oriel cream was observed after four weeks. The reduction in facial erythema is evident from the photos throughout, as well as clearance of papules and pustules. Melanin levels and TEWL levels were reduced after two weeks of treatment and further reduced after four weeks in comparison to before. Moisture levels increased after two weeks in comparison to before and continued to increase after four weeks. No sebum levels were recorded in patient H.

6.8 Discussion

The use of salt as a therapeutic agent has proved beneficial for patients with respiratory conditions such as asthma, cystic fibrosis and ARDS (Artigas *et al*., 2017; Elkins *et al*., 2006; Gibson *et al*., 2001). The use of salt to traditionally cleanse wounds is still favoured in current practise and bathing in saline has improved skin integrity and barrier function in patients with the skin condition psoriasis (Leung *et al*., 2010; Proksch *et al*., 2005). The Oriel Company carried out a private study previously which demonstrated anti-inflammatory properties and promoted cell adhesion and endothelial cell growth in keratinocytes. Based on these results and the naturally sourced composition of Oriel product, a collaboration with Oriel Company to investigate the potential of Oriel salt solution in the treatment of dermal rosacea was established.

Firstly, the toxicity of Oriel salt solution was determined in human cells, a key indicator of Oriel tolerability on the skin. In order to assess the effect of Oriel solution on human cell proliferation, HEp-2 cells and hTCEpi cells were utilized as representative cell lines for dermal and ocular rosacea, respectively. Sodium chloride (NaCl), commonly referred to as table salt, was employed as a comparative salt solution against Oriel salt in the acid phosphatase assays. HEp-2 cells exposed to concentrations of Oriel and NaCl, ranging from 50 mg/ml to 6.25 mg/ml, experienced toxic effects which inhibited cell growth (Figures 6.1 and 6.2). Concentrations of either salt solution below 3.125 mg/ml did not inhibit HEp-2 cell growth and were well tolerated. hTCEpi cells were exposed to Oriel and NaCl ranging from 50 mg/ml to 3.125 mg/ml resulted in the inhibition of cell growth as these concentrations were too toxic for cell growth (Figures 6.3 and 6.4). Concentrations below 1.563 mg/ml were well tolerated and did not significantly affect hTCEpi cell growth.

The use of salt in skin therapies is widespread in the cosmetic industry and so a HEp-2 cell proliferation assay was conducted to measure the effect of Oriel on HEp-2 cell proliferation in comparison to NaCl (Figure 6.5). HEp-2 cells were exposed to two concentrations of each salt solution for 72 hours. The Oriel and NaCl at 3.12 mg/ml significantly reduced cell proliferation by 63% and 65.5% respectively ($p < 0.01$). The 0.78 mg/ml Oriel and NaCl were more tolerated than the 3.12 mg/ml

doses. The exposure of HEp-2 cells to 0.78 mg/ml Oriel significantly decreased cell proliferation ($p < 0.05$), while 0.78 mg/ml NaCl decreased HEp-2 cell proliferation by 21%. Overall, the Oriel salt solution is tolerated below concentrations of 0.78 mg/ml in HEp2 cells and hTCEpi cells. To further analyse the effect of Oriel salt solution on the skin, HEp-2 cells were exposed to 0.78 mg/ml Oriel for 48 hours to measure the effect of Oriel on the HEp-2 proteome using LF-MS. The label-free MS/MS quantitative analysis identified nine significant proteins which were altered in abundance following HEp-2 cell exposure to Oriel treatment (Figure 6.6).

The volcano data displays four statistically significant proteins that were decreased in abundance (Figure 6.7) including microtubule-associated protein (8 fold decrease) which plays a role in the microtubule lattice required for development of cell shape, organelle organisation and is also associated with cellular components by interacting with actin and signalling proteins (Faller *et al*., 2009; Halpain & Dehmelt, 2006). The Golgi resident protein (2.4 fold decrease) plays a role in the Golgi complex by modifying and transporting protein synthesis from the endoplasmic reticulum which are coated with COPI and COPI from the coat protein complex (Anantharaman & Aravind, 2002; Sohda *et al*., 2001). The 2-oxoisovalerate dehydrogenase subunit beta (2.3 fold decrease) is a family of three enzymatic components which complex together to catalyse the conversion of alpha-keto acids into acyl-CoA (Ævarsson *et al*., 1999). The THO complex subunit 2 (1.6 fold decrease) is a member of the TREX complex which is responsible for combining proteins that play a role in mRNA export or transcription (Strasser *et al*., 2002). There are four members of the THO complex, Hpr1, Mft1, Thp2 and THO2 which has been identified in this study.

Five proteins were statistically increased in abundance (Figure 6.7) including SEC23-interacting protein (4.8 fold increase) which is part of a dimeric platform involved in the coat protein complex (COPII) formation that is responsible for vesicle transport from the endoplasmic reticulum, and SEC23 protein assists with the exiting of these vesicles by forming a concave surface on the endoplasmic reticulum membrane (Miller & Schekman, 2013; Zanetti *et al*., 2012). DNA excision repair protein ERCC-6 (3.9 fold increase), an essential member of the nucleotide excision repair pathway which processes DNA damage and is a defense mechanism in

humans against carcinogenic threats (Sancar, 1996; Li *et al*., 1994). The Ran-binding protein 3 (2.1 fold increase) plays a role in many biological processes and is directly involved in the nuclear transport of Smad2 and Smad3 signal transducers which regulate growth factor-beta signalling (Dai *et al*., 2009; Yoon *et al*., 2008). The thioredoxin mitochondrial protein (1.7 fold increase) is associated with maintaining redox homeostasis in the mitochondria in response to oxidative stress and plays a role in many biological processes such protein folding and stability, regulating homeostasis and catalysing the reduction of protein disulphide bonds (Chen *et al*., 2002; Damdimopoulos *et al*., 2002). The protein with the lowest increase in abundance was aldo-keto reductase family (1.5 fold increase) which is a superfamily with over 40 enzyme and protein members including 20-alpha-hydroxysterids dehydrogenase which is upregulated during cell differentiations and is associated with T-cell differentiation in mice (Zhang & Qin, 2013; Buhrke *et al*., 2011). HEp-2 cells exposed to Oriel revealed a minimal alteration in the abundance of statistically significant proteins, indicative that Oriel salt solution did not substantially impact the HEp-2 proteome. HEp-2 cells exposed to 0.78 mg/ml Oriel did not display a stress response and the low tolerable concentration of Oriel resulted in only subtle protein changes (Table 6.1).

Rosacea treatment typically consists of oral and topical antibiotics, with some antibiotics demonstrating anti-bacterial roles and anti-inflammatory roles, two properties desired in treating this chronic inflammatory condition (Holmes & Steinhoff, 2017; Two *et al.,* 2015b). To assess the anti-bacterial potential of Oriel salt, three different bacterial strains were exposed to the compound in susceptibility assay. *E. coli* exposed to 50 mg/ml of Oriel salt solution or NaCl resulted in significant decrease of cell growth but concentrations below 25 mg/ml were well tolerated and consistent with the control (Figures 6.10 and 6.11). *S. aureus* exposed to Oriel salt solution had significantly reduced cell growth in the presence of 0.781 mg/ml or higher (Figure 6.12). NaCl had a similar inhibitory effect on *S. aureus* growth with significant decreased cell growth between 12.5 mg/ml and 0.391 mg/ml inclusive (Figure 6.13). *B. oleronius* was the main bacterium of interest due to its strong association in the pathogenesis of rosacea. NaCl was toxic to *B. oleronius* cell growth and significantly inhibited *B. oleronius* exposed to concentration of 6.25 mg/ml or above ($p < 0.001$) (Figure 6.9). Concentrations of NaCl lower than 3.125

mg/ml were tolerated by *B. oleronius*. *B. oleronius* expose to Oriel salt solution resulted in the positive growth proliferation and *B. oleronius* growth significantly increased ($p < 0.001$) (Figure 6.8). This latter result indicates that Oriel does not display an anti-bacterial role against *B. oleronius* when in solution, which correlates with the inhibition assay (Figure 6.14A). Oriel salt prepared in solution has inhibitory effect on *B. oleronius* growth, however Oriel prepared in a cream or gel formulation does impact the bacterial growth (Figure 6.14). *B. oleronius* and *S. aureus* grown in the presence of three Oriel formulations displayed inhibition of growth by the cream and the gel, with the Oriel gel significantly inhibiting *B. oleronius* growth in comparison to the Oriel cream (Figure 6.15). The delivery method of Oriel salt may influence the anti-bacterial effect. It is important to note that the use of saline therapeutics have displayed more anti-inflammatory properties than anti-bacterial properties. The former of which is of great interest as Oriel may have the potential to reduce inflammatory erythema in the face of rosacea patients, with a possible dual role at targeting and inhibiting *B. oleronius* growth.

Following the results discussed, two pilot studies were performed to assess the effect of Oriel salt in the treatment of dermal rosacea. The first trial had twenty participants, fourteen of which had erythematotelangiectatic rosacea (ETR) and six of which had papulopustular rosacea (PPR). Patients applied 0.3% Oriel cream or 0.3% Oriel gel to the face twice to three times daily for one week. The levels of patient erythema, melanin, sebum, TEWL and moisture before and after treatment were measured to determine the effect of Oriel salt treatment on the skin of rosacea patients. The average erythema reduced by 4.2%, however patient photos represent the positive effect of Oriel treatment with reduced erythema and some clearance of papules and pustules in patient skin. The average level of melanin did not alter between ETR and PPR throughout the pilot study (Figure 6.17) and the average sebum level reduced after treatment, with a larger decrease found in PPR patients (Figure 6.18). The reduction in sebum levels may result in lower food availability for *Demodex* mites involved in the pathogenesis of rosacea (Szkaradkiewicz *et al*., 2012). The density of *Demodex* mites in the face of rosacea patients is significantly higher than normal individuals and this presence may cause micro-abrasions on the skin surface which could contribute to the development of papules and pustules on the skin (McMahon *et al*., 2014; Szkaradkiewicz *et al*., 2012; Bonnar *et al*., 1993).

The average level of TEWL reduced in both ETR and PPR patients after treatment and correlated with the increase in moisture (Figures 6.19 and 6.20). A decrease in TEWL represents improvement in the skin barrier function which is often attenuated in rosacea patients. The improvement in skin barrier function has been shown to prevent penetration of invading microorganisms in skin treated with Dead Sea salt (Proksch *et al*., 2005). The reduction in TEWL after treatment with Oriel sea salt may mechanically block the interaction between *B. oleronius* antigens and the skin surface in rosacea patients. Increased moisture in the skin may relieve patients of the symptomatic dryness and roughness often described in rosacea and other conditions (Proksch *et al*., 2005). Some of the patient images displayed, demonstrate the reduced level of erythema intensity on the face and clearance of papules and pustules (Figures 6.21-6.23).

Based on the results of the first pilot study, the concentration of Oriel was doubled to 0.6% (w/v) for the second pilot study. The length of treatment time was also lengthened with patients applying Oriel cream to the face for two weeks and then not applying Oriel for two further weeks to observe any prolonged effects of the treatment. Oriel cream was the only formulation of Oriel used in the second pilot study based on patient feedback from the previous trial. Although the gel formulation is effective at inhibiting *B. oleronius* growth *in vitro* (Figure 6.14C), patients commented that the gel enhanced the burning sensation on the skin and caused irritation in some cases. The second pilot study consisted of ten participants with ETR subtype and simultaneous PPR in some cases.

The results from the second pilot study demonstrated the potential of Oriel cream as a therapeutic agent for dermal rosacea. The average erythema level decreased after two weeks of Oriel cream application and a significant prolonged effect was recorded after four weeks ($p < 0.05$) (Figure 6.25). Most patients displayed a decrease in erythema levels over the four weeks (Figure 6.24). This can be observed more clearly in patient images throughout the trial, for example Patient E (Figure 6.30). Before the trial commenced, this female presented with ETR and symptoms included severe erythema and scaliness in the forehead. Two weeks after treatment with 0.6% Oriel cream, the level of erythema had significantly reduced

and the scaliness had been eradicated, as the patient presented with a clearer complexion. After four weeks from the beginning of the trail, a prolonged effect of Oriel cream was observed and the level of erythema remained with a decreased presentation on the forehead in comparison to before treatment.

The average level of melanin decreased in comparison to the control two weeks after Oriel treatment and four weeks after, demonstrating a prolonged effect although the reduction was limited. The average sebum levels substantially decreased in patients after two weeks of treatment and a prolonged effect was evident as the level of sebum was lower after four weeks in comparison to before the trial started (Figure 6.27). The TEWL decreased and the moisture increased, as was seen in the first pilot study also. After two weeks, the average level of TEWL decreased and remained at that level after four weeks (Figure 6.28), indicting the Oriel cream had a beneficial prolonged effect on the skin barrier function. The moisture of the skin increased after two weeks of Oriel cream application which is most likely associated with the TEWL and also the cream function itself (Figure 6.29). After four weeks the average moisture level lowered but remained slightly higher than before the trial began, postulating a limited prolonged effect of Oriel cream in rosacea skin.

Oriel sea salt solution has demonstrated anti-baterial and anti-inflammatory properties throughout this research. Oriel salt solution is tolerated below concentrations of 0.78 mg/ml in human cell models and does not induce a stress response in the proteome of HEp-2 cells. Pilot studies with 0.3% Oriel cream/gel and 0.6% Oriel cream have resulted in reduction of facial erythema, decreased sebum levels, improved TEWL, increased skin moisture, all of which have led to positive patient feedback. In conclusion, these results demonstrate the preliminary potential for the use of Oriel sea salt solution as a novel therapeutic in the treatment and management of dermal rosacea.

Chapter Seven

General Discussion

7.1 General discussion

Rosacea is a chronic inflammatory dermatological condition affecting 3% of the Irish population and over 14 million sufferers in the United States (McMahon *et al*., 2014; McAleer & Powell, 2007). Rosacea typically affects individuals between the ages of 30-50 years old and is three times more common in women than in men (Jarmuda *et al*., 2012; Gupta & Chaudhry, 2005). Rosacea is more prevalent in individuals with Fitzpatrick skin type I-III and is commonly referred to as the "curse of the Celts" (O'Reilly *et al*., 2012c; Bevins & Liu, 2007). There are four subtypes of rosacea and one granulomatous variant, established by the NRS Expert Committee and diagnostic features of each has recently been updated and specified (Tan *et al*., 2017; Two *et al*., 2015a; Crawford *et al*., 2004). The most prevalent subtype is ETR which features the classic "redness" associated with the condition, clinically referred to as persistent central facial erythema (Tan *et al*., 2017; Jarmuda *et al*., 2014). Telangiectasia is a common secondary feature of ETR and patients often describe the skin as feeling sensitive to burning and stinging sensations (Jarmuda *et al*., 2014; Barco & Alomar, 2008). PPR also features erythema and is diagnosed based on the presence of inflammatory lesions in the form of papules and pustules (Korting & Schöllmann, 2009; Barco & Alomar, 2008; Powell, 2005). Phymatous rosacea is associated with thickening of the skin and is the most disfiguring subtype of rosacea (Tan & Berg, 2013). This has led to many patients pursuing laser therapy and surgical approached for the management of this subtype (Gupta & Chaudhry, 2005; Powell, 2005). The final subtype is ocular rosacea, which is diagnosed in up to 50% of dermal rosacea patients and affects the eyes and corneal surface including telangiectasia on eyelid margin (Tan & Berg, 2013; O'Reilly *et al*., 2012b).

The aetiology of rosacea is unknown an multiple factors influence the onset of the condition and the exacerbation of inflammatory symptoms. Trigger factors are associated with the onset of rosacea conditions, some of which may determine the phenotypical appearance of a rosacea patient (Holmes & Steinhoff, 2017). Multiple factors from the exogenous environment such as diet, medication, sun exposure, exercise or alcohol may all contribute to a change in homeostasis of rosacea patient skin and contribute to endogenous factors such as lipid and sebum alteration, stress

or a change in skin homeostasis (Holmes & Steinhoff, 2017; Margalit *et al*., 2016; Holmes, 2013).

The skin microbiome consists of many micro-organisms including bacteria, fungi, viruses and *Demodex* mites, the latter of which has a strong association with rosacea (Thoemmes *et al*., 2014; Holmes, 2013; Li *et al*., 2010). Commensals in the skin have also been implicated in the pathogenesis of rosacea. *S. epidermidis*, an opportunistic bacterium, has previously been isolated from the serum of rosacea patients and proteins secreted by *S. epidermidis* have demonstrated serum reactivity in patients compared to controls (Holmes & Steinhoff, 2017; O'Reilly *et al*., 2012a; Dahl *et al*., 2004). Other commensals which may contribute to rosacea symptoms are *H. pylori, C. pneumonia* and *P. acnes*, all of which may be susceptible to a change in skin homeostasis of rosacea patients (Egeberg *et al*., 2017; Holmes & Steinhoff, 2017; Dahl *et al*., 2004). The increase of *Demodex* mite density in rosacea patients in comparison to control individuals is well established (Li *et al*., 2010; Forton *et al*., 2005; Bonnar *et al*., 1993). *Demodex* mites may also contribute to the papule development in PPR patients as they protrude though the skin barrier in the pilosebaceous (Chen & Plewig, 2014; Elston & Elston, 2014). The role of *Demodex* in the pathogenesis of rosacea is important as the mites may physically contribute to the onset of symptoms but also harbour bacteria associated with rosacea, such as *B. oleronius* (Lacey *et al.,* 2007; Delaney, 2004).

The effect of multiple trigger factors and the changes in rosacea skin microbiome may contribute to activation of the innate immune response. The higher prevalence of *Demodex* in rosacea patients skin may influx the presence of *B. oleronius* antigens exposed to the epithelial skin cells. Rosacea patients have demonstrated immune-reactivity to both the 62 kDa and 83 kDa *B. oleronius* antigens in ETR, ocular rosacea and PPR (O'Reilly *et al*., 2012c; Li *et al*., 2010; Lacey *et al*., 2007). Rosacea patients previously exposed to both of these antigens displayed the strongest immune response to the 62 kDa, 83 kDa and both antigens together, respectively. Exposure of *B. oleronius* antigens to patient serum has led to the upregulation and activation of neutrophils, inducing killing mechanisms via ROS production which can lead to tissue degradation and inflammation (O'Reilly *et al*., 2012a; Hayes *et al*., 2011). Inflammation is a key characteristic of rosacea and patients exposed to *B. oleronius* antigens have previously displayed increased

expression of pro-inflammatory cytokines, MMP secretion and increased cathelicidin, all of which contribute to the inflammatory response (Jarmuda *et al*., 2014; O'Reilly *et al*., 2012b; Bevins & Liu, 2007).

The contributing of trigger factors, *Demodex* mites, skin microbiota, neutrophils and *B. oleronius* may all induce the onset of rosacea and result in chronic skin inflammation. The role of *B. oleronius* was investigated throughout this research. *B. oleronius* is exposed to the pilosebaceous unit once the harbouring *Demodex* mite dies within the hair follicle and this environmental alteration may be critical to the survival of *B. oleronius* in response to the activated innate immune system. For example, the exposure of *B. oleronius* to surrounding mast cells or keratinocytes may induce pathogen-recognition receptors stimulated by PAMPs and DAMPs (Holmes & Steinhoff, 2017; Tan *et al*., 2017). The TLR-2 pathway has been shown to become activating upon recognition of the polysaccharide chitin, a component of the *Demodex* exoskeleton (Holmes & Steinhoff, 2017; Margalit *et al*., 2016; Steinhoff *et al*., 2013). Bacteria in turn have adapted defence mechanism in response to the immune response and cellular stress.

The effect of temperature stress on *B. oleronius* was investigated throughout this thesis, with the level of antigen expression and the *B. oleronius* proteome explored at a higher growth temperature than optimum. The primary erythema feature of rosacea, coupled with one or more of the secondary features such as telangiectasia and inflammation, may enhance blood flow through the face of the patient and elevate skin temperature (Woo *et al*., 2016; Guzman-Sanchez *et al*., 2007; Wilkin *et al*., 2004). Exogenous trigger factors may also elevate facial skin temperature including hot beverages, alcohol and spicy foods as they may induce oedema and vasodilation by exposing blood vessels closer to the skin surface (Guzman-Sanchez *et al*., 2007; Crawford *et al*., 2004; Wilkin *et al*., 2004). This increase of temperature may disrupt homeostasis and organisms may adapt to the altered environment. For example, *S. epidermidis* isolated from pustules of rosacea patients and cultured at 37ºC secreted significantly more proteins at the higher temperature, with some displayed virulent properties (Holmes, 2013; Dahl *et al*., 2004). *B. oleronius* was similarly cultured at 37ºC in comparison to the optimal growth temperature of 30ºC. The level of 62 kDa antigen expression was

significantly increased at 37ºC. This antigen shares homology with the GroEL chaperone, one of two classic heat shock upregulated in response to damage induced by temperature stress (Voigt *et al*., 2013; O'Reilly *et al*., 2012c; Periago *et al*., 2002). The level of *B. oleronius* antigen secreted from the cells was higher when cultured at 37ºC in comparison to 30ºC, which was evident using confocal microscopy. This indicates that *B. oleronius* may produce and secrete increased levels of 62 kDa antigen in response to temperature stress. The proteome of *B. oleronius* at 37ºC was investigated in comparison to the proteome at 30ºC. *S. epidermidis* displayed virulent proteins at 37ºC (Dahl *et al*., 2004) and it may be the case that *B. oleronius* produces defence proteins in response to the higher temperature of rosacea patient skin. Many proteins differentially abundant at 37ºC were associated with stress, cellular components, energy metabolism and biological processes. These proteins may enable the *B. oleronius* to survive and grow in undesirable environments, which was postulated by the increased abundance of elongation factors and stress proteins produced at 37ºC.

The heightened activity of the innate immune response in rosacea patients has been observed following the increased recruitment of neutrophils in response to *B. oleronius* antigens (O'Reilly *et al*., 2012a). Neutrophils induce oxidative stress by exposing invading pathogens to ROS produced by NADPH oxidase (Hayes *et al*., 2011; Reeves *et al*., 2002). Bacteria have adapted to this killing mechanism by producing de-toxifying proteins such as catalase and peroxidase which degrade H_2O_2, and other proteins such as SOD, thioredoxin and glutaredoxin (Fukai & Ushio-Fukai, 2011; Cabiscol *et al.,* 2000b). The skin of rosacea patients is vulnerable to endogenous factors such as the density of *Demodex* mites which may induce skin abrasions and weaken the skin barrier function, as well as tissue damage induced downstream of neutrophil activation (O'Reilly *et al*., 2012a; Hayes *et al*., 2011; Lacey *et al*., 2011). The ongoing process between neutrophil attack and bacterial defence induced by oxidative stress can exacerbate symptoms of immune-compromised rosacea patients (Margalit *et al*., 2016). To understand the effect of oxidative stress on *B. oleronius* and the impact proteins may have to the immune system or host in response to this stress was investigated by exposing *B. oleronius* cultures to H_2O_2. The growth of *B. oleronius* was not interrupted in response to H_2O_2 presence, however the differential abundance of proteins in H_2O_2 treated cells was

significant. The relationship between increased and decreased proteins involved in biological processes and molecular functions was observed in response to oxidative stress. Many glycolytic proteins increased in abundance involved with energy yielding and metabolism. Anti-oxidant proteins including peroxiredoxin and thioredoxin increased in abundance, with many sporulation and iron proteins decreasing in abundance. Iron homeostasis is vital to cell survival and the response of *B. oleronius* to oxidative stress may encourage the tight regulation of iron protein abundance in the cells and provide the bacterium the opportunity to remain dormant in order to overcome this harmful and detrimental stress (Fukai & Ushio-Fukai, 2011).

The multifactorial aetiology of rosacea (genetic, environmental, life style) is evident and *B. oleronius* and other microorganisms may contribute to the chronic inflammation. Each subtype of rosacea is diagnosed by a set of primary and secondary features, with patients suffering from more than one subtype simultaneously (Two *et al*., 2015b; Forton *et al*., 2005). Thus the treatment of rosacea is directed at symptomatic relief rather than treating individual subtypes. The management of rosacea can be controlled by patient awareness to a certain extent, for example, patients can monitor exogenous trigger factors by applying high sun protection factor to the face or avoiding specific factors that may induce their individual symptoms such as spicy food (Holmes & Steinhoff, 2017; Two *et al*., 2015b; Barco & Alomar, 2008). Topical and oral antibiotics are the predominant treatment for rosacea patients, with some antibiotics displaying a dual role of antibacterial and anti-inflammatory properties (Barco & Alomar, 2008; Gupta & Chaudhry, 2005; Del Rosso, 2004). The mainstay treatment for ocular rosacea is artificial tears, delivered onto the surface of the eye in drops, which help to lubricate the eye and flush out any pathogenic debris (Geerling *et al*., 2011; Powell, 2005). Ocular rosacea is often associated with blepharitis and conjunctiva, all of which can cause discomfort and irritation to the patient (Tan & Berg, 2013; Lacey *et al*., 2009).

Three potential agents were assessed in this research for their ability to treat ocular rosacea. The concept was to use an agent with binding capabilities that could potentially capture *B. oleronius* antigens and block their interaction with the corneal surface. The first agent was BSA, one of the most abundant serum proteins and is a

well-studied model of protein-ligand binding and interaction (Minic *et al*., 2018; Mathew & Kuriakose, 2013; Żurawska-Płaksej *et al*., 2018). Anti-62 kDa rabbit antibody was the second blocking agent explored as it is a polyclonal antibody that targets *B. oleronius* 62 kDa antigen and possibly other *Bacillus* antigens. Antibodies have also previously been used in rheumatoid arthritis treatment as anti-TNF antibody has been incorporated into the drug infliximab (Bongartz *et al*., 2006; Goodwin *et al*., 2006). The third agent which demonstrated the most potential as a blocking agent was mucin. Mucins naturally coat the ocular surface and are secreted by goblet cells in the conjunctiva (Albertsmeyer *et al*., 2010; Mantelli & Argüeso, 2008).

B. oleronius 62 kDa antigen was purified using ÄKTA-FPLC and inhibited HEp-2 cell proliferation and hTCEpi proliferation at high concentrations. This represents the damaging effect that *B. oleronius* antigen can have in an immune-compromised rosacea patient. HEp-2 cells and hTCEpi cells were also exposed to the three potential blocking agents in combination with the 62 kDa antigen. This was to determine the binding and blocking efficacy of the agents. Some potential was demonstrated in HEp-2 cell proliferation. The importance of a potential blocking agent that could bind to the *B. oleronius* antigens is vital from a treatment perspective as 50% of rosacea patients develop ocular symptoms. The level of gene expression for pro-inflammatory cytokines was explored by exposing hTCEpi cells to purified 62 kDa antigen, which resulted in increased of IL-1β, TNFα and IL-8 expression. The level of pro-inflammatory cytokine production is upregulated in rosacea patients and has been demonstrated as a downstream side effect of neutrophil recruitment (Jarmuda *et al*., 2014; Holmes, 2013). The presence of mucin during the wound healing response displayed blocking potential between the antigen and cell interaction in both HEp-2 cells and hTCEpi cells, the latter of which displayed uncontrolled growth. This may be indicative of early scarring which has previously been demonstrated with corneal cells (O'Reilly *et al*., 2012b). The exposure of *B. oleronius* antigens to hTCEpi cells has previously displayed similarities to corneal ulcer formation and increased activity of MMP and cell migration, all of which contribute to ocular inflammation (McMahon *et al*., 2014; O'Reilly *et al*., 2012b). The level of IL-1β, TNFα, IL-6 and IL-8 cytokine expression was explored in the wound healing assays of HEp-2 cells and hTCEpi

cells, with mucin demonstrating some inhibitory properties by blocking the harmful antigen potential. Overall, the mucin displayed some potential efficacy at blocking the *B. oleronius* antigen interaction with the host cells. Mucins are known for their "sticky" binding nature and the viscoelasticity of mucins may enable them to capture *B. oleronius* antigens and possibly protect the surface of the eye (Gipson, 2004; Khanvilkar *et al*., 2001).

Alternative treatments for rosacea are less common but can prove effective at relieving patient symptoms. Heat compression on the eyelid can improve tear lipid layer for ocular rosacea and cooled pasted cucumber with yogurt on the face can relieve patient oedema (Margalit *et al*., 2016; Geerling *et al*., 2011; Powell, 2005). These natural remedies alleviate symptoms and the application of Dead Sea salt on the skin of psoriasis patients has proved effective also at relieving symptoms. Following bathing in Dead Sea salt, patient skin had improved hydration levels, improved the elasticity and integrity of the skin and reduced the dryness and roughness described by patients (Proksch *et al*., 2005). In collaboration with Oriel Company, Oriel salt solution was investigated as a potential and novel treatment for dermal rosacea. Oriel salt solution displayed some antibacterial properties against *B. oleronius* and was not toxic to HEp-2 cells or hTCEpi cells below concentrations of 1.563 mg/ml. HEp-2 cells exposed to a low-dose of Oriel (0.78 mg/ml) demonstrated subtle differential abundance of proteins, indicative that Oriel salt solution does not disrupt cell homeostasis in an excessive manner. The use of salt for patient wound cleansing is still favoured as salt does not disturb the wound microbiota, does not induce tissue damage and cleanses the wound bed to prevent bacterial infection (Leung *et al*., 2010).

Two pilot studies were performed with twenty rosacea patients suffering from ETR and/or PPR subtypes in the first trial and ten ETR patients in the second trail. Patients in the first pilot study applied 0.3% Oriel cream or Oriel gel to the face for seven days. In the second pilot study, patients applied 0.6% Oriel cream to the face for two weeks and a prolonged effect with no treatment was measured after two further weeks. Both pilot studies demonstrated the potential of Oriel cream as an anti-inflammatory agent capable of significantly reducing facial erythema, the primary diagnostic feature of rosacea. The average sebum levels and TEWL levels

were reduced and the average moisture levels increased in both pilot studies, indicative of a strengthened skin barrier which acts as a physical barrier preventing pathogen penetration (Proksch *et al*., 2005). Improved moisture and hydration of the skin is important as it improves dryness and roughness in patient skin (Elkins *et al*., 2006; Dirschka *et al*., 2004).

Rosacea is a multifactorial dermatological condition that can impact on a patients psychological and emotional state. External and internal stimuli contribute to the condition and exacerbate symptoms. The elevated density of *Demodex* mites in patient skin plays a role in the pathogenesis of rosacea and physically distorts the skin surface. The change in skin microbiota and alteration in skin homeostasis may exacerbate symptoms. The effect of temperature stress and oxidative stress on *B. oleronius* has been investigated in detail, two stress factors that are predominant in the microbiome of rosacea patients. The damaging effect of *B. oleronius* antigens on HEp-2 cells and hTCEpi cells has been demonstrated with the possibility of potential blocking agents binding to *B. oleronius* antigen and preventing host cell interaction. A novel treatment for dermal rosacea has proved effective in two pilot studies. The Oriel salt solution is naturally sourced and demonstrated some anti-bacterial properties but excelled at the primary target of reducing facial erythema in rosacea patients.

In order to understand the pathogenesis and aetiology of rosacea further, a more detailed examination of trigger factors in rosacea patients would be beneficial in the future. If rosacea patients can learn to manage exogenous factors that contribute to their condition, some symptomatic relief may be achieved without the need for antibiotics in mild or possibly moderate rosacea. Future work in the area of patient treatment may also benefit the outcome of symptom relief. There is no cure for rosacea, however the condition can be managed and treated successfully in some cases. The use of a potential blocking agent such as mucin, in combination with another therapeutic agent could be investigated further to capture *Bacillus* antigens and inhibit the interaction with host cells in cases of ocular rosacea or even dermal rosacea.

Chapter Eight

Bibliography

Abu Samra, M.T. & Shuaib, Y.A. (2014). *Research Article A Study on the Nature of Association between Demodex Mites and Bacteria Involved in Skin and Meibomian Gland Lesions of Demodectic Mange in Cattle*. 2014. 1–9

Ævarsson, A., Seger, K., Turley, S., Sokatch, J.R. & Hol, W.G.J. (1999). Crystal structure of 2-oxoisovalerate and dehydrogenase and the architecture of 2-oxo acid dehydrogenase multienzyme complexes. *Nature Structural Biology*. 6 (8). 785–792

Albertsmeyer, A.-C., Kakkassery, V., Spurr-Michaud, S., Beeks, O. & Gipson, I.K. (2010). Effect of pro-inflammatory mediators on membrane-associated mucins expressed by human ocular surface epithelial cells. *Experimental Eye Research*. . 90 (3). 444–451

Anantharaman, V. & Aravind, L. (2002). The GOLD domain, a novel protein module involved in Golgi function and secretion. *Genome Biology* 3 (5). 1–7

Antunes, A., Derkaoui, M., Terrade, A., Denizon, M., Deghmane, A.E., Deutscher, J., Delany, I. & Taha, M.K. (2016). The phosphocarrier protein HPr contributes to meningococcal survival during infection. *PLoS ONE*.11 (9). 1–21

Artigas, A., Camprubí-Rimblas, M., Tantinyà, N., Bringué, J., Guillamat-Prats, R. & Matthay, M.A. (2017). Inhalation therapies in acute respiratory distress syndrome. *Annals of Translational Medicine* 5 (14). 293–293

Bantscheff, M., Lemeer, S., Savitski, M.M. & Kuster, B. (2012). Quantitative mass spectrometry in proteomics: critical review update from 2007 to the present. *Analytical and Bioanalytical Chemistry* 404 (4). 939–965

Barco, D. & Alomar, A. (2008). Rosacea. *Actas Dermo-Sifiliográficas (English Edition)* 99 (4). 244–256

Battaile, K.P., Molin-Case, J., Paschke, R., Wang, M., Bennett, D., Vockley, J. & Kim, J.J.P. (2002). Crystal structure of rat short chain acyl-CoA dehydrogenase complexed with acetoacetyl-CoA: Comparison with other acyl-CoA dehydrogenases. *Journal of Biological Chemistry* 277 (14). 12200–12207

Becerra, G., Merchán, F., Blasco, R. & Igeño, M.I. (2014). Characterization of a ferric uptake regulator (Fur)-mutant of the cyanotrophic bacterium Pseudomonas pseudoalcaligenes CECT5344. *Journal of Biotechnology* 190 2–10

Bevins, C.L. & Liu, F.-T. (2007). Rosacea: skin innate immunity gone awry? *Nature medicine*. 13 (8). 904–906.

Bikowski, J.B. & Del Rosso, J.Q. (2009). *Demodex* dermatitis: A retrospective analysis of clinical diagnosis and successful treatment with topical crotamiton. *Journal of Clinical and Aesthetic Dermatology* 2 (1). 20–25

Bongartz, T., Sutton, A.J., Sweeting, M.J., Buchan, I. & Matteson, E.L. (2006). Anti-TNF Antibody Therapy in Rheumatoid Arthritis and the Risk. *JAMA Review* 295 (19). 2275–2482

Bonnar, E., Eustace, P. & Powell, F.C. (1993). The *Demodex* mite population in rosacea. *Journal of the American Academy of Dermatology* 28 (3). 443–8

Borezee, E., Pellegrini, E. & Berche, P. (2000). OppA of Listeria monocytogenes, an Oligopeptide-Binding Protein Required for Bacterial Growth at Low Temperature and Involved in Intracellular Survival OppA of Listeria monocytogenes, an Oligopeptide-Binding Protein Required for Bacterial Growth at Low *Society*. 68 (12) 7069–7077

Brown, M., Hernández-Martín, A., Clement, A., Colmenero, I. & Torrelo, A. (2014). Severe *Demodex folliculorum*-associated oculocutaneous rosacea in a girl successfully treated with ivermectin. *JAMA dermatology* 150. 61–3

Brune, A. (1998). Termite guts: The world's smallest bioreactors. *Trends in Biotechnology* 16 16–21

Buckel, W. & Thauer, R.K. (2013). Energy conservation via electron bifurcating ferredoxin reduction and proton/Na+ translocating ferredoxin oxidation. *Biochimica et Biophysica Acta - Bioenergetics* 1827 (2) 94–113

Buhrke, T., Lengler, I. & Lampen, A. (2011). Analysis of proteomic changes induced upon cellular differentiation of the human intestinal cell line Caco-2. *Development, Growth & Differentiation* 53 (3) 411–426

Buscher, K., Ehinger, E., Gupta, P., Pramod, A.B., Wolf, D., Tweet, G., Pan, C., Mills, C.D., Lusis, A.J. & Ley, K. (2017). Natural variation of macrophage activation as disease-relevant phenotype predictive of inflammation and cancer survival. *Nature Communications* 8 (May) 1-10

Cabiscol, E., Piulats, E., Echave, P., Herrero, E. & Ros, J. (2000a). Oxidative stress promotes specific protein damage in *Saccharomyces cerevisiae*. *Journal of Biological Chemistry*. 275 (35) 27393–27398

Cabiscol, E., Tamarit, J. & Ros, J. (2000b). Oxidative stress in bacteria and protein damage by reactive oxygen species. *International Microbiology* 3 3–8

Caldas, T.D., El, A., Richarme, G. & Yaagoubi, A. El (1998). *Protein Chemistry and*

Structure : Chaperone Properties of Bacterial Elongation Factor EF-Tu Chaperone Properties of Bacterial Elongation Factor EF-Tu 273 (19) 1–6

Cartron, M.L., Maddocks, S., Gillingham, P., Craven, C.J. & Andrews, S.C. (2006). Feo - Transport of ferrous iron into bacteria. *BioMetals*. 19 (2) 143–157

Di Cera, E. (2009). Serine Proteases. *International Union of Biochemistry and Molecular Biology Life*. 61 (5) 510–515

Chang, A.L.S., Raber, I., Xu, J., Li, R., Spitale, R., Chen, J., Kiefer, A.K., Tian, C., Eriksson, N.K., Hinds, D.A. & Tung, J.Y. (2015). Assessment of the Genetic Basis of Rosacea by Genome-Wide Association Study. *Journal of Investigative Dermatology*. . 135 (6) 1548–1555

Chen, H., McCaig, B.C., Melotto, M., He, S.Y. & Howe, G.A. (2004). Regulation of plant arginase by wounding, jasmonate, and the phytotoxin coronatine. *Journal of Biological Chemistry* 279 (44) 45998–46007

Chen, W. & Plewig, G. (2015). Are *Demodex* Mites Principal, Conspirator, Accomplice, Witness or Bystander in the Cause of Rosacea. *American journal of clinical dermatology* 16. 67–72

Chen, W. & Plewig, G. (2014). Human demodicosis: Revisit and a proposed classification. *British Journal of Dermatology*. 170. 1219–1225

Chen, Y., Cai, J., Murphy, T.J. & Jones, D.P. (2002). Overexpressed human mitochondrial thioredoxin confers resistance to oxidant-induced apoptosis in human osteosarcoma cells. *Journal of Biological Chemistry*. 277 (36) 33242–33248

Commichau, F.M., Rothe, F.M., Herzberg, C., Wagner, E., Hellwig, D., Lehnik-Habrink, M., Hammer, E., Völker, U. & Stülke, J. (2009). Novel Activities of Glycolytic Enzymes in *Bacillus subtilis*. *Molecular & Cellular Proteomics* 8 (6) 1350–1360

Cox, J., Neuhauser, N., Michalski, A., Scheltema, R.A., Olsen, J. V. & Mann, M. (2011). Andromeda: A peptide search engine integrated into the MaxQuant environment. *Journal of Proteome Research*. 10 (4). 1794–1805

Crawford, G.H., Pelle, M.T. & James, W.D. (2004). Rosacea: I. Etiology, pathogenesis, and subtype classification. *Journal of the American Academy of Dermatology* 51 (3). 327–341

Dahl, M., Ross, A. & Schlievert, P. (2004). Temperature regulates bacterial protein production: Possible role in rosacea. *Journal of the American Academy of*

Dermatology 50. 266–272

Dahl, M. V, Katz, H.I., Krueger, G.G., Millikan, L.E., Odom, R.B., Parker, F., Wolf, J.E., Aly, R., Bayles, C., Reusser, B., Weidner, M., Coleman, E., Patrignelli, R., Tuley, M.R., Baker, M.O., Herndon, J.H. & Czernielewski, J.M. (1998). Topical Metronidazole Maintains Remissions of Rosacea. *Arch Dermatol*. 134 (June 1998) 679–683

Dai, F., Lin, X., Chang, C. & Feng, X.H. (2009). Nuclear Export of Smad2 and Smad3 by RanBP3 Facilitates Termination of TGF-β Signaling. *Developmental Cell* 16 (3). 345–357

Dallo, S.F., Kannan, T.R., Blaylock, M.W. & Baseman, J.B. (2002). Elongation factor Tu and E1 beta subunit of pyruvate dehydrogenase complex act as fibronectin binding proteins in Mycoplasma pneumoniae. *Mol Microbiol*. 46 (4) 1041–1051

Damdimopoulos, A.E., Miranda-Vizuete, A., Pelto-Huikko, M., Gustafsson, J.Å. & Spyrou, G. (2002). Human mitochondrial thioredoxin. Involvement in mitochondrial membrane potential and cell death. *Journal of Biological Chemistry*. 277 (36) 33249–33257

Dandekar, T., Schuster, S., Snel, B., Huynen, M. & Bork, P. (1999). Pathway alignment: application to the comparative analysis of glycolytic enzymes. *The Biochemical journal* 343 115–124

Das, M.R., Bag, A.K., Saha, S., Ghosh, A., Dey, S.K., Das, P., Mandal, C., Ray, S., Chakrabarti, S., Ray, M. & Jana, S.S. (2016). Molecular association of glucose-6-phosphate isomerase and pyruvate kinase M2 with glyceraldehyde-3-phosphate dehydrogenase in cancer cells. *BMC Cancer* 16 (1) 152

Dawoud Bani-Yaseen, A. (2011). Spectrofluorimetric study on the interaction between antimicrobial drug sulfamethazine and bovine serum albumin. *Journal of Luminescence* 131 (5) 1042–1047

Defeu Soufo, H.J., Reimold, C., Linne, U., Knust, T., Gescher, J. & Graumann, P.L. (2010). Bacterial translation elongation factor EF-Tu interacts and colocalizes with actin-like MreB protein. *Proceedings of the National Academy of Sciences of the United States of America* 107 (7). 3163–8

Dietrichs, D., Meyer, M., Schmidt, B. & Andreesen, J.R. (1990). Purification of NADPH-dependent electron-transferring flavoproteins and N-terminal protein sequence data of dihydrolipoamide dehydrogenases from anaerobic, glycine-

utilizing bacteria. *Journal of Bacteriology*. 172 (4) 2088–2095

Dietrichs, D. & Remmer Andreesen, J. (1990). Purification and comparative studies of dihydrolipoamide dehydrogenases from the anaerobic, glycine-utilizing bacteria P*eptostreptococcus glycinophilus, Clostridium cylindrosporum*, and *Clostridium sporogenes*. *Journal of Bacteriology*. 172 (1) 243–251

Dirschka, T., Tronnier, H. & Fölster-Holst, R. (2004). Epithelial barrier function and atopic diathesis in rosacea and perioral dermatitis. *British Journal of Dermatology*. 150 (6) 1136–1141

Doerfel, L.K. & Rodnina, M. V. (2013). Elongation factor P: Function and effects on bacterial fitness. *Biopolymers* 99 (11). 837–852

Donaldson, S.H., Bennett, W.D., Zeman, K.L., Knowles, M.R., Tarran, R. & Boucher, R.C. (2006). Mucus Clearance and Lung Function in Cystic Fibrosis with Hypertonic Saline. *New England Journal of Medicine* 354 (3). 241–250

Driks, A. (2002). Overview: Development in bacteria: Spore formation in *Bacillus subtilis*. *Cellular and Molecular Life Sciences*. 59 (3) 389–391

Duché, O., Trémoulet, F., Glaser, P. & Labadie, J. (2002). Salt stress proteins induced in *Listeria monocytogenes*. *Applied and Environmental Microbiology*. 68 (4) 1491–1498

Duque-Correa, M.A., Kuhl, A.A., Rodriguez, P.C., Zedler, U., Schommer-Leitner, S., Rao, M., Weiner, J., Hurwitz, R., Qualls, J.E., Kosmiadi, G.A., Murray, P.J., Kaufmann, S.H.E. & Reece, S.T. (2014). Macrophage arginase-1 controls bacterial growth and pathology in hypoxic tuberculosis granulomas. *Proceedings of the National Academy of Sciences* 111 (38) E4024–E4032

Egeberg, A., Weinstock, L.B., Thyssen, E.P., Gislason, G.H. & Thyssen, J.P. (2017). Rosacea and gastrointestinal disorders - a population-based cohort study. *British Journal of Dermatology* 176. 100–106

Elkins, M.R., Robinson, M., Rose, B., Harbour, C., Moriarty, C., Marks, G.B., Belousova, E. & Xuan, W. (2006). A Controlled Trial of Long-Term Inhaled Hypertonic Saline in Patients with Cystic Fibrosis. *The New England Journal of Medicine*. 354 (3). 229–240

Elston, C. a. & Elston, D.M. (2014). Demodex Mites. *Clinics in Dermatology* 32 (6) 739–743

Ezraty, B., Gennaris, A., Barras, F. & Collet, J.-F. (2017). Oxidative stress, protein damage and repair in bacteria. *Nature Reviews Microbiology* 15 (7). 385–396

Faller, E.M., Villeneuve, T.S. & Brown, D.L. (2009). MAP1a associated light chain 3 increases microtubule stability by suppressing microtubule dynamics. *Molecular and Cellular Neuroscience* 41 (1). 85–93

Ferrer, L., Ravera, I. & Silbermayr, K. (2014). Immunology and pathogenesis of canine demodicosis. *Veterinary Dermatology*. (March) 427-435

Fillat, M.F. (2014). The fur (ferric uptake regulator) superfamily: Diversity and versatility of key transcriptional regulators. *Archives of Biochemistry and Biophysics* 546. 41–52

Forton, F., Germaux, M.A., Brasseur, T., De Liever, A., Laporte, M., Mathys, C., Sass, U., Stene, J.J., Thibaut, S., Tytgat, M. & Seys, B. (2005). Demodicosis and rosacea: Epidemiology and significance in daily dermatologic practice. *Journal of the American Academy of Dermatology*. 52 (1) 74–87

Forton, F. & De Maertelaer, V. (2017). Two Consecutive Standardized Skin Surface Biopsies: An Improved Sampling Method to Evaluate Demodex Density as a Diagnostic Tool for Rosacea and Demodicosis. *Acta Dermato Venereologica*. (38) 1-7

Forton, F. & Seys, B. (1993). Density of Demodex folliculorum in rosacea: a case-control study using standardized skin-surface biopsy. *British Journal of Dermatology* 128. 650–659

Fu, H., Yuan, J. & Gao, H. (2015). Microbial oxidative stress response: Novel insights from environmental facultative anaerobic bacteria. *Archives of Biochemistry and Biophysics* 584. 28–35

Fujita, Y., Matsuoka, H. & Hirooka, K. (2007). Regulation of fatty acid metabolism in bacteria. *Molecular Microbiology*. 66 (4) 829–839

Fujiwara, S., Okubo, Y., Irisawa, R. & Tsuboi, R. (2010). Rosaceiform dermatitis associated with topical tacrolimus treatment. *Journal of the American Academy of Dermatology* 62 (6) 1050–1052

Fukai, T. & Ushio-Fukai, M. (2011). Superoxide Dismutases: Role in Redox Signaling, Vascular Function, and Diseases. *Antioxidants & Redox Signaling*. . 15 (6) 1583–1606

Furnari, M.L., Termini, L., Traverso, G., Barrale, S., Bonaccorso, M.R., Damiani, G., Piparo, C. Lo & Collura, M. (2012). Nebulized hypertonic saline containing hyaluronic acid improves tolerability in patients with cystic fibrosis and lung

disease compared with nebulized hypertonic saline alone: a prospective, randomized, double-blind, controlled study. *Therapeutic Advances in Respiratory Disease* 6 (6). 315–322

Gallo, R.L., Granstein, R.D., Kang, S., Mannis, M., Steinhoff, M., Tan, J. & Thiboutot, D. (2017). Standard classification and pathophysiology of rosacea: The 2017 update by the National Rosacea Society Expert Committee. *Journal of the American Academy of Dermatology* 78 167-170

Gao, Y.-Y., Di Pascuale, M. a, Li, W., Baradaran-Rafii, a, Elizondo, a, Kuo, C.-L., Raju, V.K. & Tseng, S.C.G. (2005). In vitro and in vivo killing of ocular *Demodex* by tea tree oil. *The British journal of ophthalmology*. 89 1468–1473

Geerling, G., Tauber, J., Baudouin, C., Goto, E., Matsumoto, Y., O'Brien, T., Rolando, M., Tsubota, K. & Nichols, K.K. (2011). The International Workshop on Meibomian Gland Dysfunction: Report of the Subcommittee on Management and Treatment of Meibomian Gland Dysfunction. *Investigative Opthalmology & Visual Science* 52 (4). 2050

Gibson, P.G., Saltos, N. & Fakes, K. (2001). Acute anti-inflammatory effects of inhaled budesonide in asthma: a randomized controlled trial. *Am J Respir Crit Care Med*. 163 (1). 32–36

Gipson, I.K. (2004). Distribution of mucins at the ocular surface. *Experimental Eye Research*. 78 (3) 379–388.

Gipson, I.K. (2016). Goblet cells of the conjunctiva: A review of recent findings. *Progress in Retinal and Eye Research* 54. 49–63

Gobert, A.P., Cheng, Y., Wang, J.-Y., Boucher, J.-L., Iyer, R.K., Cederbaum, S.D., Casero, R. a, Newton, J.C. & Wilson, K.T. (2002). *Helicobacter pylori* induces macrophage apoptosis by activation of arginase II. *Journal of immunology (Baltimore, Md. : 1950)*. 168 (9) 4692–4700

Goldgar, C., Keahey, D.J. & Houchins, J. (2009). Treatment options for acne rosacea. *American Family Physician*. 80 (5) 461–468

Goodwin, K., Viboud, C. & Simonsen, L. (2006). Antibody response to influenza vaccination in the elderly: A quantitative review. *Vaccine*. 24 (8) 1159–1169

Grabowska, D. & Chelstowska, A. (2003). The ALD6 gene product is indispensable for providing NADPH in yeast cells lacking glucose-6-phosphate dehydrogenase activity. *Journal of Biological Chemistry*. 278 (16) 13984–13988

Grice, E. a & Segre, J. a (2011). The skin microbiome. *Nature reviews. Microbiology*. 9 (April) 244–253

Grimm, B. (1990). Primary structure of a key enzyme in plant tetrapyrrole synthesis: glutamate 1-semialdehyde aminotransferase. *Proceedings of the National Academy of Sciences of the United States of America* 87 (11). 4169–73

Gupta, A.K. & Chaudhry, M.M. (2005). Rosacea and its management: An overview. *Journal of the European Academy of Dermatology and Venereology*. 19 (3) 273–285

Guzman-Sanchez, D.A., Ishiuji, Y., Patel, T., Fountain, J., Chan, Y.H. & Yosipovitch, G. (2007). Enhanced skin blood flow and sensitivity to noxious heat stimuli in papulopustular rosacea. *Journal of the American Academy of Dermatology*. 57 (5) 800–805

Hall, A., Karplus, P.A. & Poole, L.B. (2009). Typical 2-Cys peroxiredoxins - Structures, mechanisms and functions. *FEBS Journal*. 276 (9) 2469–2477

Halpain, S. & Dehmelt, L. (2006). The MAP1 family of microtubule-associated proteins. *Genome Biology* 7 (6). 224

Hashemian, S.M., Mortaz, E., Jamaati, H., Bagheri, L., Mohajerani, S.A., Garssen, J., Movassaghi, M., Barnes, P.J., Hill, N.S. & Adcock, I.M. (2018). Budesonide facilitates weaning from mechanical ventilation in difficult-to-wean very severe COPD patients: Association with inflammatory mediators and cells. *Journal of Critical Care* 44. 161–167

Hayes, E., Pohl, K., McElvaney, N.G. & Reeves, E.P. (2011). The cystic fibrosis neutrophil: A specialized yet potentially defective cell. *Archivum Immunologiae et Therapiae Experimentalis*. 59 (2) 97–112

Hecker, M. & Völker, U. (2001). General stress response of *Bacillus subtilis* and other bacteria. *Advances in Microbial Physiology* 44. 35–91

Herr, H. & Hee You, C. (2000). Realtionship between *Helicobactor pylori* and rosacea: it may be a myth. *Journal of Korean Med Sci*. 15. p.pp 551–554

Higgins, C.F. (2001). ABC transporters: Physiology, structure and mechanism - An overview. *Research in Microbiology*. 152 (3–4). 205–210.

Holmes, A.D. (2013). Potential role of microorganisms in the pathogenesis of rosacea. *Journal of the American Academy of Dermatology*. . 69 (6). 1025–1032

Holmes, A.D. & Steinhoff, M. (2017). Integrative concepts of rosacea pathophysiology, clinical presentation and new therapeutics. *Experimental*

Dermatology. 26 (8) 659–667

Horváth, I., Multhoff, G., Sonnleitner, A. & Vígh, L. (2008). Membrane-associated stress proteins: More than simply chaperones. *Biochimica et Biophysica Acta - Biomembranes*. 1778 (7–8) 1653–1664

Huang, W., Jia, J., Edwards, P., Dehesh, K., Schneider, G. & Lindqvist, Y. (1998). Crystal structure of b-ketoacyl-acyl carrier protein synthase II from E. coli reveals the molecular architecture of condensing enzymes. *EMBO Journal*. 17 (5) 1183–1191

Imlay, J.A. (2015). Diagnosing oxidative stress in bacteria: not as easy as you might think. *Current Opinion in Microbiology* 24. 124–131

Imlay, J.A. (2014). *The molecular mechanisms and physiological consequences of oxidative stress: lessons from a model bacterium* 24 124-131

Jahns, A.C., Lundskog, B., Dahlberg, I., Tamayo, N.C., Mcdowell, A., Patrick, S. & Alexeyev, O.A. (2012a). No link between rosacea and *Propionibacterium acnes*. *Apmis*. 120 (11) 922–925

Jahns, A.C., Lundskog, B., Ganceviciene, R., Palmer, R.H., Golovleva, I., Zouboulis, C.C., McDowell, A., Patrick, S. & Alexeyev, O.A. (2012b). An increased incidence of *Propionibacterium acnes* biofilms in acne vulgaris: A case-control study. *British Journal of Dermatology*. 167 (1) 50–58

Jarmuda, S., Mcmahon, F., Zaba, R., O'Reilly, N., Jakubowicz, O., Holland, A., Szkaradkiewicz, A. & Kavanagh, K. (2014). Correlation between serum reactivity to *Demodex*-associated *Bacillus oleronius* proteins, and altered sebum levels and *Demodex* populations in erythematotelangiectatic rosacea patients. *Journal of Medical Microbiology*. 63 258–262

Jarmuda, S., O'Reilly, N., Zaba, R., Jakubowicz, O., Szkaradkiewicz, A. & Kavanagh, K. (2012). Potential role of *Demodex* mites and bacteria in the induction of rosacea. *Journal of Medical Microbiology*. 61 (PART 11) 1504–1510

Jenssen, H., Hamill, P. & Hancock, R.E.W. (2006). Peptide antimicrobial agents. *Clinical Microbiology Reviews*. 19 (3) 491–511

Jiang, C., Kim, S.Y. & Suh, D.Y. (2008). Divergent evolution of the thiolase superfamily and chalcone synthase family. *Molecular Phylogenetics and Evolution* 49 (3). 691–701

Jing, X., Shuling, G. & Ying, L. (2005). Environmental scanning electron

microscopy observation of the ultrastructure of *Demodex*. *Microscopy Research and Technique* 68 (5). 284–289

Joblet, C., Roux, Rv., Drancourt, M., Gouvernet, J. & Raoult, D. (1995). Identification of *Bartonella (Rochalimaea)* species among fastidious gram-negative bacteria on the basis of the partial sequence of the citrate-synthase gene. *Journal of Clinical Microbiology*. 33 (7). 1879–1883

Kalinina, E. V, Chernov, N.N. & Saprin, a N. (2008). Involvement of thio-, peroxi-, and glutaredoxins in cellular redox-dependent processes. *Biochemistry. Biokhimiia*. 73 (13). 1493–1510

El Kasmi, K.C., Qualls, J.E., Pesce, J.T., Smith, A.M., Thompson, R.W., Henao-Tamayo, M., Basaraba, R.J., König, T., Schleicher, U., Koo, M.-S., Kaplan, G., Fitzgerald, K.A., Tuomanen, E.I., Orme, I.M., Kanneganti, T.-D., Bogdan, C., Wynn, T.A. & Murray, P.J. (2008). Toll-like receptor–induced arginase 1 in macrophages thwarts effective immunity against intracellular pathogens. *Nature Immunology* 9 (12). 1399–1406

Khanvilkar, K., Donovan, M.D. & Flanagan, D.R. (2001). Drug transfer through mucus. *Advanced Drug Delivery Reviews*. 48 (2–3). 173–193.

Kheirkhah, A., Casas, V., Li, W., Raju, V.K. & Tseng, S.C.G. (2007). Corneal Manifestations of Ocular *Demodex* Infestation. *American Journal of Ophthalmology*. 143. 743–750

Kim, J.W. & Dang, C. V. (2005). Multifaceted roles of glycolytic enzymes. *Trends in Biochemical Sciences*. 30 (3). 142–150

Kováryová, M. & Kollárová, M. (2008). Oxidative stress and thioredoxin system. *General Physiology and Biophysics*. 27 (2). 71–84

Korting, H.C. & Schöllmann, C. (2009). Current topical and systemic approaches to treatment of rosacea. *Journal of the European Academy of Dermatology and Venereology*. 23 (8). 876–882

Kuhle, B. & Ficner, R. (2014). A monovalent cation acts as structural and catalytic cofactor in translational GTPases. *The EMBO journal* 33 (21). 1–17

Kuhnigk, T., Borst, E.M., Breunig, A., König, H., Collins, M.D., Hutson, R.A. & Kämpfer, P. (1995). *Bacillus oleronius* sp.nov., a member of the hindgut flora of the termite Reticulitermes santonensis (Feytaud). *Canadian journal of microbiology* 41 (8). 699–706

Kumar, V., Ero, R., Ahmed, T., Goh, K.J., Zhan, Y., Bhushan, S. & Gao, Y.G.

(2016). Structure of the gtp form of elongation factor 4 (ef4) bound to the ribosome. *Journal of Biological Chemistry*. 291 (25). 12943–12950

Lacey, N., Delaney, S., Kavanagh, K. & Powell, F.C. (2007). Mite-related bacterial antigens stimulate inflammatory cells in rosacea. *British Journal of Dermatology*. 157 (3). 474–481

Lacey, N., Kavanagh, K. & Tseng, S.C.G. (2009). Under the lash: *Demodex* mites in human diseases. *The biochemist* 31 (4). 2–6

Lacey, N., Ní Raghallaigh, S. & Powell, F.C. (2011). *Demodex* mites - Commensals, parasites or mutualistic organisms? *Dermatology*. 222 (2). 128–130.

Lacey, N., Russell-Hallinan, A. & Powell, F.C. (2016). Study of *Demodex* mites: Challenges and Solutions. *Journal of the European Academy of Dermatology and Venereology*. 30 (5). 764–775

Lai, C.Y. & Cronan, J.E. (2003). β-Ketoacyl-Acyl Carrier Protein Synthase III (FabH) Is Essential for Bacterial Fatty Acid Synthesis. *Journal of Biological Chemistry*. 278 (51) 51494–51503

Lazaridou, E., Giannopoulou, C., Fotiadou, C., Vakirlis, E. & Trigoni, A. (2011). *The potential role of microorganisms in the development of rosacea*. 9 21–25

Leung, B.K., LaBarbera, L., Carroll, C., Allen, D. & McNulty, A. (2010). The Effects of Normal Saline Instillation in Conjunction with Negative Pressure Wound Therapy on Wound Healing in a Porcine Model. *Wounds*. . 22 (7). 179–187

Li, J., O'Reilly, N., Sheha, H., Katz, R., Raju, V.K., Kavanagh, K. & Tseng, S.C.G. (2010). Correlation between Ocular *Demodex* Infestation and Serum Immunoreactivity to Bacillus Proteins in Patients with Facial Rosacea. *Ophthalmology* 117 (5). 11–13

Li, K., Jiang, T., Yu, B., Wang, L., Gao, C., Ma, C., Xu, P. & Ma, Y. (2012). Transcription Elongation Factor GreA Has Functional Chaperone Activity. *PLoS ONE*. 7 (12). 1–10

Li, L., Elledge, S.J., Peterson, C. a, Bales, E.S. & Legerski, R.J. (1994). Specific association between the human DNA repair proteins XPA and ERCC1. *Proceedings of the National Academy of Sciences of the United States of America*. 91 (May). 5012–5016

Liao, G., Liu, Q. & Xie, J. (2013). Transcriptional analysis of the effect of exogenous decanoic acid stress on Streptomyces roseosporus. *Microbial Cell*

Factories 12 (1). 19

Linden, S.K., Sutton, P., Karlsson, N.G., Korolik, V. & McGuckin, M.A. (2008). Mucins in the mucosal barrier to infection. *Mucosal Immunology* 1 (3). 183–197

Ling, E., Feldman, G., Portnoi, M., Dagan, R., Overweg, K., Mulholland, F., Chalifa-Caspi, V., Wells, J. & Mizrachi-Nebenzahl, Y. (2004). Glycolytic enzymes associated with the cell surface of *Streptococcus pneumoniae* are antigenic in humans and elicit protective immune responses in the mouse. *Clinical and Experimental Immunology*. 138 (2). 290–298

Linton, K.J. & Higgins, C.F. (1998). *MicroGenomics The Escherichia coli ATP-binding cassette (ABC) proteins*. 28. 5–13

Liu, J., Sheha, H. & Tseng, S.C.G. (2010). Pathogenic role of *Demodex* mites in blepharitis. *Current opinion in allergy and clinical immunology*. 10 (5). 505–510

Liu, R.F., Huang, C.L. & Feng, H. (2015). Salt stress represses production of extracellular proteases in *Bacillus pumilus*. *Genetics and Molecular Research*. 14 (2). 4939–4948

Lüer, C., Schauer, S., Möbius, K., Schulze, J., Schubert, W.D., Heinz, D.W., Jahn, D. & Moser, J. (2005). Complex formation between glutamyl-tRNA reductase and glutamate-1- semialdehyde 2,1-aminomutase in *Escherichia coli* during the initial reactions of porphyrin biosynthesis. *Journal of Biological Chemistry*. 280 (19). 18568–18572

Mantelli, F. & Argüeso, P. (2008). Functions of ocular surface mucins in health and disease. *Curr Opin Allergy Clin Immunol.* 8 (5). 477–483

Margalit, A., Kowalczyk, M.J., Zaba, R., Kavanagh, K., Kowalczyk, J., Zaba, R. & Kavanagh, K. (2016). The role of altered cutaneous immune responses in the induction and persistence of rosacea. *Journal of Dermatological Science*. 82 (1). 3–8

Marković, O.S., Cvijetić, I.N., Zlatović, M. V., Opsenica, I.M., Konstantinović, J.M., Terzić Jovanović, N. V., Šolaja, B.A. & Verbić, T.Ž. (2018). Human serum albumin binding of certain antimalarials. *Spectrochimica Acta Part A: Molecular and Biomolecular Spectroscopy* 192. 128–139

Marks, R. & Dawber, R.P.R. (1971). Skin Surface Biopsy: An Improved Technique For The Examination Of The Horny Layer. *British Journal of Dermatology* 84

(2). 117–123

Marrakchi, H., Zhang, Y.-M. & Rock, C.O. (2002). Mechanistic diversity and regulation of Type II fatty acid synthesis. *Biochemical Society Transactions*. 30 (6). 30–33

Martínez, I., Lombardía, L., Herranz, C., García-Barrena, B., Domínguez, O. and Melero, J.A. (2009). Cultures of HEp-2 cells persistently infected by human respiratory syncytial virus differ in chemokine expression and resistance to apoptosis as compared to lytic infections of the same cell type. *Virology*. 388. 31-41

Maruyama, A., Kumagai, Y., Morikawa, K., Taguchi, K., Hayashi, H. & Ohta, T. (2003). Oxidative-stress-inducible qorA encodes an NADPH-dependent quinone oxidoreductase catalysing a one-electron reduction in *Staphylococcus aureus*. *Microbiology*. 149 (2). 389–398

Mason, D.W. & Williams, a F. (1980). The kinetics of antibody binding to membrane antigens in solution and at the cell surface. *The Biochemical journal*. 187 (1). 1–20

Mathew, T. V. & Kuriakose, S. (2013). Studies on the antimicrobial properties of colloidal silver nanoparticles stabilized by bovine serum albumin. *Colloids and Surfaces B: Biointerfaces* 101. 14–18

McAleer, M.A., Fitzpatrick, P. & Powell, F.C. (2010). Papulopustular rosacea: Prevalence and relationship to photodamage. *Journal of the American Academy of Dermatology* 63 (1). 33–39

McAleer, M. & Powell, F.C. (2007). Rosacea: Prevalence, skin type, photodamage, and flushing in an Irish population. *Journal of the American Academy of Dermatology*. 56 (2). 2007

McMahon, F., Banville, N., Bergin, D.A., Smedman, C., Paulie, S., Reeves, E. & Kavanagh, K. (2016). Activation of Neutrophils via IP3 Pathway Following Exposure to *Demodex*-Associated Bacterial Proteins. *Inflammation*. 39 (1). 425–433

McMahon, F.W., Gallagher, C., Reilly, N.O., Clynes, M., Sullivan, F.O., Kavanagh, K., O'Reilly, N., Clynes, M., O'Sullivan, F., Kavanagh, K., Reilly, N.O., Clynes, M., Sullivan, F.O., Kavanagh, K., O'Reilly, N., Clynes, M., O'Sullivan, F. & Kavanagh, K. (2014). Exposure of a Corneal Epithelial Cell Line (hTCEpi) to *Demodex*-Associated *Bacillus* Proteins Results in an Inflammatory

Response. *Investigative Ophthalmology & Visual Science* 55 (October). 7019–7028

Meers, J.L., Tempest, D.W. & Brown, C.M. (1970). 'Glutamine(amide): 2-Oxoglutarate Amino Transferase Oxido-reductase (NADP)', an Enzyme Involved in the Synthesis of Glutamate by Some Bacteria. *Journal of General Microbiology* 64 (2). 187–194

Miller, E.A. & Schekman, R. (2013). COPII - a flexible vesicle formation system. *Current Opinion in Cell Biology*. . 25 (4). 420–427. Available from: http://dx.doi.org/10.1016/j.ceb.2013.04.005.

Minic, S., Stanic-Vucinic, D., Radomirovic, M., Radibratovic, M., Milcic, M., Nikolic, M. & Cirkovic Velickovic, T. (2018). Characterization and effects of binding of food-derived bioactive phycocyanobilin to bovine serum albumin. *Food Chemistry* 239. 1090–1099

Mock, J., Zheng, Y., Mueller, A.P., Ly, S., Tran, L., Segovia, S., Nagaraju, S., Köpke, M., Dürre, P. & Thauer, R.K. (2015). Energy conservation associated with ethanol formation from H2 and CO2 in Clostridium autoethanogenum involving electron bifurcation. *Journal of Bacteriology*. 197 (18). 2965–2980

Moore, B.C. & Leigh, J.A. (2005). Markerless mutagenesis in Methanococcus maripaludis demonstrates roles for alanine dehydrogenase, alanine racemase, and alanine permease. *Journal of Bacteriology*. 187 (3). 972–979

Morita, T., Kawamoto, H., Mizota, T., Inada, T. & Aiba, H. (2004). Enolase in the RNA degradosome plays a crucial role in the rapid decay of glucose transporter mRNA in the response to phosphosugar stress in *Escherichia coli*. *Molecular Microbiology*. 54 (4). 1063–1075

Morris Jr., S.M. (2012). Arginases and arginine deficiency syndromes. *Current Opinion in Clinical Nutrition and Metabolic Care*. 15 (1). 64–70

Morya, V.K., Yadav, S., Kim, E.K. & Yadav, D. (2012). In silico characterization of alkaline proteases from different species of *Aspergillus*. *Applied Biochemistry and Biotechnology*. 166 (1). 243–257

Murakami, K., Hashimoto, Y. & Murooka, Y. (1993). Cloning and characterization of the gene encoding glutamate 1-semialdehyde 2,1-aminomutase, which is involved in delta-aminolevulinic acid synthesis in *Propionibacterium freudenreichii*. *Applied and environmental microbiology* 59 (1). 347–50

Murillo, N., Aubert, J. & Raoult, D. (2014). Microbiota of *Demodex* mites from

rosacea patients and controls. *Microbial Pathogenesis*. . 71–72 (1). 37–40

Ní Raghallaigh, S., Bender, K., Lacey, N., Brennan, L. & Powell, F.C. (2012). The fatty acid profile of the skin surface lipid layer in papulopustular rosacea. *British Journal of Dermatology*. 166 (2). 279–287

Niazi, S.A., Clarke, D., Do, T., Gilbert, S.C., Mannocci, F. & Beighton, D. (2010). *Propionibacterium acnes* and *Staphylococcus epidermidis* Isolated from Refractory Endodontic Lesions Are Opportunistic Pathogens. *Journal of Clinical Microbiology*. 48 (11). 3859–3869

Noble, R.T. & Weisberg, S.B. (2005). A review of technologies for rapid detection of bacteria in recreational waters. *Journal of Water and Health*. 3 (4). 381–392

Nyström, T. (2005). Role of oxidative carbonylation in protein quality control and senescence. *The EMBO Journal* 24 (7). 1311–1317

O'Reilly, N., Bergin, D., Reeves, E.P., McElvaney, N.G. & Kavanagh, K. (2012a). *Demodex*-associated bacterial proteins induce neutrophil activation. *British Journal of Dermatology*. 166 (4). 753–760

O'Reilly, N., Gallagher, C., Reddy Katikireddy, K., Clynes, M., O'Sullivan, F. & Kavanagh, K. (2012b). *Demodex*-associated *Bacillus* proteins induce an aberrant wound healing response in a corneal epithelial cell line: possible implications for corneal ulcer formation in ocular rosacea. *Investigative ophthalmology & visual science*. 53 (6). 3250–3259

O'Reilly, N., Menezes, N. & Kavanagh, K. (2012c). Positive correlation between serum immunoreactivity to *Demodex*-associated *Bacillus* proteins and erythematotelangiectatic rosacea. *British Journal of Dermatology*. 167 (5). 1032–1036

Pereira, S.F.F., Gonzalez, R.L. & Dworkin, J. (2015). Protein synthesis during cellular quiescence is inhibited by phosphorylation of a translational elongation factor. *Proceedings of the National Academy of Sciences* 112 (25). E3274–E3281

Periago, P.M., Periago, P.M., Abee, T., Abee, T., Wouters, J. a & Wouters, J. a (2002). Identification of Proteins Involved in the Heat Stress Response of *Bacillus cereus* ATCC 14579. *Society*. 68 (7). 3486–3495

Pesce, J.T., Ramalingam, T.R., Mentink-Kane, M.M., Wilson, M.S., Kasmi, K.C.E., Smith, A.M., Thompson, R.W., Cheever, A.W., Murray, P.J. & Wynn, T.A. (2009). Arginase-1-expressing macrophages suppress Th2 cytokine-driven

inflammation and fibrosis. *PLoS Pathogens*. 5 (4)

Peters, J.W., Miller, A.F., Jones, A.K., King, P.W. & Adams, M.W.W. (2016). Electron bifurcation. *Current Opinion in Chemical Biology* 31. 146–152

Pier, G.B. (1994). Modulation of *Pseudomonas aeruginosa* Adherence to the Corneal Surface by Mucus. *Infection and Immunity*. 62 (5). 1799–1804

Porcheron, G. & Dozois, C.M. (2015). Interplay between iron homeostasis and virulence: Fur and RyhB as major regulators of bacterial pathogenicity. *Veterinary Microbiology* 179 (1–2). 2–14

Powell, F.C. (2005). Rosacea. *The New England Journal of Medicine*. 352 (8). 793–803

Prazeres, C., Kirschning, C.J., Busch, D., Dürr, S., Jennen, L., Heinzmann, U., Prebeck, S. & Wagner, H. (2002). Role of chlamydophilal heat shock protein 60 in the stimulation of innate immune cells by *Chlamydophila pneumoniae*. *Eur. J. Immunol.* 32. 2460–2470

Proksch, E., Nissen, H.-P., Bremgartner, M. & Urquhart, C. (2005). Bathing in magnesium rich Dead Sea salt improves skin barrier function, enhances skin hydration, and reduces inflammation in atopic dry skin. *International journal of dermatology* 44. 151–157

Pye, RJ. & Burton, J.L. (1976). Treatment of rosacea by metronidazole. *Lancet.* 1. 1211-1212

Qi, Z. & O'Brian, M.R. (2002). Interaction between the bacterial iron response regulator and ferrochelatase mediates genetic control of heme biosynthesis. *Molecular Cell*. 9 (1). 155–162

Rasmusson, A.G., Svensson, Å.S., Knoop, V., Grohmann, L. & Brennicke, A. (1999). Homologues of yeast and bacterial rotenone-insensitive NADH dehydrogenases in higher eukaryotes: Two enzymes are present in potato mitochondria. *Plant Journal*. 20 (1). 79–87

Reddick, J.J., Sirkisoon, S., Dahal, R.A., Hardesty, G., Hage, N.E., Booth, W.T., Quattlebaum, A.L., Mills, S.N., Meadows, V.G., Adams, S.L.H., Doyle, J.S. & Kiel, B.E. (2017). First Biochemical Characterization of a Methylcitric Acid Cycle from *Bacillus subtilis* Strain 168. *Biochemistry* 56 (42) 5698-5711

Reeves, E.P., Lu, H., Jacobs, H.L., Messina, C.G.M., Bolsover, S., Gabella, G., Potma, E.O., Warley, A., Roes, J. & Segal, A.W. (2002). Killing activity of neutrophils is mediated through activation of proteases by K+ flux. *Nature* 416

(6878) 291–297

Rhee, S.G., Jeong, W., Chang, T.-S. & Woo, H.A. (2007). Sulfiredoxin, the cysteine sulfinic acid reductase specific to 2-Cys peroxiredoxin: its discovery, mechanism of action, and biological significance. *Kidney International* 72. S3–S8

Roos, D., Van Bruggen, R. & Meischl, C. (2003). Oxidative killing of microbes by neutrophils. *Microbes and Infection*. 5 (14). 1307–1315

Del Rosso, J.Q. (2004). Medical treatment of rosacea with emphasis on topical therapies. *Expert Opin. Pharmacother.* 5 (1). 5–13

Sancar, A. (1996). DNA Excision Repair. *Annual Review of Biochemistry* 65 (1) 43–81

Sandberg, T., Blom, H. & Caldwell, K.D. (2009). Potential use of mucins as biomaterial coatings. I. Fractionation, characterization, and model adsorption of bovine, porcine, and human mucins. *Journal of Biomedical Materials Research - Part A*. 91 (3) 762–772

Schaller, M., Gonser, L., Belge, K., Braunsdorf, C., Nordin, R., Scheu, A. & Borelli, C. (2017). Dual anti-inflammatory and anti-parasitic action of topical ivermectin 1% in papulopustular rosacea. *Journal of the European Academy of Dermatology and Venereology*. (July 2015) 1–5

Schnicker, N.J., Razzaghi, M., Guha Thakurta, S., Chakravarthy, S. & Dey, M. (2017). *Bacillus anthracis* Prolyl 4-Hydroxylase Interacts with and Modifies Elongation Factor Tu. *Biochemistry* 56. 5771–5785

Schürmann, M. & Sprenger, G.A. (2001). Fructose-6-phosphate Aldolase is a Novel Class I Aldolase from *Escherichia coli* and is Related to a Novel Group of Bacterial Transaldolases. *Journal of Biological Chemistry*. 276 (14). 11055–11061

Seo, D., Soeta, T., Sakurai, H., Sétif, P. & Sakurai, T. (2016). Pre-steady-state kinetic studies of redox reactions catalysed by *Bacillus subtilis* ferredoxin-NADP+ oxidoreductase with NADP+/NADPH and ferredoxin. *Biochimica et Biophysica Acta - Bioenergetics* 1857 (6). 678–687

Shevchenko, A., Tomas, H., Havlis, J., Olsen, J. V & Mann, M. (2006). In-gel digestion for mass spectrometric characterization of proteins and proteomes. *Nature protocols*. 1 (6) 2856–2860.

Shi, V.Y., Leo, M., Hassoun, L. & Chahal, D.S. (2015). Role of sebaceous glands in

inflammatory dermatoses. *Journal of American Dermatology* 73 (5). 856–863

Siebold, C., Flükiger, K., Beutler, R. & Erni, B. (2001). Carbohydrate transporters of the bacterial phosphoenolpyruvate: Sugar phosphotransferase system (PTS). *FEBS Letters*. 504 (3). 104–111

Sohda, M., Misumi, Y., Yamamoto, A., Yano, A., Nakamura, N. & Ikehara, Y. (2001). Identification and Characterization of a Novel Golgi Protein, GCP60, that Interacts with the Integral Membrane Protein Giantin. *Journal of Biological Chemistry*. 276 (48). 45298–45306

Soto, G., Stritzler, M., Lisi, C., Alleva, K., Pagano, M.E., Ardila, F., Mozzicafreddo, M., Cuccioloni, M., Angeletti, M. & Ayub, N.D. (2011). Acetoacetyl-CoA thiolase regulates the mevalonate pathway during abiotic stress adaptation. *Journal of Experimental Botany*. 62 (15). 5699–5711

Srivastava, S., Yadav, A., Seem, K., Mishra, S., Chaudhary, V. & Nautiyal, C.S. (2008). Effect of high temperature on *Pseudomonas putida* NBRI0987 biofilm formation and expression of stress sigma factor RpoS. *Current Microbiology*. 56 (5). 453–457

Steinhoff, M., Schauber, J. & Leyden, J.J. (2013). New insights into rosacea pathophysiology: A review of recent findings. *Journal of the American Academy of Dermatology*. 69 (6 SUPPL.1). 15–26

Stepanova, E., Lee, J., Ozerova, M., Semenova, E., Datsenko, K., Wanner, B.L., Severinov, K. & Borukhov, S. (2007). Analysis of promoter targets for *Escherichia coli* transcription elongation factor GreA in vivo and in vitro. *Journal of Bacteriology*. 189 (24). 8772–8785

Strasser, K., Masuda, S., Mason, P., Pfannstiel, J., Oppizzi, M., Rodriguez-Navarro, S., Rond??n, A.G., Aguilera, A., Struhl, K., Reed, R. & Hurt, E. (2002). TREX is a conserved complex coupling transcription with messenger RNA export. *Nature*. 417 (6886). 304–308

Suttisansanee, U. & Honek, J.F. (2011). Bacterial glyoxalase enzymes. *Seminars in Cell and Developmental Biology* 22 (3). 285–292

Suttisansanee, U., Lau, K., Lagishetty, S., Rao, K.N., Swaminathan, S., Sauder, J.M., Burley, S.K. & Honek, J.F. (2011). Structural variation in bacterial glyoxalase I enzymes: Investigation of the metalloenzyme glyoxalase I from *Clostridium acetobutylicum*. *Journal of Biological Chemistry*. 286 (44). 38367–38374

Szkaradkiewicz, a., Chudzicka-Strugala, I., Karpiński, T.M., Goślińska-Pawlowska,

O., Tulecka, T., Chudzicki, W., Szkaradkiewicz, a. K. & Zaba, R. (2012). *Bacillus oleronius* and *Demodex* mite infestation in patients with chronic blepharitis. *Clinical Microbiology and Infection*. 18. 1020–1025

Szlachcic, A. (2002). The link between *Helicobacter pylori* infection and rosacea. *Journal of the European Academy of Dermatology and Venereology*. 16 (4). 328–333

Tam, L.T., Antelmann, H., Eymann, C., Albrecht, D., Bernhardt, J. & Hecker, M. (2006). Proteome signatures for stress and starvation in *Bacillus subtilis* as revealed by a 2-D gel image color coding approach. *Proteomics*. 6 (16). 4565–4585

Tan, J., Almeida, L.M.C., Bewley, A., Cribier, B., Dlova, N.C., Gallo, R., Kautz, G., Mannis, M., Oon, H.H., Rajagopalan, M., Steinhoff, M., Thiboutot, D., Troielli, P., Webster, G., Wu, Y., van Zuuren, E.J. & Schaller, M. (2017). Updating the diagnosis, classification and assessment of rosacea: recommendations from the global ROSacea COnsensus (ROSCO) panel. *British Journal of Dermatology*. 176 (2). 431–438

Tan, J. & Berg, M. (2013). Rosacea: Current state of epidemiology. *Journal of the American Academy of Dermatology*. . 69 (6). S27–S35

Tanous, C., Kieronczyk, A., Helinck, S., Chambellon, E. & Yvon, M. (2002). Glutamate dehydrogenase activity: A major criterion for the selection of flavour-producing lactic acid bacteria strains. *Antonie van Leeuwenhoek, International Journal of General and Molecular Microbiology*. 82 (1–4). 271–278

Tatu, A.L., Clatici, V. & Cristea, V. (2016). Isolation of *Bacillus* simplex strain from *Demodex folliculorum* and observations about Demodicosis spinulosa. *Clinical and Experimental Dermatology*. . 41 (7). 818–820

Thoemmes, M.S., Fergus, D.J., Urban, J., Trautwein, M. & Dunn, R.R. (2014). Ubiquity and Diversity of Human-Associated *Demodex* Mites. *PLoS ONE*. 9 (8) 1-8

Tisma, V.S., Basta-juzbasic, A., Jaganjac, M., Brcic, L., Dobric, I., Lipozencic, J., Tatzber, F., Zarkovic, N. & Poljak-blazi, M. (2009). Oxidative stress and ferritin expression in the skin of patients with rosacea. *J Am Acad Dermatol*. 60 (2). 270–276

Tretter, L. & Adam-Vizi, V. (2000). Inhibition of Krebs cycle enzymes by hydrogen

peroxide: A key role of [alpha]-ketoglutarate dehydrogenase in limiting NADH production under oxidative stress. *The Journal of neuroscience : the official journal of the Society for Neuroscience* 20 (24). 8972–8979

Two, A.M., Wu, W., Gallo, R.L. & Hata, T.R. (2015a). Rosacea: Part I. Introduction, categorization, histology, pathogenesis, and risk factors. *Journal of the American Academy of Dermatology*. 72 (5). 749–758

Two, A.M., Wu, W., Gallo, R.L. & Hata, T.R. (2015b). Rosacea: Part II. Topical and systemic therapies in the treatment of rosacea. *Journal of the American Academy of Dermatology*. 72 (5). 761–770

Utas, S., Ozbakir, O., Turasan, A. & Utas, C. (1999). *Helicobacter pylori* eradication treatment reduces the severity of rosacea. *Journal of the American Academy of Dermatology* 40 (3). 433–435

Van Acker, H. & Coenye, T. (2017). The Role of Reactive Oxygen Species in Antibiotic-Mediated Killing of Bacteria. *Trends in Microbiology* 25 (6). 456–466

Voigt, B., Schroeter, R., Jürgen, B., Albrecht, D., Evers, S., Bongaerts, J., Maurer, K.H., Schweder, T. & Hecker, M. (2013). The response of *Bacillus licheniformis* to heat and ethanol stress and the role of the sigb regulon. *Proteomics*. 13 (14). 2140–2161

Waites, W.M., Kay, D., Dawes, I.W., Wood, D.A., Warren, S.C. & Mandelstam, J. (1970). Sporulation in *Bacillus subtilis.* Correlation of biochemical events with morphological changes in asporogeneous mutants. *Biochemical Journal*. 118 (4). 667 LP-676

Weinstock, L.B. & Steinhoff, M. (2013). Rosacea and small intestinal bacterial overgrowth: Prevalence and response to rifaximin. *Journal of the American Academy of Dermatology* 68 (5). 875–876

Wessling-Resnick, M. (2010). Iron Homeostasis and the Inflammatory Response. *Annual review of nutrition*. 30 (44). 105–122

Whitfeld, M., Gunasingam, N., Leow, L.J., Shirato, K. & Preda, V. (2011). Staphylococcus epidermidis: A possible role in the pustules of rosacea. *Journal of the American Academy of Dermatology* 64 (1). 49–52

Wieden, H.J., Gromadski, K., Rodnin, D. & Rodnina, M. V. (2002). Mechanism of elongation factor (EF)-Ts-catalyzed nucleotide exchange in EF-Tu. Contribution of contacts at the guanine base. *Journal of Biological Chemistry*.

277 (8). 6032–6036

Wilkin, J., Dahl, M., Detmar, M., Drake, L., Liang, M.H., Odom, R. & Powell, F. (2004). Standard grading system for rosacea: Report of the National Rosacea Society Expert Committee on the Classification and Staging of Rosacea. *Journal of the American Academy of Dermatology*. 50 (6). 907–912

Wilkin, J., Dahl, M., Detmar, M., Drake, L., Liang, M.H., Odom, R. & Powell, F. (2002). Standard grading system for rosacea: Report of the National Rosacea Society Expert Committee on the Classification and Staging of Rosacea. *Journal of the American Academy of Dermatology*. 46 (4). 584-587

Wilkin, J.K. (1981). Oral thermal-induced flushing in erythematotelangiectatic rosacea. *Journal of Investigative Dermatology* 76 (1). 15–18

Wittinghofer, A., Guariguata, R. & Leberman, R. (1983). Bacterial elongation factor TS: Isolation and reactivity with elongation factor Tu. *Journal of Bacteriology*. 153 (3). 1266–1271

Wohlauer, M., Moore, E.E., Silliman, C.., Fragoso, M., Gamboni, F., Harr, J., Accurso, F., Wright, F., Haenel, J., Fullerton, D. & Banerjee, A. (2012). Nebulised hypertonic saline attenuates acute lung injury following trauma and hemorrhagic shock. *Critical Care Medicine*. 40 (9). 2647–2653

Wolf, J.E. & Del Rosso, J.Q. (2007). The CLEAR trial: Results of a large community-based study of metronidazole gel in rosacea. *Therapeutics for the Clinician*. 79 (1). 73–80

Woo, P.C.Y., To, A.P.C., Lau, S.K.P. & Yuen, K.Y. (2003). Facilitation of horizontal transfer of antimicrobial resistance by transformation of antibiotic-induced cell-wall-deficient bacteria. *Medical Hypotheses*. 61 (4). 503–508

Woo, Y.R., Lim, J.H., Cho, D.H. & Park, H.J. (2016). Rosacea: Molecular mechanisms and management of a chronic cutaneous inflammatory condition. *International Journal of Molecular Sciences*. 17 (9). 1–23

Xu, X., Chen, X., Yang, P., Liu, J. & Hao, X. (2013). In vitro drug resistance of clinical isolated Brucella against antimicrobial agents. *Asian Pacific Journal of Tropical Medicine* 6 (11). 921–924

Yamasaki, K. & Gallo, R.L. (2011). Rosacea as a Disease of Cathelicidins and Skin Innate Immunity. *Journal of Investigative Dermatology Symposium Proceedings* 15 (1). 12–15

Yamasaki, K. & Gallo, R.L. (2009). The molecular pathology of rosacea. *Journal of*

Dermatological Science. 55 (2). 77–81

Yamashita, L.S., Cariello, a J., Geha, N.M., Yu, M.C. & Hofling-Lima, a L. (2011). *Demodex folliculorum* on the eyelash follicle of diabetic patients. *Arq Bras Oftalmol*. 74 (6). 422–424

Yoon, S.O., Shin, S., Liu, Y., Ballif, B.A., Woo, M.S., Gygi, S.P. & Blenis, J. (2008). Ran-Binding Protein 3 Phosphorylation Links the Ras and PI3-Kinase Pathways to Nucleocytoplasmic Transport. *Molecular Cell*. 29 (3). 362–375

Zanetti, G., Pahuja, K.B., Studer, S., Shim, S. & Schekman, R. (2012). COPII and the regulation of protein sorting in mammals. *Nature Publishing Group* 14 (2). 221

Zhang, D. & Qin, Y. (2013). The paradox of elongation factor 4: highly conserved, yet of no physiological significance? *Biochemical Journal* 452 (2). 173–181

Zhao, X. & Drlica, K. (2014). Reactive oxygen species and the bacterial response to lethal stress. *Current Opinion in Microbiology* 21. 1–6

Zhao, Y.-E., Hu, L., Wu, L.-P. & Ma, J.-X. (2012). A meta-analysis of association between acne vulgaris and *Demodex* infestation. *Journal of Zhejiang University. Science. B*. 13 (3). 192–202

Zhao, Y., Yang, F., Wang, R., Niu, D., Mu, X., Yang, R. & Hu, L. (2017). Association study of *Demodex* bacteria and facial dermatoses based on DGGE technique. *Parasitology Research* 116 945-951

Zhao, Y.E., Hu, L. & Ma, J.X. (2013). Molecular identification of four phenotypes of human *Demodex* mites (Acari: Demodicidae) based on mitochondrial 16S rDNA. *Parasitology Research*. 112 (76) 3703–3711

Zong, M., Lu, T., Fan, S., Zhang, H., Gong, R., Sun, L., Fu, Z. & Fan, L. (2015). Glucose-6-phosphate isomerase promotes the proliferation and inhibits the apoptosis in fibroblast-like synoviocytes in rheumatoid arthritis. *Arthritis Research & Therapy* 17 (1) 1-12

Zou, S.B., Hersch, S.J., Roy, H., Wiggers, J.B., Leung, A.S., Buranyi, S., Xie, J.L., Dare, K., Ibba, M. & Navarre, W.W. (2012). Loss of elongation factor P disrupts bacterial outer membrane integrity. *Journal of Bacteriology*. 194 (2). 413–425

Zouboulis, C.C., Picardo, M., Ju, Q. & Kurokawa, I. (2016). *Beyond acne : Current aspects of sebaceous gland biology and function*. 319–334

Żurawska-Płaksej, E., Rorbach-Dolata, A., Wiglusz, K. & Piwowar, A. (2018). The

effect of glycation on bovine serum albumin conformation and ligand binding properties with regard to gliclazide. *Spectrochimica Acta - Part A: Molecular and Biomolecular Spectroscopy*. 189. 625–633

Chapter Nine

Appendix

Table A3.1 Proteins identified at higher abundance in *B. oleronius* at 37ºC

Proteins that had over two matched peptides with a *t*-test probability < 0.5 and that were found to be differentially expressed at a 1.5 fold change were considered to be significantlyhigher in abundance at 37ºC. Table displays proteins with an increased fold difference >20.

Protein Annotation (* = non-imputated protein)	Peptides	Sequence Coverage %	PEP	Overall Intensity	Fold difference
Preprotein translocase subunit YajC	3	42.7	3.67E-248	3.36E+09	20.5
*Probable thiol peroxidase	11	78.3	1.18E-257	6.45E+10	20.5
*Dihydrolipoyl dehydrogenase	18	43.7	0	2.65E+10	20.4
*Peptide ABC transporter ATP-binding protein	21	65.4	9.13E-191	1.98E+10	20.3
UPF0154 protein AM506_14780	7	47.9	0	7.56E+09	19.9
UDP-N-acetyl-D-glucosamine dehydrogenase	23	60.3	1.82E-119	8.93E+09	19.7
*Aminopeptidase	23	62.3	2.84E-135	1.46E+10	19.6
Glutathione peroxidase	9	36.6	3.39E-156	4.50E+09	19.3
50S ribosomal protein L30	10	81.7	1.77E-167	6.64E+09	18.8
Chemotaxis protein CheY	10	88.3	7.08E-217	3.73E+09	18.8
2-oxoglutarate dehydrogenase E1 component	28	34.1	8.65E-162	4.43E+09	18.7
Threonine--tRNA ligase	40	54.3	3.75E-129	4.96E+09	18.6
Uracil phosphoribosyltransferase	17	76.1	3.16E-134	5.66E+09	18.5
General stress protein	11	87.6	3.08E-71	5.40E+09	18.4
*Succinyl-CoA ligase [ADP-forming] subunit alpha	21	75.7	4.53E-134	9.86E+10	18.1
*10 kDa chaperonin	10	80	5.59E-142	1.36E+11	18.1
*Electron transfer flavoprotein subunit alpha	18	56.7	5.60E-213	4.06E+10	18.0
50S ribosomal protein L23	10	62.8	1.63E-195	5.39E+09	17.5
*Chaperone protein DnaK	49	79.5	1.67E-272	5.08E+10	17.4
Chemotaxis protein	9	22.8	2.22E-138	3.69E+09	17.1
*Thioredoxin	11	51.7	2.54E-62	4.20E+10	17.1
Fe-S cluster assembly protein SufD	18	40.8	6.87E-222	4.76E+09	17.0
Ribonuclease Y	29	44.7	2.73E-24	4.32E+09	16.7
*Probable glycine dehydrogenase (decarboxylating) subunit 2	25	56.7	2.89E-170	1.99E+10	16.3
PTS glucose transporter subunit IIA	4	28.9	4.89E-173	6.87E+09	16.2
RNA polymerase sigma factor SigA	19	50.3	0	4.98E+09	16.1
Transcriptional regulator	8	79.2	2.10E-231	3.81E+09	15.9
Ferrochelatase	14	37.1	0	1.30E+10	15.7
Peptidyl-prolyl cis-trans isomerase B	1	13.3	6.14E-283	4.27E+09	15.6
General stress protein	10	56.1	0	4.83E+09	15.5

Aspartate aminotransferase	16	47	0	5.30E+09	15.4
Valine--tRNA ligase	37	44.6	0	6.90E+09	15.3
DNA-binding protein	13	82.2	8.26E-175	6.46E+09	15.2
Dephospho-CoA kinase	8	30.3	9.18E-271	4.29E+09	15.1
30S ribosomal protein S11	5	31	6.83E-201	5.82E+09	15.1
Bacitracin ABC transporter ATP-binding protein	16	57.1	0	3.00E+09	14.9
Phosphoglucosamine mutase	15	40.3	0	6.45E+09	14.9
50S ribosomal protein L35	6	54.5	2.32E-130	5.06E+09	14.5
Probable malate:quinone oxidoreductase	18	43.5	6.85E-135	4.06E+09	14.3
*Acetyl-CoA synthetase	29	53.3	1.26E-277	1.38E+10	14.2
Probable transcriptional regulatory protein AM506_05450	4	23.8	6.06E-268	3.17E+09	14.2
DNA-directed RNA polymerase subunit alpha	21	57.6	3.50E-220	7.33E+09	14.2
Leucine--tRNA ligase	18	32.5	4.39E-162	3.22E+09	14.2
Methylmalonyl-CoA carboxyltransferase	23	47.2	0	3.25E+09	14.1
*Modulator protein	22	48.4	3.19E-106	3.08E+10	13.8
*Cell division protein FtsZ	21	62.5	0	8.48E+09	13.8
Acetate kinase	16	53.5	1.60E-108	4.23E+09	13.6
ESAT-6-like protein	8	99	2.95E-185	3.62E+09	13.5
Bifunctional protein GlmU	20	48.4	0	4.41E+09	13.5
DNA polymerase III subunit beta	8	23.8	1.77E-291	2.89E+09	13.4
Capsular biosynthesis protein	5	21.9	0	5.10E+09	13.4
*Septum formation initiator	11	58.5	7.17E-83	8.06E+09	13.3
D-alanyl-D-alanine carboxypeptidase	30	59.2	8.85E-104	1.84E+10	13.3
Arginine--tRNA ligase	25	48.7	4.37E-104	6.29E+09	13.1
*UDP-3-O-(3-hydroxymyristoyl) glucosamine N-acyltransferase	9	30.8	8.05E-95	9.32E+09	13.0
tRNA uridine 5-carboxymethylaminomethyl modification enzyme MnmG	27	48.4	7.83E-57	4.65E+09	13.0
*Probable glycine dehydrogenase (decarboxylating) subunit 1	13	27	4.13E-47	7.23E+09	12.8
*Acyl-CoA dehydrogenase	32	49.3	0	9.14E+09	12.8
Serine dehydratase	11	51.8	0	3.30E+09	12.7
*50S ribosomal protein L5	18	78.8	2.32E-133	6.12E+10	12.6
*60 kDa chaperonin	66	83.3	4.97E-267	2.70E+11	12.6
*Peptidase M29	27	65.1	1.21E-27	3.86E+10	12.4
Protein GrpE	9	35.3	2.71E-173	4.07E+09	12.3
Ribose 5-phosphate isomerase	5	34.2	2.15E-82	3.29E+09	12.2
Aminomethyltransferase	19	54.3	5.01E-272	8.08E+09	12.2
Tellurite resistance protein TelA	18	44.5	1.15E-123	3.73E+09	11.9
*Fe-S cluster assembly protein SufB	22	63	0	4.97E+09	11.8
Porphobilinogen deaminase	20	53.5	0	4.59E+09	11.7
Aldehyde dehydrogenase	15	45.5	3.02E-102	1.09E+10	11.5
UDP-N-acetylglucosamine 1-	20	71.7	0	4.23E+09	11.4

carboxyvinyltransferase					
Polysaccharide deacetylase	10	44.1	0	2.76E+09	11.4
PTS lactose transporter subunit IIB	8	67	7.04E-132	4.24E+09	11.2
*50S ribosomal protein L7/L12	17	100	0	3.54E+10	11.2
Methionine aminopeptidase	12	64.1	3.88E-212	2.34E+09	11.2
Iron transporter FeoB	4	7.3	0	2.16E+09	11.0
Fur family transcriptional regulator	7	42.1	0	3.45E+09	10.9
*1,4-dihydroxy-2-naphthoyl-CoA synthase	16	52.6	7.42E-230	5.01E+10	10.8
50S ribosomal protein L9	7	34.5	2.06E-41	3.69E+09	10.7
Imidazolonepropionase	11	34	0	3.08E+09	10.6
50S ribosomal protein L13	6	40.7	3.98E-116	4.06E+09	10.5
Amino acid ABC transporter substrate-binding protein	20	55	1.84E-113	1.57E+10	10.5
Cytochrome b6	6	25.4	0	2.90E+09	10.5
*Ornithine aminotransferase	31	69.8	7.88E-17	4.30E+10	10.5
50S ribosomal protein L19	13	67.5	3.52E-220	5.68E+09	10.4
*Trigger factor	32	58.9	0	2.56E+10	10.4
Ferredoxin--NADP reductase	7	31	0	2.11E+09	10.3
Homogentisate 1,2-dioxygenase	18	63.8	5.56E-304	2.75E+09	10.3
Peptide ABC transporter permease	5	20.1	1.81E-96	3.26E+09	10.2
Xaa-Pro dipeptidase	13	43.7	3.40E-248	1.09E+10	10.1
Metallopeptidase	13	58.9	4.22E-295	4.33E+09	10.0
Regulatory protein Spx	15	83.2	1.25E-302	3.06E+09	9.9
NADH dehydrogenase	15	63.7	1.62E-158	2.86E+09	9.7
Isoleucine--tRNA ligase	38	46.7	4.39E-154	5.68E+09	9.7
Kynureninase	13	31.5	2.83E-184	2.32E+09	9.7
Putative tRNA (cytidine(34)-2-O)-methyltransferase	7	63.1	1.57E-286	2.31E+09	9.7
RsbR protein	9	47.1	0	2.42E+09	9.6
Uroporphyrinogen decarboxylase	14	54.4	1.33E-86	2.64E+09	9.5
Oligopeptide transport ATP-binding protein OppF	8	26.2	3.31E-195	2.43E+09	9.5
ATP synthase subunit delta	6	51.7	2.53E-182	3.67E+09	9.4
NAD-dependent dehydratase	7	40.7	1.83E-272	2.15E+09	9.4
Iron-sulfur cluster carrier protein	15	54.2	0	3.35E+09	9.3
4-hydroxy-tetrahydrodipicolinate synthase	10	46.6	5.57E-57	2.67E+09	9.3
30S ribosomal protein S15	6	60.7	4.31E-261	3.25E+09	9.2
Sporulation protein SpoOM	10	57.4	2.82E-128	3.24E+09	9.2
Enoyl-[acyl-carrier-protein] reductase [NADH]	13	52.7	3.73E-69	2.39E+09	9.2
*Succinyl-CoA:3-ketoacid-CoA transferase	13	73	0	9.31E+09	9.2
ATP synthase epsilon chain	7	57.5	3.52E-222	6.14E+09	9.2
DEAD-box ATP-dependent RNA helicase CshA	27	55	3.29E-247	5.93E+09	9.1

*Succinyl-CoA ligase [ADP-forming] subunit beta	37	84.7	1.83E-134	6.90E+10	9.0
Fumarate hydratase	17	31.1	2.43E-283	3.95E+09	9.0
GMP synthase [glutamine-hydrolyzing]	14	33.8	5.05E-54	2.86E+09	8.9
Glutamate--tRNA ligase	13	36.3	0	2.90E+09	8.9
Tyrosine--tRNA ligase	20	61.4	0	2.74E+09	8.9
Peptide ABC transporter permease	7	13.7	9.61E-271	4.04E+09	8.7
Kinase	6	40.9	1.88E-37	2.43E+09	8.6
Phosphoenolpyruvate-protein phosphotransferase	22	44	0	2.06E+09	8.6
*DNA-directed RNA polymerase subunit beta	80	66.9	5.20E-44	1.39E+10	8.5
Phosphoglucomutase	19	35.2	0	2.54E+09	8.5
DNA-directed RNA polymerase subunit omega	6	61.6	7.48E-128	3.16E+09	8.5
ATP-dependent Clp protease ATP-binding subunit ClpE	5	6	0	2.22E+09	8.4
*Transketolase	32	41.2	0	9.96E+09	8.4
Preprotein translocase subunit SecD	17	22.1	3.02E-168	2.49E+09	8.4
Iron transporter FeoB	12	49	7.67E-136	2.67E+09	8.3
Protein translocase subunit SecA	34	43.3	6.57E-51	2.89E+09	8.3
Sugar epimerase	7	41.8	0	2.53E+09	8.1
PalA	8	27.8	1.29E-283	1.72E+09	8.1
UPF0173 metal-dependent hydrolase AM506_20915	11	68.6	4.28E-46	2.40E+09	8.0
S-ribosylhomocysteine lyase	7	66.9	0	3.24E+09	8.0
Menaquinol-cytochrome C reductase	6	40.8	2.11E-232	3.21E+09	7.9
Dehydrogenase	10	36.4	3.14E-99	1.64E+09	7.9
NADPH dehydrogenase	12	32.2	1.34E-187	2.59E+09	7.8
D-alanine aminotransferase	3	12.1	2.73E-146	1.54E+09	7.8
ATP-dependent 6-phosphofructokinase	10	36.7	1.57E-135	2.50E+09	7.7
Peptidase M20	17	40.2	1.33E-162	2.54E+09	7.7
Deacetylase	10	44.5	0	3.86E+09	7.7
Lipoprotein	12	53.5	0	2.33E+09	7.7
*Globin	9	66.2	0	5.06E+09	7.6
*30S ribosomal protein S3	23	65.6	1.42E-24	1.62E+10	7.5
UPF0340 protein AM506_12745	8	32.8	3.08E-45	1.39E+09	7.5
Ribosome-binding ATPase YchF	21	75.4	5.16E-201	2.11E+09	7.5
50S ribosomal protein L21	5	56.9	0	4.62E+09	7.4
Kynurenine formamidase	8	47.3	0	2.22E+09	7.3
50S ribosomal protein L22	7	57.5	6.44E-94	2.18E+09	7.3
Thymidylate synthase	11	50	1.22E-238	2.06E+09	7.3
Cyclase	9	47.1	1.96E-238	3.68E+09	7.2
*Glucose-6-phosphate isomerase	22	64.4	0	1.13E+10	7.2
Nitrogen fixation protein NifU	7	69.9	0	1.67E+09	7.1
*Purine nucleoside phosphorylase DeoD-type	8	44.9	2.61E-278	1.31E+10	7.1

Pyridoxal kinase	5	15.7	0	1.86E+09	7.1
ABC transporter ATP-binding protein	20	40	0	1.77E+09	7.1
*Virulence factor	18	39.7	0	3.45E+09	7.0
ATP-dependent zinc metalloprotease FtsH	17	28.9	1.15E-237	3.15E+09	7.0
Cytidylate kinase	9	42.2	0	2.42E+09	7.0
*Cadmium transporter	20	27.3	0	7.22E+09	7.0
GTP cyclohydrolase 1	11	55.9	8.83E-234	2.83E+09	6.9
50S ribosomal protein L14	6	39.3	5.50E-254	2.26E+09	6.9
Fructose-1,6-bisphosphatase	15	65.9	1.82E-142	2.53E+09	6.9
30S ribosomal protein S10	7	52.9	0	2.69E+09	6.8
*Betaine-aldehyde dehydrogenase	21	51.5	6.89E-163	6.48E+09	6.8
Enoyl-ACP reductase	12	46.6	0	2.61E+09	6.8
Aldehyde dehydrogenase	17	49.6	2.21E-184	1.80E+09	6.8
Peptidase M20	10	33.5	7.71E-142	2.36E+09	6.7
4-hydroxy-3-methylbut-2-en-1-yl diphosphate synthase (flavodoxin)	19	65.8	1.30E-250	2.37E+09	6.7
Epimerase	11	43.7	0	1.70E+09	6.7
30S ribosomal protein S4	6	15.5	0	2.75E+09	6.6
2,3,4,5-tetrahydropyridine-2,6-dicarboxylate N-acetyltransferase	8	31.1	0	1.76E+09	6.6
*L-lactate dehydrogenase	16	33.2	1.16E-225	4.49E+10	6.6
Branched-chain alpha-keto acid dehydrogenase subunit E2	21	42.6	0	3.27E+09	6.5
UPF0435 protein AM506_05030	2	40	7.36E-186	2.01E+09	6.3
Enoyl-CoA hydratase	10	52.7	0	2.94E+09	6.3
Chorismate synthase	13	50	1.07E-185	1.66E+09	6.3
Ribonucleoside-diphosphate reductase subunit beta	9	30.1	0	3.27E+09	6.2
*Thymidine phosphorylase	15	40.3	3.35E-125	2.96E+09	6.2
50S ribosomal protein L36	4	56.8	0	2.00E+09	6.2
Septation ring formation regulator EzrA	19	38.6	1.77E-126	1.93E+09	6.1
Agmatinase	10	38.6	0	1.89E+09	6.1
Peptide methionine sulfoxide reductase MsrB	2	14.3	7.00E-75	1.88E+09	6.0
Adenylosuccinate lyase	26	62.5	0	2.29E+09	6.0
30S ribosomal protein S16	5	41.1	4.51E-68	2.42E+09	5.9
Pyruvate dehydrogenase	13	39.9	0	2.33E+09	5.9
*Elongation factor G	48	74.7	3.19E-143	8.15E+10	5.9
*Serine hydroxymethyltransferase	25	48.2	1.45E-191	2.06E+10	5.9
Sugar ABC transporter ATP-binding protein	13	50.1	2.67E-54	2.37E+09	5.9
Glutamate-1-semialdehyde 2,1-aminomutase	14	50	3.76E-198	1.74E+09	5.9
*2-oxoisovalerate dehydrogenase	22	76.1	0	1.33E+10	5.8
UPF0473 protein AM506_03120	1	28.1	0	1.59E+09	5.8
ABC transporter substrate-binding protein	11	44.8	7.59E-217	1.33E+09	5.8
Cystathionine gamma-synthase	9	34.8	0	1.54E+09	5.8

*3-oxoacyl-[acyl-carrier-protein] synthase 2	20	60.6	6.41E-303	8.33E+09	5.8
Leucine dehydrogenase	9	37.8	4.36E-120	1.94E+09	5.8
6,7-dimethyl-8-ribityllumazine synthase	9	78.2	0	1.20E+09	5.8
*Inosine-5-monophosphate dehydrogenase	50	89.7	0	5.19E+10	5.7
Dihydrolipoyllysine-residue succinyltransferase component of 2-oxoglutarate dehydrogenase complex	16	38.7	0	4.78E+09	5.7
50S ribosomal protein L16	8	64.6	0	1.99E+09	5.7
Lon protease	25	37.6	0	1.86E+09	5.7
*Transcriptional regulator	34	78.2	1.63E-42	2.44E+10	5.6
DNA helicase	24	38.1	4.97E-141	1.62E+09	5.5
Cysteine synthase	14	55.3	1.14E-201	1.92E+09	5.4
30S ribosomal protein S17	5	34.5	0	2.02E+09	5.3
*Iron siderophore-binding protein	10	24.8	0	3.74E+09	5.3
3-phosphoshikimate 1-carboxyvinyltransferase	13	37.4	0	1.23E+09	5.3
*Leucine dehydrogenase	24	74.8	2.10E-269	1.62E+10	5.3
*Succinyl-CoA:3-ketoacid-CoA transferase	5	26.4	6.84E-253	5.83E+09	5.2
*50S ribosomal protein L2	23	61.2	0	1.90E+10	5.2
tRNA-binding protein	7	42.8	0	1.23E+09	5.2
30S ribosomal protein S9	5	38.5	0	2.58E+09	5.2
Glutamate-1-semialdehyde 2,1-aminomutase	10	34.4	9.77E-176	1.48E+09	5.2
Transcriptional regulator	10	42.9	0	1.30E+09	5.1
Transcription attenuation protein MtrB	5	82.2	0	1.79E+09	5.1
UvrABC system protein A	26	38.1	4.65E-123	1.70E+09	5.1
Proline--tRNA ligase	19	35.6	5.90E-201	1.44E+09	5.0
*Adenylate kinase	18	85.6	3.13E-303	1.80E+10	5.0
3-5 exonuclease	15	57.2	0	1.91E+09	4.9
Esterase	7	52	0	1.28E+09	4.9
UDP-glucose 4-epimerase	8	36.4	8.79E-175	1.56E+09	4.9
Xylose isomerase	11	57.5	0	2.59E+09	4.9
Acetoin utilization protein AcuA	5	38.6	0	1.23E+09	4.8
*30S ribosomal protein S5	11	61.4	3.02E-34	1.55E+10	
Lipoate--protein ligase	15	58.5	0	1.80E+09	4.8
Trascriptional regulator	7	23.5	1.82E-267	2.12E+09	4.7
Permease IIC component	2	6.8	0	1.15E+09	4.7
30S ribosomal protein S12	9	47.9	5.51E-253	1.98E+09	4.7
Acyl-CoA synthetase	8	88.6	3.41E-153	3.94E+09	4.7
Transcription termination factor Rho	19	53.1	1.21E-205	1.84E+09	4.6
*Glutamyl-tRNA(Gln) amidotransferase subunit A	22	59.3	4.63E-208	3.43E+09	4.6
Cytosolic protein	8	83.8	9.23E-96	1.86E+09	4.6
UDP-N-acetylmuramyl-tripeptide	15	36.9	4.87E-204	1.79E+09	4.6

synthetase					
Catabolite control protein A	14	55.7	9.64E-271	1.39E+09	4.5
*Polyribonucleotide nucleotidyltransferase	42	59.3	0	7.94E+09	4.5
*Pyruvate carboxylase	33	37	0	2.98E+09	4.5
Zinc protease	13	37.8	0	1.56E+09	4.4
2-amino-3-ketobutyrate CoA ligase	15	33.1	0	4.18E+09	4.4
Non-canonical purine NTP pyrophosphatase	4	29.8	4.81E-06	9.37E+08	4.4
Cytochrome B6	2	16.4	2.94E-276	1.57E+09	4.4
ABC transporter substrate-binding protein	8	43.7	1.69E-61	1.66E+09	4.4
Fur family transcriptional regulator	8	73.6	0	1.74E+09	4.4
NAD kinase	8	37.2	1.83E-160	1.01E+09	4.3
DNA polymerase	23	32	0	1.77E+09	4.3
Enoyl-CoA hydratase	5	24.1	1.27E-100	1.55E+09	4.3
UPF0296 protein AM506_00685	6	86.7	0	1.41E+09	4.3
Fatty acid-binding protein DegV	6	24.6	0	8.07E+08	4.3
6-phosphogluconate dehydrogenase, decarboxylating	18	44.9	1.17E-122	1.34E+09	4.3
Cystathionine beta-lyase	8	30.7	0	1.36E+09	4.2
Beta-glucosidase	15	35.4	0	1.14E+09	4.2
Peptidase M15	8	32.4	0	1.97E+09	4.2
AMP-dependent synthetase	14	38	1.62E-257	1.18E+09	4.2
*Fis family transcriptional regulator	11	42.7	0	1.45E+10	4.2
ArsR family transcriptional regulator	5	47.5	0	1.12E+09	4.2
Putative ribosomal protein L7Ae-like	5	62.2	2.46E-225	1.53E+09	4.2
3-ketoacyl-ACP reductase	9	39.6	0	1.52E+09	4.1
D-alanine--D-alanine ligase	13	43.5	0	1.37E+09	4.1
Transcription termination/antitermination protein NusA	19	52.5	0	1.12E+09	4.1
Phosphate butyryltransferase	8	35.8	9.01E-272	1.28E+09	4.1
Transcription termination/antitermination protein NusG	5	34.5	0	1.28E+09	4.1
30S ribosomal protein S20	4	37.3	5.87E-95	8.85E+08	4.1
Ribosome-binding factor A	7	44.3	0	1.67E+09	4.0
Putative pre-16S rRNA nuclease	6	39.1	0	1.11E+09	4.0
*Chemotaxis protein CheY	18	70.2	1.59E-201	8.47E+09	4.0
*30S ribosomal protein S7	14	71.8	0	3.27E+10	3.9
Nucleoid occlusion protein	10	36.2	0	8.19E+08	3.9
Pyridoxal 5-phosphate synthase subunit PdxT	7	39.8	3.84E-152	1.67E+09	3.9
Lipid kinase	15	50	3.97E-275	1.25E+09	3.9
Spore protein	5	75	0	9.34E+08	3.9
Enoyl-CoA hydratase	13	51.1	0	7.74E+08	3.8
UPF0291 protein AM506_14795	7	62.3	0	1.49E+09	3.8
Glyceraldehyde-3-phosphate dehydrogenase	11	23.7	5.41E-215	9.62E+08	3.8
Endoribonuclease L-PSP	2	23.4	0	1.13E+09	3.8

Probable DNA-directed RNA polymerase subunit delta	12	43.9	0	1.61E+09	3.7
Cytoplasmic protein	5	51.2	0	1.05E+09	3.7
Site-determining protein	10	35.6	0	1.03E+09	3.7
Peptidase M29	9	27.3	0	1.40E+09	3.7
*Glucose-6-phosphate 1-dehydrogenase	29	59.4	1.16E-174	7.14E+09	3.6
Glycerol-3-phosphate dehydrogenase	15	30	5.13E-138	1.05E+09	3.6
Cytidine deaminase	6	39.4	0	2.00E+09	3.6
ABC transporter substrate-binding protein	11	34	0	1.35E+09	3.6
GTP-binding protein TypA	17	39.7	0	1.04E+09	3.5
Oxidoreductase	7	13.7	0	1.50E+09	3.5
Glycerol kinase	11	28.2	0	8.32E+08	3.4
Dienelactone hydrolase	6	34.9	0	1.21E+09	3.4
Peptidase	7	27.2	0	1.24E+09	3.4
Proline dehydrogenase	11	41	0	7.85E+08	3.3
CTP synthase	26	68.7	1.63E-219	1.43E+09	3.3
Chemotaxis protein CheY	9	66	2.82E-177	8.62E+08	3.3
DNA gyrase subunit A	25	34.1	3.77E-234	1.20E+09	3.2
Choloylglycine hydrolase	5	22.2	1.85E-146	5.24E+08	3.2
Chaperone protein ClpB	35	46.9	0	1.69E+09	3.2
Ring-cleaving dioxygenase	14	39	0	1.06E+09	3.2
Uridylate kinase	8	42.7	0	1.63E+09	3.2
*Peptidase M28	15	68.3	0	1.17E+10	3.1
tRNA modification GTPase MnmE	11	26.7	2.20E-169	9.77E+08	3.1
Dihydrolipoyl dehydrogenase	13	38.8	4.67E-255	2.12E+09	3.1
Glucokinase	9	31.4	0	1.26E+09	3.1
Cysteine--tRNA ligase	20	47.2	0	1.24E+09	3.0
PhoP family transcriptional regulator	17	71.1	0	1.31E+09	3.0
Guanylate kinase	10	59.8	0	7.79E+08	3.0
AAA family ATPase	11	41.3	9.15E-132	1.10E+09	3.0
UTP--glucose-1-phosphate uridylyltransferase	13	62.4	0	1.09E+09	2.9
Cysteine desulfurase	8	25.2	8.32E-146	1.04E+09	2.9
tRNA-specific 2-thiouridylase MnmA	8	24.8	0	9.33E+08	2.9
Cystathionine gamma-synthase	12	32.8	0	1.40E+09	2.9
Short-chain dehydrogenase	3	13.5	0	5.13E+08	2.9
DNA ligase	20	36.5	0	1.26E+09	2.8
Aspartate-semialdehyde dehydrogenase	13	53.6	4.16E-98	1.28E+09	2.8
Phosphopantetheine adenylyltransferase	6	57.8	0	1.03E+09	2.8
50S ribosomal protein L28	4	38.7	0	1.04E+09	2.8
Peptide chain release factor 2	9	27.8	1.18E-201	8.90E+08	2.8
1-deoxy-D-xylulose-5-phosphate synthase	7	49.1	1.11E-275	2.99E+10	2.7
DNA methyltransferase	2	36.3	0	7.70E+08	2.7
Protein-arginine kinase	12	53.9	0	1.16E+09	2.7
Lipoyl synthase	13	49.8	8.80E-95	9.81E+08	2.7
Probable butyrate kinase	12	42.7	0	7.64E+08	2.7
Heme ABC transporter ATP-binding protein	11	23.6	0	1.01E+09	2.7

3-oxoacyl-[acyl-carrier-protein] synthase 3	11	33.5	0	1.10E+09	2.6
Transcriptional regulator	4	29.5	0	7.93E+08	2.6
Translation initiation factor IF-3	6	49.1	1.59E-88	1.26E+09	2.6
Phosphatidylglycerophosphatase	3	21.7	0	7.54E+08	2.5
*Elongation factor Tu	35	90.2	0	1.32E+11	2.5
Phenylalanine--tRNA ligase alpha subunit	15	46.4	0	8.46E+08	2.5
Aspartyl/glutamyl-tRNA(Asn/Gln) amidotransferase subunit C	7	99	1.69E-215	7.59E+08	2.4
Phosphoglycerate kinase	6	9.4	4.75E-170	4.69E+08	2.4
*6-phosphogluconate dehydrogenase, decarboxylating	22	56	0	7.59E+09	2.4
Acetoin utilization protein AcuB	6	45.6	0	9.40E+08	2.4
Acetyl-coenzyme A carboxylase carboxyl transferase subunit alpha	10	28.8	5.03E-119	1.26E+09	2.4
Outer surface protein	11	40	1.74E-267	7.33E+08	2.4
Hydrolase TatD	8	36.1	2.67E-284	1.04E+09	2.3
Xylose isomerase	5	26.6	0	5.84E+08	2.3
4-diphosphocytidyl-2-C-methyl-D-erythritol kinase	6	35.9	0	4.67E+08	2.3
Molecular chaperone DnaK	8	47.4	0	6.00E+08	2.2
ABC transporter substrate-binding protein	3	17.2	0	2.62E+08	2.1
GMP reductase	8	25.7	0	6.17E+08	2.1
ADP-ribose pyrophosphatase	5	22.5	0	4.60E+08	2.1
Phenylalanine--tRNA ligase beta subunit	16	31.7	0	7.80E+08	2.1
Zinc protease	9	31.7	1.39E-266	5.92E+08	2.0
*Translation initiation factor IF-2	27	34.9	0	3.75E+09	2.0
*Lysine--tRNA ligase	41	77.8	0	9.43E+09	2.0
Ribonuclease Z	9	38	0	4.34E+08	2.0
UDP-galactose-4-epimerase	10	31	0	6.32E+08	2.0
Primosomal protein DnaI	13	57.1	0	8.29E+08	2.0
3-hydroxyacyl-CoA dehydrogenase	19	28.8	0	8.75E+08	1.9
*Probable manganese-dependent inorganic pyrophosphatase	15	50	0	7.96E+09	1.8
Cell division protein FtsA	14	30.8	0	9.50E+08	1.8
NUDIX hydrolase	7	48	0	7.37E+08	1.8
*Oligopeptidase PepB	32	41.8	2.03E-166	7.60E+09	1.8
Dihydrolipoyllysine-residue acetyltransferase component of pyruvate dehydrogenase complex	4	11.3	0	5.90E+08	1.7
RNA polymerase subunit sigma	10	54	0	6.65E+08	1.7
Adenine phosphoribosyltransferase	7	48.8	1.83E-181	7.01E+08	1.6
Tryptophan--tRNA ligase	6	31.9	2.26E-260	4.97E+08	1.6
Chemotaxis protein CheA	10	17.8	0	4.23E+08	1.5
Methionyl-tRNA formyltransferase	6	23.1	0	5.65E+08	1.5

Table A6.1 Individual patient scores from first pilot study.

Table includes individual data from rosacea patients who participated in the first pilot study. Table excludes individual scores previously mentioned in Chapter 6.

No of patient	Age	Sex	Erythema Before	Erythema After	Melanin Before	Melanin After	TEWL Before	TEWL After	Moisture Before	Moisture After	Sebum Before	Sebum After
1	55	f	22	22.38	38.28	37.45	11.1	10.9	33.43	50.5	1	208.5
2	56	f	26.25	25.39	41.26	42.3	14.2	8.5	61.15	79	77	22
3	42	f	29.02	27.01	40.88	41.12	14.9	8.8	60.93	78	67	12
5	60	m	25.5	26.06	43.1	42.17	16	20.5	28.6	48.83	0	14
6	42	m	30.4	33.86	46.01	47.17	9.2	14.4	38.37	47	6	0
7	36	f	20.86	17.72	37.21	35.72	21.3	9.6	28.5	35.63	22	0
8	27	m	23.76	19.43	36.98	35.72	14.7	16.5	29.72	52.57	178	79
9	55	m	29.46	30.69	46.29	46.15	18.1	12.1	25.27	48.13	0	2
10	39	m	28.11	35.23	27.05	34.89	18.9	13.1	27.5	43.2	13	0
11	41	m	20.87	19.98	36.06	37.8	21.7	11.6	36.25	62.3	211	192
12	36	f	16.27	17.2	31.83	34.71	10.2	15.4	40.93	48.63	22	14
13	43	f	24.61	20.31	36.75	35.38	22.1	7	59.65	59.95	277	260
14	47	m	29.29	28.79	52.49	52.49	16.7	9.4	26	28.23	81	27
16	66	m	14.17	14.4	33.88	38.5	16.8	9.8	34	39.8	215	98
17	58	f	20.34	16.02	42.43	37.8	21.8	14.8	32.8	43.9	112	109
18	51	m	23.41	23.59	50.85	49.44	31	19.5	27.9	35.8	216	89
20	29	m	24.96	22	40.62	41	21.6	14.8	25.8	42.5	116	76

Before After

Figure A6.1 Effect of Oriel application on face of patient one before and after one week of treatment.

Before After

Figure A6.2 Effect of Oriel application on face of patient two before and after one week of treatment.

Figure A6.3 Effect of Oriel application on face of patient three before and after one week of treatment.

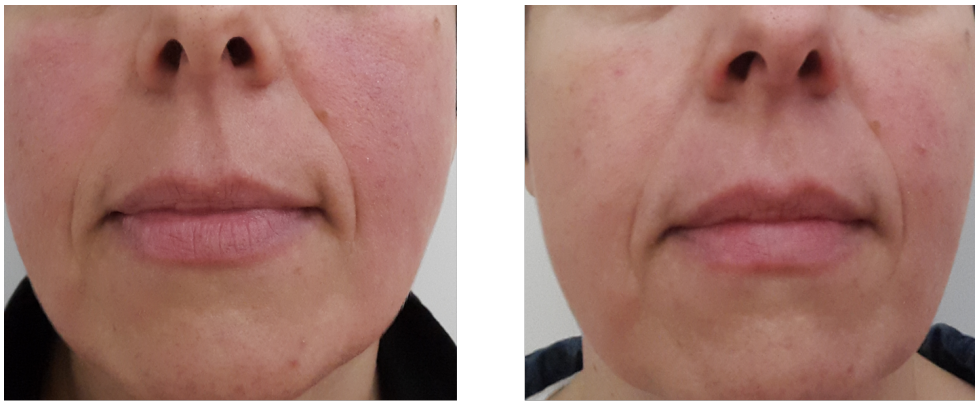

Figure A6.4 Effect of Oriel application on face of patient seven before and after one week of treatment.

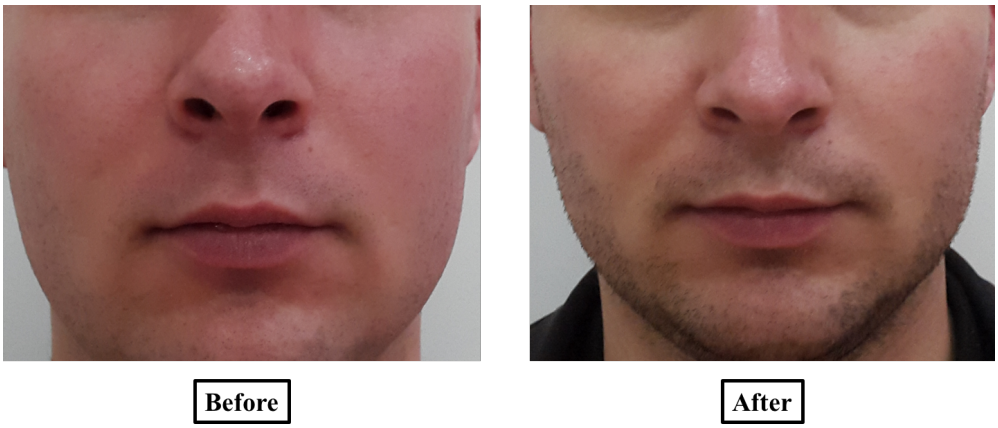

Figure A6.5 Effect of Oriel application on face of patient eight before and after one week of treatment.

Figure A6.6 Effect of Oriel application on face of patient sixteen before and after one week of treatment.

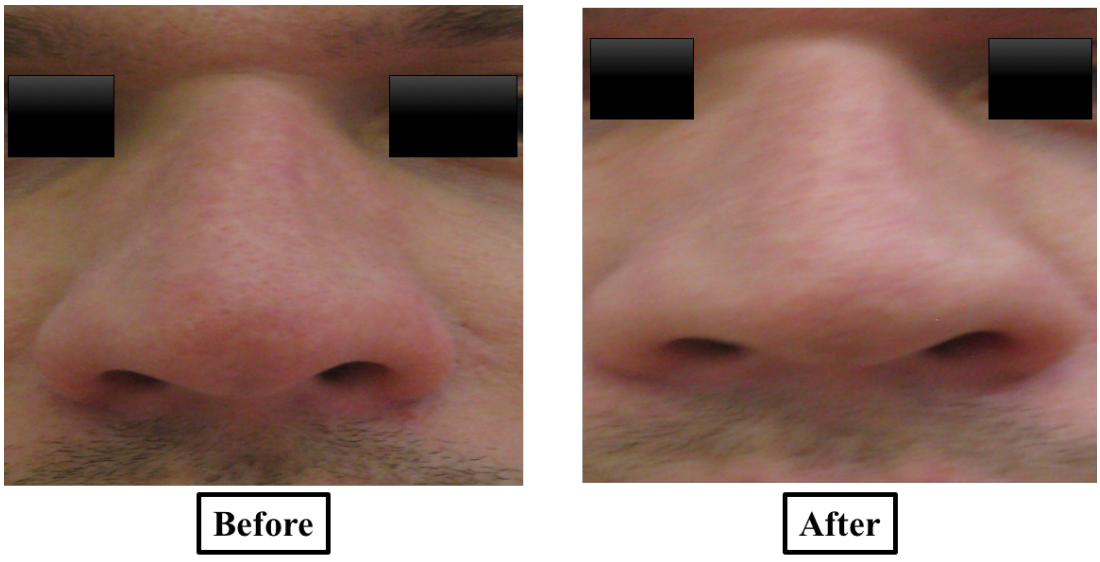

Figure A6.7 Effect of Oriel application on face of patient twenty before and after one week of treatment.

Table A6.2 Individual patient scores from second pilot study.

Table includes individual data from rosacea patients who participated in the second pilot study. Table excludes individual scores previously mentioned in Chapter 6.

No of patient	Age	Sex	Erythema Before	Erythema After 2 weeks	Erythema After 4 weeks	Melanin Before	Melanin After 2 weeks	Melanin After 4 weeks	Sebum Before	Sebum After 2 weeks	Sebum After 4 weeks
A	39	f	22.28	17.53	13.95	38.76	34.38	32.35	1	2	22
B	41	f	22	17.4	21	40.52	39.25	38.76	3	0	2
C	46	f	19.89	12.9	12.34	35.49	33.84	32.14	0	6	25
D	43	m	31.26	29.79	-	60.51	54.54	-	76	14	
F	66	f	25.65	22.71	19.23	48.82	45.16	42.43	2	2	2
I	44	f	19.94	16.08	12.59	41.65	35.83	34.6	57	7	0
J	61	f	19	16.65	17.96	38.09	36.4	35.61	15	7	8

			TEWL Before	TEWL After 2 weeks	TEWL After 4 weeks	Moisture Before	Moisture After 2 weeks	Moisture After 4 weeks
A	39	f	12.1	7	13	55.6	66.97	50.53
B	41	f	15.5	8.9	13.4	41.33	46.98	40.1
C	46	f	48.8	12.8	14.5	43.72	41.26	40.2
D	43	m	24.2	13.9		30.47	30.7	
F	66	f	9.2	8.5	7.8	34.77	55.2	48.1
I	44	f	11	15.9	11.7	44.43	58.83	53.07
J	61	f	10.3	3.4	8.5	42.33	47.28	40.8

Figure A6.8 Effect of Oriel application before treatment (left image), two weeks after treatment (middle image) and after four weeks at the end of trial (right image) in patient A.

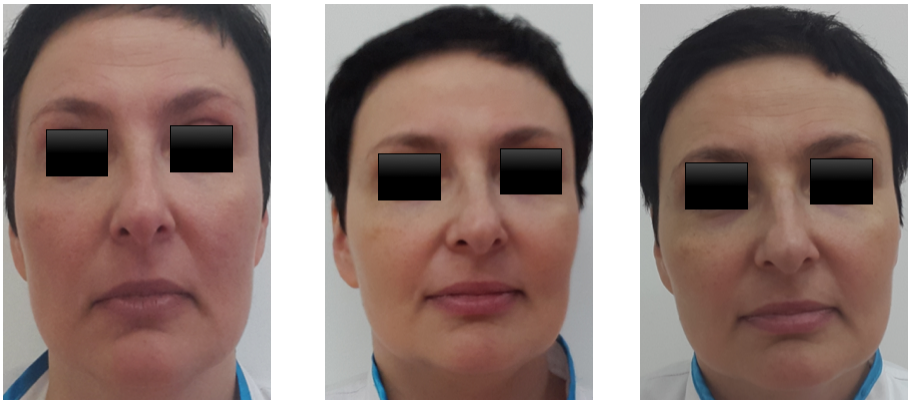

Figure A6.9 Effect of Oriel application before treatment (left image), two weeks after treatment (middle image) and after four weeks at the end of trial (right image) in patient B.

Figure A6.10 Effect of Oriel application before treatment (left image), two weeks after treatment (middle image) and after four weeks at the end of trial (right image) in patient C.

Figure A6.11 Effect of Oriel application before treatment (left image) and two weeks after treatment (right image). No image was provided after four weeks at the end of trial in patient D.

Figure A6.12 Effect of Oriel application before treatment (left image) and after four weeks at the end of trial (right image). No image was provided two weeks after treatment in patient F.

Figure A6.13 Effect of Oriel application before treatment (left image) and two weeks after treatment (right image). No image was provided after four weeks at the end of trial in patient I.

Figure A6.14 Effect of Oriel application before treatment (left image) and after four weeks at the end of trial (right image). No image was provided two weeks after treatment in patient J.